June 13-14, 2019

TU Wien

https://vss.tuwien.ac.at/

Edited by:

Katharina Ehrmann
Hamid Reza Mansouri Khosravi

Gerald Artner
Philipp Hans
Heinz Krebs
Aryan Shahabian
Daniela Wipp

Cover photo by Matthias Heisler

© 2019
Published by Book-of-Abstracts.com
Heinz A. Krebs Dipl.-Ing.
Jubiläumsstrasse 17/2
2352 Gumpoldskirchen / Austria

Printed and bound in the Czech Republic

ISBN 978-3-9504017-9-0

Contents:

Welcome Messages

from the Organizers *p 5*

by the Rector and the Vice Rector for Research and Innovation *p 7*

Announcement VSS2020 *p 8*

Guest Lectures *p 9*

Index of Contributions

AUP - Architecture & Urban Planning *p 10*

CAT – Catalysis *p 12*

ENM - Engineering in Medicine *p 15*

FUR - Fundamental Research *p 17*

LION – Lions Sponsorship *p 21*

Introductions of research fields and Abstracts

Introduction Architecture & Urban Planning *p 22*

Abstracts AUP.1 – AUP.19 *p 24*

Introduction Catalysis *p 62*

Abstracts CAT.1 – CAT.26 *p 64*

Introduction Engineering in Medicine *p 116*

Abstracts ENM.1 – ENM.13 *p 118*

Introduction Fundamental Research *p 144*

Abstracts FUR.1 – FUR.34 *p 146*

Abstracts LION.1 – LION.2 *p 214*

Author Index *p 218*

Welcome from the Organizers

We are pleased to welcome you to the 5th Vienna Young Scientists Symposium on the 13th and 14th of June 2019.

While the conference was created for you five years ago, the event now exists because of you: It has shaped up to the today's form due to your active participation and your interest in sharing your research and getting to know other fellow researchers based at your home institution. This is corroborated by the extraordinary number of contributions this year: Thank you for contributing with all the talks, posters, and discussions!

The program gives an idea about the diversity of the research going on at TU Wien. We are sure that not only our general awareness of state-of-the-art research but also our own research projects will greatly benefit from our interest in other disciplines.

We would like to thank the rectorate for their continuing support of the VSS since five years: They are the silent backbone of this conference. Furthermore, we would like to thank all reviewers for their hard work to ensure the high quality of all contributions.

Enjoy the meeting and celebrate with us science at its best!

The organizing committee wishes you a cheerful and rewarding VSS 2019!

Welcome by the Rector
and the Vice Rector for Research and Innovation

The Vienna young Scientists Symposium (VSS) is a platform, which aims at bringing highly talented individuals and promising projects together, thus demonstrating our students' enthusiasm both for broadening their own scientific horizons and for thinking outside the box, as well as their internalized interdisciplinary perspective. This initiative serves to enhance scientific research, broadens the findings of research groups and strengthens partnership with industry. The impressive volume of the abstracts compiled here rather eloquently conveys the creativity of our students and young scientists, as does this fantastic event itself.

© Raimund Appel

Scientific work at TU Wien is mainly covered by the five research focal areas of the TUW research matrix, which itself via the embedded research fields is a showcase of TUW scientific expertise.

The VSS 2019 presents research results in the fields of “Catalysis”, “Engineering in Medicine”, “Fundamental Research” and “Architecture & Urban Planning”. All these interdisciplinary topics provide vivid evidence of the existing TUW research network.

© Raimund Appel

We would like to express our gratitude towards the organizers and supporters of VSS, who contributed to realizing an outstanding event. Our young scientific talents play an important role in the research advancement for the "TU Wien of tomorrow".

Sabine Seidler, Rector of TU Wien
Johannes Fröhlich, Vice Rector for Research and Innovation

TU WIEN VSS
VIENNA young SCIENTISTS SYMPOSIUM

JOIN THE ...

6th VIENNA young SCIENTISTS SYMPOSIUM (VSS)

11-12 June 2020
TU Wien, TUtheSky
Getreidemarkt 9, 1060 Vienna, Austria

Technische Universität Wien

vss@tuwien.ac.at

vss.tuwien.ac.at

Guest Lectures

Johannes **Homa**
Lithoz GmbH

LITHOZ: FROM LAB TO WORLD MARKET LEADERSHIP IN 3D PRINTING

Karl **Milford**
University of Vienna

PHILOSOPHY OF SCIENCE AND THE RATIONALITY OF POLICY MEASURES IN SOCIETY

Ursula **Hunger**
Austrian Patent Office

THE AUSTRIAN PATENT OFFICE

Katharina **Engel**
OeAD-GmbH / Österreichischer Austauschdienst

OEAD: INFORMATION, SERVICES, AND SCHOLARSHIPS

Fridolin **Herkommer**
Arbeiterkammer Wien

KÜNSTLICHE INTELLIGENZ: AUSWIRKUNGEN AUF GESELLSCHAFT UND ARBEIT

Introduction by Rudolf Giffinger and Alireza Fadai	
AUP.1	Christos **Tsigkanos** E194 - Institute of Information Systems Engineering **ARCHITECTING DEPENDABLE CYBER-PHYSICAL SPACES**
AUP.2	Ferdinand **Reimer** E226 - Institute of Water Quality and Resource Management **SPATIAL AND TEMPORAL MODELLING OF VIENNA'S BUILDING STOCK IN RESPECT TO ITS POTENTIAL AS A SECONDARY RESOURCE MINE**
AUP.3	Klaus **Sperka** E259 - Institute of Architectural Sciences **METHOD COMPARISON OF OVERHEATING EVALUATION VIA NORMATIVE CALCULATION AND NUMERIC SIMULATION**
AUP.4	Marvin **Mc Cutchan** E120 - Department of Geodesy and Geoinformation **URBAN GROWTH PREDICTIONS WITH DEEP LEARNING AND GEOSEMANTICS**
AUP.5	Matea **Flegar** E259 - Institute of Architectural Sciences **RETROFITTING POTENTIAL OF LARGE-SCALE PREFABRICATED BUILDINGS FROM PRE-"WENDE" TIMES: A CASE STUDY OF CROATIA**
AUP.6	Judith **Mayr** E251 - Institute of History of Art, Building Archaeology and Restoration **THE SIGNIFICANCE AND PRESERVATION OF THE BUILDING TYPE "CASINO" IN THE VIENNESE BIEDERMEIER PERIOD EXEMPLIFIED ON THE STILL PRESERVED "CASINO ZÖGERNITZ"**
AUP.7	Magdalena **Wölzl** E259 - Institute of Architectural Sciences **NUMERIC THERMAL BRIDGE SIMULATION IN WINDOW CONSTRUCTION ASSESSMENT: A CASE STUDY PERTAINING TO VACUUM-GLASS WINDOWS**
AUP.8	Stefan **Pillwein** E104 - Institute of Discrete Mathematics and Geometry **DEPLOYING GRIDSHELLS MADE EASY**
~~**AUP.9**~~ **CANCELED**	~~Viktoria Eva **Lelek**~~ ~~E259 - Institute of Architectural Sciences~~ ~~**URBAN PARTERRE BUDAPEST - THE DEVELOPMENT OF STREETSCAPES IN HISTORICAL DISTRICTS OF BUDAPEST FROM THE TIME OF THE DUALISM AND THEIR EFFECT ON THE CITY TODAY**~~
AUP.10	Aryan **Shahabian** E259 – Institute of Architectural Sciences **INTELLIGENT PARAMETRIC BIM SOLUTION AND OPTIMIZER FOR DIAGRID HIGH-RISE STRUCTURES**

~~AUP.11~~ CANCELED	~~Darya **Haroshka**~~ ~~E251 - Institute of History of Art, Building Archaeology and Restoration~~ ~~**LOW-TECH APPROACH TO ARCHITECTURE AND ITS PROSPECTS**~~
AUP.12	Ceren **Sarikaya** E259 - Institute of Architectural Sciences **HOME OFFICE ILLUMINATION: THE UNDISCOVERED COUNTRY**
AUP.13	Ulrich **Pont** E259 - Institute of Architectural Sciences **4 IN A ROW: ARCHITECTURAL DESIGN AS ADAPTATION AND MITIGATION MEASURE FOR THE PROBLEMS OF TODAY?**
AUP.14	Habibe **Idiskut** E250 - Faculty of Architecture and Planning **HOW CAN INNOVATIVE SPACES FOR OUTREACH BE CREATED WITH LIMITED RESOURCES?**
AUP.15	Karoline **Walal** E259 - Institute of Architectural Sciences **ARCHITECTURE AND TECHNICAL ASPECTS OF THE SWIMMING HALL DESIGNS BY FRIEDRICH FLORIAN GRÜNBERGER**
AUP.16	Julia **Reisinger** E234 - Institute of Interdisciplinary Construction Process Management **DIGITAL PLANNING AND OPTIMISATION OF FLEXIBLE STRUCTURES FOR INDUSTRY 4.0**
AUP.17	Aída **Santana Sosa** E259 – Institute of Architectural Sciences **CHALLENGES AND OPPORTUNITIES OF COMBINING TAKT TIME PLANNING AND OFF-SITE CONSTRUCTION**
AUP.18	Michael **Jenewein** E259 - Institute of Architectural Sciences **VERIFICATION OF CONSTRUCTION DEVIATIONS USING PARAMETRIC BIM&AR**
AUP.19	Shuyin **Dong** E401 - Faculty of Architecture and Planning **TECHNOLOGICAL SOLUTIONS AND THEIR DETERMINING FACTORS IN SEALING WOODEN GRANARY IN SOUTH CHINA**

Introduction by Gareth Parkinson and Florian Rudroff	
CAT.1	Hamid R. **Mansouri** E163 - Institute Applied Synthetic Chemistry **ACTIVITY AND STABILITY IMPROVEMENT OF CYCLOHEXANONE MONOOXYGENASE BY PROTEIN ENGINEERING**
CAT.2	Igor **Sokolović** E134 - Institute of Applied Physics **ATOMIC INSIGHT INTO THE ADSORPTION OF MOLECULAR O_2 ON THE RUTILE TiO_2(110) (1x1) SURFACE**
CAT.3	Vera **Truttmann** E165 - Institute of Materials Chemistry **CHIRAL AU NANOCLUSTERS - A STEP TOWARDS HETEROGENEOUS ASYMMETRIC CATALYSIS**
CAT.4	Lorenz **Lindenthal** E165 - Institute of Materials Chemistry **NANOPARTICLE EXSOLUTION: ENHANCING CATALYST REACTIVITY UNDER REACTION CONDITIONS**
CAT.5	Thomas **Haunold** E165 - Institute of Materials Chemistry **SURFACE SCIENCE STUDIES OF Li AND Co_3O_4(111) THIN FILMS**
CAT.6	Xia **Li** E165 - Institute of Materials Chemistry **POLARIZATION-DEPENDENT SFG SPECTROSCOPY OF NEAR AMBIENT PRESSURE CO ADSORPTION ON Pt(111) AND Pd(111)**
CAT.7	Klaus **Dobrezberger** E165 - Institute of Materials Chemistry **HYDROGENATION OF CO_2 CATALYSED BY Cu AND Pd NANOPARTICLES SUPPORTED ON ZnO AND CARBON**
CAT.8	Sreejith P **Nandan** E165 - Institute of Materials Chemistry **HETEROGENIZATION OF MOLECULAR OXO/THIO METALATE CATALYSTS FOR SOLAR FUEL GENERATION**
CAT.9	Noelia **Barrabes** E165 - Institute of Materials Chemistry **ON THE REACTIVITY OF $Au_n(SR)_m$ NANOCLUSTERS CATALYSTS: LIGAND, STRUCTURE AND SUPPORT EVOLUTION**
CAT.10	Marcin **Magierło** AGH University of Science and Technology, Kraków, Poland **SYNTHESIS OF MCM-41 FROM FLY ASH**
CAT.11	Oliwia **Ligęza** AGH University of Science and Technology, Kraków, Poland **WASTE MANAGEMENT OF ENERGY SECTOR WASTE - FLY ASH FROM BURNING CRUDE OIL AS CATALYSTS**

CAT.12	Gabriela **Radwańska** AGH University of Science and Technology, Kraków, Poland **THE USE OF FLY ASH FOR THE PRODUCTION OF NICKEL-BASED CATALYST**
CAT.13	Michał **Nowotarski** AGH University of Science and Technology, Kraków, Poland **ANALYSIS OF THE POSSIBILITY OF USING MCM-41 MESOPOROUS MATERIAL FROM FLY ASH TO REMOVE NO_x FROM WASTE GASES**
CAT.14	Charlie **Lim** E163 - Institute of Applied Synthetic Chemistry **SYNTHESIS OF CHIRAL CYCLOOCTADIENE LIGANDS FOR RHODIUM CATALYSIS**
CAT.15	Richard **Fried** E163 - Institute Applied Synthetic Chemistry **DEVELOPMENT OF ENVIRONMENTALLY-FRIENDLY DYES**
CAT.16	Paulina **Summa** AGH University of Science and Technology, Kraków, Poland **COMPARISON OF STRUCTURE OF HYDROTALCITE MATERIALS PREPARED BY DIFFERENT SYNTHESIS METHODS**
CAT.17	Raffael **Rameshan** E165 - Institute of Materials Chemistry **DEVELOPMENT OF A LAB-BASED IN-SITU NAP-XPS SYSTEM FOR ELECTRO-CATALYSIS RESEARCH**
CAT.18	Christoph **Rameshan** E165 - Institute of Materials Chemistry **CHARACTERIZATION OF NOVEL DOPED PEROVSKITE CATALYSTS - TAILORED EXSOLUTION OF METAL NANOPARTICLES**
CAT.19	Agnieszka **Szymaszek** AGH University of Science and Technology, Kraków, Poland **SELECTIVE CATALYTIC REDUCTION OF NO_x WITH AMMONIA OVER CATALYSTS DERIVED FROM FLY ASH**
CAT.20	Jakub **Sobala** AGH University of Science and Technology, Kraków, Poland **THE PROCESS OF MINERAL CARBONATION OF FLY ASH WITH A HIGH CONTENT OF CALCIUM OXIDE FROM THE GROUP HCFA**
CAT.21	Katharina **Novak** E166 - Institute of Chemical, Environmental and Bioscience Engineering **PRODUCTION OF ISOBUTANOL FROM CO_2 IN A TWO-STEP PROCESS**
CAT.22	Markus **Latschka** E165 - Institute of Materials Chemistry **KINETIC STUDIES ON BIMETALLIC Au CATALYSTS: INFLUENCE OF WATER**

CAT.23	Hao **Chen** E134 - Institute for Applied Physics **PROBING ACTIVE PHASE OF Pt-Fe MODEL CATALYSTS USING STM**
CAT.24	Joseba **Lizarazu** Universidad del País Vasco (UPV/EHU), San Sebastián, Spain **STUDY OF Ni CLUSTERS ON Al_2O_3 FOR SABATIER REACTION**
CAT.25	Gernot **Pacholik** E165 - Institute of Materials Chemistry **Co, Ni AND K AS PROMOTERS IN CO_2 HYDROGENATION ON MoS_2 BASED CATALYSTS**
CAT.26	Clara **Garcia** E165 - Institute of Materials Chemistry **Pd DOPING EFFECT ON THE CATALYTIC PROPERTIES OF GOLD NANOCLUSTERS SUPPORTED ON OXIDES**

Introduction by Stefan Baudis and Christian Hellmich	
ENM.1	Franziska **Gantner** E308 – Institute of Materials Science and Technology **FABRICATION OF HIGH-VOLUME 3D 2-PHOTON POLYMERIZATION MICROSTRUCTURES**
ENM.2	Barbara **Dellago** E163 - Institute of Applied Synthetic Chemistry **ACETAL MOIETIES AS BIODEGRADABLE FUNCTIONALITY IN PHOTOPOLYMERS FOR BONE REGENERATION**
ENM.3	Johannes **Kalliauer** E202 – Institute for Mechanics of Materials and Structures **MOLECULE-TO-BEAM HOMOGENIZATION, APPLIED TO DNA**
ENM.4	Vedran **Nedelkovski** E317 - Institute of Lightweight Design and Structural Biomechanics **AFM-BASED MICROBEAM BENDING OF HUMAN CORTICAL BONE AT THE LAMELLAR LEVEL**
ENM.5	Sebastian **Kratz** E163 - Institute of Applied Synthetic Chemistry **RAPID PROTOTYPING, MANUFACTURING AND APPLICATION OF ORGAN-ON-A-CHIP AND CELL BASED LAB-ON-A-CHIP SYSTEMS**
ENM.6	Jie **Sun** CEST Centre of Electrochemical Surface Technology, Wr. Neustadt, Austria **SURFACE MODIFICATION OF Ti-BASED MATERIALS FOR BIOMEDICAL APPLICATION**
ENM.7	Malte **Hartmann** E308 - Institute of Materials Science and Technology **LITHOGRAPHY-BASED CERAMIC MANUFACTURING IN DIGITAL DENTISTRY**
ENM.8	Babak **Dabiri Razlighi** E354 - Institute of Electrodynamics, Microwave and Circuit Engineering **SIMULATION OF THE CARDIOVASCULAR AND AUTONOMIC NERVOUS SYSTEM FOR OPTIMIZATION OF AURICULAR VAGUS NERVE STIMULATION**
ENM.9	Andreas **Fellner** E101 - Institute of Analysis and Scientific Computing **NEURAL SIGNALLING MODELLED WITH FINITE ELEMENT METHOD**
ENM.10	Sogand **Sajedi** E101 - Institute of Analysis and Scientific Computing **COCHLEAR IMPLANTS FOR CAT AND MAN & WHAT WE LEARN FROM A MODELING STUDY**
ENM.11	Joschka **Hellmeier** E134 - Institute for Applied Physics **DNA ORIGAMI AS A NANOSCALE PLATFORM FOR T-CELL ACTIVATION**

ENM.12	Veronika **Pfannenstill** École Polytechnique Fédérale de Lausanne (EPFL), Lausanne, Switzerland **DETECTOR DEVELOPMENT FOR NANOMOTION BASED MONITORING OF CELL STATES**
ENM.13	Ruth **Leskovar** E101 - Institute of Analysis and Scientific Computing **A DYNAMIC CAUSAL SYSTEM SIMULATION APPROACH FOR ANATOMIC JOINTS**

Introduction by Andreas Körner and Florian Libisch	
FUR.1	Manuel **Ederer** E136 - Institute of Theoretical Physics **MULTIPHOTON DOUBLE IONIZATION OF HELIUM**
FUR.2	Christian **Schmidrathner** E325 - Institute of Mechanics and Mechatronics **BUCKLING OF A CLAMPED-CLAMPED BEAM DUE TO INITIAL CURVATURE**
FUR.3	Thomas **Fabian** E136 - Institute for Theoretical Physics **EDGE FREE GRAPHENE NANOSYSTEMS**
FUR.4	Claudio **Navacchi** E120 - Department of Geodesy and Geoinformation **MONITORING OF ALPINE SNOW CONDITIONS USING C-BAND SAR**
FUR.5	Thaddäa **Rath** E308 – Institute of Materials Science and Technology **DEVELOPING A NEW SUBSTITUTE FOR IVORY USING LITHOGRAPHY BASED ADDITIVE MANUFACTURING**
FUR.6	Benjamin **Klebel** E138 - Institute of Solid State Physics **ELECTRONIC TRANSPORT MEASUREMENTS UNDER UNIAXIAL PRESSURE IN CUPRATE SUPERCONDUCTORS**
FUR.7	Alexander **Fuss** E141 - Atomic and Subatomic Physics **BACKGROUND SIMULATION STUDIES FOR THE CRESST AND COSINUS DIRECT DETECTION DARK MATTER EXPERIMENTS**
FUR.8	Dmitry **Ponomarev** E101 - Institute of Analysis and Scientific Computing **INVERSE MAGNETISATION PROBLEM FOR THE ANCIENT ROCKS: A FRUITFUL ENCOUNTER OF HARMONIC ANALYSIS AND PALEOMAGNETISM**
FUR.9	Hoai Maria **Nguyen Thu** E308 - Institute of Material Science and Technology **REPROCESSING OF HIGH DENSITY POLYETHYLENE**
FUR.10	Marianna **Kharlamova** E165 - Institute of Materials Chemistry **FILLING OF SINGLE-WALLED CARBON NANOTUBES WITH LEAD HALOGENIDES**
FUR.11	Katarina **Kumpf** Center for Electrochemical Surface Technology, Tulln/Donau, Austria **STUDY OF INTERACTIONS OF CHEMIRESISTORS ARRAYS TOWARDS VOCs**

FUR.12	Teresa **Liberto** E207 - Institute of Material Technology, Building Physics, and Building Ecology **CONTROLLING THE ELASTICITY OF CALCITE SUSPENSIONS WITH SIMPLE IONS**
FUR.13	Bernadette **Kirchsteiger** E164 – Institute of Chemical Technologies and Analytics **SEMI-VOLATILE ORGANIC TRACE QUANTIFICATION OF EMISSION SAMPLES WITH PTR-TOF-MS**
FUR.14	Latifeh **Nasseri** E308 - Institute of Material Science and Technology **THERMAL AND FRICTIONAL AGING IN TRIBOLOGY - STATUS ANALYSIS OF ENGINEERING AND HIGH-PERFORMANCE THERMOPLASTICS**
FUR.15	Ayse Nur **Koyun** E165 - Institute of Material Chemistry **BITUMEN AGEING AND ITS EFFECT ON THE SURFACE MICROSTRUCTURES**
FUR.16	Niusha **Lasemi** E165 - Institute of Materials Chemistry **LASER ASSISTED SYNTHESIS OF GRAPHITE ENCAPSULATED ALLOY NANOPARTICLES FOR ENERGY CONVERSION APPLICATIONS**
FUR.17	Stefan **Krimmel** E302 - Institute for Energy Systems and Thermodynamic **PERFORMANCE CHARACTERIZATION OF A TECHNOLOGY FOR THERMAL ENERGY STORAGES**
FUR.18	Elżbieta **Jószczuk** AGH University of Science and Technology, Kraków, Poland **THE USE OF FLY ASH FOR THE SYNTHESIS OF INSULATING MATERIALS**
FUR.19	Agata **Popiela** AGH University of Science and Technology, Kraków, Poland **THE USE OF THE HYDROTHERMAL METHOD FOR SORBENTS SYNTHESIS**
FUR.20	Ibuki **Kobayashi** Tokyo University of Science, Tokyo, Japan **SYNTHESIS OF NOVEL ALLOY CLUSTERS USING LIGAND EXCHANGE REACTION**
FUR.21	Christoph **Fuger** E308 - Institute of Materials Science and Technology **INFLUENCE OF TANTALUM ON THE PHASE STABILITY AND MECHANICAL PROPERTIES OF WB_2 THIN FILMS**
FUR.22	Hana **Šimonová** E207 – Institute of Material Technology, Building Physics and Building Ecology **FRACTURE PARAMETERS OF ALKALI-ACTIVATED MATRIX BASED COMPOSITES**

FUR.23	Agnieszka **Kuźmik** AGH University of Science and Technology, Kraków, Poland **MODIFICATION OF THE LABORATORY EQUIPMENT USED TO ASSESS THE SPONTANEOUS COMBUSTION SUSCEPTIBILITY OF COAL**
FUR.24	Stefanie **Winkler** E101 - Institute of Analysis and Scientific Computing **COMPARISON OF DATA MODELLING POSSIBILITIES IN HYBRID MODELS**
FUR.25	Thomas **Glechner** E308 - Institute of Materials Science and Technology **TUNING STRUCTURE AND MECHANICAL PROPERTIES OF Ta-C COATINGS BY N-ALLOYING AND VACANCY POPULATION**
FUR.26	Lisa **Mayerhuber** CEST Centre of Electrochemical Surface Technology, Wr. Neustadt, Austria **NEW TOOLS FOR THE ON-SITE DETECTION OF WATER POLLUTANTS: ION-SELECTIVE ELECTRODES AND LATERAL FLOW DEVICES**
FUR.27	Richard **Mócsa** CEST Centre of Electrochemical Surface Technology, Wr. Neustadt, Austria **DEVELOPMENT OF A NOVEL OPTOELECTRONIC SENSOR PLATFORM**
FUR.28	Markus **Ostermann** E164 - Institute of Chemical Technologies and Analytics **PRODUCTION OF VERY FINE GRAINED TUNGSTEN CARBIDE POWDERS BY THE $WO_2(OH)2$ TRANSPORT REACTION**
FUR.29	Anh Dung **Tran** E163 - Institute of Applied Synthetic Chemistry **RADICAL INDUCED CATIONIC FRONTAL POLYMERIZATION OF EPOXY SYSTEM**
FUR.30	Elisabeth **Rauchenwald** E164 - Institute of Chemical Technologies and Analytics **CHARACTERISATION OF NANOSTRUCTURED HARD COATINGS PRODUCED BY CHEMICAL VAPOUR DEPOSITION**
FUR.31	Stephan **Sponar** E141 - Atomic and Subatomic Physics **EXPERIMENTAL STUDIES OF MEASUREMENT UNCERTAINTY RELATIONS STUDIED IN NEUTRON OPTICS**
FUR.32	Amphai **Wejwithan** E230 - Institute of Transportation **RESPONSIBLE TOURISM TO CLIMATE CHANGE: A SYSTEM APPROACH FOR ALTERNATIVE SUSTAINABLE TRANSPORT**
FUR.33	Matthias **Lanzinger** E192 - Institute of Logic and Computation **FIXED-PARAMETER TRACTABLE FRAGMENTS OF CONJUNCTIVE QUERIES AND CONSTRAINT SATISFACTION PROBLEMS**

FUR.34 Bonny **Dongre**

E165 - Institute of Materials Chemistry

POINT DEFECT PHONON SCATTERING: FUNDAMENTALS AND IMPORTANCE

Lions Award 2019	
LION.1	M. Josef **Taublaender** E163 - Institute of Applied Synthetic Chemistry **ORGANIC HIGH-PERFORMANCE MATERIALS VIA HYDROTHERMAL SYNTHESIS**
LION.2	Thomas **Bruckmüller** E315 - Institut für Fahrzeugantriebe und Automobiltechnik **LADEINFRASTRUKTUR FÜR ELEKTROFAHRZEUGE: BEDARF, KOSTEN UND AUSWIRKUNGEN AUF DIE ENERGIEVERSORGUNG IN ÖSTERREICH BIS 2030**

Research Field *Architecture & Urban Planning*

Chairs and Reviewers:

Giffinger, Rudolf
Univ.Prof. Mag.rer.nat. Dr.techn.

E280 - Institute of Spatial Planning
rudolf.giffinger@tuwien.ac.at

Fadai, Alireza
Associate Prof. Dipl.-Ing. Dr.techn.

E259 - Institute of Architectural Sciences
alireza.fadai@tuwien.ac.at

Introduction

Cities are facing complex challenges in front of globalization, climate change and urbanization processes. Cities should increase the capacities of infrastructures, reduce energy consumption and restrict emissions implementing corresponding new technologies. Especially urban agglomerations have above-average volume of building construction, due to population growth but also due to the constant changes in life form (e.g. increasing single-person households) and changes in the social structure of the public sector (education, health) and in private sector (relocation of industries, reclassification of traffic areas, changes in trade - shopping centers in urban versus retail in urban ground floor zones).

The corresponding discussion of 'Smart City' reflects these technical needs but in a rather heterogonous understanding – technical against citizen centered. However, Smart City initiatives are fostering and implementing innovations. In particular, ICT and web 2.0 are offering new possibilities of technology driven developments in the different domains of urban development: economy, mobility, housing, environment, but also in domains of governance and participation.

For instance, construction industry is expected to obtain a higher level of resource efficiency and improved environmental performance through the use of improved raw materials and processing techniques. At the same time, the buildings' functional requirements have also changed dramatically. Thus, research aims at the development of resource-efficient construction typologies considering most relevant properties and characteristics of buildings and their materialization.

Today, there is a wide range of strategies, activities in planning, architecture, and construction as well as research regarding the implementation of projects impacting energy efficiency, quality of urbanistic structures or participatory decision finding, and decision making. However, empirical evidence in different activities or, in general, on urban development still shows problematic trends in terms of energy consumption, emissions, mobility structures or social polarization due to the excluding power or the non-expected impacts of new technologies. Hence, research in Architecture and Urban Development Planning on the 'urban fabric' and its meaning for sustainable development in terms of economic performance, social inclusion, and design and construction quality and on environmental impacts is urgently demanded.

This track of the symposium covers therefore research performed at TU Wien that is predominantly focusing on questions of urban innovations impacting sustainable development. Thus, contributions are welcome with focus on urban innovations and their meaning for sustainable development coming from the areas of Architecture, Urban and Regional or Landscape Planning, Engineering, Energy, Social Sciences, as well as from Computational Science.

ARCHITECTING DEPENDABLE CYBER-PHYSICAL SPACES

Christos Tsigkanos

E194 – Institute of Information Systems Engineering, TU Wien, Austria

We increasingly live in cyber-physical spaces – spaces that are both physical and computational, and where the two aspects are intertwined. Such spaces are software-intensive systems, as computational elements heavily interact with physical entities [1], especially with internet-of-things devices and along active human agents, where the physical space determines many of such interactions. This can be witnessed in a variety of settings, ranging from smart infrastructures based on sensors deployed on cities to visionary multi-functional living spaces that can be spatially re-organized in a dynamic way.

Cyber-physical spaces are much more dynamic than traditional –physical– spatial environments used to be. Humans, robots or devices moving around connected to networks are examples of entities dynamically performing actions while operating in a composite space. Such dynamics have to be considered in the design of systems operating within spatial environments, as certain dependability guarantees about their behaviour should be fulfilled [2]. Moreover, as for any other software-intensive system, maintaining a cyber-physical space which "operates" in a dynamic environment is faced with the manifold challenges that a self-adaptive system brings and demands for operational management to observe a constantly changing space and potentially react to environmental changes [7].

The current practice of designing space-intensive systems is weak in facing these emerging challenges, which appear in numerous contemporary applications. For example,

- How can a smart hospital be designed such that response of medical personnel is guaranteed [3]? In case of an emergency, after medical personnel are notified (i.e. through networked mobile devices), they should physically reach a location within a certain time.
- How can quality-of-service be maximized by a smart bike-sharing system in a smart city [4]? Utilization of bikes differs on time of day, location, riders' behaviour and exogenous events.
- How can assurances be obtained about a swarm of unmanned aerial vehicles providing autonomously emergency response in a city within a disaster scenario [2]? Challenges arise when non-human agents need to coordinate within an urban disaster setting – including limited connectivity, uncertainty and a constantly changing physical space.

In such challenging scenarios, the boundary between the physical and the computational aspects gets increasingly blurry. Design of systems operating within physical spaces is largely disconnected from the computational components enabling smart functionalities, a great concern especially in safety-critical applications dominated by mobile connectivity, active agents and complex dynamic behavior. As a consequence, dynamic space-dependent systems cannot be automatically – and formally – analyzed with respect to various qualitative or quantitative requirements. Moreover, runtime support to recognize and manage dynamic spatial changes in space, essentially some form of automated operational management based on systematic model-driven engineering, is largely missing.

An Emerging Research Agenda. This talk will show an avenue for research which can be characterized as rethinking cyber-physical spatial environments from a software engineering perspective. Specifically, we advocate that bridging architecture and urban planning with software systems engineering has significant potential for future living and urban spaces which should be dependable. Spatial environments are increasingly dynamic cyber-physical spaces, where the physical world and the computational world are heavily interwined and interacting with each other. Obtaining assurances of satisfaction of requirements concerning e.g., security [5], reliability [3] or safety [2] etc. becomes challenging, something which has to be considered during both design and operation.

In a walk through exemplar problems which have been tackled in the past [2, 3, 6], we will observe how CityGML or BIM descriptions can give rise to models amenable to automated analyses of dynamic behaviours on spaces populated with humans, robots, or mobile devices. Analysis amounts to assessing if some collective behaviour that is highly space-dependent, violates certain requirements that the overall system should exhibit. Requirements may state some behaviour that is about position of mobile entities in space, actions or state of internet-of-things devices, or roaming human agents.

Early results from experiments conducted based on prototypical implementations will be illustrated, showing potential benefits of our vision of supporting architects and system designers in the challenging task of reasoning on dynamic cyber-physical spaces adopting software engineering principles. This can be considered as a second happy marriage of two disciplines which, although apparently being far apart from each other, share a considerable amount of challenges and body of knowledge.

REFERENCES

[1] Christos Tsigkanos, Timo Kehrer, and Carlo Ghezzi. Architecting dynamic cyber-physical spaces. *Computing*, 98(10):1011–1040, 2016.

[2] Christos Tsigkanos, Timo Kehrer, and Carlo Ghezzi. Modeling and verification of evolving cyber-physical spaces. In *ACM SIGSOFT Symposium on the Foundations of Software Engineering*, pages 38–48, 2017.

[3] Christos Tsigkanos, Timo Kehrer, Carlo Ghezzi, Liliana Pasquale, and Bashar Nuseibeh. Adding static and dynamic semantics to building information models. In *Proceedings of SEsCPS@ICSE16*, pages 1–7. ACM, 2016.

[4] Vincenzo Ciancia, Diego Latella, Mieke Massink, and Rytis Pakauskas. Exploring spatio-temporal properties of bike-sharing systems. In *IEEE International Conference on Self-Adaptive and Self-Organizing Systems Workshops (SASOW)*, pages 74–79. IEEE, 2015.

[5] Christos Tsigkanos, Liliana Pasquale, Claudio Menghi, Carlo Ghezzi, and Bashar Nuseibeh. Engineering Topology Aware Adaptive Security: Preventing Requirements Violations at Runtime. In *Proc. of the 22nd IEEE International Requirements Engineering Conference*, 2014.

[6] Christos Tsigkanos, Nianyu Li, Zhi Jin, Zhenjiang Hu, and Carlo Ghezzi. On early statistical requirements validation of cyber-physical space systems. In *Proceedings of SEsCPS@ICSE18*, pages 13–18. ACM, 2018.

[7] Christos Tsigkanos, Liliana Pasquale, Carlo Ghezzi, and Bashar Nuseibeh. On the interplay between cyber and physical spaces for adaptive security. *IEEE Transactions on Dependable and Secure Computing*, 15(3):466–480, 2018.

SPATIAL AND TEMPORAL MODELLING OF VIENNA'S BUILDING STOCK IN RESPECT TO ITS POTENTIAL AS A SECONDARY RESOURCE MINE

Ferdinand Reimer

E226 Institute for Water Quality and Resource Management, Technische Universität Wien, Vienna

INTRODUCTION

The European Union strives to boost the recycling and reuse of construction materials in the building sector. Materials of interest are, among others, concrete, gypsum and glass as well as various wood products, and metals.

To assess the material quantities in the urban building park and subsequently examine the material recoverability, different modelling approaches were applied in case studies all around the globe. These approaches vary in the types of materials they focus on, in the respective methodology and tools used, and in the quality and quantity of the underlying data.

Based on the experience from other studies, I am developing a new modelling approach and test it for the city of Vienna. The goal is to assess the volume and material composition of the building stock in terms of historical trends, the present situation, and furthermore, as a future projection of how the building stock will likely develop.

MODEL DATA AND DESIGN

I have developed a model prototype and limited the spatial system boundaries around the 18th city district. Several different sources of data for this district are available. For historical data, there is a city map from 1920 [1] in vector graphics format, a building directory from 1928 [2], which is an index of all buildings present at that point of time listing several properties for every building, and furthermore, a historical map of the building age in 1920 [3] for every building.

The combination of these data sources allows for each building the reconstruction of the building age and dimensions in the past. While the buildings' area is relatively certain due to a proportionally adequate map, the respective heights and volumes of these historical buildings are subject to qualified estimates.

In a subsequent step, also the material composition of the historical buildings has to be determined via the use of building archetypes that define characteristic materials used due to a buildings' construction period and its primary type of use.

For the examination of the historical changes in time of the building stock there are contemporary data available from the cities open government data platform [4]. The comparison of the buildings between 1920 with 2018 allows the tracing of construction and demolition activities over the last 100 years.

After the 1920 and 2018 situation of the building stock has been sufficiently covered, a system dynamics approach is designed to make use of the previous analysis and give an outlook to estimate expected future urban development, incorporating various chosen socio-economic and technical factors of influence to simulate their potential impact on the process of construction and demolition cycles.

RESULTS AND DISCUSSION

Preliminary results on the development of the buildings stock are given in Figure 1. The map shows which buildings have been constructed before 1920 and are still present, which buildings have been demolished and re-build and which have been built on previously open property grounds.

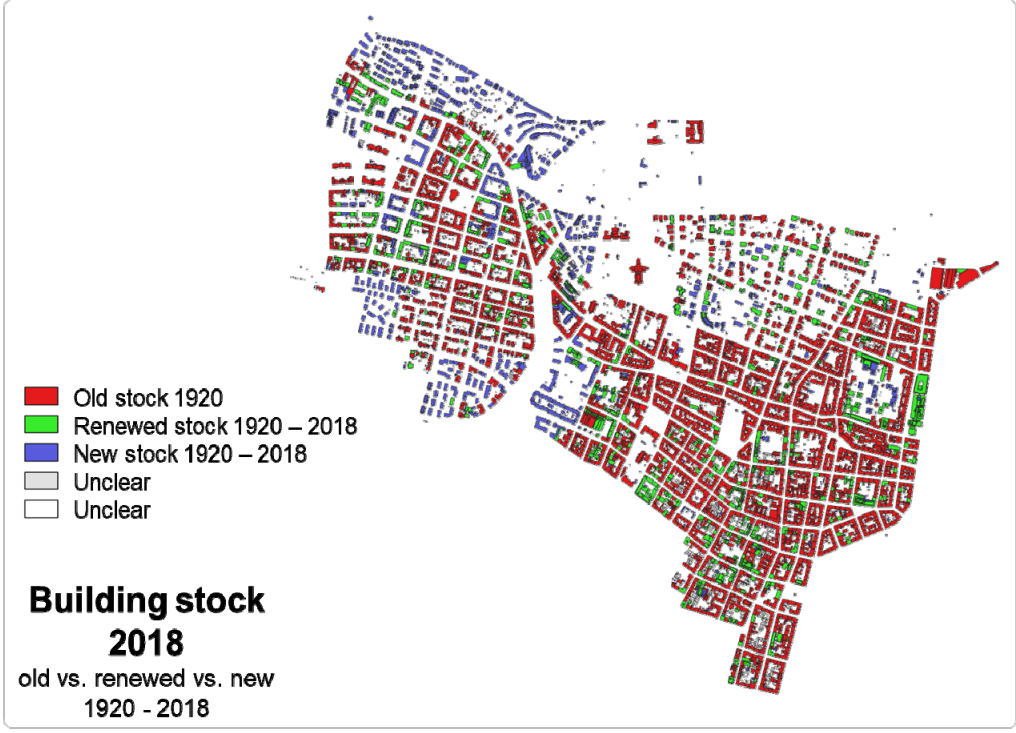

Figure 1: Inter-temporal comparison of buildings between 1920 and 2018, with resulting information about changes of the building stock in time

I have learned that the building stock models are mostly constrained by the availability of data. Furthermore, it is very important to give a qualified statement about the reliability of data, as in some cases it is merely possible to produce estimates. In other cases, it becomes clear that data are very reliable. One example is the 1920 city map [1], where the area and shape of the buildings in the map still fits perfectly well to the same building still existing in modern maps.

CONCLUSION

The compilation of historical and contemporary data is a viable option to model urban changes in time. The precision and reliability of the results depends on the available datasets and in turn, the question whether a dataset is adequate depends on the intended use of the resulting model.

To evaluate the quality of different modelling approaches and develop a coherent framework for the modelling of the urban building stock, increased efforts for the cross-examination of different studies and their methods is recommended.

REFERENCES

[1] Wiener Stadt- und Landesarchiv, *Grundlagenkarte des 18. Wiener Gemeindebezirkes für den Zeitpunkt um 1920*. Bereitgestellt von F. Hauer am Mittwoch, den 23. August 2017.
[2] Salzberg, J.W., *Häuser-Kataster der Bundeshauptstadt Wien (1927-1929). Band 9: 18. und 19. Bezirk*. 1928: Wien.
[3] Wiener Stadt- und Landesarchiv, *Historischer Atlas von Wien (17. Lieferung). Baualter 1920, 1. bis 20. Bezirk*. 2015
[4] Wiener Magistratsabteilung 41, Flächen-Mehrzweckkarte. Abrufen von https ://www.data.gv.at/katalog/dataset/stadt-wien_flchenmehrzweckkartevektordatenwien am 3. März 2018.

METHOD COMPARISON OF OVERHEATING EVALUATION VIA NORMATIVE CALCULATION AND NUMERIC SIMULATION

Klaus Sperka[a], Ulrich Pont[b,*], Ardeshir Mahdavi[b]

[a]Graduate Student of Building Science and Technology, TU Wien, Vienna, Austria
[b] E259.3 (Dept. of Building Physics and Building Ecology)

INTRODUCTION

The avoidance or at least mitigation of summer overheating is a topic that constantly gains importance within the AEC-community (Architecture-Engineering-Construction) in recent years. This is, on the one hand, due to the climate-change-induced increase of hot periods in summer time, and, on the other hand, caused by microclimatic implications in the urban surroundings, known as the Urban Heat Island effect. Currently different methods of assessment of building designs toward summer overheating tendency are available: (i) Normative methods of different degree of complexity for instance based on the Austrian standards [1]. These methods regularly are used for certification that a certain building design or retrofit project is to a certain degree safe against severe summer overheating. Such certifications are required for different purposes, e.g. for getting a subsidy grant or receiving a building permit; (ii) sophisticated simulation-based methods that consider a wide range of input data and allow for close to any enquiry being worked upon. In comparison to the normative methods, such methods require a higher resolution of input data regarding climate data, occupant behaviour, and physical characteristics of the surround building components. Both methods are widely in use, but deliver results in different resolutions. Due to the different output data characteristics, planners often struggle to understand if certain results from simulation can be mapped onto the normative performance indicators and vice versa. Moreover, aspects that need to be considered in recent times – such as changing boundary conditions due to climate change and increased impact of the Urban Heat Island effect – cannot or only to very limited extent integrated in the normative approaches. Needless to say, this is suboptimal and needs to be addressed in close future as the normative procedure is one decision criteria for or against a granted building permit. In this contribution we illustrate our efforts pertaining to comparing and mapping results of the normative approach and the simulation-based assessment on a set of case study building designs (roof top extensions of an existing *Gründerzeit* building in Vienna). The present study is in its preliminary phase, thus we can only provide an outlook onto expected results.

METHODOLOGY

Case study buildings: For this study, a set of different designs for a rooftop extension of an existing Viennese *Gründerzeit* building have been chosen as case study. This is due to the increased summer overheating risk connected with this specific design task (large envelope area in comparison to occupied volume, often direct exposure to sunlight, limited possibility to integrate thermal mass compartments into the design). Figure 1 illustrates some of the roof top extension designs.

Figure 1: Some of the rooftop extension designs

Utilized summer overheating evaluation methods: The normative evaluation utilized in this study is based on the Austrian Standard B8110-3 [1]. In this standard both a simplified and a more detailed version are encompassed. The standard provides as results in both simplified and detailed approach operative temperatures for a virtual summer day (15th of July), which is assumed to be part of a heat period. The average operative temperature during day time and night time is then expressed in quality classes (A+ to D). The method can only be applied to single rooms, not to a set of rooms or an overall building. The numeric methodology utilizes the software EnergyPlus [2]. A wide range of output data can be generated in this tool, ranging from different temperature outputs (radiative temperatures, air temperatures, operative temperature) to heat flux through components to cooling demand calculations. Moreover, the simulation not only can be applied to single rooms, but also to a set of zones that together can form up to a whole building. Needless to say, the numeric simulation requires a more detailed set of input data encompassing hourly weather data including solar radiation data, detailed information about the physical properties of the building envelope, and – maybe most difficult to set – detailed occupancy data (including operation of windows, ventilation behaviour, presence, use of appliances and gadgets in different zones, etc.). Previous studies and works will be employed to setup the required input data in a convenient fashion [3][4].

WORKPLAN, COMPARISON CONCEPT AND EXPECTED RESULTS

In a first step, the different roof top extension designs will be evaluated, and the most critical spaces in each design will be identified. These spaces will be used for the normative procedure, and also be set as a zone in the numeric simulation. Subsequently, a comparison of the required input data and their overlap and differences will be conducted. Based on this information, a reasoning of result differences in later stages can be performed, as well as a sensitivity analysis. In a further step, all of the rooftop design variations will be subjected to both simulation and normative evaluation. Thereby, the resulting Key Performance Indicators will be analysed on potential comparison mechanisms. Besides direct mapping, alternative concepts, such as linear regression analysis or ranking-based comparison methods (compare [5]) will be evaluated as potential instruments for comparison. In subsequent steps, both the building design properties (for instance thermal mass) and the boundary conditions (e.g. integrating different climate change scenarios, or considering the urban heat island effect) will be varied, so that a sensitivity analysis can be performed. A major objective of the overall work is to find conclusions, whether and to which extent both simulation (which is considered to be “closer” to reality) and normative calculations provide sufficient planning support regarding summer overheating mitigation (or in best cases avoidance) assessment.

REFERENCES

[1] ÖNORM B 8110-3: Wärmeschutz im Hochbau Teil 3: Vermeidung sommerlicher Überwärmung; Ausgabe: 2012-03-15; Austrian Standards Institute/Österreichisches Normungsinstitut (ON)

[2] Department of Energy: EnergyPlus; https://energyplus.net/

[3] A. Wurm, U. Pont, F. Tahmasebi, A. Mahdavi: Overheating risk in buildings: A case study of the impact of alternative construction solutions and operational regimes; in: (Printed) Proceedings of CESB 2016: Central Europe towards sustainable building 2016 - innovations for sustrainable future, P. Hàjek, J. Tywoniak, A. Lupisek (ed.); Prague, Czech Republic (2016), ISBN: 9788027102488; Paper ID 1319 (p.1325-1332), 8 pages.

[4] W. Pereira, A. Bögl, T. Natschläger: Sensitivity analysis and validation of an EnergyPlus model of a house in Upper Austria, Energy Procedia 62 (2014) 472 – 481

[5] U. Pont, A. Mahdavi: Evaluation of Prescriptive Indicators for Building Performance - A Ranking Based Approach; Applied Mechanics and Materials, 12th Envibuild - Buildings and Environment - From Research to Application Proceedings of the 12th International EnviBUILD Conference (7th & 8th September 2017) (2019), 887; 172 - 180.

URBAN GROWTH PREDICTIONS WITH DEEP LEARNING AND GEOSEMANTICS

Marvin Mc Cutchan, Simge Özdal Oktay , Ioannis Giannopoulos

E120 - Department of Geodesy and Geoinformation

INTRODUCTION

This work outlines a novel approach for the prediction of urban growth. The method extracts semantic information of geospatial data and predicts if urban and non-urban areas are going to change in the future, using a deep neural network. The scored prediction accuracy is higher than any other urban growth prediction model. This superiority is based on two novelties: (1) The effective modeling of the geospatial configurations using semantics, (2) the use of deep learning. The proposed method is therefore an effective tool to predict one of the global challenges of urban sprawl and support the future development strategies.

EXPERIMENTS/FUNDAMENTAL OF THE PROBLEM/EXAMINATIONS

Spatial predictions are identified as one of the key aspects of Digital Earth [1]. Accordingly, spatio-temporal predictions, such as urban growth and land cover change, provide an effective tool for minimizing urban sprawl, which is a complex phenomenon that has severe environmental, social, and economical consequences. Taking the necessary measures against these negative consequences requires sound urban development strategies [2, 3]. Predictions of dynamic urban patterns have an essential role in providing optimal solutions for impact assessment of alternative scenarios and planning policies [4]. However, analysis and interpretation of these temporal, irregular urban patterns require innovative approaches.

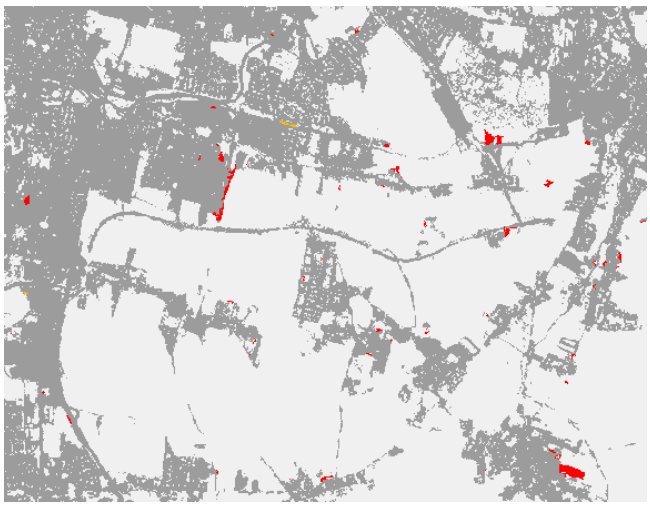

Figure 1: Urban (dark grey) and non-urban (light grey) areas.Red areas indicate areas which changed from non-urban to urban.

The proposed methodology starts by obtaining linked data from LinkedGeoData for 2012. This data is semantically annotated vector data. The semantic information expresses the type of an geo-object such as restaurant, path, bus station as well as its geometry. OWL classes in an OWL ontology describe this semantics. The geometry can be a linestring, a point or a polygon. Afterwards, data on the imperviousness change from 2012 to 2015 is obtained from Copernicus. This data describes which non-urban areas have changed to urban areas , vice versa, as well as did not change. Thus, there are 4 different classes: (1) Urban to non-urban, (2) non-urban to urban, (3) urban no change and (4) non-urban no change. The propsed method ultimately enables to predict these changes for 2015 by utilizing the data from LinkedGeoData. For this purpose the methods transforms the obtained linked data into feature vectors. Each feature describes the spatial constellation of geo-objects of different OWL classes to a specific location. Every feature vector is than labeled with one of the four urban change classes for the corresponding location. Subsequently a deep neural

network is trained and tested with these feature vectors in a 10 fold cross validation manner. Approximately 50.000 samples were used for that purpose. Finally a confusion matrix is generated in order to assess the accuracy of the predictions.

RESULTS AND DISCUSSION

The overall accuracy of the presented urban growth prediction is 87.7%. The kappa coefficient is 0.81. The results not only proof the feasibility of the method but as well as its superiority compared to other urban growth prediction models. Additionally, it demonstrates that a task such as urban growth prediction which commonly is based on remotely sensed imagery, can instead rely on geospatial semantics and therefore reveal its potential for this type of task. Furthermore deep learning has been identified as a promising tool machine learning algorithm for spatial predictions.

CONCLUSION

The presented method enables to predict the growth of urban areas and therefore provides a vital tool to control urban sprawl and support a sustainable development of cities. Additionally it provides an approach which is capable to perform spatial prediction with geospatial semantics. Several potential future works can be identified: Such as the use of advanced sensory for extracting geospatial semantics of the environment in order to increase the prediction accuracy. Within that scope Augmented Reality could be used to derive a deeper understanding of the semantics of the environment and therefore provide better spatio-temporal predictions. Another fruitful topic is the data fusion with remotely sensed imagery in order to discriminate classes more efficiently. It has to be noted that the presented approach is generic. Thus, other phenomena than urban change can be subject to such a prediction, such as real estate price development or spatial density for crime.

REFERENCES

[1] M.F. Goodchild. The use cases of digital earth. International Journal of Digital Earth, 389 1(1):31–42, 2008. URL: https://doi.org/10.1080/17538940701782528, arXiv:https: 390 //doi.org/10.1080/17538940701782528, doi:10.1080/17538940701782528.

[2] Michael P Johnson. Environmental impacts of urban sprawl: A survey of the literature and 408 proposed research agenda. Environment and Planning A: Economy and Space, 33(4):717– 409 735, 2001. doi:10.1068/a3327.

[3] OECD. Rethinking Urban Sprawl. 2018. URL: https://www.oecd-ilibrary. 420 org/content/publication/9789264189881-en, doi:https://doi.org/https: 421 //doi.org/10.1787/9789264189881-en.

[4] Martin Herold, Noah C. Goldstein, and Keith C. Clarke. The spatiotemporal 395 form of urban growth: measurement, analysis and modeling. Remote Sensing 396 of Environment, 86(3):286 – 302, 2003. Urban Remote Sensing. URL: http: 397 //www.sciencedirect.com/science/article/pii/S0034425703000750, doi:https:// 398 doi.org/10.1016/S0034-4257(03)00075-0.

RETROFITTING POTENTIAL OF LARGE-SCALE PREFABRICATED BUILDINGS FROM PRE-"WENDE" TIMES: A CASE STUDY OF CROATIA

Matea Flegar[a], Ulrich Pont[b,*], Ardeshir Mahdavi[b]

[a]Graduate of the Msc-Programme Building Science and Technology, TU Wien, Vienna, Austria
[b]E259.3 – Department Building Physics and Building Ecology

INTRODUCTION

It is a widely known fact that buildings contribute largely to both worldwide GHG (green-house-gas) emissions and energy consumption. To change that, not only new buildings have to be designed following the principles of low- to zero-energy building, but also the building stock has to be addressed. In many European countries, an extensive stock of prefabricated buildings from pre-"Wende"-times (this means constructed prior to the fall of the Soviet Union) can be found, which particularly are of interest for large-scale retrofit measures. This is due to two major reasons: First of all, many of these prefabricated buildings were generated by industrial mass production of building components (e.g. wall-elements) and were several times combined in identical or rather similar fashion. Thus, retrofit measures can be designed in a feasible and easily applicable way, once the specific element has been subjected to a retrofit planning. The second reason is that such buildings often form the backbone of large residential communities, and as such cannot easily be replaced. Given the large extent of built volume and the poor thermal quality of such constructions, retrofit measures often seem to be more an urgent need than a luxury. This contribution focuses on a specific type of prefabricated houses in Croatia, known as building type JU-61, and on potential retrofit measures. The contribution is based on a recently written master thesis [1].

JU-61 (producer Jugomont) apartment blocks consist of modular units that form rooms with a floor plan size of 360 x 480 cm. To ensure the functional connections between the different units, a shift of connection walls by one third of the length or width of the system was considered. Figure 1 and 2 illustrate the building construction of a neighbourhood in Remetinečki gaj in (Novi-)Zagreb, and a typical two unit floor plan.

METHODOLOGY

A major challenge in retrofitting buildings is to balance the cost efficiency with the occupants' thermal comfort levels and the technical legislation constraints. In a first step, a sample building of the buildings in Remetinečki gaj was selected. This building can be considered as representative of typical JU-61 buldings in size, volume, number of residential units, as well as regarding damages and current state. Figure 3 illustrates this building. The building features 5 floors, a total height of 16.8 m, all together 35 residential units, and a total gross building area of 2675 m² (net ara 1814 m²). The building spans from south to north, thus it's major transparent components face east and west direction.

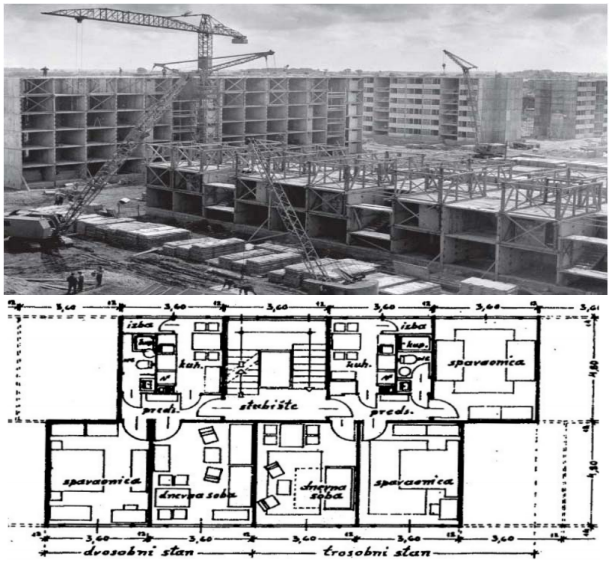

Figure 1 (top): Construction work in Remetinečki gaj in 1961 (private archive of architect Bogdan Budimirov)
Figure 2 (bottom): Typical Floor plan of JU-61

Figure 3: The case study building in today's shape.

Non-load-bearing opaque wall elements of the building are rear-ventilated panels, filled with a layer of mineral wool (4cm), an air gap, and – as a finishing – a corrugated metal plate. These metal panels provide inside why the buildings are also known as "tin-cans". Load-bearing elements are made of reinforced concrete (15cm), a thin insulation (4cm), and a similar corrugated metal plate. Today's condition of the building can be considered as bad. Beside from some private initiatives of individual occupants little to no maintenance work or refurbishment efforts have been undertaken in recent years. To assess the current energy performance and potential improvement scenarios, numeric simulation has been deployed, both on an overall building level [2], as well as on a thermal-bridge assessment scale [3]. Details regarding the input data assumptions and approximations made due to lack of data can be found in [1]. In addition to a base case scenarion that is based on today's condition, five different retrofit scenarios have been assessed. These encompass replacement of windows, increasing the insulation layers in the opaque elements, and the reconstruction of roof and floor constructions.

RESULTS AND DISCUSSION

For the base case, the simulation resulted in a heating demand of 136 $kWh.m^{-2}.a^{-1}$ and a cooling demand of 22 $kWh.m^{-2}.a^{-1}$. The different retrofit scenarios suggested heating demand reductions of 17 to 58% and cooling demand reductions of 5 to 33%. Regarding the amortization times of different retrofit scenarios, it can be said that all of the examined interventions pay off in between 12 and 17 years. In any of the suggested improvement scenarios, a careful detailing has to be conducted, given that the windows in their currently existing position do not show overlap/adjacencies with the insulation layers. This might become tricky in terms of thermal bridge / condensation risk aspects, if not considered properly.

CONCLUSION & FUTURE RESEARCH

The present study showed the potential of retrofit measures if applied to the "Tin Can" houses of Croatia (JU-61 prefabricated Jugomont residential builings). The saving potential is a considerable one, however, pay off times have to be considered carefully given the already long lifetime of these buildings. Furthermore, an ecological footprint comparison of the different retrofit scenarios still needs to be carried out.

REFERENCES

[1] M. Flegar: "Performance-based optimization potential of a widely used prefabricated building type: A case study of Zagreb"; Supervisor: A. Mahdavi, U. Pont; TU Wien2018; final examination: 2018-06-21.

[2] Department of Energy EnergyPlus, https://energyplus.net/

[3] AnTherm (www.antherm.eu)

THE SIGNIFICANCE AND PRESERVATION OF THE BUILDING TYPE "CASINO" IN THE VIENNESE BIEDERMEIER PERIOD EXEMPLIFIED ON THE STILL PRESERVED "CASINO ZÖGERNITZ"

Judith Mayr

E251 - Institute of History of Art, Building Archaeology and Restoration

INTRODUCTION

In the year 1837 Ferdinand Zögernitz opened a Casino, built in the Biedermeier-style, in Vienna´s former suburb Oberdöbling, today 19th district, with a performance by Johann Strauß Father. Thanks to the horse-drawn railway, which had its last stop at the Casino and the countless performances by well-known bandleaders, it developed into one of the most popular entertainment destinations of the Viennese. The building changed owners often and was subject of numerous renovations over time, but in contrast to the other dance and concert venues of the area, it still remains today. To preserve this jewel, it was put under monumental protection in 2008.

The content of the research is the firstly taken detailed analyzation of the building's history and historical use. Thanks to newly found records, it was possible to define and evaluate the numerous renovations of the object and enlarge the current knowledge regarding its history and also its connection to important historical individuals, buildings and events.

In addition, it was integrated in the building type „Casino"; it's importance for the city of Vienna was expressed for the first time and examined for its structural characteristics. Due to the lack of references regarding this field, similar examples were studied and analyzed.

A proposal for a preservation and revitalization concept that allows further use of the building in its original purpose, was worked out based on the analysis of the existing structure. Since structural alteration works have already begun before work on this research commenced, the occurred and future demolition works will be analyzed and evaluated in their accordance with the lawful treatment of protected historic monuments.

CONTEXT

Due to hunting trips of the emperor Karl VI. and his daughter Maria Theresia, the small and rural village of Oberdöbling established in the beginning of the 19th century, to one of the most popular places for weekend and summer holidays for the Viennese bourgeoisie. The ever-increasing influx affirmed the economic conditions and thus also the development of the popular inns, which led in a further step also to the establishment of the Casino Zögernitz.

From a temporal point of view, the year of construction of the Casino Zögernitz can be put in order in the Biedermeier era, where such venues reached their high point. This can be explained by the prevalent political situation and therefore increased entertainment culture. After the Congress of Vienna, emperor Franz I. and his foreign minister Prince Metternich used control, censorship and surveillance to regain the old regulations and therefore the population concentrated on nature, their families and homes and tried to distract themselves by celebrating. Restaurants were converted to dance-locations and more venues were newly built. An especially high increasement of such buildings, called "Casinos" or "Etablissements", can be found in the suburban villages, due to their proximity to nature and with it connected the romanticizing of the country life, which is characteristic for the philosophy of the era.

In general Casinos were normally used for enjoyment purposes and describe a combination of a restaurant, café and dance hall. They can be traced back to the Italian renaissance, where such buildings were also used for gambling games, besides the normal usage for social meetings. The "Casino Pio" in the Vatican Gardens can be regarded as the first example of this building type. Casinos reached Vienna first at the end of the 18th century where different kind of entertainments were offered to small prices, which increased the importance of such buildings for the social life.

THE CASINO ZÖGERNITZ - HISTORY

The Casino Zögernitz in particular got newly built in the years 1836 and 1837, by request of the already successful restaurant owner Ferdinand Zögernitz and his wife Theresia, who bought the plot of land in 1835 and opened it on 21st June 1837. The building at that time contained a Restaurant, a banquet hall, a café, dining rooms in the upper floor and generous gardens. It soon developed to one of the most popular venues of the Viennese. The constant changing requests of the audience and the zeitgeist required a lot of alterations at the building: Dining rooms were added and floors expanded. These circumstances increased, when the newly build horse-drawn railway in the 1870 brought the guests directly to the Casino.

Over the years Casinos lost their importance and plans were made to sell the Zögernitz. In 1903 the owners of the popular "Ottakringer Brauerei" bought the house and, together with their tenants Alfred and Maria Stegbauer, awoke the sleeping beauty with numerous renovations and extensions. 1919 the Stegbauers took over the building and brought the house in everyone's mind by using the garden for the construction of the first open-air cinema in Vienna. During the second world war the house was used for storage and afterwards converted to the "Manhattan´s Casino" by the US-Army. 1947 the family Stegbauer regained possession of the building and converted it into a Hotel, and the dance hall was mainly used as a recording studio.

2008 the building was put under monumental protection and bought by a private investor. He initiated the break-down of all of the over the years added building-parts, and plans are made to renovate the remaining structure. In addition, two apartment buildings are built in the garden at the moment, which led to demonstrations by the residents of Oberdöbling.

PRESERVATION AND REVITALIZATION CONCEPT

Here the questions on how to deal with an example of this building-type and how to preserve its characteristics raise themselves. Is it possible to maintain the object in its initial type of use in this modern day of age, and how can it be combined with the monumental protection? To prove it`s potential, a proposal for a preservation and revitalization concept was worked out, which can be also used as an introductory guide for other remaining examples of this building type. The concept founds itself on the definition of the building type, which clarifies the Casino as a social center for the surrounding inhabitants.

Nonetheless the way of entertainment changed over the years, the building could regain its importance as a cultural center and be open for the population for events but also for private purposes. Open and wide spaces with flexible room partitions could allow a flexible way of usage of the house with multiple options. The goal is to preserve the characteristics of this building type and to preserve it for later generations.

NUMERIC THERMAL BRIDGE SIMULATION IN WINDOW CONSTRUCTION ASSESSMENT: A CASE STUDY PERTAINING TO VACUUM-GLASS WINDOWS

Magdalena Wölzl[a], Ulrich Pont[a*], Peter Schober[b], Matthias Schuss[a], Ardeshir Mahdavi[a]

[a]E259.3 Dept. of Building Physics and Building Ecology, TU Wien
[b]Holzforschung Austria

INTRODUCTION & PROJECT DESIGN

This contribution is a work report on recent efforts in the field of computational assessment of contemporary, highly insulating window designs based on vacuum glazing. Thereby, recent developments of the third-party funded project FIVA (Fensterprototypen mit integriertem Vacuumglas – window prototypes with implemented vacuum glazing), follow-up of the successful MOTIVE and VIG-SYS-RENO projects (reported on in previous contributions at the VSS conference series), are discussed.

As already indicated in past publications [1][2], the availability of durable vacuum glass panels allow for the construction of new window constructions, which – if designed in an appropriate fashion - offer a similar thermal performance than conventional triple glazing windows, but featuring smaller system size, thickness, and weight. Based on the ideas developed in the MOTIVE project, the authors could assemble a research and development team together with stakeholders from renowned window construction companies (Internorm, Gaulhofer, Katzbeck, Svoboda, Wick) as well as with stakeholders of supportive technology suppliers (IeB Eisele, Maco). This R&D team is now (ongoing efforts from 2018 – 2020) investigating into progressing the ideas of MOTIVE into higher technology-readiness-levels toward new window constructions for the market that implement vacuum glazing. The project consists of several work packages addressing different aspects, such as fundamental construction principles, implementation of supportive technologies, acoustical performance, and thermal performance of different construction concepts. To successfully establish useful and operable window construction, an iterative ping-pong-process between the technical design work and virtual testing of the thermal performance via numeric thermal bridge simulation was implemented. The specifics of the simulation efforts of window constructions that integrate vacuum glass are illustrated in this contribution.

SIMULATION SETTINGS

The numeric simulation tool used to generally investigate into the thermal performance of the vacuum glazing – based window constructions was AnTherm [3], a finite point solving modelling and simulation tool. As in any other finite point/finite element tool a crucial element is the smallest cell size. As vacuum glass products regularly encompass a very small vacuum gap between two glass panes, the minimum cell size needs to be dimensioned based on the gap thickness. Thus the minimum cell dimension was set to 0.1 mm. In the currently happening simulation efforts, the simulations have been based on (extreme) steady state boundary conditions (20°C inside temperature, -10°C external temperature, and focus on 2D assessment. Both aspects will be changed (to

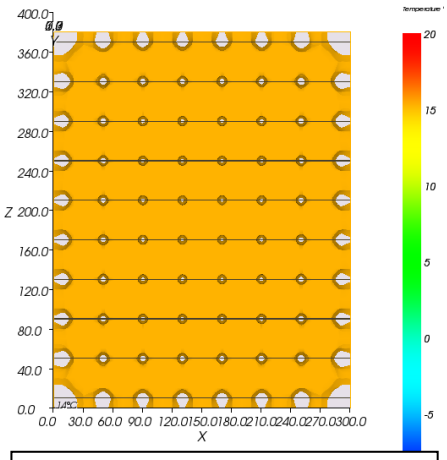

Figure 1: Temperature distribution on a vacuum glass pane (first published in [4])

transient and 3D-assessment), once major design decisions have been conducted regarding the different, currently developed window designs.

PRELIMINARY PREVIEW ON RESULTS

(i) Performance of typical vacuum glazing panes: Figure 1 shows simulation model and heat map on a typical vacuum glazing (including pillars and edge seal). The temperature differences between undistorted field and pillars are clearly visible, however in a negligible range (due to the very small dimension of the pillars in comparison to the overall window pane).

(ii) Result example (glazed versus wooden transom): As a sneak preview two transom designs (one consisting of a traditional wooden element, the other of two overlapping vacuum glass panels) are shown. Thereby, surface temperatures suggest that the by-far "lighter" appearance of the vacuum glazing element transom features a thermal performance that is comparable to the "bulky" wooden transom.

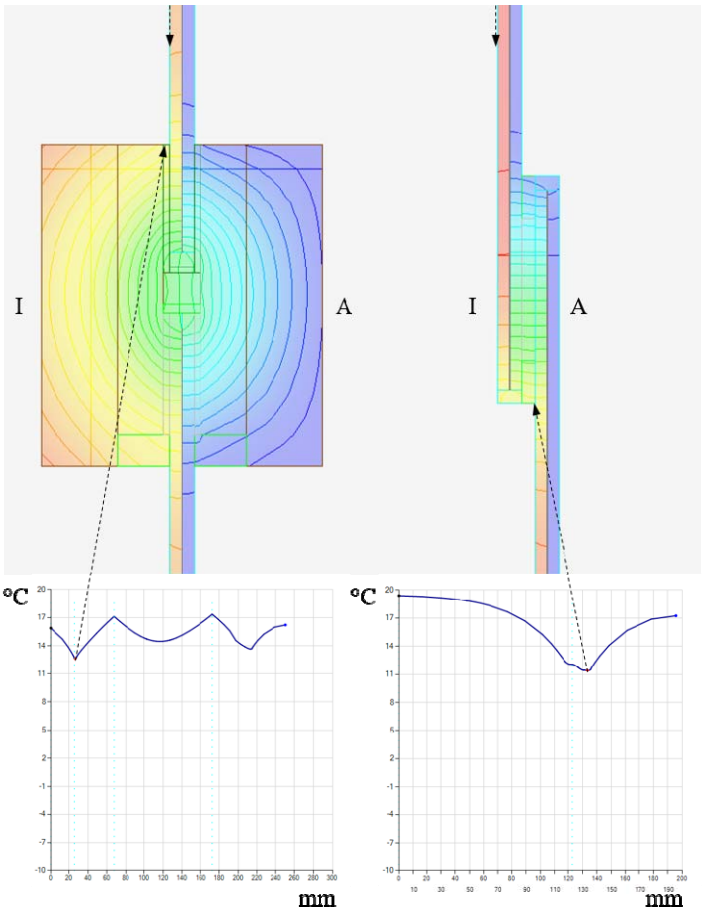

Figure 2: False-colour image and inside surface temperature distribution of two different transom designs (left: Wooden element, right: overlapping vacuum glazing panels)

CONCLUSION & ACKNOWLEDGEMENT

This extended abstract provided a glimpse on ongoing efforts pertaining to the thermal performance evaluation of novel vacuum-glass based window designs. Thereby, the principle performance of vacuum glass was illustrated, as well as a small case study pertaining to the performance of transom elements. The presented research efforts were in part funded by the Austrian Research Promotion Agency (FFG, project FIVA, project number: 867352).

REFERENCES

[1] O. Proskurnina, U. Pont, M. Schuss, E. Heiduk, P. Schober, A. Mahdavi: "A computational inquiry into the application of vacuum glazing in building retrofit"; in: "Proceedings of Vienna Young Scientists Symposium 2016", B. Ullmann et al. (Ed.); (2016), ISBN: 978-3-9504017-2-1; S. 26 - 27.

[2] U. Pont, P. Schober, M. Schuss, A. Mahdavi: "Exploring the technical requirements of vacuum glazing for contemporary window constructions";; in: "VSS - Venna young scientists symposium", P. Hans, G. Artner, J. Grames, H. Krebs, H. Mansouri Khosravi, T. Rouhi (Ed.); Book-of-Abstracts, (2018), ISBN: 978-3-9504017-8-3; S. 80 - 81.

[3] AnTherm – Numeric thermal simulation environment (www.antherm.eu)

[4] U. Pont, A. Mahdavi: "A comparison of the performance of two- and three-dimensional thermal bridge assessment for typical construction joints"; in: "Building Simulation Applications Proceedings", M Baratieri, V. Corrado, A. Gasparella, F. Patuzzi (Hrg.); bu.press (publisher of the Free University of Bozen-Bolzano), 3. (2017), ISSN: 2531-6702; Paper-Nr. 75, 8 P.

DEPLOYING GRIDSHELLS MADE EASY

Stefan Pillwein

E104 - Institute of Discrete Mathematics and Geometry

INTRODUCTION

Making structures light is an important goal for architects and engineers. One approach to light structures are gridshells. There is a special class within the family of gridshells, where members are so slender, that they bend. These “elastic gridshells” utilize the elastic potential of their members produce beautifully curved structures and can still be surprisingly stiff. Building them is not easy: In the design stage, the physical behaviour has to be simulated to know how it actually will look. During construction, many members need to be arranged, requiring scaffolding, falsework, cranes or other equipment [1]. We present a new type of elastic gridshell, that tackles these issues. It can be assembled flat on site and pulled into shape. During its deployment, members rotate around the joint and bend. Our design method is composed of several steps, where algorithms simplify the job and optimize for user goals.

EXPERIMENTS/FUNDAMENTAL OF THE PROBLEM/EXAMINATIONS

The design of a gridshell is usually based on a surface, that should be approximated. To develop an initial concept of arranging the members, geometry comes into play. Since we deal with a surface and want to place rods (idealized by their center lines) on the surface, we use geodesic curves to do so. Geodesic curves are a special curves on surfaces, that have nice properties for our specific problem. Randomly picking geodesics and joining them at their intersections with rotational joints produces curved 3d structures. Since not all surfaces can be made flat without tearing (in fact only developable surfaces can be), networks geodesics generally can not be flattened either.

To come up with a network of geodesics that reflects the nature of the surface, we have developed a method, that slightly adjusts the locations of the member’s intersections and makes the grid flattenable (see Fig.1). Pulling apart the closer of the two corners of the grid makes the structure buckle out of plane again. It basically acts as a one degree of freedom system (see the result of pulling in Fig.2). To simulate the deployed network of rods, we define and minimize elastic energies as in state of the art simulations [2] [3]. To calibrate the parameters of our simulation we compare our it against point cloud scans of claped rods. Observing from the results one can see that constraining the structure to

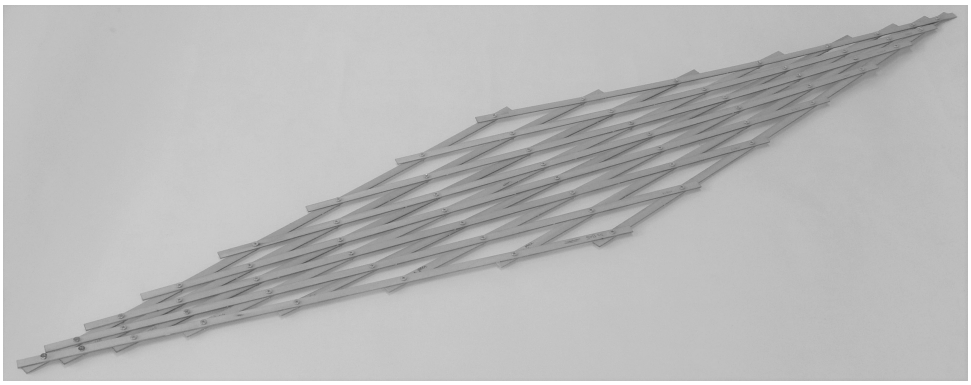

Figure 1: Example of a grid in planar state

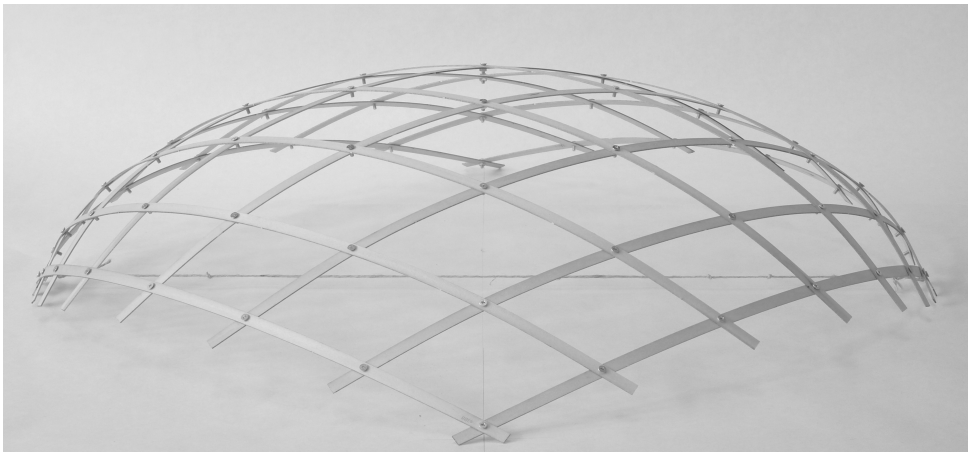

Figure 2: Grid of Fig.1 in deployed state

be flattenable comes with a price: in the deployed state, the structure does not approximate the design surface as well as without this constraint. We minimize this defect in a subsequent shape optimization algorithm. In this algorithm, we slightly adjust the placement of the geodesics and re-evaluate the design to approximate the design surface better, keeping the constraint of planarity upright.

RESULTS AND DISCUSSION

With our method we can compute 1-DoF structures, that are initially flat and can easily be pulled into shape, resulting in curved structures, that approximate a given design surface. Because of their planarity in the initial state, they are easy to assemble. Enforcing planarity however, can result in deviations of the shape of the deployed structures and the design shape. A subsequent optimization step can reduce the deviations, but not fully prevent them. Observing from the different design surfaces we tested, we can see that some kinds of surfaces are better suited for our method than others. By now we can not specify details of what makes a surface suited despite avoiding high curvature, this will be one of the scopes of our future work. [5]

CONCLUSION

We present a method, that supports the design and construction of elastic gridshells. Starting from a free form surface, a designer can use our method to create a flattenable gridshell, that can be easily deployed without any additional measures than pulling two corners apart.

REFERENCES

[1] Quinn, G., Gengnagel, C., Bletzinger, K., “Simulating Pneumatic Erection of Strained Grid Shells via Dynamic Relaxation”, Proceedings of IASS Annual Symposia, IASS 2016 Tokyo Symposium: Spatial Structures in the 21st Century – Bending Active and Flexible Structures, pp. 1-10(10), 2016

[2] Bergou, M., Wardetzky, M., Robinson, S., Audoly, B., Grinspun, E., “Discrete Elastic Rods”, ACM Trans. Graph. August 2008, 27, 3, 63:1–63:12, 2008

[3] Bergou, M., Audoly, B., Vouga, E., Wardetzky, M., Grinspun, E., “Discrete Viscous Threads”, ACM Trans. Graph. July 2010, 29, 4, 116:1–116:10, 2010

[4] Rabinovich, M., Hoffmann, T., Sorkine-Hornung, O., “Discrete Geodesic Nets for Modeling Developable Surfaces”, ACM Trans. Graph. February 2018, 37, 2, 16:1–16:17, 2018

[5] Pillwein, S., Birsack, M., Leimer, K., Musialski, P., Paper currently under review.

URBAN PARTERRE BUDAPEST
THE DEVELOPMENT OF STREETSCAPES IN HISTORICAL DISTRICTS OF BUDAPEST FROM THE TIME OF THE DUALISM AND THEIR EFFECT ON THE CITY TODAY

Viktória Éva Lélek

E259 - Institute of Architectural Sciences

The development of major European cities in the 20th century was characterized by industrialization and urbanisation. The accelerated mobility and the spread of the motorised vehicles has changed the way cities were growing and transforming. The new innovations of transportation have taken on a dominant role on the streets, redefining public space. The ground floor, which was planned primarily for commercial or other semi-public uses, has lost its importance as a smooth transition between public and private space. Smaller forms of operation were neglected due to mass production until they have been rediscovered in the 21st century.

The 8th district of Budapest has been chosen for examination. It is located east of the Danube and has been defined as a public administration unit at the time of the Austro-Hungarian Empire. The analysis does not focus on the historic monumental buildings, but mainly on so-called "Gründerzeit" houses, whose ground floor zone has an unregulated mixture of uses today. In addition, there is the possibility of a comparison with Vienna, as the two cities show many similarities in urban structures and architecture of the 19th century.

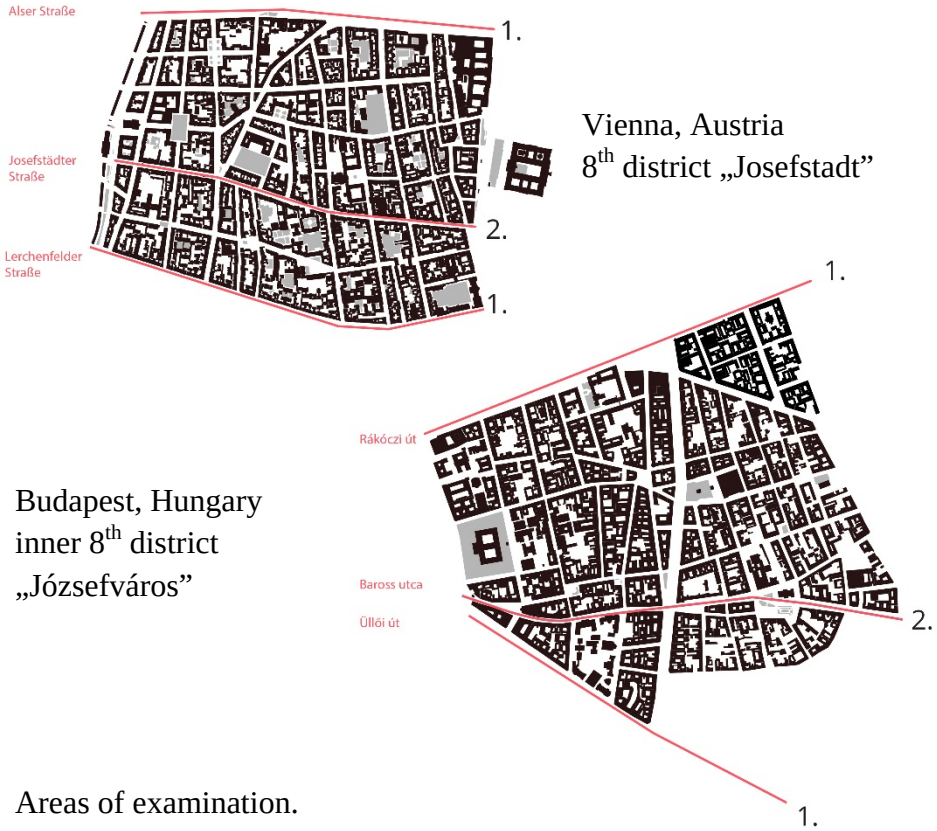

Figure 1. Areas of examination.

1. district border, primary East – West connection road
2. the second most important East – West connection road

The master thesis consists of three parts. It starts with a detailed analysis of the city history, topography and urban structures from the 19th century until today. Historical and current building regulations will be compared to understand the complex basis for city expansion. The second part takes a city block under examination and leads back to the roots of the structural origins in formal farmlands. The third part builds up from a selection of eight “Gründerzeit” houses that are investigated both as parts of a city planning system and as individual buildings as well, in terms of construction, materials and spatial program.

Figure 2 & 3. Photographs of the selected buildings in Budapest.

A two months residence on site in Summer 2018 has supported the collection of the necessary data and plans, which serve as the basis for a field study and a detailed plan analysis. The pictures, figure two and three show the current situation in the 8th district. The selected eight houses build one small street that leads to an important radial street.

The so-called Urban Parterre Model of this selected street is produced in a BIM program. It allows us to investigate the architectural design of the building. The spatial program is connected to the program of the street itself, which has radically changed by the end of the 20th century. The topic of motorised individual vehicle and its effects on this program is an important part of the study. Rethinking the establishment and organisation of the automobile leads to suggestions for future district developments.

The results of this research process lead us to a wider knowledge about former architectural practice and to a better understanding of the city structures of today. The aim is to create a basic knowledge that helps dealing with the challenges in “Gründerzeit” districts in the future.

INTELLIGENT PARAMETRIC BIM SOLUTION AND OPTIMIZER FOR DIAGRID HIGH-RISE STRUCTURES

Aryan Shahabian, Alireza Fadai

E259-02 – Research Unit of Structural Design, Institute of Architectural Sciences

INTRODUCTION

With the aim of improving the functionality and resource-efficiency, many research projects in recent years have focused on various characteristics of high-rise structures–e.g., comparing the performance of different structural systems, components and materials, geometric optimization and integration with other systems [1-4]. A common section in their research design is the appliance of simulation-based case studies. Due to the large number of structural elements in tall buildings, one of the challenging and time-consuming stages of such studies is the initial geometric modeling phase prior to the structural analysis. The significance of the structural models is remarkable as they also act as the base for other models (architectural, mechanical, electrical, etc.) because they include all the main axes of beams, columns, core walls and boundaries of floors. Any inaccuracy, missing or superfluous objects in the models may cause errors during the process or incorrectness in outputs. For high-rise structures with relatively complex geometries, e.g., diagrids, especially with non-orthogonal overall forms, the procedure of preparing a single preliminary geometric model of the whole structure—when done manually—may approximately take hours to days.

This paper presents an intelligent multiparametric BIM solution which is able to generate multiple models of diagrid high-rise structures (with core, and cylindrical overall form or regular polygonal plan shape) in an accurate and quick manner. Moreover, it is capable of applying the geometric optimization method for diagrid structures–developed by K.S. Moon et al. [3]–to the models.

METHODOLOGY AND RESULTS

By employing the principles of Algorithmic Thinking [5,6] and by means of the programming and visual programming languages of Python and Grasshopper, an algorithm was designed and developed in the environment of the computer-aided design application of Rhinoceros (version 5.0). The reasons for this selection were: (1) the high-accuracy and advanced geometric functionality of Rhinoceros; (2) the inclusive parametric platform of Grasshopper which makes it possible to connect models to several other parametric engineering platforms at the same time or for further studies (3) simplicity, robustness and the open-source nature of Python and its growing libraries.

The algorithm has two main parts: One starts with multiple potentially independent variables as input parameters (e.g., number of segments of the base polygon, geometric density of the diagrid pattern, number of floors, floor-to-floor height, radius of the inner and outer tubes, spans of the main and secondary beams, etc.) and geometric model of different elements, collected in separated groups, as outputs (e.g., slabs, various beams, diagrid elements, core walls, etc.). Using the genetic algorithm of Galapagos [7], the second part is an optimizer which is an evolutionary solver loop connecting the aforementioned outputs and inputs. The numerical values of the optimal angles for the diagrid elements (the findings of the research by K.S. Moon et al.[3]) is merged as the fitness criteria in this phase. It is worth mentioning that the algorithm is intelligent enough to avoid logical errors and producing useless models (overlapped geometries, or empty set outputs which may cause errors in running other potentially interconnected BIM applications).

Figure 1 shows a few models generated as a test example. **The test example specifications: (1) Hardware and Operating System**: Processor: Intel® Core™ i7-4720HQ CPU @ 2.60GHz, Video Cards: Intel(R) HD Graphics 4600, NVIDIA GeForce GTX 960M, HDD: 1TB, RAM: 16GB, OS: Windows 8.1 64-bit; **(2) Building Spec. (given parameters):** number of floors: 40, floor-to-floor height 4.08m, core radius: 9.5m, envelope radius: 21m, etc.; **(3) Example Question:** What is the optimum number of segments of the polygon (plan shape)?; **(4) Answer:** 64, found in approx. 7 seconds, number of generated and tested models: 47.

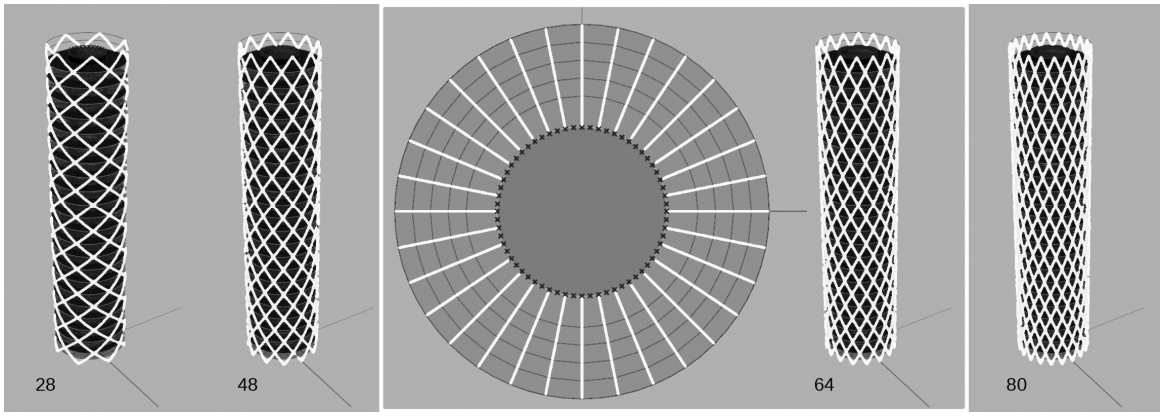

Figure 1. Four of the 47 generated models in approx. 7 seconds (from left to right polygons with 28, 48, 64, and 80 segments). A plan view example shows the modeled slab, core wall and beams elements–in the middle of the figure.

DISCUSSION AND CONCLUSION

The presented BIM solution significantly accelerates the process of accurate geometric model generation and structural optimization. Regarding the former, as the geometry of cylindrical diagrid systems is relatively more complex than those of most of other typical structural systems in tall buildings (e.g., orthogonal rigid frame, framed tube or truss-tube with rectangular plan shapes [8]), the outputs of this solution could also serve as blueprints to generate the other types. Alternatively, parts of the algorithm could be deactivated or modified for further customized setups.

REFERENCES

[1] Trabucco, D., Wood, A., Vassart, O., Popa, N., & Davies, D. (2015). *Life cycle assessment of tall building structural systems*. Chicago: Council on Tall Buildings and Urban Habitat.

[2] Foraboschi, P., Mercanzin, M., & Trabucco, D. (2014). Sustainable structural design of tall buildings based on embodied energy. *Energy and Buildings*, 68, 254-269.

[3] Moon, K. S., Connor, J. J., & Fernandez, J. E. (2007). Diagrid structural systems for tall buildings: characteristics and methodology for preliminary design. *The Structural Design of Tall and Special Buildings, 16(2)*, 205-230..

[4] Shahabian, A. (2015). Integration of solar-climatic vision and structural design in architecture of tall buildings. In *Proceedings of International Conference CISBAT 2015 Future Buildings and Districts Sustainability from Nano to Urban Scale* (No. CONF, pp. 179-184). LESO-PB, EPFL. doi:10.5075/epfl-cisbat2015-179-184

[5] Futschek, G. (2006, November). Algorithmic thinking: the key for understanding computer science. In *International conference on informatics in secondary schools-evolution and perspectives* (pp. 159-168). Springer, Berlin, Heidelberg. (Accessed: 30th August 2018)

[6] Shahabian, A. Algorithmic thinking for architects and designers. die Angewandte (2017). Available at: https://www.dieangewandte.at/en/news/detail?artikel_id=1488903145804. (Accessed: 27th February 2019). doi:10.13140/RG.2.2.31396.12164

[7] Rutten, D. (2010, September). Evolutionary principles applied to problem solving. In *AAG10 conference, Vienna*.

[8] Ali, M. M., & Moon, K. S. (2007). Structural developments in tall buildings: current trends and future prospects. *Architectural science review*, 50(3), 205-223.

LOW-TECH APPROACH TO ARCHITECTURE AND ITS PROSPECTS

Darya Haroshka

E251 - Institute of History of Art, Building Archaeology and Restoration

INTRODUCTION

The topic of low-tech architecture has been researched for several decades by now and has a scientifically approved definition; as an *antithesis of High Tech, it involves the recycling of materials and components and the use of traditional construction, insulation and natural means of heating and ventilation. Low Tech recognises the environmental damage done by High Tech through the excessive use of resources* [1]. However, despite its benefits, low-tech approach to architecture has not been widely implemented yet and has been put into practice mainly in an experimental way so far.

FUNDAMENTAL OF THE PROBLEM

There are several reasons for the author of this abstract to research the topic of low-tech architecture and its possible implementation and propagation, among which are the following:

- Overproduction and overconsumption of technical appliances, which are used in the construction field, leaded by aggressive marketing and greenwashing
- Waste issues in contrast to long living constructions
- Complicated controlling of systems and appliances, which are being installed in contemporary buildings requires additional education of the users, as incorrect usage may lead to their inefficient performance or early breakdown
- Sophisticated appliances, which are being installed in contemporary buildings in order to sustain the required comfort conditions, require regular maintenance and are vulnerable to errors

Officially recognised contemporary sustainable approach to architecture is aiming for reduction of ecological footprint, it is being widely applied and promoted to be the optimal solution for the future. However, it still presumes and applies massive amounts of highly sophisticated equipment and such material combinations, which are difficult to separate and, as a result, recycle, producing tons of waste in the long run. Therefore, the author of this research finds it necessary to develop a critical view and reconsider the definition of *sustainable architecture* and its implementation nowadays.

Furthermore, in many cases contemporary architecture seems to create problems in favour of design of the visual appearance of buildings and then solve them by adding more equipment. Therefore, a few more questions arise. Firstly, if this kind of approach makes sense and, secondly, if these advanced devices actually simplify the life of occupants or do they become overwhelming in terms of effort that has to be put into the controlling and maintenance of contemporary buildings. Modern pace of life is stressful enough to make our living and working spaces a matter of concern on a daily basis.

In addition, technical appliances have much shorter lifetime, than the buildings, where they are installed, are supposed to serve. Therefore, regular maintenance and timely replacement of these

appliances has to be taken into consideration in the long-term view. This, again, inevitably causes large amounts of waste we have to deal with. The flow of production and construction industries, which can be illustrated as a transformation of rapidly fading natural resources into waste, has to be changed.

For example, if we look at the quality of construction of Renaissance buildings, their main core, the walls are on their places, as on the day they have been erected. Would contemporarily constructed buildings survive the same time test?

Picture 1: Historical buildings on the main square of the town of Telč, Czech Republic

However, in no way the author of this paper wants to deny the necessity of those modern conveniences, which supply us with the comfort conditions, which are required for sustaining contemporary quality of life, leaving them out of question in this research. Only those appliances, which are over the daily necessities, are going to be observed in the scope of this research.

The research includes analysis of building approaches of various modern building examples. Each example demonstrates high performance and at the same time has managed in its own way to avoid at least one conventional appliance (e.g. mechanical heating, cooling or ventilation system) and reduce energy consumption of the building without reduction of personal comfort conditions and quality of construction. Examples, analysed during the research represent different efficient methods of how technical appliances can be replaced with various means of design or constructive solutions. Therefore, low-tech approach to architecture aims to design contemporary buildings in such a way, so that they would rely less on appliances and can function and sustain the required comfort conditions with minimum effort from the side of their occupants.

RESULTS AND DISCUSSION

The research proves the necessity of reconsidering the use of technical appliances in contemporary buildings and finding solutions, more efficient and alternative to conventional. The results of the conducted research so far represent a classification of different low-tech strategies, further to be examined in a more detailed way.

CONCLUSION

The author is aiming to continue research on the topic of low-tech architecture on existing examples and, in particular, on methods of its implementation on practice as well as simulating the building performance in order to apply low-tech approaches on newly constructed buildings in the most efficient way in the long run.

REFERENCES

[1] James Stevens Curl, Susan Wilson, “Oxford Dictionary of Architecture”, 3rd Ed., 2016

HOME OFFICE ILLUMINATION: THE UNDISCOVERED COUNTRY

Ceren Sarikaya[a], Ulrich Pont[b,*], Ardeshir Mahdavi[b]

[a]Graduate Student of Building Science and Technology, TU Wien, Vienna, Austria
[b]E259.3 (Dept. of Building Physics and Building Ecology)

INTRODUCTION

Sufficient and satisfactory illumination levels are considered to be of utmost importance for health, well-being, and productivity of occupants of buildings. As such, the consideration of illumination aspects in the framework of building planning and interior design is playing a key role in contemporary work of architects. Moreover, there are a number of international standards as well as national laws and guidelines in most countries that define minimum thresholds for illumination, glare avoidance and daylight penetration of spaces (e.g. [1]). Building planning needs to consider these regulations. Thus, most planning processes for larger office facilities encompass a consultant for lighting aspects. This is not necessarily true for other planning tasks, as fewer regulations exist for other building usages, especially residential use. In the case of small scale home offices situated within residential units, regularly the occupants, who often are non-specialists in lighting design, design their workplaces themselves. Little is known about the in-fact lighting conditions in such home-office places, especially those that could be named “micro offices”. Thus, the present contribution literally sheds light upon this topic by presenting the results of recent efforts pertaining to investigate into a set of small scale home offices in Izmir, Turkey.

METHODOLOGY

Case study home offices: All together 9 different home offices that encompass 10 work places (1 in each residential unit, except one encompassing two work spaces) were examined (named A-J). The involved professions that can be found in the offices can be considered as diverse and include lawyers, journalism free-lance IT professionals as well as architects and industrial designers. Figure 1 illustrates some floor plans of the examined offices. In each of the spaces the task area of the specific work place was identified, and in further evaluation steps clearly distinct from other areas of the corresponding space (living, sleeping, kitchen, etc.).

Figure 1: Some of the small scale floor plans (not scaled, orientation arrows pointing in north direction)

Deployed evaluation methods: For the purposes of this study, we deployed both measurements and numeric simulation tools. The used simulation environment was the well-known simulation tool Dialux [2]. The measured Key Performance Indicators included illumination inside and outside of the residential units. In particular, the outside illuminance was measured during daytimes parallel to the illumination levels on the work planes, but also of the remaining apartment, to be able to derive

daylight factors. Furthermore, night-time measurements were conducted to assess the artificial lighting in the workspaces / residential units.

RESULTS & DISCUSSION

Figure 2 illustrates the results of the artificial light assessment via simulation and field measurement (these happened in the evenings and encompassed 56 to 104 measurement positon per workplace). In all of the offices average and median illumination levels were below the two threshold values (500 lux respectively 300 lux) named in typical standards for workplaces [1] in both simulation and measurements. Generally speaking, the average deviation between simulation results and field measurements was quite small (around 1%). In some cases very well lit evaluation points could be found, which indicates that per se luminaries might offer sufficient lighting levels, but are positioned in an unfortunate way. Some of the other results indicate that the general availability of artificial lighting seems sparse and could and should be subjected to improvement. Regarding the daylight availability, some of the offices offered quite large average daylight factor values on the workplaces, while others did not feature satisfactory daylight availability (daylight factor values between 0.24 to 9.93). Generally speaking, the quality of the indoor illumination in all of the examined micro offices can be considered as dissatisfactory, especially if compared to large scale offices, which regularly have been subjected to light planning.

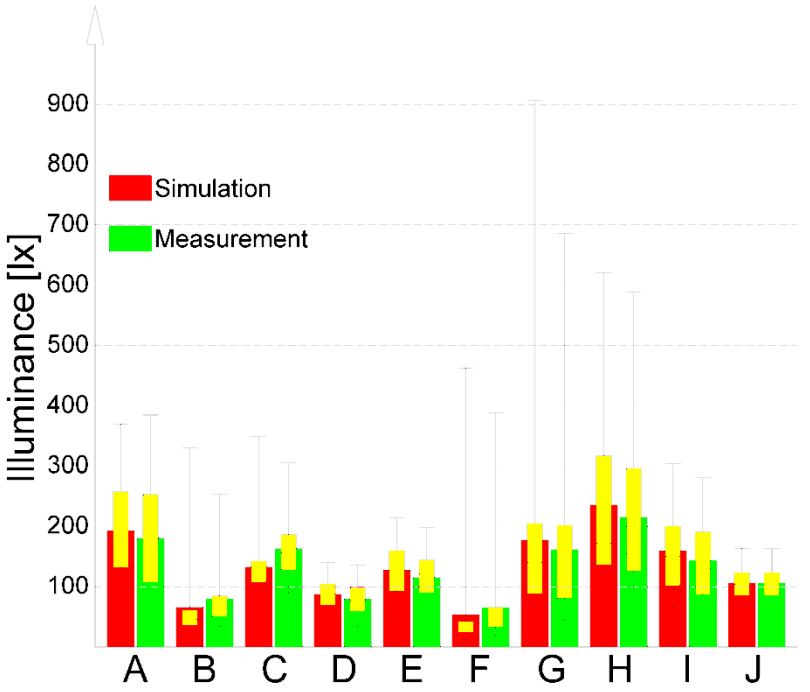

Figure 2: Illumination levels in workplaces A-J. red: simulation; green: field measurement.

CONCLUSION AND FUTURE RESEARCH

The next step in this research effort is an optimisation effort. For the examined offices, low-cost improvements should be checked upon via the simulation models. More general, future research efforts should encompass a larger sample of home offices from different regions of the world and different job disciplines, the derivation of a “checklist” for home offices to generate good lighting conditions, and – a bit farfetched – the development of an mobile phone app that can support the setup of home offices based on some basic planning parameters, such as location, orientation of transparent building components, and available luminaries. Such an app could utilize existing simulation tools and corresponding knowledge, but offer valuable planning support to home office planning without a designated consultant specialized upon lighting.

REFERENCES

[1] European Standard Series EN 12464 - Light and lighting - Lighting of work places. (different issueing dates).

[2] Software Dialux (www.dial.de)

4 IN A ROW: ARCHITECTURAL DESIGN AS ADAPTATION AND MITIGATION MEASURE FOR THE PROBLEMS OF TODAY?

Ulrich Pont[a], Sigrun Swoboda[b], Andreas Jonas[b], Peter Schober[c], Florian Waldmayer[d], Heinz Priebernig[d], Ardeshir Mahdavi[a]
{Sara Alasu, Maximilian Baumgartner, Nikola Buncic, Daniela-Vasilica Cucu, Juan Arturo Hernandez Barrera, Georg Holzmann, Eleni Marmaridou, Sofia Milet Oliver, Mais Msto, Valentina Pajtak, Jessic Parizek, Chaeran Park, Anastasia Proreschnew, Barbara Razek, Renata Rios-Capapé Gans, Lola Sánchez Valldecabres, Helene Teufl, Elitsa Tsankova, Eduardo Vidal, Edita Vinca, Daniel Can Wittek, Melissa Wittek, Melanie Würrer}[e]

[a]E259.3 – Department Building Physics and Building Ecology
[b]E259.1 – Digital Architecture and Planning
[c]Holzforschung Austria, Franz-Grillstraße 7, 1030 Wien
[d]E253.4 - Project and Building Management
[e]Students of Architecture as well as Building Science and Technology Programs

INTRODUCTION

This contribution describes an academic effort conducted in Winterterm 2018/2019 at the Faculty of Architecture and Planning of the TU Wien. Thereby, a collaborative teaching effort established in the year (see [1]) before was continued and furtherly improved. Such as in the year before (coupled design studio of the Master Programme Architecture and project course of the Master of Building Science Programme "Building Envelope 4.0) Master students from Building Science and Architecture programmes were asked to form groups and to collaboratively develop clever design ideas and to proof their performance. The topic of the winter term 2018/2019 did – unlike the year before – not focus on just one solitaire building, but rather addressed a convolute of buildings situated along a heavy-traffic street (Operngasse) in Vienna. The buildings addressed in the course are highlighted in Figure 1.

Figure 1: Buildings along the Operngasse that have been addressed in the design studio / project course. Note: In the right lower, half the "Freihaus" complex of TU Wien can be seen.

Thereby, each group of students was assigned one building. Their task was to improve not only the singular building regarding appearance (façade) and internal organisation (plan layout, usage, occupant comfort, etc) but also to think about interrelations between the different buildings in term of urban structure of the neighbourhood. Given the idea to integrate greenery in buildings, an additional task was to consider façade and roof greenery as good as possible in the retrofits. Challenges related to the design studio included the existing plan layout of the buildings (all but one

building were built around 1937 and featured *Gründerzeit* plan layouts, but severely lower ceiling heights than the original *Gründerzeit buildings*) that could be considered as far from today's requirements, and the rather slim structural elements (slabs, columns). Moreover, the thermal and acoustical performance of these old buildings required comprehensive improvement. Regarding the one and only newer building, an office building with a rather regular plan layout dating back to the late 1970ies and early 1980ies, the major challenge was to find ways to integrate as good as possible residential units. All of the building suffer from vacancies along the ground floor street façade, thus solutions addressing that issue were also part of the task. The progress in the design studio was structured into (i) concept phase, (ii) design phase, (iii) evaluation phase, and (iv) detailing and work-planning phase. Students, in contrast to many other design studios, had to work out technical solutions for their design and to think about the construction effort connected with their suggested interventions.

RETROFIT CONCEPTS

The retrofit concepts spanned a wide range of different interventions. Some of the concepts just performed minimal invasive changes, such as punctual addition of boxes that host plants and a watering system. Others added an additional layer in front of the façade that serves as a second skin. The interstitial space between can be used for balconies, growing space for plants, or ventilation purposes. Two other design concepts suggested the addition of kinematic shading elements before the façade layer. Finally, some concepts totally opened the façade of the building or even performed subtractive interventions onto the building (office building). Close to all designs optimized their design in the direction of factory prefabrication to shorten construction times. Figure 2 illustrates some of the developed designs.

Figure 2: Examples of improved Operngassen facades.

CONCLUSION

The outcome of the design studio / project course unravelled a large demand by students toward interdisciplinary courses. In detail, the combination of design skills, technical assessments and a long-term "big picture" view is something that is severely missing in today's planning practice, and thus in many academic efforts. However, the generation of well-performing, aesthetically attractive, and technically feasible architecture requires multidisciplinary approaches and the utilization of technical skills (e.g. simulation utilization) and knowledge-based approaches. As such, we plan to continue with this collaboration and to think about 1:1 realizations (of course in small scales) encompassing building greenery.

REFERENCES

[1] U. Pont, S. Swoboda, A. Jonas, P. Schober, Florian Waldmayer, Heinz Priebernig, A. Mahdavi, M. Alhayek, S. Acar, Z. Bajka, D. Beigl, C. Casian, A.K. Chrysochou, L.M. Faurbjerg, G. Holzmann, P.P. Korpitsch, J.A. Marx, H. Meisenender, M. Pospichal, D. Radulovic, T.-I. Rosca, K. Sperka, N. Summhammer, E. Tsankova, A. Wadi, X.X. Zhou: "Interfacing Architectural Design and Industtry 4.0 concepts: A case study"; Literature Number 1, Journal, Page, Year in: "VSS - Venna young scientists symposium", P. Hans, G. Artner, J. Grames, H. Krebs, H. Mansouri Khosravi, T. Rouhi (ed.); Book-of-Abstracts, (2018), ISBN: 978-3-9504017-8-3 p 52 - 53.

HOW CAN INNOVATIVE SPACES FOR OUTREACH BE CREATED WITH LIMITED RESOURCES?

Habibe Idiskut

E 006 443 - Faculty of Architecture and Planning at TU Wien

INTRODUCTION

Urban innovations impacting sustainable development also happen in unexpected small spaces, for example when universities open their doors to young people for different outreach activities. These small spaces are places of encounter for scientists and young people, yet their design is often neglected. Especially in engineering and natural sciences, the focus is more on the subject and the tools than on the room and the people in it. Our outreach with robotics team is interdisciplinary (physics, psychology, computer science, architecture, mechanical and electrical engineering, literature science) and diverse (gender, age, backgrounds). In a team where every member is contributing with their field of expertise and talents, our architect noticed the need to adapt the outreach rooms to the young people's needs [1].

How young people perceive an out-of-school activity in a setting where they visit a university to hear about robots is also influenced by how they perceive the space where all this happens. Their behaviour is dependent on five important parameters which define a room and their perception. These parameters are:

1.) light

2.) acoustic

3.) furniture

4.) textures & colours and

5.) room dimensions.

Children need a lot of space to move during outreach activities. And the impression of the room is very important for the children otherwise they feel bored and do not want to be an active part of the workshop. Therefore, the innovators lab needed to be adapted. Since there was no budget for this, the adaptation was done with limited resources.

INNOVATOR LAB

For the workshops with the kids we needed our own room and in this room the kids should not feel crowded. As we started with our workshops we had few opportunities to use it as our workshop rooms. One of our rooms we called "innovator lab", which was at the beginning a room we used as a stockroom. It was not possible to use this for any of our workshops because there was no space left were the children could stand free. Furthermore we needed place where the children could be an active part of it and could try out some tests. Therefore we started to put everything out of the room and cleaned it. Afterwards we measured out the room and reused some of the interior equipments which we carried out of the room. Now we had a room with working places and also a lot of daily light which were not blocked from the huge cupboards. As a further step we started to think about how we could show up our prototypes and results from our workshops. So we arrayed six shelves

symmetrically on the wall above our pin board. On the pin board we designed some posters as an illustration so we were able to explain our projects easier to the children. And after each workshop we watch the children and their behaviour and can decide which changes are still needed.

Below on the illustration and picture it is recognizable that the stockroom is completely dissolved and got a new function of the room. The room gets more daily sunlight because the windows are not covered by any furniture and also this light streams can get through the glazed walls of the room so that the whole hallway can get more sunlight as well. The room is separated in three sections so in the middle of the room, a hallway which leads to the window, is readable. And also a spot between all working stations was developed, so that the children have enough space as well to follow the workshop.

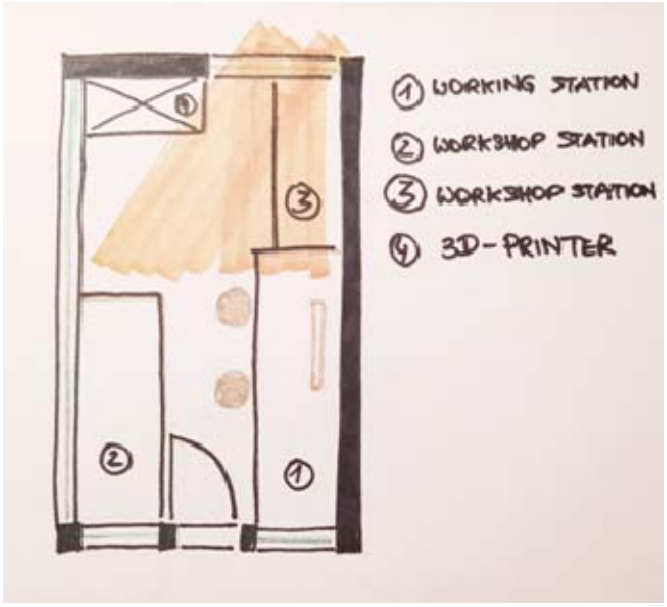

Picture 1: sketch of the floor plan of the innovator lab

Picture 2: situation of the innovator lab

LESSONS LEARNED

During my work with the outreach team in the role as an architect I learned that it is very important to be also able not only to create new spaces and build them, but also think about given resources and reuse them.

CONCLUSION AND OUTLOOK

Children are very inquisitive if you shape your workshops as interesting as possible, they will follow you as well. Therefore it is very important to be in a comfortable place. But is it really that important to be just in an airy and bright room which is big enough to move around? We live in the so called “digital era” and it is also possible to connect our knowledge in architecture with other multimedia, so we can make spaces more interactive and interesting for children. To conclude: schools and other educational institutions are not only places of “enforced encounter” it should also be a place of “playful learning”.

REFERENCES

[1] Julean, D., 2016. Why Architects See Things Differently An Architectural Approach On Teaching Space Perception, European Scientific Journal, Special Edition, April 2016

ARCHITECTURE AND TECHNICAL ASPECTS OF THE SWIMMING HALL DESIGNS BY FRIEDRICH FLORIAN GRÜNBERGER

Karoline Walal[a], Ulrich Pont[b],* , Ardeshir Mahdavi[b]

[a]Graduate of the Msc-Programme Building Science and Technology, TU Wien, Vienna, Austria
[b]E259.3 – Department Building Physics and Building Ecology

INTRODUCTION

In the year 1968, the Viennese government decided to implement a new concept regarding public swimming pool halls ("Bäderkonzept"). Thereby, it was decided that a network of easily accessible and affordable swimming pool halls should be constructed. The idea behind was to re-establish the bathing culture of earlier times in Vienna, and to generate facilities for sport and recreation of the population. As a key, 1m² of swimming pool surface area was intended for 333 inhabitants of Vienna. It is obvious that with the facilities available in Vienna at that time, this key could not be reached. Thus, the architect Friedrich Florian Grünberger (Figure 1) developed the so called *Bezirkshallenbäderprogramm* (district indoor swimming pool program). Based on this concept a set of very similar swimming pool halls has been constructed in Vienna. While Grünberger in the 1960ies and 1970ies was a well-known architect specialized on recreational facilities – he was even called the bathpope of Vienna (der Bäderpapst von Wien) -, today little knowledge about him is preserved. This seems a bit surprising, given that the majority of his swimming bath design from the backbone of Vienna's public bath infrastructure of today. One of Grünberger's major developments was the concept of the so-called *Europabad*, a porotypical plan-layout for an indoor swimming pool hall (Figure 2).

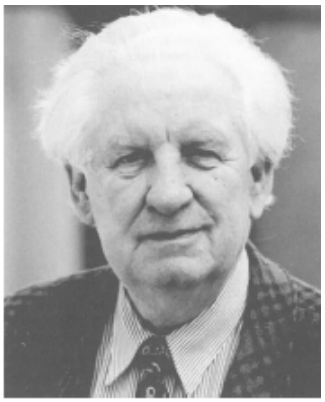

Figure 1 (left): Portrait of Friedrich Florian Grünberger [1].

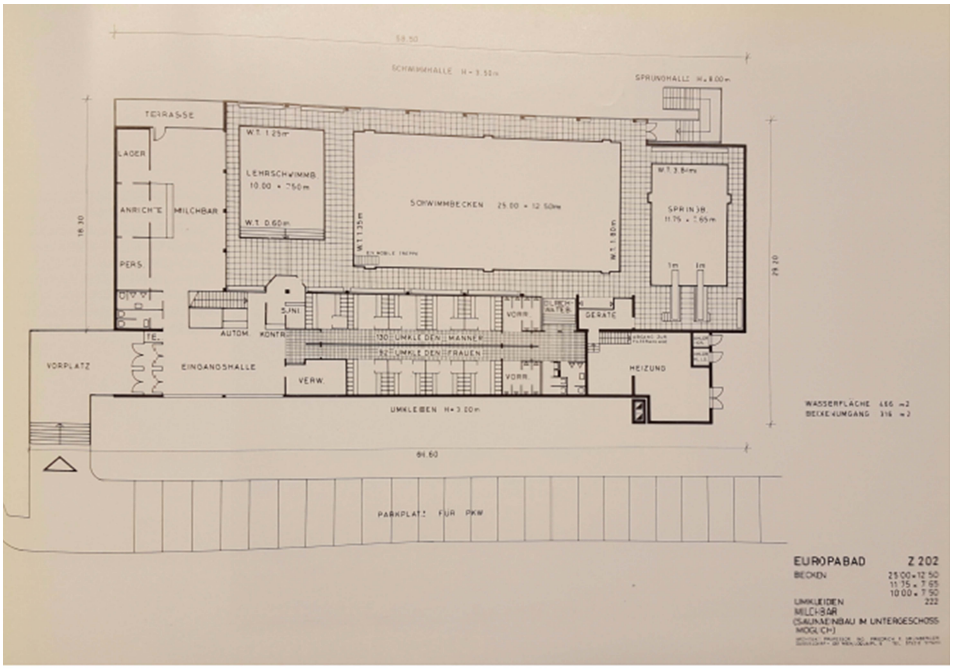

Figure 2 (right): Plan layout of the Europa-Bad concept by F.F. Grünberger [2]

In a first attempt to rediscover some of the knowledge about both the architect and his ouvre, it was decided to propose a master thesis that focusses on some technical aspects of one of Grünberger's swimming pool halls of Vienna. The findings discussed below are based on this master thesis [3].

THE FLORIDSDORFER BAD

The Swimming pool hall in Floridsdorf was designed by F.F. Grünberger, and built between 1964 and 1967. It was the first Swimming pool hall that was built after the second world war. During the planning process the bath was designated as a multi-role swimming pool hall, which required the attachment of number of facilities. For instance, to allow for the usage during competitive swimming a spectators stand had to be integrated. The building is a reinforced concrete skeleton construction and is separated in different parts (one for the pool, one for the change rooms, and one for administration/entry part; a fourth part encompassing a gym has been added in the 1990ies). The layout is thus significantly different from those of later baths designed by Grünberger, following the *Bezirkshallenbäderprogramm.*

Today, the swimming pool hall is still in heavy use, being the only of the public Viennese baths (beside the privately operated Stadthallenbad) that can host swim competitions.

During the early 2000s, the operation of the bath regarding energy usage was changed to contracting in most of the Viennese bahts. Contracting is a Private-Public-Partnership model, where private companies support the public owner in implementing energy-saving measures, and – in return – is paid a part of the saved money. Interestingly, the implemented measures suggested by the private energy contracting firms, regurarly do not touch the existing building envelope, but rather the technical infrastructure of the buildings that is necessary for keeping up the required water temperature and quality. Beside the old swimming pool halls of Amalienbad and Theresienbad, there has not been any major thermal retrofit to the envelopes of Grünbergers buildings.

The contracting efforts could be considered as rather successful in the special case of the Floridsdorfer bad. The energy consumption out of Vienna's district heating could be lowered by 34% due to integration of solar panels on the roof. Gas and electricity consumption could be decreased by 4 and 21%, and the water consumption by 67%-

CONCLUSION

The master thesis conducted about the Floridsdorfer Bad and Florian Friedrich Grünberger revealed a larger research necessity which has to encompass multiple streams: (i) the energy performance of the swimming bath halls needs to be more explainable for non HVAC-engineers; Moreover, the impact of potential envelope retrofit measures needs to be examine; (ii) Comfort and performance indicators such as noise levels, thermal comfort, and daylight availability need to be investigated; (iii) Today's state of the Grünberger baths has to be documented and compared to the original realizations. Thereby, the methods of building archaelogoy/research could be utilized; (iv) the meaningfulness of Grünbergers baths has to be examined from a viewpoint of art history/building history; (v) As a central platform for the different other research streams, it might be wise to generate BIM (Building Information Modelling) models of the Grünberger baths. The mentioned aspects are currently collected and prepared onto a fundamental research proposal addressing Viennes indoor swimming pool halls.

REFERENCES

[1] Weihsmann, H. (ed). 2005.: *In Wien gebaut*

[2] Grünberger .F. (1974) *Fünfundzwanzig Jahre Architekt* (aus Anlass der Ausstellung F.F: Grünberger, 25 Jahre Architekt; Künstlerhaus Wien, September 1974; Wien: Tusch-Druck.

[3] K. Walal: "Architectural & Technical Aspects of Swimming Hall Design by Friedrich Florian Grünberger"; Supervisor: A. Mahdavi, U. Pont; TU WIen, 2018; final examination: 2018-06-19

DIGITAL PLANNING AND OPTIMISATION OF FLEXIBLE STRUCTURES FOR INDUSTRY 4.0

Julia Reisinger

E234-2 - Department for Integrated Planning and Industrial Building

INTRODUCTION

Industry 4.0 incorporates a highly networked, digitalized and therefore individualized production enabled through the Internet of Things (IoT), generating cost-effective production in batch size 1. The production cycles are extremely short and therefore the production systems are constantly changing. Due to the short product cycles and rapid product changes in industry, it is necessary for industrial buildings to be able to adapt quickly and easily to changing conditions [1],[2]. Thus, sustainable operation of industrial plants for Industry 4.0 require flexible and adaptable production, building, structural and building services equipment (BSE) systems.

FUNDAMENTAL OF THE PROBLEM

The sequential approach in building design where production, building and BSE planning are separated in time and run consecutively, the slow pace of digitization in the AEC (Architecture, Engineering, and Construction) industry and the rigid building systems in industrial buildings constitute the greatest constraints for the realization of Industry 4.0-compliant industrial construction plants. The bearing structure, as the element with the longest service life and the lowest level of flexibility in the building, plays the key role. The supporting system affects and limits the reusability of the whole production system the most. The non-flexible building systems cannot be adapted quickly and efficiently to support production changes, which usually results in cost-intensive modifications or in demolition and rebuilding of the plants, influencing the lifecycle costs and the environmental impact negatively.

RESEARCH DESIGN AND METHODOLOGY

This study aims to enable the design of flexible, versatile production facilities, from the perspective of structural design, using integrated planning methodology and digital BIM (Building Information Modelling)-based parametric tools.

The main objective is to create a framework for an innovative parametric structural design application. The use of parametric design tools in the early planning stages enables the rapid expansion of potential solutions and the development of variant studies, which is difficult in BIM at the early planning stage. A Framework for an “Parametric Structural Design and Optimisation for Industry 4.0” (PARASOLI 4.0) App is developed and is intended to enable the analysis and calculation, as well as the optimisation and prediction of flexible structural systems, coupled to the BIM model. PARASOLI 4.0 aims to enable the planning, optimisation and prediction of flexible structural systems for Industry 4.0, taking into account the temporal changes of the production, building, energy and media systems through scenario formations in the early design stage, based on criteria such as cost, time and quality. It should serve as a decision-making tool via visual management - by linking to the BIM-model - and an evaluation tool.

Based on the generated workflow for the integrated planning process, the information necessary for the data exchange and specific data exchange requirements are prepared by classification, filtering and pre-processing of the geometric and non-geometric data. For a seamless import from the BIM

model to the structural analysis software (FEM - Finite Element Method), a project-specific classification system is to be developed, which enables an optimal central data storage. By creating this seamless connection between BIM and FEM software PARASOLI 4.0 is optimally coupled with the structural analysis software. The various sub discipline information, requirements and data of production planning, BSE and architecture, which are dependent on the structural design in industrial construction 4.0, will be integrated (see picture 1).

To achieve these goals, the methods of process analysis and process definition from the management sciences, digital modelling and data analysis, as well as the embedding of FEM and other numerical calculation methods from the research field of structural analysis and mechanics in the digital models, by means of algorithm development, are applied.

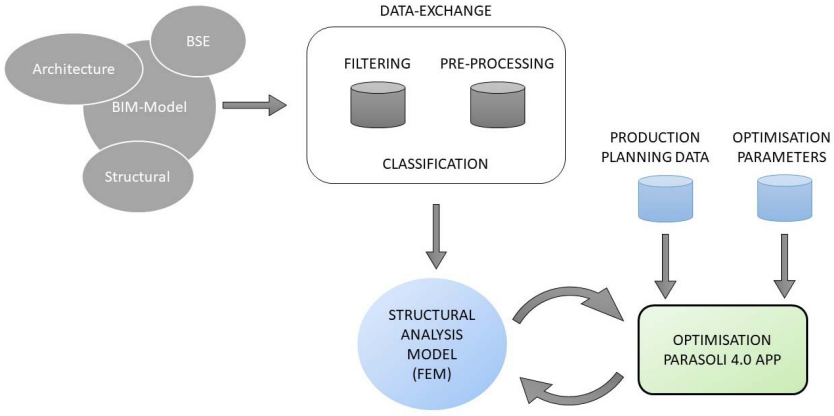

Picture 1: Modelling of the data coupling including PARASOLI 4.0

EXPECTED RESULTS

PARASOLI 4.0 aims to achieve 20% more efficient design processes and 20% less emissions in the building's manufacturing and operating phases. The proposed framework serves for prediction, optimisation and decision support by means of scenarios formation and evaluation and should allow the determination of the optimal structural variant. This results in an increase in the overall service life of the building, as rescheduling or even demolition can be avoided. As a result, negative ecological effects and life cycle costs can be minimized.

CONCLUSION

The objectives in industrial design to meet the needs of industry 4.0 are the maximum flexibility of the horizontal structure (free floor plan and flexible layout design), as well as the flexible vertical building structure (reconfigurable structure). In order to allow the flexibility of the structure, the parametric structural design and its optimisation is proposed as part of the integrated design methodology, which couples the planning participants, their processes and partial models by means of BIM and parametric design tools. Due to the high information content in combination with real-time scenarios formation, the overall life cycle of industrial construction can be positively influenced and the information from architecture, engineering and production planning can be integrated and exchanged along the life cycle. Hence, the production systems should be quickly and efficiently adaptable to market requirements through the framework developed.

REFERENCES

[1] Bracht, U. (2018): *Digitale Fabrik. Methoden und Praxisbeispiele.* 2. Aufl. 2018. Berlin, Heidelberg: Springer Berlin Heidelberg (VDI-Buch).

[2] Wiendahl, H., Reichardt, J., Nyhuis, P., (2014): *Handbuch Fabrikplanung. Konzept, Gestaltung und Umsetzung wandlungsfähiger Produktionsstätten. 2.*, überarb. und erw. Aufl., [elektronische Ressource]. München: Hanser. Online verfügbar unter http://dx.doi.org/10.3139/9783446437029.

CHALLENGES AND OPPORTUNITIES OF COMBINING TAKT TIME PLANNING AND OFF-SITE CONSTRUCTION

Aída Santana Sosa

E259 - Institute of Structural Design

INTRODUCTION

While other industries have steady increased their productivity, in construction sector has stood still becoming an urgent challenge [1]. Off-site construction has been seen as an effective method to reformulate construction from traditional site-based wasteful practices towards industrialization [2]. Besides, the term Lean Construction (LC) was formulated in 1992 as an adaptation of the Toyota Production System (TPS) suggesting that the sector should learn from the so-called Lean Management [3]. LC was then defined as a production system that tracks and eliminates every task with no value to the end product (*muda*) and follows continuous improvement principles (*Kaizen).* Under the umbrella of LC exist several tools focused on resource and flow efficiency, such as Integrated Planning (IP), Last Planner® System (LPS) and Takt Time Planning (TTP) among others. Through this approach the interaction of off-site construction as a method to industrialize construction and TTP to optimize activities is explored to highlight efficient practices based on just value-adding tasks.

OFF-SITE CONSTRUCTION AND TAKT TIME PLANNING

Prefabrication has been linked since decades to mass production, where all elements look alike with no customization and run along a production line within a Push Planning. At present it can be understood as a systematic work methodology where standard sub-pieces, when combined, form an end-product with bare constrictions. Since parallel work can be executed on-site and in a factory under optimal conditions, construction time can be reduced by overall 25% [4]. For an optimized management, a Pull Planning as a main pillar of LC should be implemented, where specific products and components are delivered only after being asked, easing a smooth production flow and a Just In Time (JIT) delivery with no overproduction, nor stock and nor waiting time (*muda).*

The *Takt* principle was firstly formulated by Porsche and is considered as the *beat* of construction, referred to the time for one trade to finish its activities. Accordingly, TTP is a method used to streamline those activities in a construction sequence with the purpose to harmonize and accelerate the flow [5]. Although TTP can be applied to non-repetitive activities [6], the basis of an effective TTP relies on detecting repetitive elements and the so-called smallest multiple units (SMU) [5]. Consequently, a systematic approach based on standardized prefabricated elements, components and joints seems to be the best scenario for applying it effectively. Despite theories have explained how to apply TTP and its potential benefits, there is a lack of documentation about practical approaches and analysed empirical data [7].

WORKSHOP AND RESULTS

In the field of this research a workshop was conducted consisting in three rounds simulations of a production line, where elements and prefab components were delivered from different sub-producers in a semi-structured timeline, being together assembled, further delivered to quality control management and finally to the client. Each participant assumed a role and agreed the interdependence with their closest partner understanding how the production line works. A TTP was

given where some constraints related to transport logistic and order and delivery capacity were included to simulate real conditions. The first simulation started and although each trade worked on their activities as efficiently as possible delivering their components according to their production speed and the TTP given, the production line not able to deliver the whole product to the client. Furthermore, delays and errors occurred throughout the line in the delivery of some components and elements, being out of the *takt*, and implying rework, over-processing, waiting time and deficient production rate. The factors constraining a right workflow were discussed in a collaborative workshop where changes and potential improvements were proposed, and the TTP consequently adjusted. Although there were significant improvements in the second simulation, a considerable amount of stock was produced traduced to overproduction, inventory, poor quality, and unneeded transport and movements. Within the second collaborative meeting, the Pull Planning main principles were explained, and thereafter implemented in the production planning optimizing again the TTP for both flow and resource efficiency. In the third simulation, the production line got optimized in a way that trades were able to produce all components on *takt*, even when errors occurred, since they were detected earlier in the production process and sent back to be fixed, while the whole process stood on sequence. Furthermore the number of workers was optimized, the over processing and unneeded movements were minimized and no overproduction from components nor inventory or stock from elements occurred.

CONCLUSION

The combination of off-site construction as a system to industrialize construction, with TTP as a method to optimize activities appear to bring several benefits to the sector in terms of productivity and flow efficiency. However, it is important to highlight that TTP as an isolated tool would not be enough to effectively align the activities and uncover potential improvements. Such an approach implies a tight involvement and trust-based relationship between producers, sub-producers and specially workers, since they know exactly how the tasks should be done. That is the main foundation of the LPS formulated by Glenn Ballard [8], and should be the basis of an optimized TTP. Aiming to quantify the benefits of such a combination and stablish some applicable principles, practical approaches should be implemented and analysed.

REFERENCES

[1] Teicholz P Goodrum P M and Haas C T 2001 *U.S. Construction Labor Productivity Trends*, 1970-1998 In: Journal of Construction Engineering and management Volumen 127 Issue 5

[2] Gibb A 2001 *Standardization and Pre-Assembly- Distinguishing Myth from Reality Using Case Study Research* In: Construction Management and Economics 19 (3) 8

[3] Koskela L 1992 Volumen 72 *Technical report: Center for Integrated Facility Engineering CIFE Application of the New Production Philosophy to Construction* Stanford University

[4] Smith R E 2015 *Solid Timber Construction – Process, Practice, Performance*. Off-site Studies University of Utah, Integrated Technology in Architecture Center, College of Architecture and Planning

[5] Lange A 2016 *Lean Construction. Practical Insights for innovating Construction Management.*

[6] Linnik M, Berghede K and Ballard, G 2013 *An experiment in takt time planning applied to non-repetitive work* 21st Annual Conference of the International Group for Lean Construction (Fortaleza, Brazil)

[7] Frandson A G, Seppänen O, and Tommelein I D2015 *Comparison between location based management and takt time planning* 23rd Annual Conference of the International Group of Lean Construction (Perth, Australia)

[8] Ballard H G 2000 *The last planner system of production control* Doctoral Thesis School of Civil Engineering Faculty of Engineering of the University of Birmingham

VERIFICATION OF CONSTRUCTION DEVIATIONS USING PARAMETRIC BIM&AR

Michael Jenewein

E259.1 - Institute of Architectural Sciences - Digital Architecture and Planning

INTRODUCTION AND MOTIVATION

This PhD project deals with the detection of constructive deviations between a Building Information Model (BIM) from planning stage and the as-built situation after construction by use of Augmented Reality (AR) directly on the building site. BIM has become a feature in design and planning [1] but with limited investigations how it can be integrated on-site [2]. This work presents an approach for tracking dimensional deviations with BIM&AR.

Reasons for building deviations and the gap between planning model and built model are misinterpreted plans, errors in the building process or deviating decisions of local site management that are not corrected afterwords in the planning database. State of the art in measuring building deviations is surveying with total stations, laser scanners [3] or photogrammetry [4]. Corrections of the planning database by use of measured data are normally made later in the office. This project proposes an approach for integrating AR tracing of existing constructions by comparing as-planned and as-built data in real world on the construction site with the advantage of saving time and costs [5].

REREARCH PROJECT

AR tracing of constructive deviations will only be possible based on a parametric real time model. In this project Unity is used as parametric modeler and Vuforia as implemented AR tool. The individual BIM elements of the database are structured in layers. A scale model with an axis spacing of 12 m by 12 m and a grid of 3 m with standardized industrial components such as truss girders enables to explore simulated deviations in an office environment. The constructive dimensions in the scale model correspond to real-world components.

AR tracking is done by a webcam and a target with additional markers. The AR setup has been optimized by camera calibration and test cases with different viewing angles and lighting conditions. An iPad interface enables wireless remote editing of the parametric BIM&AR database. Measurements can be made directly on-site in AR with a virtual ruler.

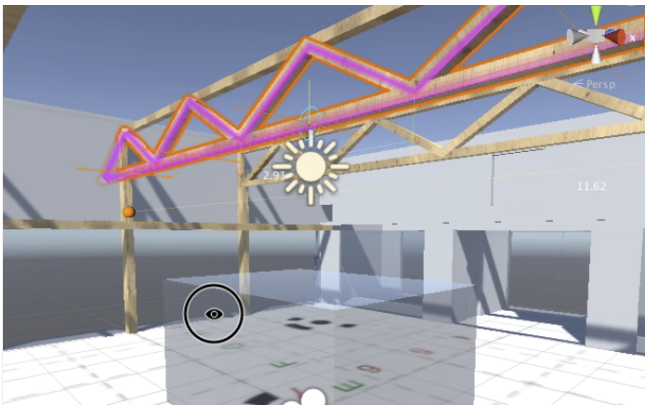

Figure 1: Interior AR view of a parametric truss girder

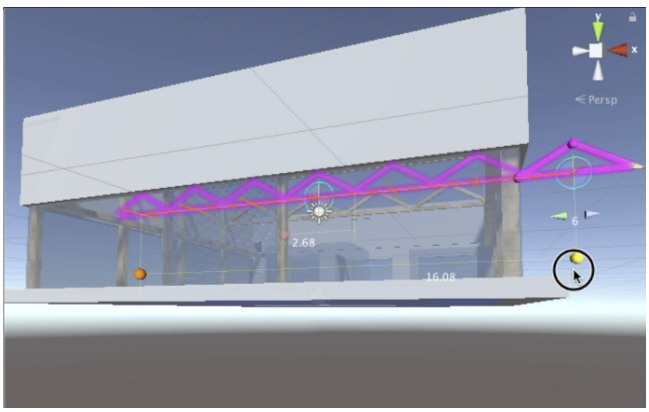

Figure 2: BIM with a scaled truss girder in AR view

RESULTS AND DISCUSSION

Experience shows that the parametric BIM&AR setup is very sensitive to subtile changes of single components. But basically the on-site tracing of construction deviations by comparing as-planned and as-built data with AR works. Technically it is essential to have a calibrated AR setup with AR camera and AR tracking. Lighting conditions and viewing angles also have to be considered. The remote connection to the BIM&AR database via iPad and WiFi enables user independent location on the construction site.

CONCLUSION

Building Information Modeling (BIM) and Augmented Reality (AR) are key technologies for the future. The combination of BIM&AR will enhance the process of as-built information extraction to improve on-site effectiveness [6]. In order to verify the findings of the model stage under real conditions the results of the PhD work will be implemented in an industrial real-world test case in scale 1:1. The planned evaluation in an example environment directly on a construction site will help to derive a robust and reliable method for "Verification of Construction Deviations using Parametric BIM&AR".

REFERENCES

[1] Automation in Construction, Kristen Barlish and Kenneth Sullivan *"How to measure the benefits of BIM — A case study approach"*, http://www.sciencedirect.com, 2012.

[2] Automation in Construction, Xiangyu Wang and Peter E.D. Love and Mi Jeong Kim and Chan-Sik Park and Chun-Pong Sing and Lei Hou *"A conceptual framework for integrating building information modeling with augmented reality"*, http://www.sciencedirect.com, 2012.

[3] Journal of Civil Engineering and Management, 22 October 2013, p.1-10, Mill, Tarvo and Alt, Aivars and Liias, Roode *"Combined 3D building surveying techniques – terrestrial laser scanning (TLS) and total station surveying for BIM data management purposes"*, https://journals.vgtu.lt/index.php/JCEM/article/view/3949, 2013.

[4] ISPRS - International Archives of the Photogrammetry, Remote Sensing and Spatial Information Sciences, Tuttas, S. and Braun, A. and Borrmann, A. and Stilla, U. *"Comparision of photogrammetric point clouds with BIM building elements for construction progress monitoring"*, https://www.int-arch-photogramm-remote-sens-spatial-inf-sci.net/XL-3/341/2014/isprsarchives-XL-3-341-2014.pdf, 2014.

[5] Automation in Construction, Xiangyu Wang and Martijn Truijens and Lei Hou and Ying Wang and Ying Zhou *"Integrating Augmented Reality with Building Information Modeling: Onsite construction process controlling for liquefied natural gas industry"*, http://www.sciencedirect.com, 2014.

[6] Automation in Construction, Chu, Michael and Matthews, Jane and Love, Peter E.D. *"Integrating mobile Building Information Modelling and Augmented Reality systems: An experimental study"*, http://www.sciencedirect.com, 2017.

TECHNOLOGICAL SOLUTIONS AND THEIR DETERMINING FACTORS IN SEALING WOODEN GRANARY IN SOUTH CHINA

Shuyin Dong

Vienna University of Technology, Faculty for Architecture and Planning

INTRODUCTION

Being one of the most easily accessible natural material, wood was generally used by farmers for building their granaries in the pre-industrial society. However, the wood shrinkage was an inevitable problem which carpenters needed to deal with in the granary construction. It would lead to that gaps occurs in walls and floor of the wooden granary, thus causes loss of cereals.

Investigations carried on the building crafts of wooden granaries in several different ethnic areas of South China shows that carpenters from different cultural backgrounds developed a diversity of special technological solutions in sealing local granaries, aiming at ensuring the sealing performance of a granary. The further study tries to reveal various determining factors in shaping a building technology.

RESEARCH

Granaries are essential building types in the Chinese society that were based on agriculture up to the middle of the 20th century. Due to the unique requirements of storing grain, the craft of granary construction has been developed into a type of specialized building technologies in many cultural regions in the pre-industrialized period. So it is with China. However, the traditional building technology of Chinese granaries is long-ignored in the academic field.

This article would focus on an inconspicuous but essential technical detail of the wooden granary: the sealing treatment. The sealing treatment is directly related to the wooden shrinkage problem, thus many carpenters began to consider it since logging. Meanwhile, a variety of special joints had been created for solving this problem in different regions.

The following examples are selected for a further examination in the article. Based on a series of first-hand measurements and oral interviews with local carpenters, this section aims to provide information about the different sealing treatments under different building traditions in these ethnic groups' areas of South China.

1) A Tibetan granary in Sha'er Zhong, Sichuan. It is a log construction granary embedded in a tower dwellings. For ensuring the sealing of this granary, locals made the granary as a load-bearing structure.

2) A Wa granary in Wending, Yunan. Limited by their primitive tools, the wooden components produced by locals were mostly small and irregular. Thus local carpenters invented a special paneling method to enclose their granaries.

3) A Dong granary in Dengcen, Guizhou. Local carpenters carefully designed a series of construction procedure to ensure the sealing of the granary.

4) A Hmong granary in Dongmen, Guizhou. A special movable joint was invented for meeting the sealing requirement of the granary.

CONCLUSION

This study aims to reveal these unique building technologies of wooden granaries through refined measurements, utilization records and precise studies of details typical and unique to the respective building type. Based on the study of the local environmental and societal factors and interviews with local carpenters, the study further indicates that determining factors in shaping the wooden building technology of sealing are not only carpentry tools and tree species, but local society background and climate as well.

REFERENCE

[1] Herrle, P.(2017).Tibetan Houses: Vernacular Architecture of the Himalayas and Environs.

[2] Ryser,M.(1997). Osttibetische Bauernhäuser in ihrer Umgebung. Überblick über die tibetischen Siedlungs- und Wohnformen in einem Teilgebiet der chinesischen Provinz Sichuan.

[3] Zwerger,K.(2013).Die Architektur der Dong.

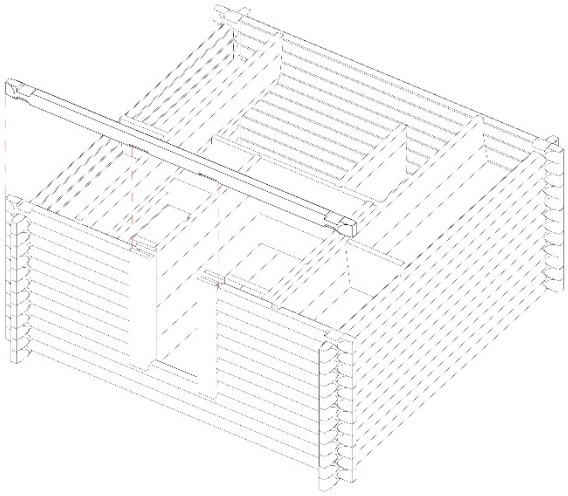

Image of the Tibetan log granary

Research Field *Catalysis*

Chairs and Reviewers:

Parkinson, Gareth
Associate Prof.

E134 - Institute of Applied Physics
gareth.parkinson@tuwien.ac.at

Rudroff, Florian
Assistant Prof. Dipl.-Ing. Dr.techn.

E163 - Institute of Applied Synthetic Chemistry
florian.rudroff@tuwien.ac.at

Introduction

Catalysis pervades the global economy and plays a central role in the production of fuels, chemicals, plastics, foods, and pharmaceuticals. While the catalyst industry is worth some $15 billion annually, the total value of products reliant on at least one catalysed reaction exceeds $15,000 billion per annum. This extremely large number is difficult to comprehend, and it is perhaps easier to appreciate the importance of catalysis when we know that ≈80% of everything produced, anywhere in the world, undergoes at least one catalysed step in its manufacture. Even minor improvements in catalytic performance have major cost saving implications, and developing more energy efficient, greener catalysts is a major challenge for the scientific community in these times of dwindling natural resources and heightened environmental concerns. As we transition from our reliance on fossil fuels to a future based on renewable energy, the importance of photo-, electro-, metal-, organo-, and biocatalysis will continue to grow as many energy capture and storage technologies involve the conversion of renewable energy sources into chemical energy.

One of the major challenges today is that the best catalysts always tend to be expensive, they lack operational stability, are often unselective and accessibility is limited. A good catalyst is cheap, highly active and can be reused as many times as possible. Furthermore, it would be appreciable if a novel catalyst for a given reaction can be rationally designed, based on fundamental understanding of their mechanism to avoid tedious experimental work like the classical trial and error approach.

For example, in metal catalysis many catalysts are composed of rare and expensive metals like platinum and iridium. It would be advantageous if we could discover new catalysts based on earth abundant materials. In biocatalysis, the production, isolation and purification of an enzyme is quite elaborate and waste intensive. Furthermore, the operational space is rather limited to a small set of reaction conditions.

This symposium covers all catalysis research performed at TU Wien. At one end of the research spectrum, there are those very close to industrial applications fighting to achieve vital improvements in activity and selectivity, and at the other end, there is much fundamental research into how materials interact with reactants at the atomic scale. Today, theory is more and more involved in discovering mechanisms in catalysis, and there is an increasing attempt to screen potential catalysts for important reactions computationally. By its very nature, catalysis sits at the border of physics and chemistry, and addresses the Computational Science, Materials and Matter, and Energy and Environment focus areas. As such, we welcome and invite contributions from diverse research fields and all Faculties at TU Wien involved in catalysis research.

ACTIVITY AND STABILITY IMPROVEMENT OF CYCLOHEXANONE MONOOXYGENASE BY PROTEIN ENGINEERING

Hamid R. Mansouri[a], Leticia Christina P. Goncalves[a], Andreas S. Bommarius[b], Saima Feroz[c], Florian Rudroff[a] and Marko D. Mihovilovic[a]

[a] E163, Institute of Applied Synthetic Chemistry, TU WIEN
[b] Georgia Institute of Technology, Atlanta, United State of America
[c] COMSATS Institute of Information Technology, Islamabad, Pakistan
hamid.khosravi@tuwien.ac.at

INTRODUCTION

Among the great number of flavin-dependent monooxygenases, Baeyer–Villiger monooxygenases (BVMOs) have been studied most for their application as a biocatalyst. These interesting biocatalysts are capable of oxidizing carbonyl atoms into the corresponding esters or lactones[1] and performing heteroatom oxidation reactions, like sulfoxidations. BVMOs usually exhibit high chemo-, regio- and/or enantioselectivity while converting a wide variety of substrates. The prototype BVMO, cyclohexanone monooxygenase (CHMO) is a promising biocatalyst for industrial reactions owing to its broad substrate spectrum and the excellent stereoselectivity. However, the low stability of BVMOs in general and especially for CHMO is an obstacle for their exploitation in industry. [2,3] This unmet need is the main objective of this study.

EXPERIMENTS

Cyclohexanone monooxygenase (CHMO) originating from *Acinetobacter* NCIB 9871 as a prototype BVMO was chosen for this study. To improve the thermostability of $CHMO_{Acinteo}$, we have used a data-driven protein design method that requires fewer homologous sequences than the traditional consensus approach and utilizes structural information to limit the number of variants created. [4] After choosing the residues for mutagenesis, site-directed mutagenesis method has been performed to implement the mutations. The library of mutants has been examined for their characteristics, especially the thermal stability, melting temperature, and activity. After creating the first library with single point mutations, the best variants were determined. To boost the effect of the mutation, the best single point mutations were combined and a new series of mutants created which contained more than one mutation. We also did implement the literature known mutation in our new library. The overview of the experimental part can be seen in figure 1.

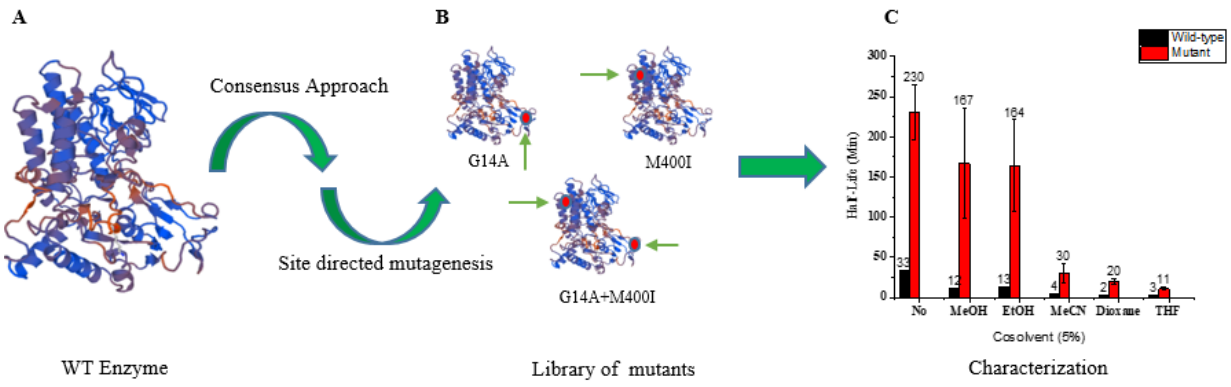

Figure 1. Overview of the study. A; the enzyme of interest was chosen. B; the predicted mutations based on the consensus approach have been implemented in the enzyme sequence, the variants with the combination of mutations created. C; the enzyme characteristic like organic solvent tolerance, half-life time and activity have been determined.

RESULTS AND DISCUSSION

The combination of single point mutations gave rise to a library of 14 mutants. Then, activity, melting temperature, and thermostability for all mutants have been evaluated. We have found several single point mutants with increased activity and thermodynamic stability. After the combination of improved variants, we ended up with a mutant (S2), composed of 7 single point mutations, which showed about 40% higher activity, 2-fold enhanced thermostability and 2°C increase in the melting temperature than the wild-type. S2 as the best variant was used for another round of mutation. The literature known mutations were combined with S2 and lead us to 6 new variants. These new variants examined for their characteristic. There was an increase in melting temperature and thermal stability in all mutants. The new mutants showed either the same or even higher activity in comparison to wildtype. S8 showed the highest improvement in the case of melting temperature by 5 °C and S7 showed the highest thermal stability by more than 8 fold improvement.

CONCLUSION

We successfully prepared a semi-rational library of CHMO mutants. The improvement in activity, thermostability and also melting temperature achieved with the used method. We can conclude that the consensus approach would be an efficient method to predict the mutations and can be used for further studies in the family of BVMOs. This study also can help us to determine the residues which can be important for the stability of this class of enzyme.

REFERENCES

[1] H. Leisch, K. Morley, P. C. K. Lau. Chemical Reviews, 4165-4222, 2011.

[2] U. Bornscheuer, G. Huisman, R. Kazlauskas, S. Lutz, J. Moore, K. Robins. Nature, 185– 194, 2012.

[3] L. Goncalves, D. Kracher, S. Milker, F. Rudroff, M. J. Fink, R. Ludwig, A. Bommarius, M. Mihovilovic. Advanced Synthesis & Catalysis, 2121-2131, 2017.

[4] K. M. Polizzi, J. F. Chaparro-Riggers, E. Vazquez-Figueroa,A.S. Bommarius. Biotechnology Journal , 531-536, 2006.

ATOMIC INSIGHT INTO THE ADSORPTION OF MOLECULAR O_2 ON THE RUTILE TiO_2(110) (1X1) SURFACE

Igor Sokolović[a], Michele Reticcioli[b], Martin Čalkovský[a], Cesare Franchini[b], Michael Schmid[a], Ulrike Diebold[a], Martin Setvin[a]

[a]E134 - Institute of Applied Physics, TU Wien
[b]Center for Computational Materials Science, Faculty of Physics, University of Vienna, Vienna, Austria

INTRODUCTION

Transition metal oxides attract significant research attention due to their various application possibilities and intriguing phenomena at their surfaces [1, 2]. Rutile TiO_2 is considered a prototypical example of this class of materials and its (110) facet is the most studied transition metal-oxide surface up to date [1]. It attracts attention for its possible applications in photocatalysis [3], photochemical solar cells [4], memsistors [5] and a transparent conductors [6].

The use of local-probe techniques in a controlled environment of ultra-high vacuum (UHV), together with quantum-mechanical simulations, is a well-established approach for resolving fundamental questions related to the applications. This research focuses on the interaction of O_2 molecules with the reduced rutile TiO_2(110) surface; a long-standing question on this material, which still does not have a widely-accepted solution [7].

EXAMINATIONS

We employed the non-contact atomic force microscopy (AFM) as a non-intrusive local technique. The AFM, in constant height imaging mode, provides atomic resolution as can be seen in panels (a-b) of the Figure. The Figure clearly shows the as-adsorbed molecular oxygen with atomic resolution, together with the rows of bridging oxygen atoms (with some bridging oxygen vacancies) characteristic for this surface. The theoretical treatment utilizes U-corrected density functional theory (DFT). The precise ground state of the clean, reduced surface, was determined in previous studies [8,9] and can be seen in the panel (c) of the Figure. It is characterized by the presence of electronic small polarons induced by the presence of electron-donating bridging oxygen vacancy. This theoretical approach enables us to non-ambiguously determine the charge associated with each of the adsorbed molecular species, illustrated in panel (d) of the Figure.

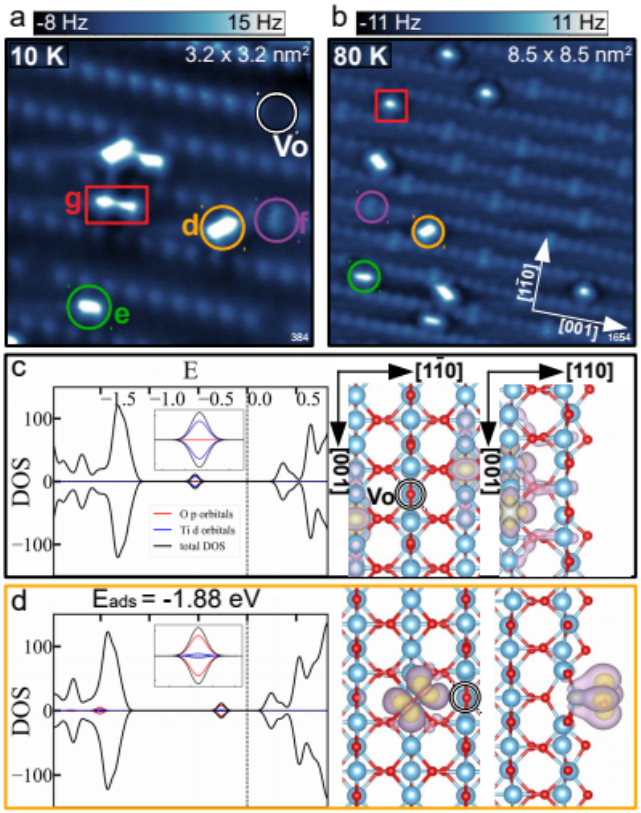

Adsorption of molecular O_2 to the reduced rutile TiO_2 (110) surface: (a,b) constant-height AFM images of the surface exposed to O_2 (c,d) DFT calculations of the adsorption showing charge transfer to the adsorbed O_2.

RESULTS AND DISCUSSION

The O_2 molecules adsorb to the reduced TiO_2 (110) surface in three molecular configurations below 100 K: one type of O_2 molecule filling the oxygen vacancy and two types of O_2 molecules adsorbed on Ti_{5c} sites. All the adsorbed O_2 are predicted by the DFT+U to have undergone a charge transfer from the polaron-hosting Ti_{6c} sites, making them chemisorbed (ionosorbed) in the peroxo form. The chemisorbed character of the molecules is confirmed by their presence on the surface after annealing up to room temperature. The increase in temperature also reveals dissociation channels. As already indicated by a STM study [10], we find that the application of bias voltage between the sample and the tip also dissociates the adsorbed O_2, which explains the current ambiguities in the literature and highlights the importance of nc-AFM in this research. The assignment of the calculated properties of the adsorbed O_2 to the experimentally observed ones is further confirmed by comparing the measured and calculated force-distance curves. This procedure, in particular, supports the adsorbed O_2^{2-} charge assignment, a long-standing discussion in the literature. The effect of UV light on the adsorbed molecules is investigated, and the possible reaction pathways are observed.

CONCLUSION

This research unambiguously identified the adsorption configurations of molecular O_2 on the reduced rutile TiO_2 (110) surface, and determined all the adsorbed species to be chemisorbed with two excess electrons O_2^{2-}. The methodology used in this research can be applied to adsorption studies of other gases on this surface [11], and to other reducible transition-metal oxide surfaces.

REFERENCES

[1] Diebold U., *Surface Science Reports* 48, 53 (2003).

[2] Fujishima A., Zhang X., and Tryk D. A., *Surface Science Reports* 63, 515 (2008).

[3] Henderson M.A., *Surface Science Reports* 66, 185 (2011).

[4] Linsebigler, A.L., Lu, G. and Yates Jr, J.T., *Chemical Reviews* 95, 735 (1995)

[5] Szot, K., Rogala, M., Speier, W., Klusek, Z., Besmehn, A., and Waser, R., *Nanotechnology* 22, 254001 (2011).

[6] Furubayashi, Y., Hitosugi, T., Yamamoto, Y., Inaba, K., Kinoda, G., Hirose, Y., Shimada, T. and Hasegawa, T., *Applied Physics Letters* 86, 252101 (2005).

[7] Henderson, M.A. and Lyubinetsky, I., *Chemical Reviews* 113, 4428 (2013).

[8] Setvin, M., Franchini, C., Hao, X., Schmid, M., Janotti, A., Kaltak, M., Van de Walle, C.G., Kresse, G. and Diebold, U., *Physical Review Letters* 113, 086402 (2014).

[9] Reticcioli, M., Setvin, M., Schmid, M., Diebold, U., and Franchini, C. , *Physical Review B* 98, 045306 (2018).

[10] Scheiber, P., Riss, A., Schmid, M., Varga, P. and Diebold, U., *Physical Review Letters* 105, 216101 (2010).

[11] Reticcioli, M., Sokolović, I., Schmid, M., Diebold, U., Setvin, M. and Franchini, C., *Physical Review Letters* 122, 016805 (2019).

CHIRAL Au NANOCLUSTERS - A STEP TOWARDS HETEROGENEOUS ASYMMETRIC CATALYSIS

Vera Truttmann, Noelia Barrabés*, Günther Rupprechter

E165 - Institute of Materials Chemistry

INTRODUCTION AND MOTIVATION

Monolayer protected Au nanoclusters (NCs) usually consist of less than 100 metal atoms stabilized by organic ligands. Unlike nanoparticles, they can be synthesized with atomic precision, leading to monodisperse clusters of specific size, structure and properties [1]. Therefore, these clusters are perfect materials to be applied in catalysis, in particular to study structure-activity relationships.

For some Au nanoclusters, existence of intrinsic structural chirality has been reported. Besides, the chirality can also be introduced to previously achiral clusters by binding of chiral protecting ligands [1]. Thus, combining this with the possibility to obtain atomically defined structures, chiral Au nanoclusters are ideal candidates as catalysts in asymmetric catalysis. This research area is currently dominated by homogeneous catalysis featuring mainly chiral coordination complexes. However, moving towards heterogeneous systems would yield several benefits, e.g. concerning catalyst stability, separation or recyclability.

We therefore aim to find a suitable strategy for preparing chiral Au nanocluster surfaces. As shown in Figure 1, there are two different routes possible: (1) deposition of chiral Au nanoclusters on suitable support materials or (2) supporting of precursor clusters and introducing of chirality by ligand exchange on the surface with chiral ligands. In both cases, prior investigations must be carried out: To pursue pathway (1), the chiral clusters must first be synthesized and thoroughly characterized in solution; for (2), the feasibility of ligand exchange on a surface must be determined. Within this work, we therefore want to present our first steps towards well-defined supported chiral Au NCs, investigating the accessibility of both routes.

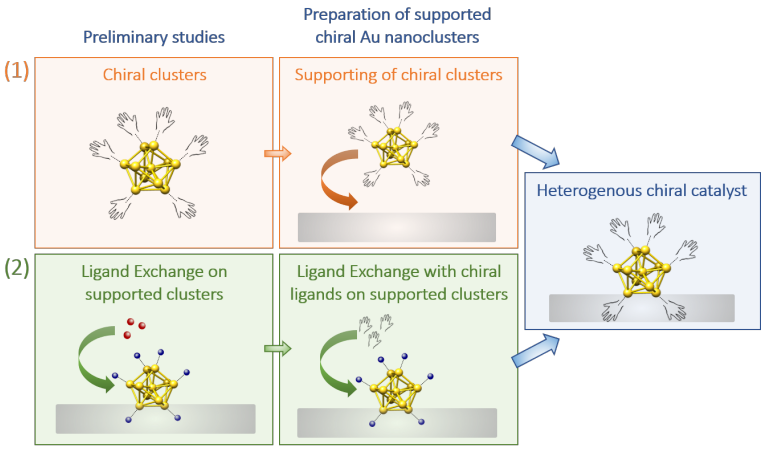

Figure 1: Strategies for obtaining chiral Au nanocluster surfaces

EXPERIMENTAL

The Au nanoclusters in this study were prepared by modified Brust procedures [2]. For the preparation of chiral clusters, different cluster sizes and geometries (Au_{11}, Au_{25} and biicosahedral Au_{25}) and chiral ligands (thiols and phosphines; mono- and bidentate) were used. Thorough analysis was performed (UV-Vis, MS, NMR, IR, elemental analysis, stability tests), with special emphasis on probing the chiral properties by (vibrational) circular dichroism ((V)CD) spectroscopy.

For the ligand exchange-on-surfaces approach (2), the model reaction of Au_{11} and two different thiols (L-glutathione (GSH) and 2-phenylethanethiol (2-PET)), which is well documented in liquid

phase [3,4], was chosen. Therefore, the $Au_{11}(PPh_3)_7X_3$ clusters were supported on Al_2O_3 and SiO_2 and then exposed to solutions of the thiol exchange ligands. The samples before and after reaction were analyzed by several techniques, including PM-IRRAS, STEM, EXAFS, ss-NMR and DRS.

RESULTS AND DISCUSSION

All synthesized Au nanoclusters with chiral ligands showed signals in CD spectroscopy, proving the chirality of the system. However, the signal intensities differed strongly depending on the specific cluster-ligand system. In general, higher degree of chirality transfer from the ligands to the whole cluster structure could be achieved using bidentate chiral ligands. This is mainly confirmed by the fact that these clusters do not only exhibit a CD signal in areas where the chiral ligands are absorbing, but also in the higher-wavelength areas of Au nanocluster HOMO-LUMO transitions. In addition, these clusters are also generally more stable, which makes them ideal candidates for the following catalytic tests and supporting experiments.

As is shown in Figure 2, very interesting data could be obtained for the ligand exchange on surfaces: Contrary to the same reaction in solution, when the cluster size is increasing from Au_{11} to Au_{25} regardless of the chemical nature of the exchange thiol [3,4], the supported Au_{11} preserved its small core size when reacted with GSH. However, the samples reacted with 2-PET showed alterations of the cluster structure, which are related to etching and decomposition processes. Moreover, the presence of thiolates in all reacted samples could be confirmed by PM-IRRAS and elemental analysis (LA-ICP-MS, ICP-OES), indicating at least partial ligand exchange [5].

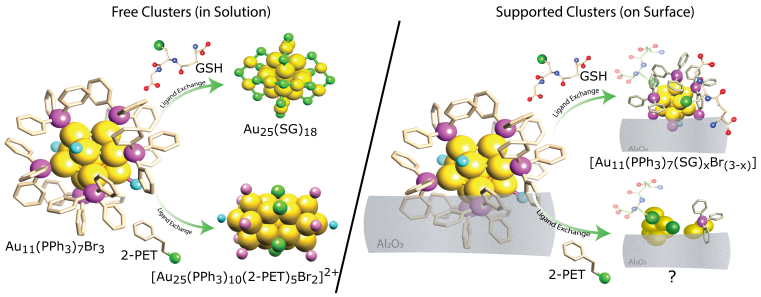

Figure 2: Ligand exchange of Au_{11} in solution vs. on a surface

CONCLUSIONS

In our work, we aim to obtain supported chiral Au nanoclusters for application in heterogeneous catalysis. We thereby focused on two different routes for their preparation and approached them by performing necessary preliminary studies. For the supporting approach (1), we managed to synthesize and characterize a set of chiral clusters, whose most promising candidates will be selected for catalytic testing and supporting. In addition, we were able to prove the feasibility of ligand exchange on surfaces (2) by studies on an Au_{11}-thiol model system. However, to apply this as a general synthesis tool, further tests and refinement of the method will be necessary.

REFERENCES

[1] R. Jin, C. Zeng, M. Zhou and Y. Chen; Chem. Rev., 116 (18), 10364-10413, 2016.

[2] M. Brust, M. Walker, D. Bethell, D. J. Shiffrin and R. Whyman; J. Chem. Soc., Chem. Commun.., 0 (7), 801-802, 1994.

[3] L. C. McKenzie, T. O. Zaikova and J. E. Hutchison; J. Am. Chem. Soc., 136 (38), 13426-13435, 2014.

[4] Y. Shichibu, Y. Negishi, T. Watanabe, N. K. Chaki, H. Kawaguchi and T. Tsukuda; J. Phys. Chem. C, 111 (22), 7845-7847, 2007.

[5] V. Truttmann, I. Illes, A. Limbeck, E. Pittenauer, M. Stöger-Pollach, G. Allmaier, T. Bürgi, N. Barrabés, and G. Rupprechter; To be submitted.

NANOPARTICLE EXSOLUTION: ENHANCING CATALYST REACTIVITY UNDER REACTION CONDITIONS

Lorenz Lindenthal[a], Janko Popovic[a], Johannes Raschhofer[a], Raffael Rameshan[a], Andreas Nenning[b], Alexander Karl Opitz[b], Christoph Rameshan[a,*]

[a]E165 - Institute of Materials Chemistry
[b]E164 - Institute of Chemical Technologies and Analytics

INTRODUCTION

In heterogeneous catalysis surfaces decorated with uniformly dispersed, catalytically highly active (nano)particles are a key requirement for excellent performance. Besides the standard catalyst preparation routines, e.g. impregnation or precipitation, with limitations in terms of controlling exactly the desired catalyst structure (i.e. particle size distribution or dispersion of nanoparticles), we present here an innovative, time efficient route to exactly tailor the catalyst surface directly under reaction conditions.

Perovskite-type oxides are a large class of materials with many interesting properties. Their general chemical formula is ABO_3, the possibility of choosing different elements for the cations and of doping either of the sites allows to adjust these properties and makes them highly versatile.

An emerging concept in catalyst design, and the scope of our ERC project, is to selectively and reversibly tune and modify the surface chemistry/structure of Perovskite-type catalysts by electrochemical polarisation in operando[1]. The catalysts can incorporate catalytically highly active elements, either as a main component or as dopants. Upon electrochemical polarisation (applying voltage to the system), these elements emerge from the oxide lattice to form catalytically active clusters or nanoparticles on the surface (by exsolution), figure 1. In consequence, this leads to a strong modification or enhancement of catalytic selectivity and activity.

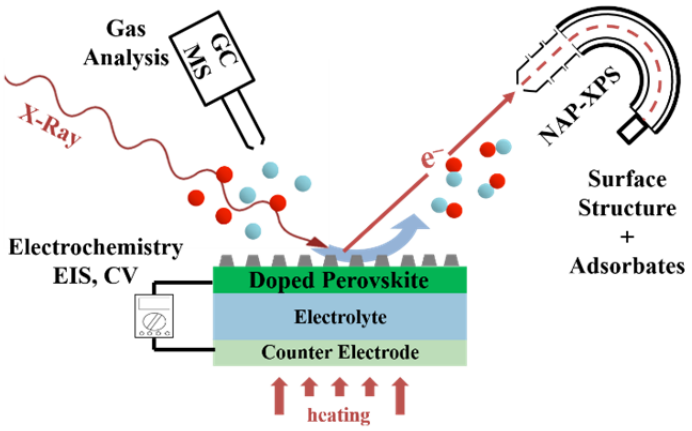

Figure 1: Setup for operando measurements

EXPERIMENTAL

Different perovskite materials were prepared via a modified Pecchini method[2]. Structural characterization was done by (in situ) XRD, XPS and SEM. Catalytic testing was performed in a custom made tubular flow reactor with gas analysis by micro GC and MS. We investigated the water-gas shift reaction (WGS) and the reverse WGS (rWGS). For experiments with electrochemical polarization, electrochemical cells (figure 1) were prepared by depositing electrodes on (100)-oriented 9.5 mol % yttria-stabilized zirconia (YSZ) single crystals using pulsed laser deposition. With these cells, we performed in-situ NAP-XPS experiments for direct correlation (simultaneous experiments) of surface chemistry with catalytic activity, selectivity and the applied polarization, using our lab based in-situ NAP-XPS system.

RESULTS

For the newly synthesized perovskite materials, we could show by in-situ XRD and SEM the formation of nanoparticles on the surface (by exsolution) under reducing conditions, figure 2. The different perovskites were compared with respect to their reduction behaviour. We found that a doping with Co facilitates the exsolution process.

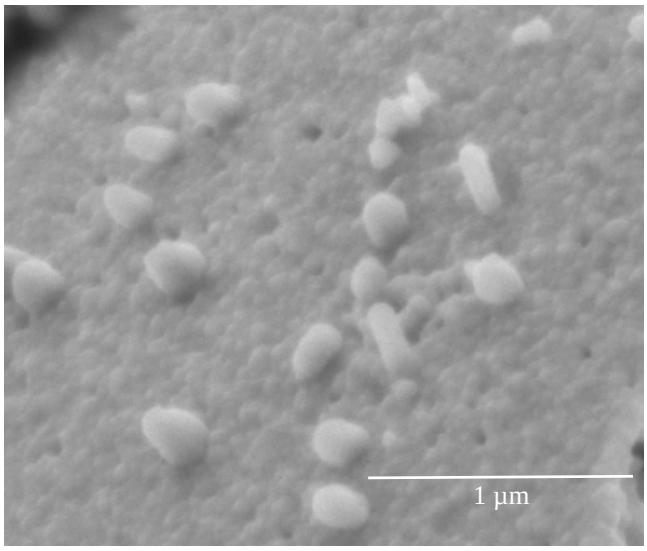

Figure 2: SEM after Fe nanoparticle exsolution from $Nd_{0.9}Ca_{0.1}FeO_3$

On the other hand, we compared the catalytic performance of the various perovskites for WGS and rWGS. The catalyst doped with Co had a significantly higher catalytic activity for rWGS than all the other materials. This is due to the fact, that it is the only catalyst where exsolution is possible under the chosen reaction conditions. The exsoluted nanoparticles consist of catalytically active elements and have a large surface area, thus greatly enhancing the performance of the catalyst. We confirmed nanoparticle formation from the Co doped catalyst during rWGS by operando XRD experiments and SEM.

CONCLUSION

The structural changes when exsolution occurs have a great impact on catalytic reactivity. Therefore, our goal is a deeper understanding of the process and the ability to control it accurately. This enables the precise tuning of the catalyst surface and thereby the regulation of the catalytic behaviour. A thorough investigation of the exsolution process is possible with our in-situ NAP-XPS system.

ACKNOWLEDGEMENT

This project has received funding from the European Research Council (ERC) under the European Union's Horizon 2020 research and innovation programme (grant agreement n° 755744 / ERC - Starting Grant TUCAS).

REFERENCES

[1] Mao, X. W.; Tian, W. D.; Wu, J.; Rutledge, G. C.; Hatton, T. A., Journal of the American Chemical Society 2015, 137 (3), 1348-1355.

[2] Pechini, M. P., Method of Preparing Lead and Alkaline Earth Titanates and Niobates and Coating Method Using the Same to Form a Capacitor, U.S. Patent 3.330.697, July 11th, 1967

SURFACE SCIENCE STUDIES OF Li AND Co_3O_4(111) THIN FILMS

Thomas Haunold, Christoph Rameshan, Günther Rupprechter

E165 Institute of Materials Chemistry

INTRODUCTION

Over the past decades, cobalt oxides have served as inexpensive key materials for many applications. These range from heterogeneous catalysis of important oxidizing reactions (e.g. low-temperature CO oxidation[1, 2], preferential oxidation of CO (PROX)[3-5], Ostwald synthesis of nitric acid by oxidation of ammonia[6], and oxidation of hydrocarbons[1, 7]), to the Fischer-Tropsch synthesis of hydrocarbons and liquid fuels[8], and the conversion of volatile organic compounds (VCOs)[9]. Recently, Co_3O_4 has also been investigated as potential anode material for Li ion batteries (LIBs)[10, 11], featuring high theoretical discharge capacities. However, the formation of a solid electrolyte interface (SEI) competes with reversible Li^+ ion intercalation and thus reduces the capacity of LIBs[12]. A similar behavior is observed in solid-state batteries where metallic Li anodes are used.

EXPERIMENTAL

The most effective approach to explain and improve the functionality of cobalt oxides is to conduct experiments at a microscopic or even atomic level. This can be achieved by preparation and study of model-systems. Therefore, Co_3O_4 and Li thin films were prepared by physical vapor deposition (PVD) under ultrahigh vacuum (UHV) conditions. Film growth was monitored visually in real-time using low energy electron microscopy (LEEM). Afterwards, thin film characterization was carried out by X-ray photoelectron spectroscopy (XPS), low energy electron diffraction (LEED) and temperature-programmed desorption (TPD).

RESULTS AND CONCLUSION

The catalytic activity of Co_3O_4(111) thin films was investigated under working conditions using CO oxidation as test reaction. Experiments were performed within a flow reactor supplying a stoichiometric mixture of reactants ($CO:O_2$ = 2:1) at mbar pressure while the catalyst was heated stepwise over a wide temperature range. Product (CO_2) formation was observed *via* mass spectrometer (MS), starting at roughly 200 °C, which agrees well with previous results reported in the literature[13]. Regardless of morphology (cobalt oxide thin films, powders, nanorods), the stability of the Co_3O_4 phase, particularly the presence of Co^{3+} at the surface, defines the temperature window of catalytic activity. Moisture (even trace amounts) in the feed led to a decrease of CO conversion due to water dissociation (formation of hydroxyl groups) and blocking of active sites. However, this deactivation process is reversible upon heating to higher temperatures.

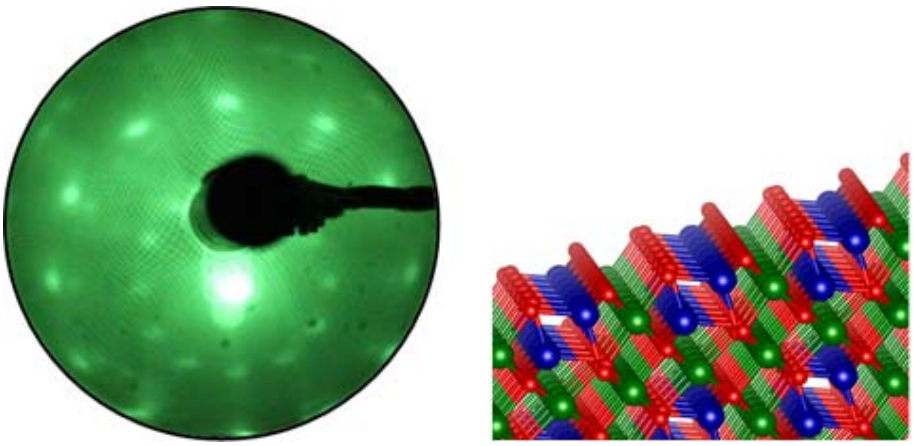

Figure 1: LEED pattern of Co_3O_4(111) (left) and surface structure (right; red: O^{2-}, blue: Co^{2+} and green: Co^{3+})

ACKNOWLEDGMENTS

This work was supported by the Austrian Science Fund (FWF) through the international DACH program I 1041-N28 (COMCAT) and project SFB FOXSI (F4502-N16).

REFERENCES

[1] Y. F. Y. Yao, *Journal of Catalysis 33.1*, (**1974**) 108-122
[2] X. Xie, Y. Li, Z.-Q. Liu, M. Haruta, W. Shen, W., *Nature: 458*, (**2009**) 746-749
[3] G. Marbán, I. López, T. Valdés-Solís, A. B. Fuertes, *International Journal of Hydrogen Energy 33(22)*, (**2008**) 6687-6695
[4] L. Lukashuk, K. Föttinger, E. Kolar, C. Rameshan, D. Teschner, M. Hävecker, A. Knop-Gericke, N. Yigit, H. Li, E. McDermott, M. Stöger-Pollach, G. Rupprechter, *Journal of Catalysis 344*, (**2016**) 1-15
[5] L. Lukashuk, N. Yigit, R. Rameshan, E. Kolar, D. Teschner, M. Hävecker, A. Knop-Gericke, R. Schlögl, K. Föttinger, G. Rupprechter, *ACS Catal 8(9)*, (**2018**), 8630-8641
[6] K. Shojaee, B. S. Haynes, A. Montoya, *Applied Surface Science 316*, (**2014**) 355-365
[7] Z. Tian, N. Bahlawane, F. Qi, K. Kohse-Höinghaus, *Catalysis Communications 11(2)*, (**2009**) 118
[8] H. Oosterbeek, *Physical Chemistry Chemical Physics 9(27)*, (**2007**) 3570-3576.
[9] T. Garcia, S. Agouram, J. F. Sanchez-Royo, R. Murillo, A. M. Mastral, A. Aranda, I. Vazquez, A. Dejoz, B. Solsona, *Applied Catalysis a-General 386* (1-2), (**2010**) 16-27
[10] H. C: Liu, S. K. Yen, *Journal of Power Sources 166(2)*, (**2007**) 478-484
[11] Y. Dou, J. Xu, B. Ruan, Q. Liu, Y. Pan, Z. Sun, S. X. Dou, *Advanced Energy Materials 6(8)*, (**2016**) 1501835
[12] M. B. Pinson, M. Z. Bazant, *Journal of the Electrochemical Society 160(2)*, (**2013**) A243-A250
[13] Jansson, J.; Palmqvist, A. E. C.; Fridell, E.; Skoglundh, M.; Osterlund, L.; Thormahlen, P.; Langer, V., On the catalytic activity of Co3O4 in low-temperature CO oxidation. *Journal of Catalysis*, *211(2)*, (**2002**), 387-397

POLARIZATION-DEPENDENT SFG SPECTROSCOPY OF NEAR AMBIENT PRESSURE CO ADSORPTION ON Pt(111) AND Pd(111)

Xia Li, Matteo Roiaz, Verena Pramhaas, Christoph Rameshan, and Günther Rupprechter

E165-Institute of Materials Chemistry, TU Wien.

INTRODUCTION

For many years, the surface science approach to heterogeneous catalysis was restricted to gas pressures of 10^{-6} mbar and below, giving rise to the well-known "pressure gap" problem [1,2]. This limitation was overcome when surface-sensitive methods were developed that could be operated at least in the mbar pressure range. Sum frequency generation (SFG) vibrational spectroscopy has high surface sensitivity and selectivity, most importantly, it is non-destructive and without vacuum-limitation, which make it popular in the study of surface/interface sciences including the catalysis reactions. Polarization-dependent (PD-) SFG has been proven an excellent tool in providing the microscopic information of adsorbed molecules at interfaces, such as molecular structure, orientation, symmetry, chirality, and dynamics [3-5]. However, the detail analysis of CO on model catalysts (Pt(111) and Pd(111)) is still lack. This is because usually only one polarization-combinations (i.e. PPP) spectra could be measured before [6,7], resulting in the missing of the orientation information.

EXPERIMENTS

The experiments on Pt(111) and Pd(111) single crystals were performed in a new UHV surface analysis system equipped with an SFG-compatible UHV-high pressure cell [8]. Both Pt and Pd surfaces were cleaned by circles of Ar^+ ion bombardment (beam energy 1.3 keV at 5 x 10^{-6} mbar of Ar) at room temperature and subsequent annealing at 1200 K for 2 min. If necessary, oxidation in 1 x 10^{-6} mbar O_2 was used to remove carbon contamination. The surface structure of single crystal was examined by low energy electron diffraction (LEED). SFG was performed using a Nd:YAG (neodymium-doped yttrium aluminum garnet, Nd: $Y_3Al_5O_{12}$) fundamental radiation of a PL 2241 laser (EKSPLA, 1064 nm, 30 mJ/pulse), with a 20 ps pulse width and 50 Hz repetition rate. The visible beams (532 nm) and tunable IR beam (1000-4300 cm^{-1}) are spatially and temporally overlapped on the single crystal surface in a co-propagating geometry at an incidence angle of 58.5° (α_{Vis}) and 55° (α_{IR}) with respect to the surface normal, respectively. The polarization of visible beam and SFG signal can be switched between P and S using Glan-Taylor prism and a half-wave plate, while the IR polarization was kept as P because S-polarized field would be canceled on a metal surface [9].

RESULTS AND DISCUSSION

SSP and PPP spectra of near ambient pressure CO on Pt(111) at room temperature have been obtained, as shown in Fig. 1. However, no SSP signal of CO on Pd(111) was observed. Moreover, PPP signal of CO on Pd(111) was much smaller than on Pt(111) (Fig. 2a) [10]. Similar increase of SSP and PPP spectra with increasing CO pressure showed that the orientation of CO molecules on Pt(111) surface was independent of the gas pressure.

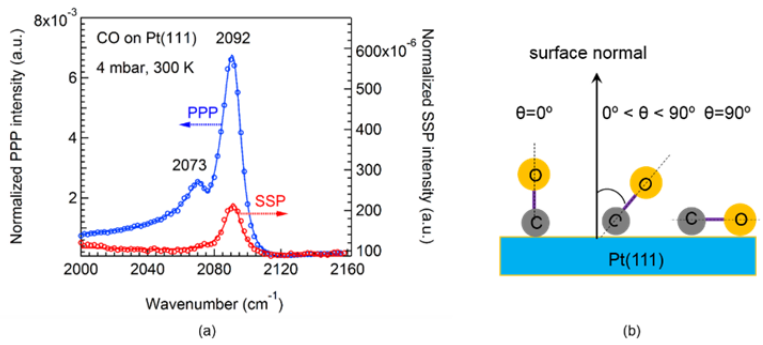

Fig. 1 Polarization-dependent SFG spectra of CO adsorption on Pt(111) at 4 mbar and 300 K. Symbols refer to experimental data. Blue circles: PPP polarization; Red circles: SSP polarization; Solid lines represent the global fitting curves with Lorentzian lineshapes. b Schematic diagram of tilt angles of CO on a Pt surface.

A modelling analysis of influences of incidence angles (α_{IR} and α_{Vis}) and refractive indices of substrates on the SFG intensity and orientation, as well as the relationship of SFG intensity, orientation and molecular hyperpolarizability ratio (R), has been discussed in detail (e.g. Fig. 2). Results showed that SFG spectral intensity is much more sensitive to α_{Vis} than α_{IR}. Based on a larger simulated I_{PPP}/I_{SSP} =48, and a smaller experimental PPP signal of CO on Pd(111), the effective surface number density of CO molecules should be smaller than that of CO on Pt(111) [10].

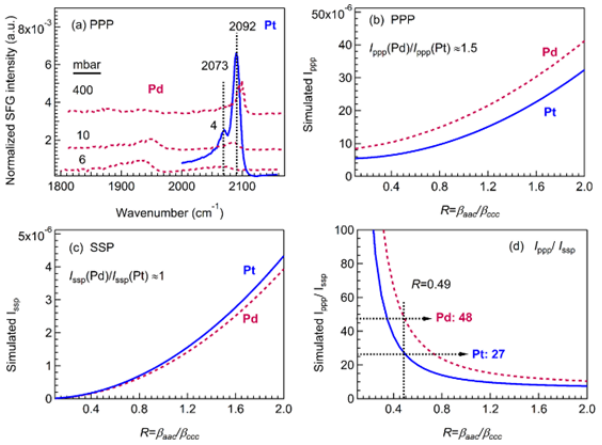

Fig. 2 Comparison of spectral intensity of on-top CO on Pd(111) and Pt(111). a. Experimental PPP spectra at 300 K, Ippp(Pd) < Ippp (Pt). Dark red: CO on Pd(111). Blue: CO on Pt(111): 4 mbar. b. Simulated Ippp versus R. c. Simulated Issp versus R. d. Ippp/Issp versus R. The following parameters were used in the simulation: ωIR = 2090 cm^{-1},α_{IR} = 55°; ω_{Vis} = 532 nm, α_{Vis} = 58.5°; Ns = 1, βccc = 1, and θ = 0°.

CONCLUSION

An exact value of molecular hyperpolarizability ratio of CO molecules, R=0.49 (assumed tilting angle of 0°), has been determined according to the polarization-dependent SFG spectra of CO on Pt(111) surface. Pressure-dependent SFG spectra on Pt(111) (10^{-4} to 36 mbar) did not indicate any orientation change of adsorbed CO. A proper experimental configuration (especially α_{Vis}) plays important role in measuring SSP and PPP spectra with good signal-to-noise ratio. Weaker PPP and non-SSP signals of CO on Pd(111) implied a smaller surface number density of ordered CO molecules.

REFERENCES

[1] G.A. Somorjai, G. Rupprechter, *J Chem Educ*, **1998**, 75, 162-176.
[2] G. Rupprechter, in: B. Gates, H. Knoezinger (Eds.), Advances in Catalysis, Academic Press, Cambridge, **2007**, 133-263.
[3] X. Li, G.H. Deng, R.J. Feng, K. Lin, Z. Zhang, Y. Bai, Z. Lu, Y. Guo, *Chinese Chem Lett*, **2016**, 27, 535-539.
[4] H.F. Wang, W. Gan, R. Lu, Y. Rao, B.H. Wu, *Int Rev Phys Chem*, **2005**, 24, 191-256.
[5] P. Galletto, H. Unterhalt, G. Rupprechter, *Chem Phys Lett*, **2003**, 367, 785-790.
[6] C. Klunker, M. Balden, S. Lehwald, W. Daum, *Surf Sci*, **1996**, 360, 104-111.
[7] B. Bourguignon, S. Carrez, B. Dragnea, H. Dubost, *Surf Sci*, **1998**, 418, 171-180.
[8] M. Roiaz, V. Pramhaas, X. Li, C. Rameshan, G. Rupprechter, *Rev Sci Instrum*, **2018**, 89.
[9] F.M. Hoffmann, *Surf Sci Rep*, **1983**, 3, 107-192.
[10] X. Li, M. Roiaz, V. Pramhaas, C. Rameshan, G. Rupprechter, *Top Catal*, **2018**, 61, 751-762.

HYDROGENATION OF CO_2 CATALYSED BY Cu AND Pd NANOPARTICLES SUPPORTED ON ZnO AND CARBON

Klaus Dobrezberger, Julian Stropp, Julie Neuhauser, Anna Aspalter, Martin Huber, Karin Föttinger, Günther Rupprechter

E165 - Institute of Materials Chemistry at TU Wien

INTRODUCTION

Cu/ZnO and Pd/ZnO nanoparticle catalysts have been widely studied for hydrogenations. In this work, ZnO supported Cu and Pd nanoparticle catalysts are used for CO_2 hydrogenation and the dependence on parameters such as temperature, pressure and reduction temperature were analyzed. Palladium is more active than copper and forms a PdZn phase at higher reaction temperatures. Alloying cannot be observed with copper. Sintering effects were observed by electron microscopy. Palladium initially has smaller particles than copper, but they sinter strongly. The long-term stability was also investigated and it was concluded that all catalysts have relatively good stability over the reaction time. At atmospheric pressure mainly CO was formed, whereas at a pressure of 20 bar also methane and traces of methanol were produced.

EXPERIMENTS / FUNDAMENTAL OF THE PROBLEM / EXAMINATIONS

The increased use of CO_2 to produce higher quality chemicals may be a future approach for recycling CO_2. Cu and Pd particles on different supports (oxides) can serve for this purpose, with ZnO being frequently used. Cu is often commercially applied but has the disadvantage that it oxidizes and is less catalytically active than palladium. Palladium, on the other hand, is expensive. Therefore, a way should be found to combine the positive aspects of both metals and to minimize their disadvantages. For this purpose, besides monometallic catalysts (Cu/ZnO, Pd/ZnO), bimetallic PdCu catalysts, in particular, were produced, characterized and kinetic tests were performed for the hydrogenation of CO_2 to various products [1], [2].

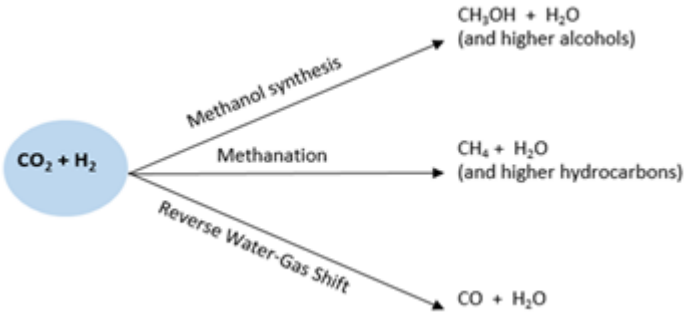

Figure 1. Main pathways for the hydrogenation of CO_2. These pathways are related to temperature, pressure and catalyst.

RESULTS AND DISCUSSION

The selectivity of the reaction depended on the reaction temperature, the pressure and the respective catalyst. Since CO_2 is a thermodynamically stable molecule, high temperatures but also the oxide are required for activation. The formation of PdZn alloys, which form in Pd/ZnO catalysts, also plays a role in the catalytic activity [3], [4]. It was found that at atmospheric pressure the palladium catalysts have a much higher catalytic activity than the copper nanoparticles. In contrast, no difference in activity could be observed at a pressure of 20 bar. Interestingly, the bimetallic PdCu catalysts are catalytically more active at 20 bar pressure than the monometallic Cu and Pd nanoparticles. Pressure is necessary for the production of methane gas. At atmospheric pressure, for example, no methane was formed, but at 20 bar the selectivity to methane increases. Measurements

have shown that pretreatment with hydrogen is not necessary for reactions at elevated pressures, which is of great industrial importance. Furthermore, Pd and Cu nanoparticles were also applied to graphene as support. Interestingly, even with these catalysts, there is an activity for CO_2 hydrogenation, although there is no oxide support.

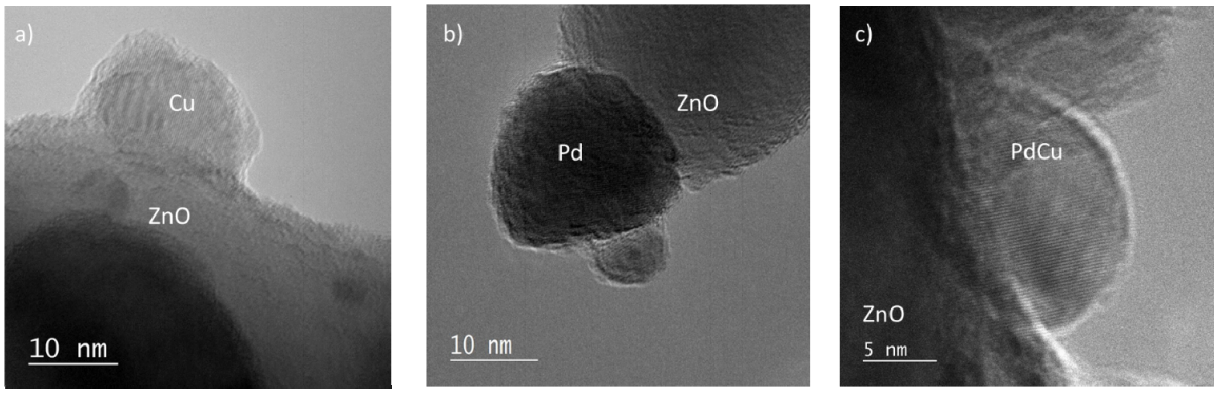

Figure 2. HR-TEM images of Cu/ZnO (a), Pd/ZnO (b) and PdCu/ZnO (c) nanoparticle catalysts

CONCLUSION

By combining different characterization methods the catalytic activity of monometallic and bimetallic copper and palladium nanoparticles supported on zinc oxide could be determined and the influence of the metal composition, the different synthesis methods and the behaviour of the particle distribution on catalysis could be investigated. These results can provide important insights into industrial applications (production of CO, CH_4 and CH_3OH), as it has been found that bimetallic catalysts actually provide higher catalytic activity than monometallic catalysts. Further spectroscopic measurements (especially in-situ) will be necessary for the future to complete the characterization.

ACKNOWLEDGEMENTS

Supported by the Austrian Science Fund (FWF) via Doctorate School Solids4Fun (W1243) and SFB FOXSI (F4502-N16).

REFERENCES

[1] X. Jiang, N. Koizumi, X. Guo, and C. Song, “Bimetallic Pd-Cu catalysts for selective CO_2 hydrogenation to methanol,” *Appl. Catal. B Environ.*, vol. 170–171, pp. 173–185, 2015.

[2] J. Díez-Ramírez, J. A. Díaz, P. Sánchez, and F. Dorado, “Optimization of the Pd/Cu ratio in Pd-Cu-Zn/SiC catalysts for the CO2hydrogenation to methanol at atmospheric pressure,” *J. CO2 Util.*, vol. 22, no. September, pp. 71–80, 2017.

[3] H. H. Holzapfel, A. Wolfbeisser, C. Rameshan, C. Weilach, and G. Rupprechter, “PdZn surface alloys as models of methanol steam reforming catalysts: Molecular studies by LEED, XPS, TPD and PM-IRAS,” *Top. Catal.*, vol. 57, no. 14, pp. 1218–1228, 2014.

[4] K. Föttinger and G. Rupprechter, “In situ spectroscopy of complex surface reactions on supported Pd-Zn, Pd-Ga, and Pd(Pt)-Cu nanoparticles,” *Acc. Chem. Res.*, vol. 47, no. 10, pp. 3071–3079, 2014.

HETEROGENIZATION OF MOLECULAR OXO/THIO METALATE CATALYSTS FOR SOLAR FUEL GENERATION

Sreejith P Nandan[a], Ashwene Rajagopal[b], Alexey Cherevan[a]*, Carsten Streb[b], Dominik Eder[a]*

[a] E165 Institute of Materials Chemistry, Technical University of Vienna, 1060 Vienna, Austria
[b] Institute of Inorganic Chemistry-1, Ulm University, 89081 Ulm, Germany

INTRODUCTION

One of the main challenges of today's society is the impending energy crisis, which is tightly linked to global warming and ever-increasing greenhouse gas emissions. A strong shift in our political and economic decisions is inevitable, as evidenced by the rapidly growing reliance on renewable energy sources and the corresponding research hype in the field of materials science. One solution for this issue is the concept of solar fuels that can be generated by means of photocatalytic (PC) water splitting and CO_2 reduction, both of which are highly demanding redox reactions that require a delicate design of the PC system (see Figure). To accomplish this multifaceted task, we propose a novel strategy that will complement the advantages of homogeneous and heterogeneous PC and eliminate the drawbacks.

Polyoxometalates (POMs) and polythiometalates (PTMs) have captured the attention of chemists and material scientists over the past decades with their structural and compositional tunability along with their functional properties [1]. POMs are basically molecular metal oxide clusters of early transition metals in their high-valent states, while PTMs are molecular metal sulphides that have recently emerged as 0D analogues to low-dimensional MoS_2 nanostructures. Both of them have been studied extensively as versatile catalysts for homogeneous reactions. Most recently, POM and PTM clusters triggered a lot of attention as first fully-inorganic homogeneous water oxidation and water reduction catalysts, respectively [2,3]. However, similar to other molecular photocatalysts (PCs), they [A] suffer from rapid self-aggregation that leads to the shielding of active sites. Besides, [B] almost all reported POM/PTM PC systems are not able to complete the light absorption and require the presence of a molecular photosensitizer such as $[Ru(bpy)_3]^{2+}$. These two issues pose a strong limitation hindering the development of the field and its commercialization.

OBEJCTIVES

In my Ph.D. project, I aim to address these challenges of *molecular PC* using an innovative approach that takes inspiration from *heterogeneous PC* and combines the advantages of both fields. I am currently on my second year and my project is entitled "Heterogenization of molecular oxo/thio metalate catalysts for solar fuel generation". Briefly, in my project I am wiring the catalytically relevant POM/PTM clusters to high-surface-area semiconducting substrates (shown in Figure) that are capable of complementing the light absorption step (Step 1 in Figure) of a PC process. Besides, we expect this POM/PTM heterogenization approach to provide a better accessibility of the active sites, along with preventing the catalytic species from deactivation.

RESULTS AND DISCUSSION

I have started my work by examining several PTM clusters that have recently been reported to be catalytically active towards HER in homogeneous phase (i.e. their molecular form). I first successfully synthesized various Mo-based PTMs (eg. $Na_2[Mo_3S_{13}]$ clusters) and performed

systematic studies on their electrostatic immobilization on TiO_2 nanoparticles (NPs) chosen here as a model photoactive substrate.

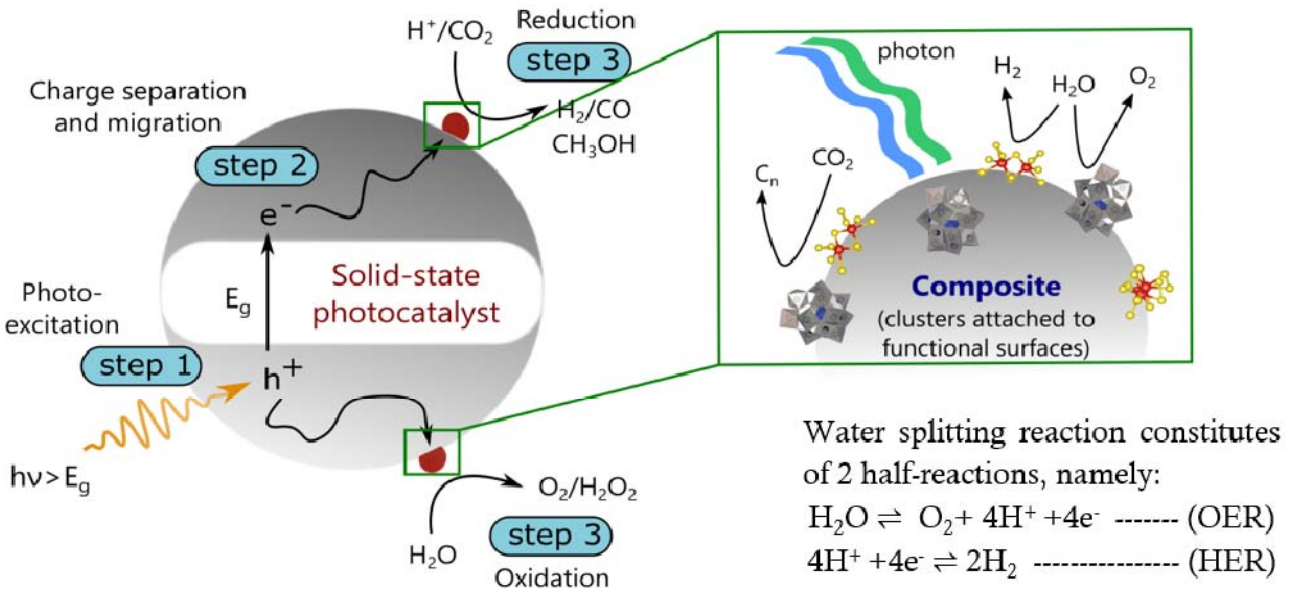

Figure 1: Schematic for heterogeneous photocatalysis and immobilization of the POM/PTM clusters on the surface (zoomed view)

I have carefully optimized immobilization protocols investigating attachment kinetics (how quick does the deposition occur) and loading degree (how much of the PTM can I put on the TiO_2 surface) as a function of solvent and PTM type. In this poster, I will demonstrate various HER experiments and the observation that the PTM-TiO_2 composites show an improved and stable activity towards HER over the benchmark reference TiO_2. These results confirm that fuctional properties of solid-state substrates (light absorption) and molecular compounds (catalytic activity) can be combined and even lead to synergistic functions (stabilization) demonstrating the feasibility of our approach. Most recently, I have started working on Co-based POMs for oxygen evolution reaction (OER) – necessary step for both CO_2 reduction and water splitting. Due to complex structure of these clusters, I am working on the development of novel attachment protocols to ensure formation of stable POM-substrate composites. I will also present a range of characterization techniques that we applied to study the resulting composites including SEM-EDX, XPS and ICP-OES.

CONCLUSION

Thus, electrostatic immobilization of POM/PTMs on TiO_2 nanoparticles have been accomplished and experimental data is shown on how efficiently these clusters can be utilized as co-catalysts in heterogeneous photocatalytic water splitting reactions. I will further work on (a) developing synthetic protocols for optimised immobilization of molecular oxo/thio clusters on photoactive substrates by covalent approach (b) conducting fundamental studies on interfacial processes and substrate effects, and (c) exploring their potential as high-performance PCs towards solar-to-fuel conversions

REFERENCES

[1] D. Long et al. Angew. Chem., 2010, 49, 1736
[2] Q. Yin et al. Science, 2010, 328, 342
[3] J. Kibsgaard et al. Nat. Chem., 2014, 6, 248

ON THE REACTIVITY OF $Au_n(SR)_m$ NANOCLUSTERS CATALYSTS: LIGAND, STRUCTURE AND SUPPORT EVOLUTION

Noelia Barrabés, Stephan Pollitt, Clara García, Vera Truttmann, Günther Rupprechter

E165 - Institute of Material Chemistry at TU Wien

INTRODUCTION

In nanocatalysis, a great challenge is to obtain truly homogenous and well-defined highly active nanostructures on surfaces. Ligand protected metal nanoclusters is an emerging class of functional nanomaterials consisting of less than 100 atoms, with atomic precision, well-defined molecular structure. These properties are also sensitive to the metal composition, which allows tuning properties by removing, adding or replacing (doping) one or more au atoms with heteroatoms. We successfully doped different cluster sizes by metal as Pd, Pt, Cu or Ag, producing bimetallic and trimetallic nanoclusters with atomic precision. Insights in the structural and properties changes were obtained by several spectroscopic studies (XAFS, XPS, MALDI…) correlated with DFT calculations[1, 2].

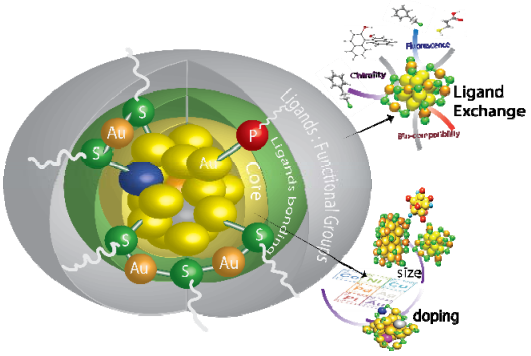

Figure 1: Scheme monolayer protected clusters and the possible route for fine-tunning of their properties (doping and ligand exchange)

Heterogeneous catalytic research of atomically precise gold nanoclusters is an emerging field opening new opportunities for accurate studies of size-dependent properties, atomic structure effects and reaction mechanisms in catalysis. An enhancement of the catalytic properties by metal nanoclusters has been observed, when compared to classical nanoparticles of similar size. By *in situ* spectroscopic techniques we study the influence of the cluster structure and support material in their stability and reactivity, during pretreatment and in different gas and liquid phase reactions

RESULTS AND DISCUSSION

Generally, the supported nanoclusters undergo ligand removal treatments, in order to increase the active surface accessible for reaction. We studied the structural changes of different atomic sizes of $Au_x(SC_2H_4Ph)_y$ (x=25,38 and 144) supported on various metal oxides (CeO_2, Al_2O_3 and SiO_2) upon thermal treatments and reaction conditions. *In situ* XAFS measurements revealed the strong influence of the cluster structure and support material in their stability.[3-5] Whereas high stability of the cluster is obtained with CeO_2 and SiO_2 supports, Al_2O_3 leads to an increase in particle size. These studies confirmed that the cluster core structure was stable upon deposition and post-treatment, but focused only on the Au kernel. However, the fate of the thiolates (ligands) during deposition of the clusters on an oxide support and post-treatments was not considered. Up to now, it was believed that the ligands of cluster catalysts

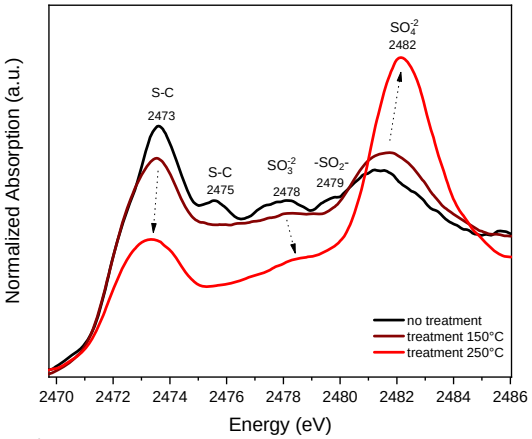

Figure 2: XANES spectra at S K-edge of Au_{38}/CeO_2 catalysts fresh and treated at 150°C and 250°C under oxygen atmosphere

"disappeared" (into the gas phase) upon activation. The field is in fact moving towards applications and many involve the deposition of clusters on solid surfaces (supports). This motivated us to study the fate of the thiolate ligands upon supporting clusters on surfaces. S K-edge measurements revealed for first time ligand migration from the gold clusters to the support, manifested by formation of unexpected oxidized sulfur species on the support.[3] The redistribution and oxidation of the ligands modified the support surface, a factor that may alter its properties.

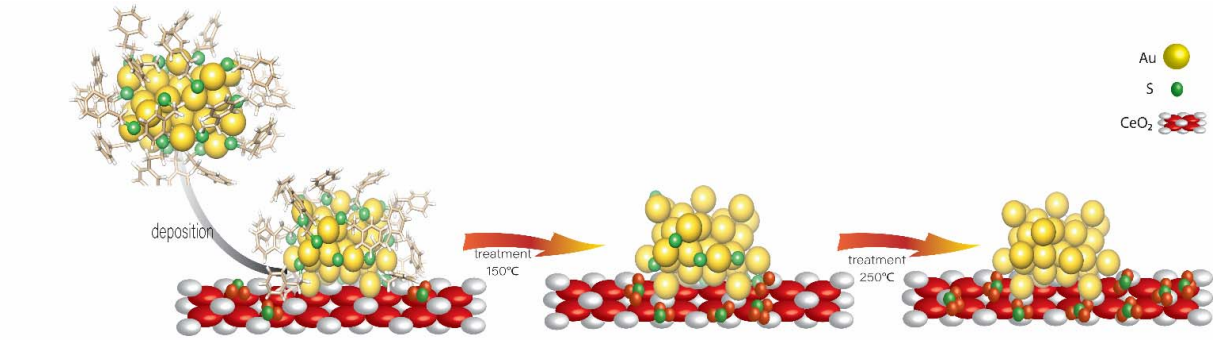

Figure 2. Scheme of thiolate ligands evolution upon cluster deposition on CeO_2 and oxidative treatments

In situ XAFS Au L_3-edge studies under CO oxidation reaction conditions show the high stability of the main core cluster structure but a reversible mobility of the Au-S units[6]. The flexibility of the cluster structure and the mobility of atoms was observed in our previous work by in situ QXAFS of metal exchange reaction between Au_{38} and Ag_xAu_{38-x} clusters[7]. The mobility of the Au-S units can explained the different catalytic behaviour depending on the treatment also confirmed by *in situ* DRIFTS measurements.

CONCLUSION

Insights into the interaction between the monolayer protected nanocluster and the oxide support are obtained leading to a better understanding on the different catalytic behavior of this class of nanocatalysts. In summary, we have shown that upon supporting thiolate protected gold clusters, the thiolates are redistributed between cluster and support, leading to oxidized sulfur species that alter the electronic and adsorption properties of the support. This effect has completely been neglected up to now but we believe that it must be taken into account to fully understand the complex selectivity patterns of supported thiolate-protected clusters in catalysis.

REFERENCES

[1] Sels, A., et al., Nanoscale, 2016. **8**(21): p. 11130-11135.
[2] Barrabés, N., B. Zhang, and T. Bürgi, JACS, 2014. **136**(41): p. 14361-14364.
[3] Zhang, B., et al.,. ChemCatChem, 2018. **10**(23): p. 5372-5376.
[4] García, C., et al.,. Catalysis Today, 2019, *in press*
[5] Zhang, B., et al.,. Journal of Physical Chemistry C, 2015. **119**(20): p. 11193-11199.
[6] Pollitt, S., et al,. 2019: *in preparation.*
[7] Zhang, B., et al., Physical Chemistry Chemical Physics, 2018. **20**(7): p. 5312-5318.

SYNTHESIS OF MCM-41 FROM FLY ASH

Marcin Magierło, Paweł Baran, Jakub Szczurowski, Katarzyna Czerw, Katarzyna Zarębska

AGH University of Science and Technology, Cracow, Poland
e-mail: baranp@agh.edu.pl

INTRODUCTION

MCM-41 is a mesoporous material with a hierarchical structure from a family of silicate and alumosilicate solids [1,2]. It consists of a regular arrangement of cylindrical mesopores that form a one-dimensional pore system. It is characterized by an independently adjustable pore diameter, a sharp pore distribution, a large surface and a large pore volume. MCM-41,is widely used as catalytic cracking and also separations [3].

GOAL

The aim of these studies was to obtain mesoporous materials from fly ash, which is waste from the energy sector.

EXPERIMENTS

The starting material for the synthesis of MCM-41 wasfly ash from the Polish heat and power plant. The other ingredients were: CTAB - surfactant, NaOH, methyl acetate and distilled water. The chemical composition of used fly ash was determined using the XRF method. SEM analysis was performed to determine the porous structure and morphology. A point analysis of the chemical composition of grains - EDS was added to the study. Preparation of MCM-41 sieve from fly ash included two stages: extraction of Si and Al from fly ash, and proper synthesis based on the obtained filtrate. Two methods have been used, in order to extract silicon and aluminum from fly ash:

- the solution that remained from the synthesis of zeolites in the hydrothermal reaction

- fusion of fly ash with sodium hydroxide following with dissolution of the solid formed, in water

The obtained filtrate was placed in an oven, surfactant and methyl acetate were added. The resulting material was transferred to a mechanical stirrer and mixed, and then cooled to room temperature. Next the pHmeter was adjusted and material was mixed.

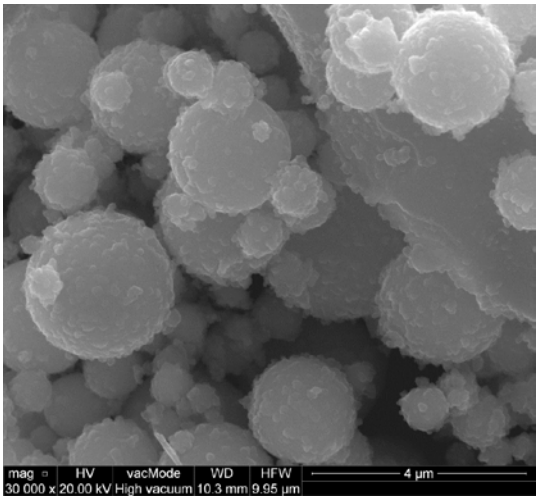

SEM photomicrograph of the fly ash used

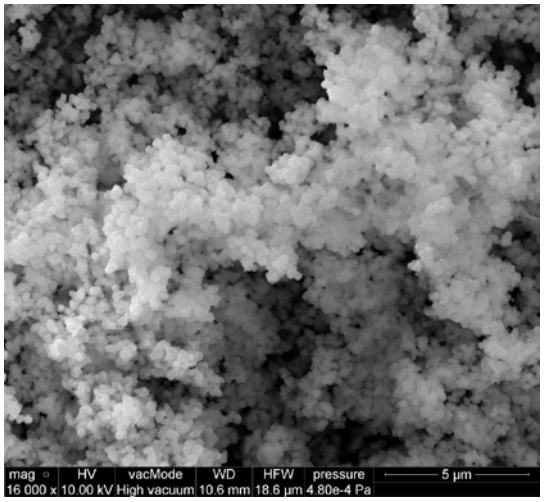

SEM photomicrograph of the obtained MCM-41

RESULTS

As a result of the synthesis, four samples were obtained. The resulting products were subjected to XRD analysis. First samples (S1, S2) which were synthesized from the filtrate remained after fusion of fly ash with NaOH did not show mesoporous properties. However, it was achieved with remaining two samples (S3, S4) obtained on the basis of synthesis of zeolites in a hydrothermal reaction. For further description, SEM analysis and low-temperature nitrogen adsorption were performed. The characteristics of the pores were determined based on the DFT and BJH methods. After obtaining the results it was found that both the pore diameter and their volume are located near the border of the range of microporous materials with mesoporous ones. Therefore, it was decided to carry out the test, using the Dubinin-Raduszkiewicz method (Table 1).

Table 1. Selected properties of samples

Parameter	S3	S4
Dominant pore diameter (DFT) [nm]	2,703	2,583
Dominant pore diameter (BJH) [nm]	2,001	1,999
Dominant pore volume (DFT) [cm^3/g]	0,405	0,356
Dominant pore volume (BJH) [cm^3/g]	0,311	0,279
S_{BET} [m^2/g]	864,85	756,384
S_{DR} [m^2/g]	614,42	569,088
S_{DFT} [m^2/g]	670,236	610,514
S_{BJH} [m^2/g]	251,74	139,365

CONCLUSION

The difference in the way the materials were obtained undoubtedly influenced the result. The concentration of aluminum and silicon was not analyzed in the solutions used for synthesis, therefore it is not possible to state whether the reason for not receiving the expected products from filtrates after fusion is the result of low Si and Al concentrations or their inappropriate ratio.

SUMMARY

It might have seemed that the ash fusion with NaOH will allow higher concentrations of silicon and aluminum to be obtained in the filtrate compared to the hydrothermal solution solution. However upon the conducted analyzes, the presence of MCM-41 type material was found for the synthesis of which the filtrate was based on the hydrothermal reaction of obtaining zeolites. No MCM-41 structures were found for samples obtained from fused solutions.

REFERENCES

[1] Selvam, P., Bhatia, S., Recentadvanced in processing and characterization of periodic mesoporous MCM-41 silicate molecular sieves. Industrial& Engineering ChemistryResearch. 2001, 40, 3237-3261

[2] Xu, X., Song, Ch., Andresen, J.M., Miller, B.G., Scaroni, A.W., Adsorption of carbondioxide from fluegas of natural-fired boiler by a novel nanoporous „molecular basket" adsorbent. Fuel Processing Technology, 2005, 86, 1457-1472.

[3] Zhao, X.S., Ma, Q., Lu, G.Q.M., Comparison of MCM-41 with hydrophobic zeolites and activated carbon. Energy and Fuels, 1998, 12, 1051- 1054.

WASTE MANAGEMENT OF ENERGY SECTOR WASTE - FLY ASH FROM BURNING CRUDE OIL AS CATALYSTS

Oliwia Ligęza, Natalia Czuma, Paweł Baran, Wojciech Nowak, Katarzyna Zarębska

AGH University of Science and Technology, Cracow, Poland
email: zarebska@agh.edu.pl

INTRODUCTION

Due to the increased world population and demand for electricity, the level of greenhouse gases and pollutions is still growing. During last years' scientists were trying to provide new technologies to reduce the amount of emitted NO_x and utilize the waste from energy sector. One of the most promising methods may be fly ash waste (due to its chemical composition [1]) implicated as catalyst used in Selective Catalyst Reduction, which is based on conversion of nitrogen oxides to elementary nitrogen. The main aim of this study was to check the possibilities of application fly ash from burning crude oil as low-cost and eco-friendly catalyst to be used in that process.

EXPERIMENTS

As catalyst properties are connected with surface area and the amount of active centres the main point was to test the surface of starting sample, N_2 low-temperature adsorption was the method used [2]. The obtained values seemed not to be high enough that is why developing the surface was needed. As a first step, CO_2 activation has been applied because of ability of this gas to enlarge the amount of porous structure and what is connected with that increase active surface. Nitrogen adsorption has been applied once again afterwards.

The samples were also purified with mixture of acids to reduce the amount of substances known of their poisonous properties for work of catalyst. One sample was activated for 15 minutes and the other one for 30 minutes to check also if time may have influence on samples.

RESULTS AND DISCUSSION

After using CO_2 on samples the specific surface area has increased 5 to 6 times depending on time of gas application on starting samples (Table 1). This may have significant outcome for catalysts, which mechanisms are based on surface interactions, and because of that more molecules may react witch each other [3].

Table 1. Specific surface area of samples.

Sample	Specific surface area, m^2/g
Non-activated starting sample	2,5
15 minutes activated sample	13,0
30 minutes activated sample	16,0

Using mixture of acids - HCl, HNO_3 and HF - had impact on the chemical composition of the fly ash and caused decrease in amount of undesirable elements. On the other hand, the content of elements, which are active in Selective Catalytic Reduction, has increased (Table 2). That may provide longer time of lasting catalyst and its better work parameters [4].

Table 2. Amount of undesirable components in samples.

	Sample		
Component	Non-activated	15 minutes activated	30 minutes activated
P	733,2 ppm	723,6 ppm	716,9 ppm
S	10,066 %	8,373 %	8,201 %

CONCLUSION

This study has shown that it may be possible to manage waste from energy sector and instead of storage - use them to prepare active and selective eco-friendly catalysts from the fly ash for Selective Catalytic Reduction. Numerous studies among them will be conducted to obtain catalysts with the highest possible conversion rate and selectivity.

REFERENCES

[1] O. Gorce, F. Baudin, C. Thomas, P. Da Costa, G. Djéga-Mariadassou "*On the role of organic nitrogen-containing species as intermediates in the hydrocarbon-assisted SCR of NOx*", Elsevier, Applied Catalysis B: Environmental, 54, 69-84.

[2] G. Fagerlund "Determination of specific surface by the BET method" Materials and structures, Volume 6, Issue 3, pp 239–245, 1973 .

[3] Masel, R. I. "*Principles of adsorption and reaction on solid surfaces*." Wiley series in chemical engineering. New York: Wiley, 1996

[4] R. Dębek, K. Zubek, M. Motak, P. Da Costa, T. Grzybek „*Effect of nickel incorporation into hydrotalcite-based catalyst systems for dry reforming of methane*", Research on Chemical Intermediates, 41, 2015, 9485-9495.

THE USE OF FLY ASH FOR THE PRODUCTION OF NICKEL-BASED CATALYST

Gabriela Radwańska, Natalia Czuma*, Paweł Baran, Monika Motak, Katarzyna Zarębska

AGH University of Science and Technology, Cracow, Poland
*nczuma@agh.edu.pl

INTRODUCTION

The necessity to reduce carbon dioxide emission causes that more and more researchers' attention is directed to chemical methods of carbon dioxide utilization. Selected nickel-based catalysts [1] are used in selected processes, embedded in various supports [2]. The catalyst support should fulfill the following tasks: increasing the surface area of the active phase and increasing the catalyst strength. In the presented studies, a zeolite synthesized from fly ash was proposed as a catalyst carrier.

EXPERIMENTS

The catalyst support proposed was zeolite from fly ash. This material was obtained by fusion synthesis method [3]. The starting material for the synthesis was fly ash from the Polish heat and power plant. The obtained material was examined using the XRD technique.

IMPREGNATION-DEPOSITION OF THE ACTIVE PHASE

10% (10% Ni Zeolite X) and 15% (15% Ni Zeolite X) nickel% wt. (from Ni $(NO_3)_2$ solution * $6H_2O$) were applied to the support. In order to introduce the active phase, the wet incipient impregnation procedure was applied. After the impregnation process, the samples were dried and subjected to a calcination process.

PRELIMINARY CATALYST ANALYSIS

After the calcination process, the XRD test was carried out (Chart 1a). It was aimed at determining whether nickel oxide crystals are present in the catalyst structure.

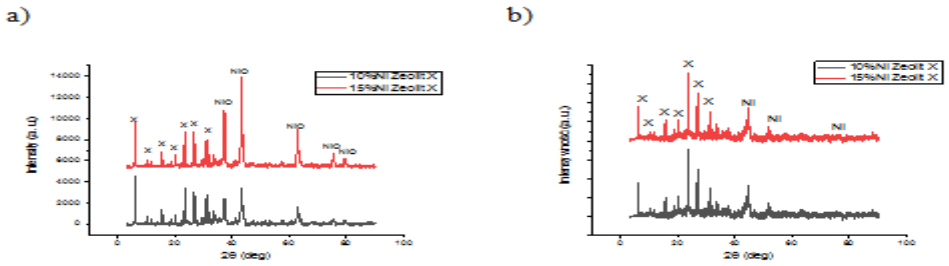

Chart 1:Diffractograms of catalysts a) after the calcination process, b) after reduction

The next catalyst investigation step was the TPR analysis of both the pure catalyst support and the impregnated samples. The results of the analysis of all samples are presented in Chart 2.

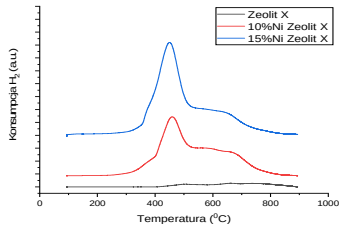

Chart 2: Results of TPR analysis

Impregnated samples after TPR testing were again tested using XRD (Chart 2.b). The material surface area measurementallowed to determine that for the 10% Ni impregnated material, the specific surface area was 191m^2/g and for the 15% Ni impregnated sample S_{BET} was 190 m^2/g.

RESULTS ANDDISCUSSION

As a result of the synthesis process zeolite was obtained from fly ash, its presence was confirmed by XRD. The impregnation and calcination process led to the appearance of NiO crystals. Due to the necessity of obtaining nickel at zero oxidation level, material reduction in a hydrogen atmosphere was carried out. The obtained TPD curves allow to observe that during the reduction of impregnated zeolite, hydrogen consumption increases. The curve for zeolite X allows to state that in the non-impregnated material there is also a process of reduction. After the reduction process, the diffraction patterns of impregnated samples clearly show that nickel oxides have undergone a reduction process. The value of the specific surface compared to the starting material has been reduced.

CONCLUSION

Research confirms that synthesis of zeolite from fly ash is possible. This material can be used as a catalyst carrier. The introduction of nickel in the impregnation process was successful, as evidenced by S_{BET}, XRD and TPD tests. The obtained material is perspective as a catalyst for selected processes of chemical utilization of carbon dioxide.

REFERENCES

[1] Czuma N., Zarębska K., Baran P., Additives for the hydrothermal fly ash zeolites synthesis, SGEM 2016, 2-5 November, 2016, Vienna, Austria :conference proceedings.
[2] Wierzbicki D., Debek R., Motak M., Grzybek T., Gálvez M. E., Costa P. Da, Catal. Commun., t. 83, 2016, s.
[3]Grzybek T., Klinik J., Czajka P., Samojeden B., The structure and DeNOx catalytic properties of carbon composites promoted with nickel oxides, Polish Journal of Environmental Studies ; ISSN 1230-1485. — 2006 vol. 15 no. 6A, s. 62–65

ANALYSIS OF THE POSSIBILITY OF USING MCM-41 MESOPOROUS MATERIAL FROM FLY ASH TO REMOVE NOx FROM WASTE GASES

Michał Nowotarski, Bogdan Samojeden, Paweł Baran, Natalia Czuma, , Katarzyna Zarębska

AGH University of Science and Technology, Cracow, Poland
e-mail: baranp@agh.edu.pl

INTRODUCTION

N_2O, commonly called nitrous oxide, is a greenhouse gas whose molecules absorb heat. The concentration of nitrous oxide from the beginning of the industrial revolution in the atmosphere increased by approximate 16%, which resulted in a strengthening of the greenhouse effect by 4-6% [1]. This leads mainly to the intensification of the stratospheric ozone decomposition process and consequently, the increase in the amount of UV radiation reaching the earth's surface. For this reason, researchers are looking for new ways to reduce NOx. In the presented research, a mesoporous MCM-41 material was proposed synthesized from fly ash as a catalyst carrier. In selected processes, catalysts based on cobalt and copper are used [2].

EXPERIMENTS

The proposed catalyst carrier was the Mesoporous MCM-41 material, which was obtained from fly ash remaining after the combustion of hard coal in the Polish thermal power plant. This material was obtained by means of extraction and synthesis. The obtained material was subjected to the XRD test.

MODIFICATION OF MCM-41 MESOPOROUS MATERIAL

In order to modify the MCM-41 mesoporous material, two samples were selected, and then each of them was divided into two parts by weight. Division resulted in samples 3a, 3b and 4a and 4b, which were then subjected to the process of applying ions to adsorbent surfaces. To the four conical flasks, the weighed amounts of MCM-41 mesoporous material and the corresponding solution were added. Then it was shaken, filtered, then the samples were calcined. The products so obtained were subjected to selective catalytic reduction of nitrogen oxides using NH_3 as a reducing gas [3].

DEPENDENCE OF NO CONVERSION RATE ON TEMPERATURE

Samples of mesoporous material activated with Cu^{2+} ions achieve a higher degree of conversion (within 70%) for lower temperatures, whereas as the temperature rises, this value decreases. The exception is the first measurement for sample 3a, where the conversion rate is much lower. In the case of samples modified with Co^{2+} ions, the value of conversion is much smaller, it is 30% for material 3b at high temperatures, while for sample 4b it is kept low by several percent. The data show that by far the largest N_2O production was recorded for sample 3a material Mesoporous MCM-41 activated with Cu^{2+} ions. Comparing the amount of produced NO with the degree of NO conversion, we can see that even at 300 ° C, where the reaction of nitrous oxide was the lowest, this amount is still higher than the produced N_2O. As the temperature rises, the amount of N_2O formed is increasing, which may indicate a greater contribution of the NH_3 oxidation process.

For sample 4a also modified Cu^{2+} production of nitric oxide is high but comparing it with the degree of NO conversion it can be seen that the amount of nitric oxide removed is much higher. As with the conversion rate, sample 4a retains the most stable amount of N_2O production as the temperature

increases. From the graph we are not able to deduce which of the reactions of dinucleotide oxide formation could have a larger share in the obtained results.

RESULTS AND DISCUSSION

Sample 3a shows a high level of N_2O production. As the temperature rises, the amount of NO increases, while the conversion rate decreases. In the changing conditions of the process, the sample 4a of the MCM-41 mesoporous material activated by Cu^{2+} appears to be the most stable, NO conversion rate oscillates around 70% and the amount of N_2O produced at 160ppm. Due to its stability, it can be concluded that from all the mesoporous material samples tested in the above work it is most useful for removing NOx from waste gases. Sample 4b modified with Co^{2+} ions shows the lowest values of NO conversion and proportionally the highest N_2O production. Of the MCM-41 samples tested in the above work, it can be assessed as the worst material for removing nitrogen oxides from flue gases. Looking at the results of sample 3b of activated Co^{2+}, it should be noted that this material at low temperatures, desirable due to the location of the SCR installation behind the electrostatic precipitator it has low conversion rates and the amount of N_2O produced is higher. Only at upper temperatures there is a significant increase in the conversion rate in the production of NO.

CONCLUSION

This above work presents research on the use of MCM-41 mesoporous material made from fly ash to remove nitrogen oxides from waste gases. The best results were obtaine with sample 4a by Cu^{2+} activation. It showed high stability changing process conditions, achieving a conversion rate of NO at the level of 70% and the amount of N_2O produced at 160ppm, with an initial concentration of NO equal to 800ppm.

REFERENCES

[1] Czuma N., Zarębska K., Baran P., Additiv es for the hydrothermal fly ash zeolites synthesis, SGEM 2016, 2-5 November, 2016, Vienna, Austria :conference proceedings.
[2] Wierzbicki D., Debek R., Motak M., Grzybek T., Gálvez M. E., Costa P. Da, The influence of lanthanum incorporation method on the performance of nickel-containing hydrotalcite-derived catalysts in CO2 methanation reaction. Catal. Commun., t. 83, 2016, s.
[3] Grzybek T., Klinik J., Czajka P., Samojeden B., The structure and DeNOx catalytic properties of carbon composites promoted with nickel oxides. Polish Journal of Environmetal Syudies, 2006, 15(6A), 62

CHIRAL CYCLOOCTADIENE LIGANDS FOR RHODIUM CATALYSIS

Charlie Lim[a], Manuel Spettel[a], Robert Pollice[b], Michael Schnürch[a]

[a]E163 - Institute of Applied Synthetic Chemistry
[b]ETH Zürich, Zürich, Switzerland

INTRODUCTION

The scaffold of organic molecules is dominated by the presence of carbon-hydrogen (C-H) and carbon-carbon (C-C) bonds. Considering this dominance of carbon atoms, it is only natural that carbon-carbon bond forming transformations are of fundamental interest for organic chemists. Numerous approaches towards C-C bond forming reactions have been realized – including the highly useful transition-metal catalysed cross-coupling reactions. However, the major drawback with such transformations is the need for at least one pre-functionalized coupling partner. This is where C-H functionalization proves to be superior. The selective C-H functionalization, an uprising and promising field within the plethora of C-C transformations, allows the direct coupling of non-pre-functionalized substrates and results in a more atom- and step-efficient synthesis of complex molecules.

Our group has previously reported the direct alkylation of benzylic amines *via* C-H functionalization by utilizing terminal olefins as alkylating agents.[1] Additionally, the introduction of the gaseous short-chain olefins was reported by *in-situ* generation of the olefins *via* Hoffmann-elimination from the corresponding tetraalkylammonium salts.[2]

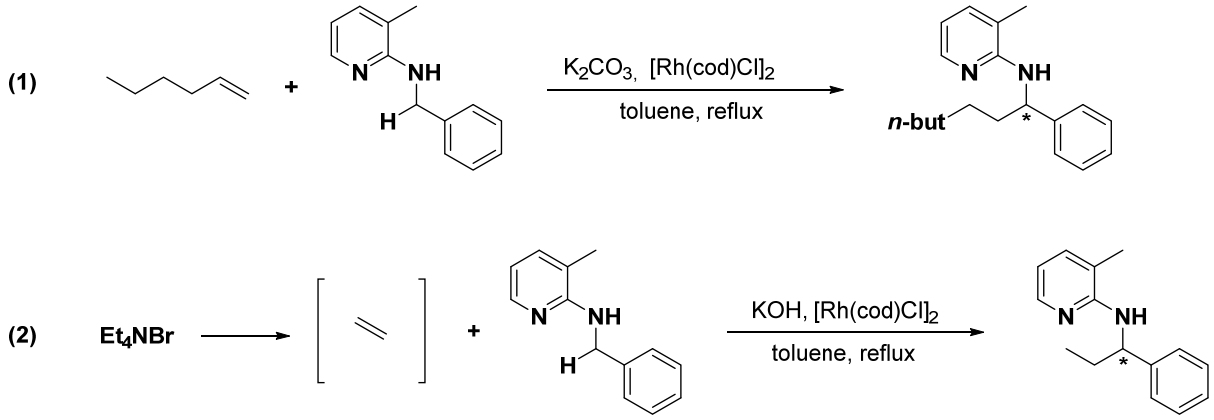

Scheme 1: (1) Direct alkylation of benzylic amines via C-H functionalization with terminal olefins (2) Utilizing alkylammonium salts as olefin source *via* Hoffmann-elimination

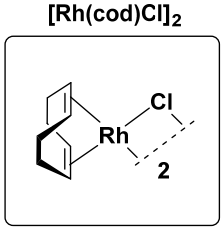

So far, the potentially enantioselectivity of this reaction was of less attention. Within this project, we are aiming for chiral modification of the cyclooctadiene ligand on the rhodium catalyst (Scheme 2).

Scheme 2: Rhodium catalyst used in the reaction

CHIRAL CYCLOOCTADIENE LIGANDS

We have synthesized three different cyclooctadiene derivatives (Scheme 3) for the investigation of the enantioselective induction. The ligands were synthesized and coordinated onto the rhodium as racemic mixture.[3] According to the Grützmacher method, the enantiomerically pure **(*R*)-1** was obtained by optical resolution *via* fractional crystallization of the diastereomers [Rh((*R*)-Ph_2-cod(*R*)-DABN)]BF_4 and [Rh((*S*)-Ph_2-cod(*R*)-DABN)]BF_4.[4] The optical resolution of **(*dl*)-2** and **(*dl*)-3** *via* the Grützmacher method is currently pending.

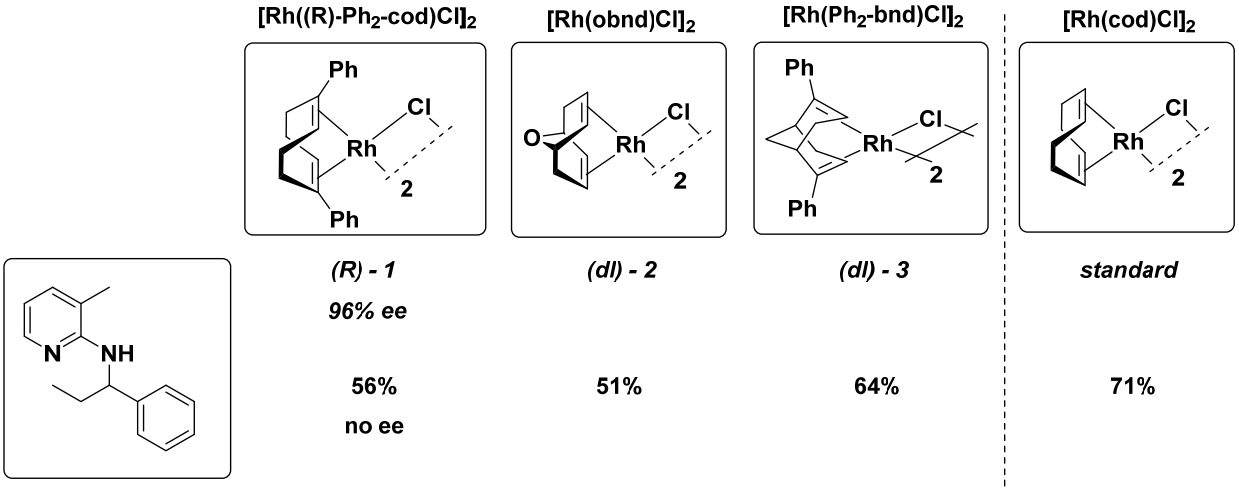

Scheme 3: Overview of synthesized catalysts bearing modified cod-ligands

RESULTS AND DISCUSSION

All of the racemic catalysts were tested in the Hoffmann-approach (reaction (2) in Scheme 1) and showed general catalytic activity (Scheme 3). In case of the enantiomerically pure catalyst **(*R*)-1**, the product was obtained as a racemic mixture. The absence of any ee indicates the racemization of the catalyst. This may be caused by dissociation of the diene ligand and re-coordination with the other face.

CONCLUSIO

To avoid the racemization by the proposed dissociation/re-coordination process, we are currently investigating cod-derivatives **(*dl*)-2** and **(*dl*)-3** bearing a bridge-moiety in their backbone. This bridge-moiety would trap the conformation and thus prevent racemization.

REFERENCES

[1] R. Pollice, N. Dastbaravardeh, N. Marquise, M. D. Mihovilovic, M. Schnurch, *ACS Catal* **2015**, *5*, 587-595.
[2] M. Spettel, R. Pollice, M. Schnurch, *Org Lett* **2017**, *19*, 4287-4290.
[3] (a) A. Takahashi, M. Aso, M. Tanaka, H. Suemune, *Tetrahedron* **2000**, *56*, 1999-2006;
(b) A. Kina, K. Ueyama, T. Hayashi, *Org Lett* **2005**, *7*, 5889-5892;
(c) G. Bassioni, F. S. Delgado, M. Jaeggy, F. H. Kohler, S. Nogai, C. Ruiz-Perez, *Z Naturforsch B* **2005**, *60*, 1143-1148;
(d) Y. Otomaru, A. Kina, R. Shintani, T. Hayashi, *Tetrahedron: Asymmetry* **2005**, *16*, 1673-1679.
[4] F. Läng, F. Breher, D. Stein, H. Grützmacher, *Organometallics* **2005**, *24*, 2997-3007.

DEVELOPMENT OF ENVIRONMENTALLY-FRIENDLY DYES

Richard Fried[a,b], Felix Spiegel[a,b], Ilinca Oprea[a,b], Laura Kühner[a,b], Esther Rühe[b], Tobias Griessler[b], Karin Fleck[a,b], Florian Rudroff[a], Marko Mihovilovic[a]

[a]E163 - Institute of Applied Synthetic Chemistry
[b]Vienna Textile Lab, Vienna, Austria

INTRODUCTION

Textile industry is a large sector of economy, having a global impact. Dying of textiles creates enormous environmental pollution as it involves toxic chemicals such as azodyes or heavy metals[1]. Development of alternatives is of utmost importance for reducing pollution and lowering environmental impact of this globally acting industry branch.

At the Institute of Applied Synthetic Chemistry environmentally-friendly tools for synthesis are explored, such as multi-step biocatalysis or whole-cell systems. Microorganisms applied as biosynthesis factories may provide solutions for difficult synthetic tasks such as the production of complex dye molecules. Bacteria like *Janthinobacterium lividum*[2] or *Serratia marcescens*[3] were reported to produce coloured metabolites that can be used for textile dying. Producing colorants by fermentation instead of petroleum-based chemistry offers substantial improvements in environmental impact by consuming renewable resources and saving energy in the process.

EXPERIMENTS

The aim of the project was to find bacterial dyes (coloured secondary metabolites) and apply them in dying of most commonly used textile materials, e.g. cotton, linen, silk, wool, polyester. Microorganisms came from a project partner's library. Two well-known organisms were selected (*Janthinobacterium lividum* and *Serratia marcescens*) for conducting proof of concept experiments. Dyes produced by these two model organisms are the diindoles violacein/deoxyviolacein (*J. lividum*) and the tripyrrole prodigiosin (*S. marcescens*). Other organisms with unidentified dyes will follow in the same workflow.

Dye-producing microorganisms were cultivated in shaking flasks at TU Vienna and at 1.5-L-reactor scale at BOKU Vienna. Bacterial dyes were separated from biomass and purified according to standard preparative chemistry. Biomass was extracted with ethanol, crude extract dried and solvent removed. Dry crude extract was purified using silica gel flash chromatography. 1H-NMR measurements were made and compared to reference spectra from literature.

Dying of textile materials was performed by dipping textile samples into ethanol solution of crude or purified extracts. The solvent was removed and textiles subjected to a heat fixation step. Quality of dying with violacein/deoxyviolacein was assessed by ISO standard textile tests. ISO standard methods for wash fastness (ISO 105-C06), perspiration fastness (ISO 105-E01 and ISO 105-E04) and light fastness (ISO 105-B02) were applied. Results of these tests may range from 1 (very poor) to 5 (excellent). Light fastness has a different range, from 1 (worst) to 8 (best).

RESULTS AND DISCUSSION

Violacein/deoxyviolacein and prodigiosin could be successfully produced by aerobic fermentation in shaking flask and reactor. Their identity was confirmed by 1H-NMR measurements of purified substances. Classical dip dying method was suited to apply colour to textile materials (Figure 1).

Successfully dyed materials include plant fibres (cotton, linen), animal fibres (silk, wool) and man-made fibres (viscose, polyester, polylactic acid). Results of standardised textile tests for dyed cotton, silk and polylactic acid are displayed in Table 1. Washing fastness and perspiration fastness showed satisfying values. Colour change of dyed sample and staining of white reference textiles (by bleeding) were low, as scores around 4 (good) show. Light fastness still has to be improved; score is around 2 (poor).

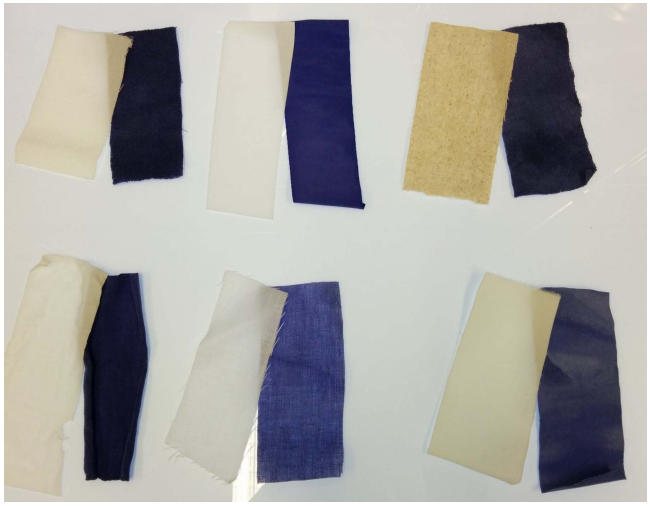

Figure 1: Textiles dyed with violacein.
Top: wool fabric, polyester, cotton-banana-mixed fibre.
Bottom: modal, linen, cotton.

Table 1: Results of ISO textile testing methods

	Wash fastness		**Perspiration fastness**		**Light fastness**
	Colour change	*staining*	*Colour change*	*staining*	
Cotton	3-4	3-4	3-4	3-4	2-3
Silk	3-4	4	3-4	3-4	1-2
PLA	4-5	3	4	4	1-2

CONCLUSION AND OUTLOOK

This proof of concept project showed that secondary metabolites of certain microorganisms are suited to dye different textile materials with good dying characteristics. Isolation and purification of the dyes are work-intensive tasks but may be facilitated by advanced extraction methods. Solid-phase extraction with suitable material may be successful, similar to Domröse et al.[4]. Low light fastness was identified as the most important challenge for the application of dyes from microorganisms. Methods for improving light fastness are already envisioned[5]. Biotechnologically produced dyes may present an environmentally-friendly alternative to synthetic dyes for textile industry. Their production and application may save resources, energy and water to decrease environmental impact of textile industry greatly.

REFERENCES

[1] United Nations Environment Programme: Global Chemicals Outlook - Towards Sound Management of Chemicals. GPS Publishing, 2013, ISBN: 978-92-807-3320-4.

[2] Hoshino et al.; Violacein and related tryptophan metabolites produced by *Chromobacterium violaceum*: biosynthetic mechanism and pathway for construction of violacein core. Appl Microbiol Biotechnol, 91, 6, 1463-75, 2011.

[3] Williamson et al.: The biosynthesis and regulation of bacterial prodiginines. Nat. Rev. Microbiol. 4, 887–899, 2006.

[4] Domröse et al.: Efficient recombinant production of prodigiosin in *Pseudomonas putida*. Frontiers in Microbiology, 6, 972, 2015.

[5] Zarkogianni et al.: Colour and fastness of natural dyes: revival of traditional dyeing techniques. Coloration Technology, 127, 18–27, 2010.

COMPARISON OF STRUCTURE OF HYDROTALCITE MATERIALS PREPARED BY DIFFERENT SYNTHESIS METHODS

Paulina Summa, Agnieszka Szymaszek, Monika Motak, Bogdan Samojeden

AGH University of Science and Technology, Cracow, Poland

INTRODUCTION

Hydrotalcites, due to adjustable composition[1] are widely examined as a catalyst for processes such as dry reforming of methane[2],[3], carbon dioxide hydrogenation[4], selective catalytic reduction[5]. Size of an active center is of importance in catalytic processed, that's why reduction of elemental cell determines uniform distribution of the material, increases the active surface and prevents from sintering[6].

EXPERIMENTS

Samples containing Mg and Al in molar ratio 3:1 and Ni, Mg and Al in molar ratio 1:2:1 subsequently were prepared via three alternative methods, and later were characterised with XRD (Panalytical Empyrean diffractometer, equipped with Cu anode as a source of X-ray radiation, the patterns were recorded over the 2θ range 3 to 90° in steps of 0.013°).

Coprecipitation at low supersaturation

Preparation was carried according to methodology proposed by Cavani[1] with the constant pH in range 8.5-9.

Urea hydrolysis

Solution containing metal nitrates precursors was mixed with urea solution, in molar ratio of urea to to nitrate ions of 4:1, basing on the methodology by Zeng et al.[7].

Solution combustion synthesis

Solutions with nitrate precursors in chosen molar ratios were prepared with stoichiometric amount of urea, in accordance to form oxides, and 0.2 g Na_2CO_3 per 1 g of solid mixture. Such solution was heated to 50℃ for 1 hour under constant stirring. Then, solution was combusted at 450℃. Powder obtained from each combustion was cooled down and put to the 0.1M solution of Na_2CO_3 for 5 minutes, under dynamic stirring. After that time, samples were washed with distilled water and dried in 70℃ as it was suggested by Davila et al.[8].

RESULTS AND DISCUSSION

Different preparation methods of hydrotalcites do result in different size of the crystallites and presence of additional phases. Both size and phase composition may be influenced with the temperature of the process, pH and time. Pure hydrotalcite phase was obtained only with urea hydrolysis, also, this method resulted in the smallest size of crystallites.

Table 1 **Comparison of the composition and crystallite size of the prepared samples**

Method	Sample	XRD composition	Crystallite size of hydrotalcite [nm]
Coprecipitation at low supersaturation	Mg-Al	Hydrotalcite, Al_2O_3, $CaCO_3$	7.04
	Ni-Mg-Al	Hydrotalcite, Al_2O_3, $CaCO_3$	19.97
Urea hydrolysis	Mg-Al	Hydrotalcite	7.25
	Ni-Mg-Al	Hydrotalcite	15.68
Solution combustion synthesis	Mg-Al	Hydrotalcite, Al_2O_3,	15.11
	Ni-Mg-Al	Hydrotalcite, $Mg_{0.4}Ni_{0.6}O$	21.19

CONCLUSION

According to this research, the most precise method of hydrotalcite preparation is urea hydrolysis, which provides a highly crystalline, one-phase product with small size of the crystallites. Solution combustion synthesis leads to formation of relatively big crystallites and additional oxide phases. Coprecipitation gave satisfactory size of the crystallite in Mg-Al sample, however additional phases were present.

ACKNOWLEDGEMENTS

This work was financed by AGH Grant 11.11.210.373

REFERENCES

[1] E. S. Publishers, 'Hydrotalcite-type anionic clays: preparation, properties and applications, I I (I99 I) 173-301 Elsevier Science Publishers', *Catal. Today*, vol. 11, pp. 173–301, 1991.

[2] R. Dębek, M. Motak, T. Grzybek, M. Galvez, and P. Da Costa, 'A Short Review on the Catalytic Activity of Hydrotalcite-Derived Materials for Dry Reforming of Methane', *Catalysts*, 2017.

[3] R. Dębek, M. Motak, M. E. Galvez, P. Da Costa, and T. Grzybek, 'Catalytic activity of hydrotalcite-derived catalysts in the dry reforming of methane: on the effect of Ce promotion and feed gas composition', *React. Kinet. Mech. Catal.*, 2017.

[4] D. Wierzbicki, R. Debek, M. Motak, T. Grzybek, M. E. Gálvez, and P. Da Costa, 'Novel Ni-La-hydrotalcite derived catalysts for CO2methanation', *Catal. Commun.*, vol. 83, pp. 5–8, 2016.

[5] D. Wierzbicki *et al.*, 'Copper, cobalt and manganese: Modified hydrotalcite materials as catalysts for the selective catalytic reduction of NO with ammonia. the influence of manganese concentration', *Comptes Rendus Chim.*, 2015.

[6] J. Hagen, *Industrial catalysis: A practical approach*. 2015.

[7] H. Y. Zeng, X. Deng, Y. J. Wang, and K. B. Liao, 'Preparation of mg-ai hydrotalcite by urea method and its catalytic activity for transesterification', *AIChE J.*, 2009.

[8] V. Dávila, E. Lima, S. Bulbulian, and P. Bosch, 'Mixed Mg(Al)O oxides synthesized by the combustion method and their recrystallization to hydrotalcites', *Microporous Mesoporous Mater.*, vol. 107, no. 3, pp. 240–246, 2008.

DEVELOPMENT OF A LAB-BASED IN-SITU NAP-XPS SYSTEM FOR ELECTRO-CATALYSIS RESEARCH

R. Rameshan[a], J. Raschhofer[a], T. Huber[b], J. Popovic[a], C. Rameshan[a]

[a] Technische Universität Wien, Institute of Materials Chemistry, Vienna, Austria
[b] Huber Scientific, Vienna, Austria

We present the development of a lab-based near ambient pressure X-ray photoelectron spectrometer (NAP-XPS) that is specially designed for investigations of electro-catalytic systems under realistic operating conditions. The new system allows catalytic measurements in flow mode with online reaction analysis while simultaneously characterising in-situ surface composition and electrochemical properties.

Key requirements are a flow reactor environment that can be operated up to 10 mbar H_2 (or other gas mixtures) with operating temperatures between RT and 800°C (peak temperatures of 1000°C possible). The sample stage has special design to allow simultaneous characterisation by impedance spectroscopy and to obtain current-voltage curves. For electro-catalytic experiments, the sample surface can be polarized. The attached gas analysis allows to follow catalytic reactions in real time by MS.

In addition, we present additional software implementation developed in LabVIEW for control and safety (interlocks) as well as for user-friendly data processing.

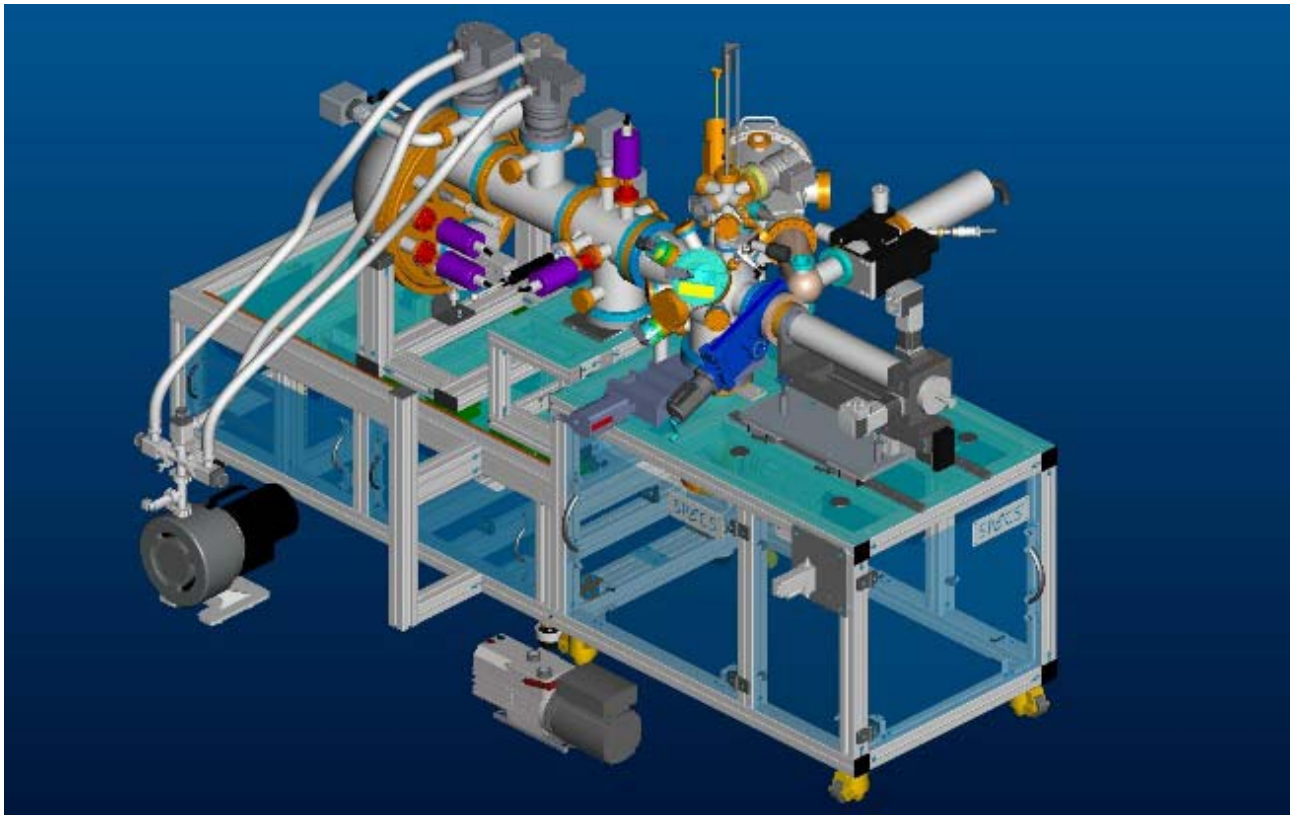

Figure 1: 3D Model of the in-situ NAP-XPS system

ACKNOWLEDGEMENT:
This work has received funding from the European Research Council (ERC) under the European Union's Horizon 2020 research and innovation programme (grant agreement n° 755744 / ERC - Starting Grant TUCAS).

CHARACTERIZATION OF NOVEL DOPED PEROVSKITE CATALYSTS – TAILORED EXSOLUTION OF METAL NANOPARTICLES

Lorenz Lindenthal[a], Janko Popovic[a], Johannes Raschhofer[a], Thomas Ruh[a], Raffael Rameshan[a], Andreas Nenning[b], Alexander K. Opitz[b], Christoph Rameshan[a]

[a]E165 - Institute of Materials Chemistry
[b]E164 - Institute of Chemical Technologies and Analytics

INTRODUCTION

Perovskite-type oxides are a large class of materials with many interesting properties, including piezo- and pyroelectricity, mixed ionic-electronic conductivity and high catalytic activity. Thus, there is a wide range of applications, for example the use as sensors or as electrode materials in solid oxide fuel cells. Their general chemical formula is ABO3, with two different cations A (bigger) and B (smaller). The ideal structure is cubic, but it is often distorted as can be seen for La0.9Ca0.1FeO3 (figure 1). The high versatility of the material class is due to the possibility of adjusting the properties by choosing different elements for the cations. Doping either one or both of the cation sites opens up an even larger matrix for materials design.

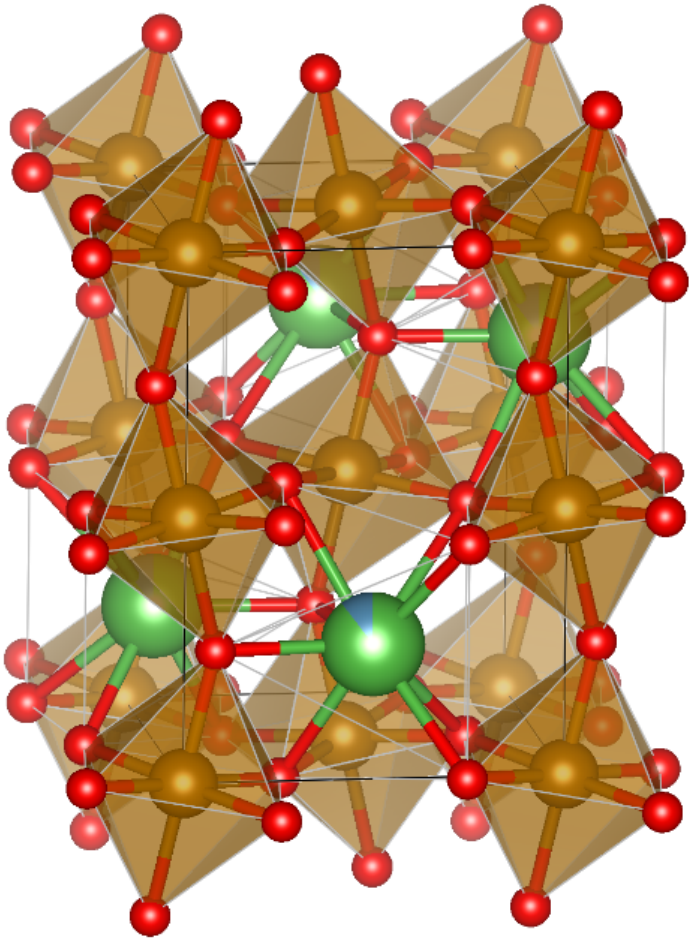

Figure 1: Distorted perovskite structure of $La_{0.9}Ca_{0.1}FeO_3$, data from XRD measurement (La/Ca-green/blue, Fe-brown, O-red).

In terms of catalysis, another recently shown outstanding property of perovskites is the exsolution of metal nanoparticles under reducing conditions. This surface modification (by migration of cations to the surface) can change the catalytic activity and selectivity of the perovskite surface completely and is the core topic of our ERC project.

RESULTS AND DISCUSSION

Several perovskite-type oxides (e.g. LaxCa1-xFeO3 or NdxCa1-xFeO3), that are promising catalyst materials, have been synthesised and subsequently characterised. These perovskites are promising catalyst materials for several energy related reactions, such as the (reverse) water gas shift reaction. Using different reducing conditions, the stability and reducibility of the synthesized perovskites were investigated in-situ. X-ray diffraction (XRD) allowed structural determination, while X-ray photoelectron spectroscopy (XPS) gave additional chemical information on the surface state. These characterisations have been complement by additional analytical methods. It was possible to show the reversible exsolution of metal nanoparticles in an ideal metastable window.

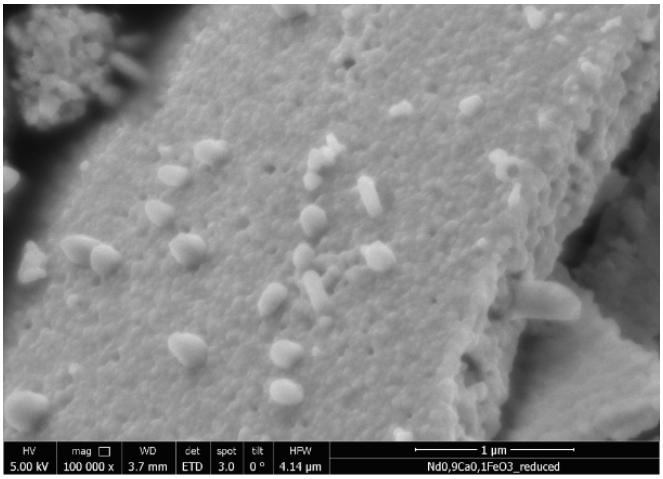

Figure 2: SEM picture of exsoluted nanoparticles on $Nd_{0.9}Ca_{0.1}FeO_3$.

ACKNOWLEDGEMENT

This project has received funding from the European Research Council (ERC) under the European Union's Horizon 2020 research and innovation programme (grant agreement n° 755744 / ERC - Starting Grant TUCAS)

SELECTIVE CATALYTIC REDUCTION OF NO_X WITH AMMONIA OVER CATALYSTS DERIVED FROM FLY ASH

Agnieszka Szymaszek, Paulina Summa, Bogdan Samojeden, Monika Motak

AGH University of Science and Technology, Kraków, Poland

INTRODUCTION

The generation of adverse pollutants caused by combustion of fossil fuels is nowadays a significant environmental problem. One of the most abundant and complex anthropogenic by-product of coal combustion is fly ash (FA). The term fly ash refers to particles which are collected from flue gas by mechanical or electrostatic precipitator. The physicochemical properties of this solid waste are determined by the type of combusted coal. Inappropriate disposal of FA can result in degradation of the soil and poses great danger to the environment [1-3]. Therefore, there is a pressing need to find an effective method for fly ash utilization. Over the past few years, much attention has been also directed to NO_x abatement and the most effective current method is selective catalytic reduction with ammonia (NH_3-SCR). According to the scientific literature, supported transition metals and their oxides can be potentially used as more economical substitutes of the commercial catalyst [4-5]. In view of the above, in this study the suitability of fly ash for the synthesis of NH_3-SCR catalysts supports was investigated. The concept of this kind of modification was motivated by the fact, that contaminating fly ash could be utilized with simultaneous abatement of another adverse compound. Hence, the idea is a promising opportunity to meet the objectives of the circular economy.

EXPERIMENTS

In the research, the catalytic performance in NH_3-SCR of the fly ash-derived catalysts containing transition metal oxides was investigated. Before the modification, the coal fly ash was dried in the oven at 100^{o}C for 24 h. Subsequently, it was treated with 1 M solution of HNO_3 with the FA/acid ratio of 1:10. The slurry was left to react at 100^{o}C for 4 or 24 h. The mixture was continuously filtered, washed and dried at 100^{o}C for 24 h. Transition metals were introduced on the fly ash-based support via impregnation by metal nitrates. The structure of prepared materials was characterized by XRD and FTIR, the S_{BET} and texture were determined by the low-temperature N_2 sorption. The type and aggregation state of active metal species were analyzed by UV-vis-DRS. Subsequently, the obtained samples were subjected to NH_3-SCR catalytic tests.

RESULTS AND DISCUSSION

Catalyst characterization

The physicochemical characterization of the prepared materials had a significant contribution into the understanding of their properties. The specific surface area analyzed by low temperature N_2 sorption increased significantly after the treatment with acidic medium. FTIR analysis indicated the presence of characteristic absorption bands ascribed to anions and cation-oxygen bonds, hydroxyl groups and hydroxyl groups linked to Mg-, Al- and Ca- lattice. The results of XRD analysis indicated the presence of characteristic reflections of SiO_2, Al_2O_3, CaO and Fe_2O_3. These compounds are considered to influence the catalytic activity of the material in NH_3-SCR. UV-vis-DRS analysis confirmed that active metal phase occurs in different forms, including isolated cations, metal oxides and spinels.

Catalytic tests

The results of NH_3-SCR catalytic tests for the fly ash-based catalyst containing nickel and iron are presented in Chart 1 and Chart 2. The peak conversion of about 55% is reached at 200°C and stays constant until the temperature does not exceed 275°C. The decrease of catalytic activity above this temperature is probably caused by oxidation of ammonia, which undesired side-reaction of NH_3-SCR. The conclusion is with agreement with the results of N_2O concentration in this temperature range. Increased amount of N_2O in flue gas from about 300°C indicates that NH_3 is being oxidized.

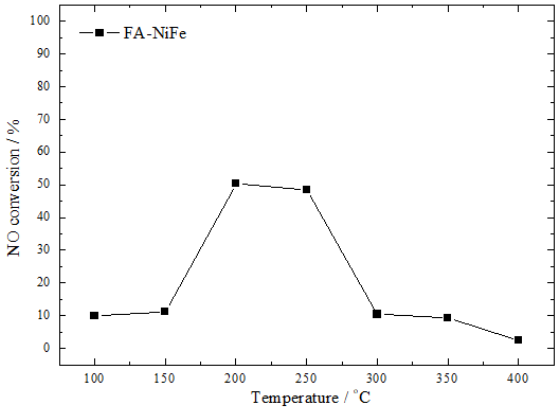

Chart 1: NO conversion for fly ash-based catalyst containing nickel and iron (reaction conditions: 800 ppm NO, 800 ppm NH_3, 3.5 % vol. O_2, balance He).

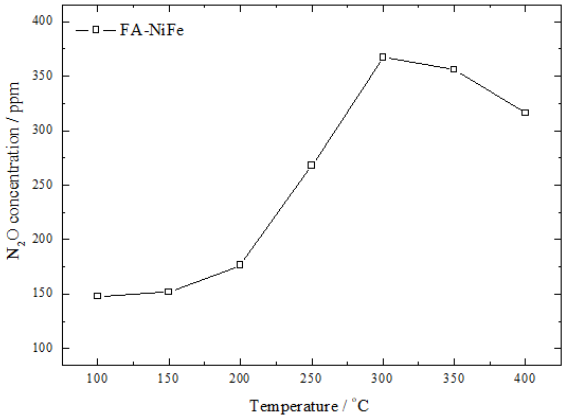

Chart 4: N_2O concentration for fly ash-based catalyst containing nickel and iron (reaction conditions: 800 ppm NO, 800 ppm NH_3, 3.5 % vol. O_2, balance He).

CONCLUSIONS

The chemical treatment of fly ash with acidic medium had significant impact on structural and catalytic properties of the material. Especially, the specific surface area was greatly increased which results in better catalytic activity in NH_3-SCR. Metal oxides present in the fly ash-based supports are predicted to enhance catalytic performance. Inclusion of active metals, e.g. iron and nickel influenced NO conversion, however further catalytic tests over materials containing copper and cobalt are predicted.

ACKNOWLEDGEMENT

The research financed by Grant AGH 11.11.210.373

REFERENCES

[1] T. Hemalatha, A. Ramaswamy, A review on fly ash characteristics - Towards promoting high volume utilization in developing sustainable concrete, Journal of Cleaner Production 147, 546-559, 2017.

[2] T. Matsunaga, J. K. Kim, S. Hardcastle, P. K. Rohatgi, Crystallinity and selected properties of fly ash particles, Materials Science and Engineering A325, 2002, 333-343.

[3] Z. T. Yao, X. S. Ji, P. K. Sarker, J. H. Tang, L. Q. Ge, M. S. Xia, Y. Q. Xi, A comprehensive review on the applications of coal fly ash, Earth-Science Reviews 141, 2015, 105-121.

[4] M. Motak, Ł. Kuterasiński, P. Da Costa, B. Samojeden, Catalytic activity of layered aluminosilicates for VOC oxidation in the presence of NO_x, Comptes Rendus Chimie 18, 2015, 1106-1113.

[5] D. Wierzbicki, R. Dębek, J. Szczurowski, S. Basąg, M. Włodarczyk, M. Motak, R. Baran, Copper, cobalt and manganese: Modified hydrotalcite materials as catalysts for the selective catalytic reduction of NO with ammonia. The influence of manganese concentration, Comptes Rendus Chimie 18, 2015, 1074-1083.

THE PROCESS OF MINERAL CARBONATION OF FLY ASH WITH A HIGH CONTENT OF CALCIUM OXIDE FROM THE GROUP HCFA

Jakub Sobala[a], Natalia Czuma[a], Piotr Zabierowski[a], Agnieszka Ćwik[a,b.c,*], Ignasi Casanova[b,c], Katarzyna Zarębska[a]

[a] AGH University of Science and Technology in Cracow, Faculty of Energy and Fuels,
[b] Institute of Energy Technologies, Universitat Politčcnica de Catalunya,
[c] Barcelona Research Center in Multiscale Science and Engineering
Campus Diagonal-Besňs, 08930 Barcelona, Spain
zarebska@agh.edu.pl

INTRODUCTION

Currently, it is estimated that about 50% world emission of carbon dioxide comes from coal burning in the power stations [1]. One of the most hazardous substance which is produced by the energy sector is fly ash with a high content of calcium oxide, included to the group HCFA- High Calcium Fly Ash. It is estimated that annual production of fly ash is around 750 mln. tonnes, of which only use 16% in the industry [2]. In Europe, more than 50% of the total production of fly ash is HCFA [3]. Fly ash is mostly used for production of cement, building materials and as the component in road construction. If calcium oxide content in fly ash is more than 10% it is included to the group HCFA. Mineral carbonation is one of the safest and environmentally benign technologies for Carbon Capture and Storage. This mechanism consists of the fixation of carbon dioxide into calcium and/or magnesium bearing minerals to form stable carbonates. Due to the method of mineral carbonation process it is possible to reduce carbon dioxide emissions and in the same time neutralize fly ash, which is used as one of the substrates in this reaction. This process has two steps. First, the hydration of CaO is taking place and next, it is followed by carbonation of calcium hydroxide [4].

EXPERIMENTS

The aim of our research was to examine the mineral carbonation process of calcium fly ash. The experiments were conducted at three different temperatures: 298, 323 and 343 K and a pressure range of CO_2 from 0.4 to 1.5 MPa.

RESULTS AND DISCUSSION

One of the examined materials was biomass fly ash. The main components are: silicon dioxide (51,33%), calcium oxide (12,01%) and aluminium oxide (10,42%). The maximum sequestration capacity was achieved for biomass fly ash at 343 K and 0.711 MPa, and it was 29,382 dm^3 CO_2/kg of fly ash, it has been observed that the biggest values were obtained at the highest selected experimental parameters. The second material was fly ash from power station, the main are: silicon dioxide (37,12%), calcium oxide (15,34%) and aluminium oxide (13,14%). The maximum sequestration capacity was achieved at 298 K and 0,527 MPa, and it was 25,937 dm^3 CO_2/kg fly ash. In contrary to biomass fly ash, the biggest value was obtained at the lowest temperature, however at the highest pressure.

CONCLUSION

The experiment shown that increasing the pressure and temperature enhances the process of carbonation in case of biomass fly ash. However, it has been concluded that for fly ash from power plant increasing the temperature does not influence the effectiveness of carbonation process. It has been proven that HCFA has a big potential in the carbonation process. Thanks to carbonation process, the reduction CO_2 emission is possible, whats more it may allow to find a new way of fly ash utilization.

REFERENCES

[1]. M. Peters, B. Köhler, W. Kuckshinrichs, W. Leitner, P. Markewitz, and T. E. Müller, 'Chemical technologies for exploiting and recycling carbon dioxide into the value chain', *ChemSusChem*, vol. 4, no. 9, pp. 1216–1240, Sep. 2011.

[2] Z. T. Yao *et al.*, 'A comprehensive review on the applications of coal fly ash', *Earth-Sci. Rev.*, vol. 141, pp. 105–121, Feb. 2015.

[3] A. Fauzi, M. F. Nuruddin, A. B. Malkawi, and M. M. A. B. Abdullah, 'Study of Fly Ash Characterization as a Cementitious Material', Procedia Eng., vol. 148, pp. 487–493, Jan. 2016.

[4] Carbonation of high-calcium fly ashes and its potential for carbon dioxide removal in coal fired power plants / Agnieszka ĆWIK, Ignasi Casanova, Kwon Rausis, Nikolaos Koukouzas, Katarzyna ZARĘBSKA // Journal of Cleaner Production ; ISSN 095

PRODUCTION OF ISOBUTANOL FROM CO_2 IN A TWO-STEP PROCESS

Katharina Novak, Christoph Herwig, Stefan Pflügl*

E166 - Institute of Chemical, Environmental and Bioscience Engineering

INTRODUCTION

The effects of climate change as a result of high greenhouse gas emissions force the industrial sector to reduce its carbon footprint, especially as it accounts for 44 % of the emissions in Austria[1]. Additionally, a high amount of energy is required for the transportation sector, mainly in the form of hydrocarbons, which offer a cheap energy source and are easily storable.

Finding a solution for these two challenges and concurrently investing into the transition towards a biobased future led to the design of a two-step process. In the first step, acetate is produced from CO_2 and H_2 by the acetogenic bacterium *Acetobacterium woodii*. The produced acetate is subsequently used in a second step for the conversion into isobutanol by genetically engineered *Escherichia coli*. Its property as a two-step process makes the system a highly flexible platform for the production of various fuel alcohols and chemicals.

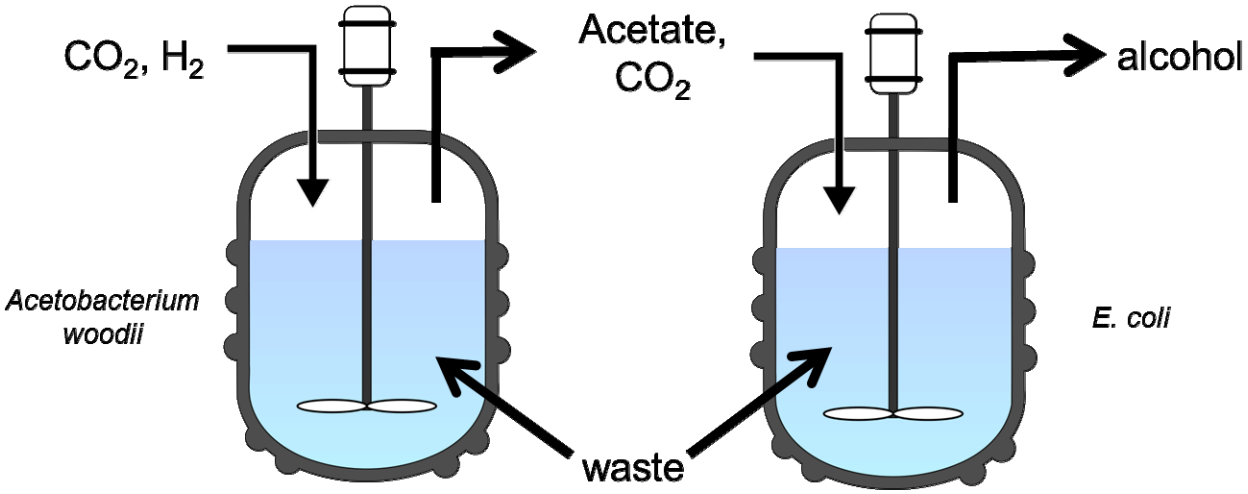

Picture 1: Overviw of the two-step process for CO_2 fixation and alcohol prodcution

Biotechnological CO_2 fixation is challenging, because CO_2 is chemically inactive and it can be used as a carbon but not as an energy source. Hence, for biological utilization, an energy input is needed. This can be in the form of sunlight as for photoautrotrophic organisms, but also hydrogen gas from renewable resources and waste streams, with the last two being investigated in this work. Conventional cultivation media for the acetogen *Acetobacterium woodii* usually contain high amounts of expensive complex media components. For industrial applications, the omittance of this component is of great interest, which was shown to be possible in this work. Although the productivity was decreased in batch processes, good productivities of 11 g l^{-1} d^{-1} were shown in a chemostat operation.

Subsequently, acetate is taken up by *E. coli* in a second stage and converted into isobutanol. However, acetate utilization is challenging due to the low energy production from this carbon source in the bacterial cell. Genetic engineering of the acetate uptake system has been shown to

improve the utilization of acetate as a sole carbon source as well as in a co-utilization system with glucose[2].

For isobutanol production, a strain with high productivities was selected during a screening process from a genetic construct library. During bioreactor cultivations, important process parameters were optimized, resulting in the production of 9 g/l isobutanol, which could even be further increased in fed-batch cultivations. Out of four waste streams tested, two were successfully used for alcohol production, underlining the potential of the imagined process.

Until now, all parts of the imagined two-step process for CO_2 fixation and isobutanol production were investigated successfully. The next steps will be to improve the isobutanol production on acetate as a carbon source as well as to finally put all puzzle pieces together in order to investigate the whole process in its full complexity.

REFERENCES

[1] http://www.umweltbundesamt.at/umwelt/luft/treibhausgase/

[2] Novak K, Flöckner L, Erian AM et al. Characterizing the effect of expression of an acetyl-CoA synthetase insensitive to acetylation on co-utilization of glucose and acetate in batch and continuous cultures of E. coli W. Microbial Cell Factories 2018;17:109.

KINETIC STUDIES ON BIMETALLIC Au CATALYSTS: INFLUENCE OF WATER

Markus Latschka[a], Andreas Nagl[a], Jenoff E. De Vrieze[b], Sotiria Mostrou-Moser[c], Jeroen A. van Bokhoven[c], Mark Saeys[b], Karin Föttinger[a,*]

[a] E165 - Institute of Materials Chemistry
[b] Laboratory for Chemical Technology, Technologiepark 914, B-9052 Gent, Belgium
[c] Institute of Chemical and Bioengineering, Vladimir-Prelog-Weg 1-5/10. 8093 Zürich, Switzerland

INTRODUCTION

Acetaldehyde is an important base chemical, at present it is mainly produced by the Wacker-Hoechst process, which requires petrochemical starting materials. Acetaldehyde can also be made by the oxidation of ethanol and ethanol can be produced renewably from biomass[1].

Normally gold is catalytically very inactive, but when the gold particles have a small diameter like below 30 nm, the catalytic activity is getting much better for a number of reactions. Then also oxygen can absorb on the gold surface even at room temperature. The catalytic activity of the gold catalyst per unit surface area for CO oxidation is about 100 times better when the gold is on a TiO_2 support as for the pure gold particles[2].

Therefore, supported gold nanoparticles have been studied as catalysts for the oxidation of alcohols to aldehydes with oxygen in the gas phase. When the reaction takes place in an aqueous solution the corresponding carbon acid is formed instead of the aldehyde[3]. The reason why the acetaldehyde is further oxidized to acetic acid only in the liquid phase reaction has not yet been determined.

When two metals are combined in a catalyst, the advantages of both individual metals can appear. However, also a synergistic effect can occur resulting in new functionalities of the catalyst[4].

EXPERIMENTS / FUNDAMENTAL OF THE PROBLEM / EXAMINATIONS

Our group at the TU Wien synthesized gold nanoparticles on rutile wet-chemically via deposition-precipitation, while the silver was added via wetness impregnation. The bimetallic catalyst consists of 5 wt% gold and 1 wt% silver on rutile, the monometallics contain the same amount of the respective metals.

For the characterization of the catalysts, STEM-HAADF images were taken (FEI Tecnai F20 FEG-TEM). From these measurements a particle size distribution was obtained and thereby a quantification of the surface atoms of the precious metals.

Around 20 mg of the catalyst diluted with quartz sand were loaded into a continuous-flow fixed-bed quartz reactor to determine the reaction kinetics for ethanol oxidation to acetaldehyde. Prior to the reaction, the catalysts were pretreated with 20 % oxygen and 5 % hydrogen, both diluted in He, at 400 and 300 °C, respectively. The reaction took place with 1.1 mL/min of ethanol (introduced with a bubbler) and oxygen (total flow ~ 50 mL/min). In addition to the bimetallic catalyst, the monometallic Au and Ag references were tested as well.

The results obtained were compared with kinetic studies of ethanol oxidation in the liquid phase on the same catalysts, which were carried out by a collaborating group at the ETH Zurich. In the aqueous phase, the main product is acetic acid instead of acetaldehyde. To explore the reason for this and the influence of water, we added water during the gas phase ethanol oxidation.

The results of the catalytic studies in the gas and the liquid phase were compared with theoretical calculations, which were performed within a cooperation with the Saeys group at the University of Gent with the VdW-DF2 functional.

RESULTS AND DISCUSSION

In Figure 1 the TEM images of the pretreated Au and AuAg/TiO_2 catalysts can be seen. Both catalysts have a similar particle size distribution with small nanoparticles of around 3 nm. The monometallic silver catalyst showed the same result.

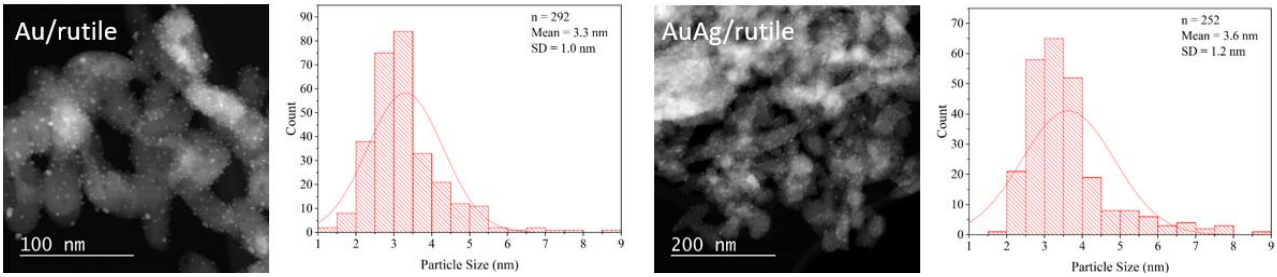

Figure 1: STEM-HAADF-Images and the resulting size distribution of the Au nanoparticles on rutile (left) and the AuAg nanoparticles on rutile (right).

Figure 2 shows the reaction rate of acetaldehyde formation on the three catalysts increasing with temperature. As expected, the monometallic gold catalyst had a better performance than the silver catalyst. The synergetic effect of the two precious metals in the bimetallic catalyst can be seen very well. The reaction rate is significantly higher than on the monometallic catalysts. Compared to reaction in liquid phase, an interesting behaviour occurred. Besides the fact that acetic acid is the main product in aqueous solution, the monometallic Au catalyst showed a higher conversion than the bimetallic AuAg one. In addition, other metal combinations like AuRu and AuPt were tested and the performance of these catalysts was completely reversed. For the gas phase the order by the activity was AuAg > Au > AuRu > AuPt and for the liquid phase it was AuAg < AuRu < Au < AuPt. The reason for the different behaviour might be related to the presence of water.

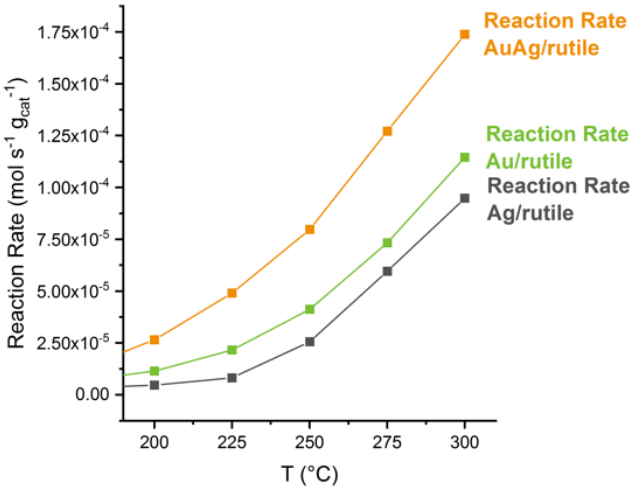

Figure 2: Reaction rate for acetaldehyde for both monometallic and the bimetallic catalyst.

CONCLUSION

The synergetic effect of silver and gold in the gas phase reaction of ethanol to acetaldehyde could has been proven. The influence of water on the catalysts during the reaction is still under investigation. Theoretical calculations should also help to elucidate the reaction pathways.

REFERENCES

[1] Baerns M. et al., Technische Chemie, 595-597, 2013

[2] Haruta M., Catalysis Today 36, 153-166, 1997

[3] Enache D. et al., Science VOL 311, 362-365, 2006

[4] Zaleska-Medynska A. et al., Advances in Colloid and Interface Science 229, 80-107, 2016

PROBING ACTIVE PHASE OF Pt-Fe MODEL CATALYSTS USING STM

Hao Chen[a,b], Yun Liu [b], Fan Yang,[b,*], Ulrike Diebold [a] , Xinhe Bao[b,*]

[a] E134 - Institute for Applied Physics, TU Wien
[b] State Key laboratory of Catalysis, Dalian Institute of Chemical Physics, Dalian, China

INTRODUCTION

Platinum Iron (PtFe) bi-component catalysts display prominent low-temperature activity towards preferential oxidation of the CO in the excess of H_2 (PROX) for the purpose of removal of trace CO in H_2 proton exchange membrane fuel cell (PEMFC), a promising and high efficient hydrogen energy converter from chemical energy to the electric energy[1]. FeO nanostructures supported on the Pt(111), which contain density of coordinated unsaturated Fe (CUF) atoms at the metal/oxide interface, highly activate the O_2 molecules and therefore solve the CO-poisoning problem of Pt-based catalysts. In contrast, at the absence of the H_2 atmosphere, this FeO active phase would undergo deactivation with the reactivity of CO oxidation quickly dropping down.

The objective of this work is to get a better understanding of how the FeO active phase responds to the reaction condition and the corresponding deactivation mechanism. Furthermore, we investigated the active phase of PtFe alloy model catalyst, whose powders show high activity and enhanced stability of the CO oxidation in the excess /absence of H_2[2].

EXPERIMENTS / FUNDAMENTAL OF THE PROBLEM / EXAMINATIONS

In this work, both low temperature and near ambient pressure Scanning Tunneling Microscopy (LT-STM &NAP-STM), were used for the in-situ investigation of the fine structure of well-defined FeO/Pt(111) and PtFe surface alloy model catalyst before and after exposure to reaction gas.

Preparation of supported FeO/Pt(111): The FeO nano-islands were deposited onto the Pt(111) surface by evaporating Fe atoms in 1.3×10^{-7} mbar O_2 at the clean Pt substrate temperature between 150 and 300 K. The as-deposited FeO nano-islands were then annealed to 600 K, leading to the formation of well-ordered Fe-edge terminated FeO nanostructures.

Preparation of FePt surface alloy: The PtFe surface alloy was prepared through the deposition of low coverage Fe ($\Theta_{Fe} < 1$ ML) onto Pt substrate at 460 K or high coverage Fe ($\Theta_{Fe} > 1$ ML) with post-annealing at 650 K. The as-prepared alloy surface exhibited network of stripes and consisted of Pt skin layer and Pt_3Fe layer underneath.

RESULTS AND DISCUSSION

The triangular Fe-edge terminated FeO nano-islands would reversibly transform to the O-edge terminated FeO at ~10^{-8} mbar O_2. However, this bilayer FeO would gradually turned to the tri-layer FeO_2 when directly exposed to 0.26 mbar O_2. In contrast, FeO nano-island could remain stable under the PROX reaction gas with the pressure even increased to 1 bar.

Significant morphology changes occurred when the PtFe surface alloy exposed to $5x10^{-7}$ mbar O_2. A large density of nanoclusters, characteristic of one protrusion in the middle surrounded by dark contour, dominated the surface and could be attributed to the embedding Fe_3O_X nanostructures. Furthermore, massive segregation of subsurface Fe took place when exposed to the 0.05 mbar O_2, which dramatically increased the density of oxide-metal interface. Meanwhile, this PtFe surface alloy model catalyst also showed better activity of CO oxidation than Pt(111) at room temperature.

CONCLUSION

The bilayer FeO nanostructures exhibited advantages towards O_2 activation through the reversible transformation from Fe-edge to O-edge at lower O_2 pressure and remain stable even at realistic PROX condition. However, It would gradually transformed to tri-layer FeO_2 after exposure to O_2 at the near ambient pressure, which was the main deactivation mechanism of PtFe catalysts at H_2-lean reaction condition.

PtFe surface alloy, consisting of Pt-skin layer and Pt_3Fe subsurface layer, exhibited high reactivity and enhanced stability towards CO oxidation. Extremely small embedding Fe_3O_X nanoclusters formed at lower lower O_2 pressure. In contrast, significant segregation took place and supported FeO_X nanoclusters from subsurface layer dominated the surface after exposure to O_2 at the near ambient pressure. The newly-formed FeO_X nanoclusters with considerable metal/oxide interface and this segregation process should be responsible for high reactivity of CO oxidation and enhanced stability, respectively.

Since now, we have demonstrated the high performance of PtFe model catalysts in the solid-gas interface towards CO oxidation. However, the real PtFe catalysts of PEMFC operate at the solid-gas-liquid ternary phase interface, that is, the FeO/Pt nanoclusters are surrounded by the liquid atmosphere. So next step, we will keep on surveying whether the activity and stability of FeO/Pt(111) still remains at liquid atmosphere[3].

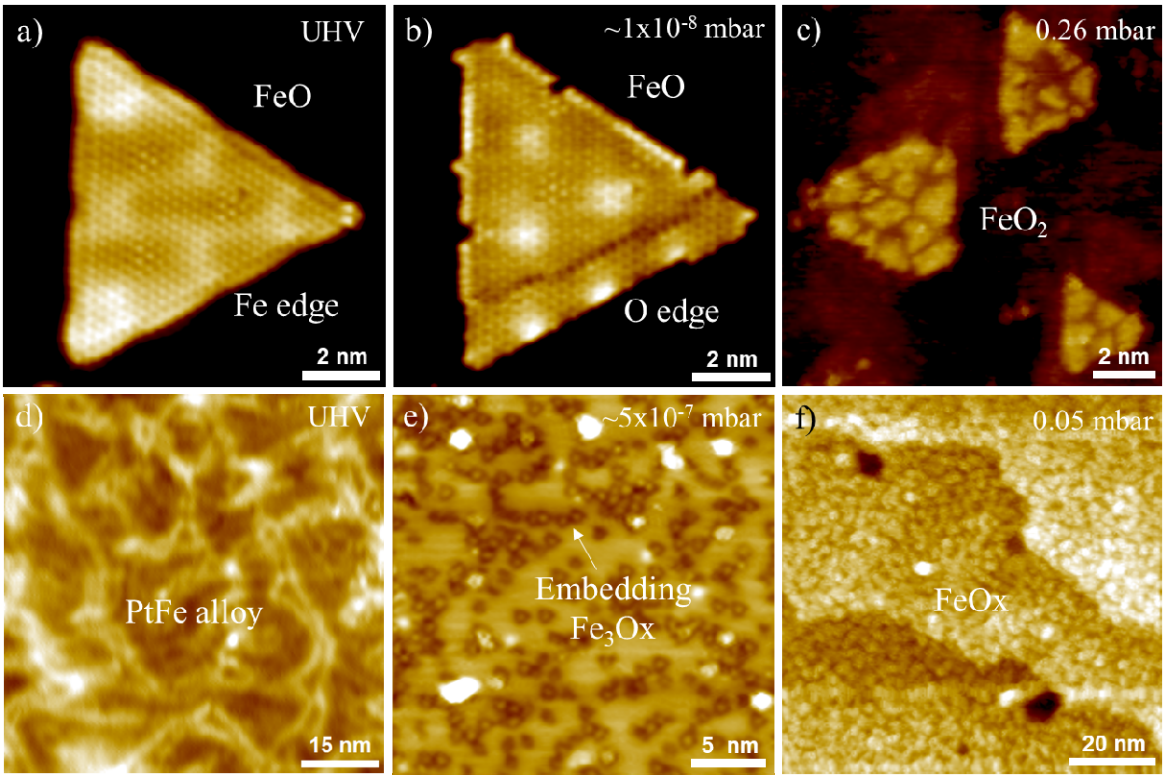

Fig.1 STM image of (a-c) FeO/Pt(111) and (d-f) PtFe alloy exposed to O_2 from UHV to NAP.

REFERENCES

[1] Fu, Q., et al., Interface-confined ferrous centers for catalytic oxidation. Science, 2010. **328**(5982): p. 1141-4.

[2] Xu, H., et al., Highly active Pt-Fe bicomponent catalysts for CO oxidation in the presence and absence of H_2. Energy & Environmental Science, 2012. 5(4): p. 6313-6320.

[3] Balajka, J., et al., Apparatus for dosing liquid water in ultrahigh vacuum. Rev. Sci. Instrum, 2018. **89**(8): p. 083906.

STUDY OF NI CLUSTERS ON Al_2O_3 FOR SABATIER REACTION

Joseba Lizarazu[a], Oihane Sanz[a], Oihana Amorrortu[a], Noelia Barrabes[b], Günther Rupprechter[b], Mario Montes[a]

[a] Dpto. Química Aplicada/Facultad de Química, Universidad del País Vasco (UPV/EHU), San Sebastián (España)

[b] Institute of Materials Chemistry, Technische Universität Wien, Vienna (Austria)

INTRODUCTION

One of the most promising approaches in *carbon capture and utilization* is the Sabatier reaction, leading to the removal of carbon dioxide pollution and at the same time converting it in energy. The Sabatier reaction produces methane from carbon dioxide and hydrogen ($4H_2 + CO_2 \rightarrow CH_4 + 2H_2O$)[1]. Ni-based catalysts are the most widely investigated materials for Sabatier reaction due to their high activity, high selectivity and low cost. The main drawback of Ni-based catalysts is carbon formation that is strongly influenced by temperature and operating pressure [2]. Nickel particle size or nickel dispersion are frequently discussed as factors influencing the CO/CH_4 selectivity of CO_2 hydrogenation. Nanosized metal clusters have demonstrated exceptional properties and play an important role in many catalytic applications.

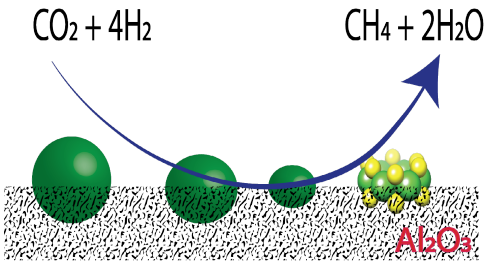

In this work, we evaluated the influence of particle size in the catalytic behavior of Ni/Al_2O_3 catalysts in the Sabatier reaction. Four different preparation routes are explored, from the conventional incipient wetness impregnation or deposition-precipitation to the preparation of Ni nanoclusters.

EXPERIMENTS

Powder catalysts were synthetized with 15% of Ni supported in Al_2O_3. To obtain this type of powder catalysts, three techniques have been developed: Two catalysts were prepared using `All in one method´; which consists in preparing an aqueous suspension with all that is necessary, that is, the support, the metal precursor salt and the additives. These two catalysts were named as `Ni_tdu_pva´ and `Ni_tdu´. Another catalyst was prepare using pore volume impregnation method named as `Ni_imp´. By this technique, the precursor salt of the metal, to be supported, is introduced into a volume corresponding to the pore volume of the support, and finally, the last catalyst was prepared by precipitation-deposit method (Ni_PD), a homogeneous precipitation with the presence of a support that in our case was alumina. To obtain the powder catalysts, the solutions were dried at 120 ºC and calcinated for two hours at 550 ºC. To control the particle size and structure we prepare $Ni_6(SC_2H_4Ph)_{12}$ nanoclusters based on reported methods [3] and supported on Al_2O_3 by impregnation.

The physical-chemical properties of the prepared catalysts were studied by several techniques such as: N_2 physisorption (BET), CO chemisorption, X-ray Diffraction, Temperature programmed reduction/adsorption/desorption (TPR/D/O) and the catalytic performance has been tested in the Sabatier reaction at CO_2/H_2 feed molar ratio of 1:4. Kinetic tests have been done between 150-500 ºC at atmosphere pressure, with a feed molar ration of CO_2/H_2 1:4. In all the test flow reactor was

used, loaded with 200mg of catalysts, and the outgas connected for analysis with a GC-chromatograph.

RESULTS AND DISCUSSION

The preparation protocol had a strong effect on the surface of the catalysts. Table 1 showed differences in dispersion and particle size depending on the sample. PVA and PD protocols leads to higher dispersion and smaller particle size.

These results were correlated with the reduction profiles shown in Fig.1. Therefore, high homogeneous surfaces with smaller particle sizes are required to optimize the catalytic performance. Then, the next step is the atomically precise nanoclusters. The preliminary results showed the possibility to obtain highly pure Ni_6 cluster.

CONCLUSION

The PVA and PD methods lead to the most homogeneous surface and optimal candidate for better catalytic performance. However, the straightforward and highly reproducible route is the PVA. Then, once the nanocluster catalysts will be prepared, the final comparison in catalytic activity will be obtained.

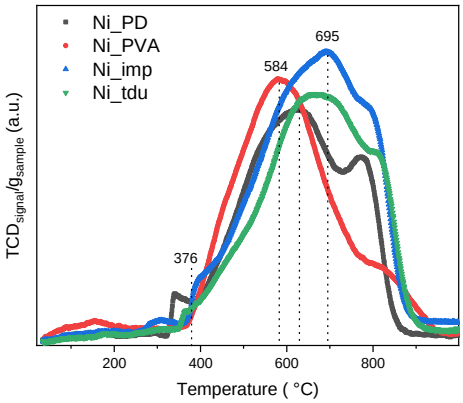

	Metallic surface (m^2/g_{sample})	Dispersion (%)	Grade of reduction (%)	Dp Ni^0 (nm)
Ni_tdu_pva	20.65	20.7	65.19	4.89
Ni_tdu	11.66	11.7	74.72	8.66
Ni_PD	21.07	21.1	68.87	4.79
Ni_imp	13.62	13.6	70.2	7.42

Figure 1: *(left)* H_2 reduction profiles by TPR and *(right)* Physic-chemical characterization results

REFERENCES

[1] M. Saric, J.W. Dijkstra, W.G. Haije, J. CO2 Util, **2017**, 20, 81-90

[2] K. Stangeland, D. Kalai, H. Li, Z. Yu, Energy Procedia, **2017**, 105, 2022-2027

[3] Kagalwala H., et al. *Inorganic chemistry*, **2013**, 52, 9094-9101.

CO, NI AND K AS PROMOTERS IN CO_2 HYDROGENATION ON MoS_2 BASED CATALYSTS

Gernot Pacholik, Ludwig Enzlberger, Karin Föttinger *

E165 - Institute of Materials Chemistry

INTRODUCTION

CO_2 is a well know greenhouse gas and the amount in the atmosphere is still rising. The goal of this work was to study recycling and utilization of carbon dioxide in flue gas by catalytic reduction. Flue gas contains about 10 – 15 vol.% CO_2, oxygen, water and traces of sulfur containing substances like H_2S. There are several ways to convert CO_2 into valuable compounds using different catalysts. For example: Ni based catalysts for CH_4 formation, $Cu/ZnO/Al_2O_3$ for methanol production or MoS_2 based catalysts for alcohol synthesis. However, the sulfur contamination in the flue gas leads to deactivation of many catalysts. MoS_2 based catalysts should not be affected by sulfur containing feed gas. Co-Mo-S materials are known as hydrodesulfurization catalysts and are also active for CO_2 hydrogenation. [1] Therefore, in this work, we have studied MoS_2 based catalysts in order to learn about correlations between synthesis and composition, structural and catalytic properties.

EXPERIMENTS

In this work different formulations of Co-Mo-S and Ni-Mo-S catalysts were prepared hydrothermally [2], [3] and by precipitation [4] and compared to each other. Different supports (activated carbon and alumina) were used. Catalysts with and without potassium promoter were synthesized. Catalytic properties were tested in a plug flow reactor up to 20 bar. Reaction orders of the reactants and apparent activation energies of the product formation were calculated. A long-term test was done to ensure the stability of the catalyst.

The catalysts were characterized by TPD (temperature programmed desorption), TPR (temperature programmed reduction), TPO (temperature programmed oxidation), XRD (X-ray diffraction) and N_2 physisorption and the changes of the catalyst during the reaction were investigated.

RESULTS AND DISCUSSION

Products were mainly CO, methane and traces of methanol. Fig. 1 shows the yield of CO and CH_4 over different Co-Mo-S catalysts. The effect of potassium as promoter was investigated. Catalysts with potassium promoter produced much less CH_4 and more CO under the given conditions. There was no dependence on the support.

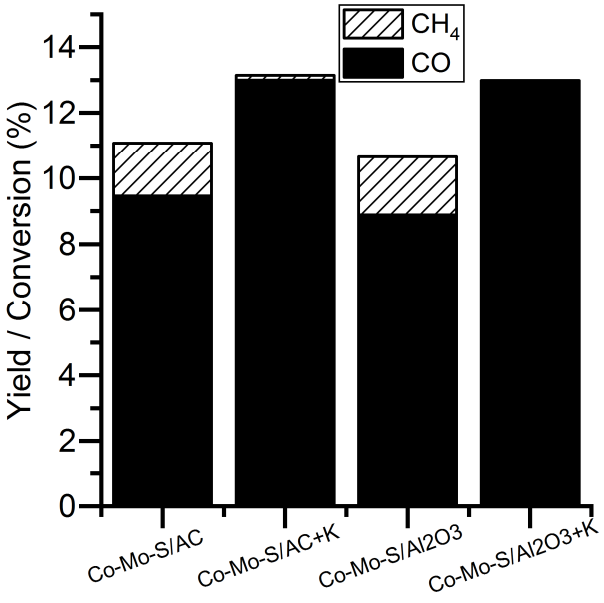

Fig. 1: Yield of CO and CH_4 at 330 °C, 21 bar, 3000 $mlN/(g_{catalyst}*h)$

Fig. 2 shows the conversion of a MoS_2 + K catalyst compared to a Co-Mo-S + K catalyst. The conversion of the Co-Mo-S + K catalyst was higher at the given conditions. The Co-Mo-S + K catalyst showed a lower selectivity to CH_4.

A long-term test over 200 hours showed a constant conversion of CO_2 over the catalyst.

Under reducing conditions, the catalyst was stable below 500 °C, whereas under oxidizing condition above 300 °C SO_2 was formed.

XRD showed a change of the cobalt sulfide phase during the reaction.

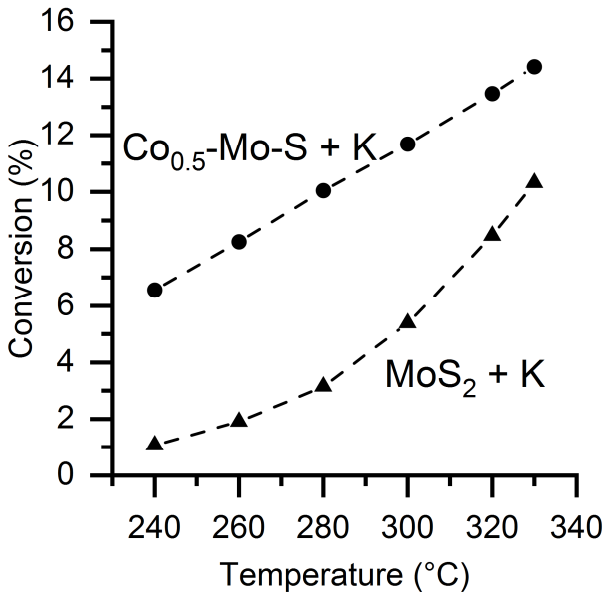

Fig. 2: Conversion of CO_2 over MoS_2 + K and Co-Mo-S + K, 21 bar, 300 mlN/($g_{catalyst}$*h)

CONSLUSION

Co, Ni and K are efficient promoters of MoS_2 based catalysts to increase the formation of CO and inhibit the CH_4 production. The catalyst was stable under working conditions.

ACKNOWLEDGEMENTS

We thank OMV for supporting this project.

REFERENCES

[1] M. D. Porosoff, B. Yan, and J. G. Chen, “Catalytic reduction of CO2 by H2 for synthesis of CO, methanol and hydrocarbons: challenges and opportunities,” Energy Environ. Sci., vol. 9, pp. 62–73, 2016.

[2] H. Li et al., “Nanosheet-structured K–Co–MoS2 catalyst for the higher alcohol synthesis from syngas: Synthesis and activation,” J. Energy Chem., 2018.

[3] D. Li et al., “The performances of higher alcohol synthesis over nickel modified K2CO3/MoS2 catalyst” Fuel Process. Technol., vol. 88, no. 2, pp. 125–127, 2007.

[4] S. Liu, H. Zhou, Q. Song, and Z. Ma, “Synthesis of higher alcohols from CO2 hydrogenation over Mo–Co–K sulfide-based catalysts” J. Taiwan Inst. Chem. Eng., vol. 76, pp. 18–26, 2017.

Pd DOPING EFFECT ON THE CATALYTIC PROPERTIES OF GOLD NANOCLUSTERS SUPPORTED ON OXIDES

Clara García, Noelia Barrabés*, Günther Rupprechter

E165 - Institute of Materials Chemistry, TU Wien, Vienna, Austria

INTRODUCTION

Atomically designed metal clusters offer the possibility to design well-defined and truly homogeneous surfaces leading to optimal catalysts for reaction mechanism studies. Thiolate-protected metal clusters supported on metal oxides have been shown enhanced catalytic activity in several reaction processes, both in liquid phase and gas phase [1]. These structures can be tuned by different strategies: modifying the ligands (ligand exchange reactions), by size (variating the synthetic procedure) or by heteroatom doping (variating the metal composition). In the case of $Au_{25}(SR)_{18}$ clusters, Pd have a preferential position in the core centre, leading to an increase in stability and reactivity [2,3]. Previously we studied the effect of support and nanocluster size on the catalytic properties in liquid phase oxidation reactions (cyclohexane oxidation) [4,5]. Clear influence was observed, related with the cluster stability. Therefore, we further investigate the effect of Pd doping in the cluster structure stability under pretreatment and reaction conditions, in addition to the catalytic properties.

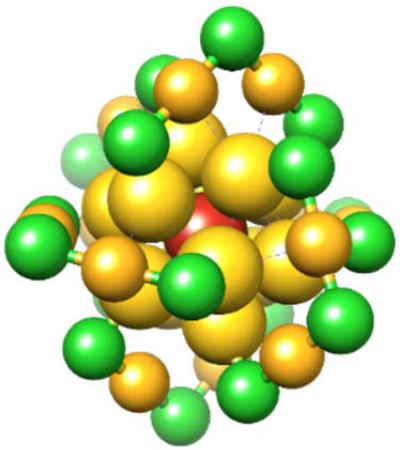

Figure 1. *$PdAu_{24}(SR)_{18}$ core structure (●Pd, ●Au^0, ●Au^+, ●S)*

EXPERIMENTS

$PdAu_{24}(SC_2H_4Ph)_{18}$ and $Au_{25}(SC_2H_4Ph)_{18}$ have been synthesized and supported on SiO_2 and TiO_2 based on reported methods [1]. The samples have been pretreated to remove the ligand shell previous the catalytic test in the cyclohexane oxidation reaction. At each step, fresh, pretreated and after reaction, the samples have been characterized by several techniques (MALDI, UV-Vis, STEM, TPR, XAFS)

RESULTS AND DISCUSSION

In our recent work [5], kinetic measurements and operando ATR pointed out a significant support effect in the selectivity towards cyclohexanone and cyclohexanone, as well as a pronounced cluster modification towards bulk during the reaction was observed depending on size (Au_{25} vs Au_{144}) and support (TiO_2 vs. SiO_2) by HERFD-XAS (Fig. 2). Therefore, introduced the Pd doping aiming for higher structure stability during the reaction and enhanced catalytic behaviour. Preliminary STEM-HAADF analysis of the supported $PdAu_{24}$ clusters revealed that the particle size is preserved during the catalytic

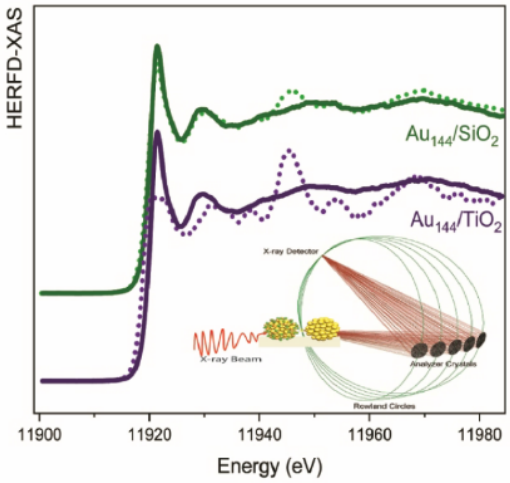

Figure 2. *HERFD-XAS spectra before and after reaction*

oxidation of cyclohexane reaction. The kinetics test show an enhancement in activity and selectivity to the desired products.

CONCLUSION

The application of supported thiolate protected gold clusters for catalysis is an emerging field. However, to date it was mostly assumed that the clusters remained intact during the catalytic reaction. The current work represents one of the first cluster structure studies, revealing how size, support, composition and reaction environments affect stability, which may help to further develop catalysis by thiolate metal nanoclusters.

REFERENCES

[1] R.C. Jin et al, Nano Today, 2018. 18: p. 86-102.

[2] Negishi et al., Phys. Chem. Chem. Phys., 2010, 12, 6219–6225

[3] Sels et al. Nanoscale, 2016, 8, 11130–11135

[4] Zhang et al, J. Phys. Chem. C 2015, 119, 11193−11199

[5] C. García, S.Pollitt, M. van der Linden, V.Truttmann, M.Stöger-Pollach, N.Barrabés, G.Rupprechter, Catalysis today, 2019, *in press*.

Research Field *Engineering in Medicine*

Chairs and Reviewers:

Baudis, Stefan
Dipl.-Ing. Dr. techn.

E163 – Institute of Applied Synthetic Chemistry
stefan.baudis@tuwien.ac.at

Hellmich, Christian
Univ.-Prof. Dipl.-Ing. Dr. techn.

E202 – Institute of Mechanics of Materials and Structures
christian.hellmich@tuwien.ac.at

Introduction

Engineering and medicine have always been closely linked disciplines. This becomes obvious taking a look inside an operating theater back then and now. However, the relationship between engineering and medicine is more profound and recognizable within almost every aspect of medical research and modern health care. For instances, the term "medical device" covers a range of items, incl. apparatus, materials but also software for the diagnosis, treatment, monitoring and prevention of diseases, injuries and handicaps, but also for the investigation, the replacement or the modification of anatomy or physiological processes.

In this symposium we would like to cover all aspects of Engineering in Medicine, including materials, design and constructs, but also innovative processes for the manufacturing of medical devices, e.g., 3D printing, novel technologies for the actuation and signal transduction of devices, the simulation of biomaterials and biological systems, i.e., mechanobiology and biomechanics, and advanced tools for the experimental characterization of biomaterials, incl. advanced mechanics testing as complement to the standard materials science canon of methods.

We want to put an emphasis on the technologies available at TU Wien, especially unique methods being employed along the whole process chain from the design and simulation of materials and constructs, the synthesis, preparation and processing of these materials, the experimental testing of semi-finished and finished products through to the testing of medical devices in pre-clinical or clinical settings.

This very broad topic of this symposium reflects in at least three of the six research focuses of TU Wien, Computational Science and Engineering, Materials and Matter, and Information and Communication Technology, and emphasizes the interdisciplinary nature of all research activities in this field. Hence we welcome and invite contributions from all related faculties of TU Wien, including Civil Engineering, Electrical Engineering and IT, Informatics, Mechanical and Industrial Engineering, Physics and Technical Chemistry.

FABRICATION OF HIGH-VOLUME 3D 2-PHOTON POLYMERIZATION MICROSTRUCTURES

Franziska Gantner, Peter Gruber, Markus Lunzer, Wolfgang Steiger, Aleksandr Ovsianikov

E308-02-3 - Research Group for 3D Printing and Biofabrication

INTRODUCTION

Multi-photon polymerization is a versatile tool within additive manufacturing technologies with rapidly growing applications including photonics [1], biofabrication and tissue engineering approaches [2]. 2-photon absorption, a non-linear optical process, occurs when two photons are absorped simultaneously by a molecule to exite it to an energy state higher than the energy of individual photons. In 2-photon polymerization (2PP) this phenomenon is employed to create arbitrary and complex 3-dimensional (3D) structures with feature resolutions down to a few hundred nanometres. A pulsed laser is tightly focused into photosensitive resin and moved in a 3D manner to locally crosslink polymers with high temporal and spatial control [3]. Typically, the overall size of the fabricated structures is no more than some 100 μm in each dimension. Despite the ongoing progress in the field of 2PP, fabricating larger structures while preserving sub-micrometre features remains challenging [4]. Due to this, most attempts to up-scale 2PP-structures are made in only one or two dimensions [5]. However, by adapting and optimizing the structuring technique and the material composition it is possible to produce constructs that are up-scaled in all three dimensions which results in not only large-scale but also high-volume 2PP-objects that show high-resolution features.

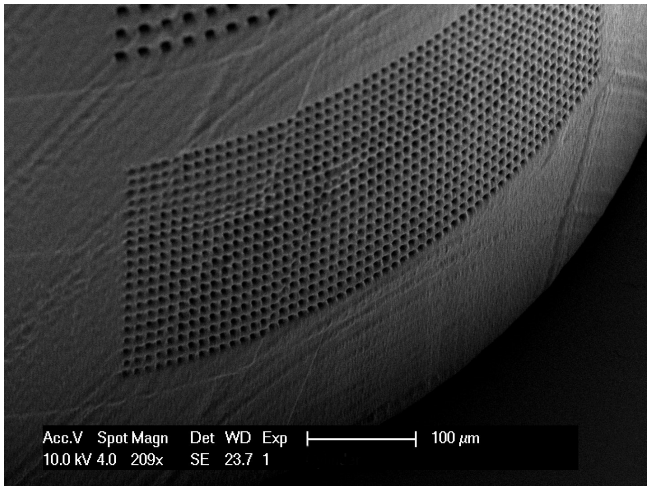

Figure 1: Close-up SEM-image of a high-volume structure with stitching areas and features with a size down to 5 μm.

EXPERIMENTS/FUNDAMENTAL OF THE PROBLEM/EXAMINATIONS

The main challenge when up-scaling in beam propagation direction are optical abberations that lead to an inhomogenious structuring process. This limits the focusing optics and impairs the printing resolution. To overcome this problem a sample mount with a wider objective working range (WOW-2PP) [6] was used. This technique enables to keep the focal spot distance in the material constant and reduces aberrations to a minimum. The objective used for the structuring process shows a limited field of view (FOV) that restricts the structuring area. To fabricate objects that exceed this FOV the printing area needs to be segmented. Therefore a high processing accuracy of the printing stage, suitable printing parameters and the spatial arrangement of the structured layers, called stitching, are fundamental (Fig.2). To create high-volume objects WOW-2PP was combined with an angular stitching arrangement. Since 2PP is a quite time consuming process it is crucial to fabricate larger structures with a high throughput system. Therefore a thorough understanding of the performance of the structuring materials is essential.

Further, large-scale structures show different mechanical behaviour than regular sized objects which is challenging the processed materials and may lead to undesirable effects such as tension and shrinkage. To overcome those problems two different categories of materials were tested and optimized.

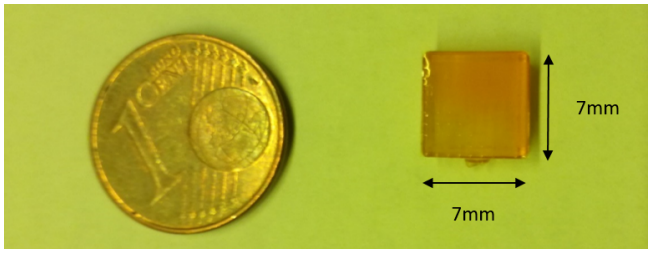

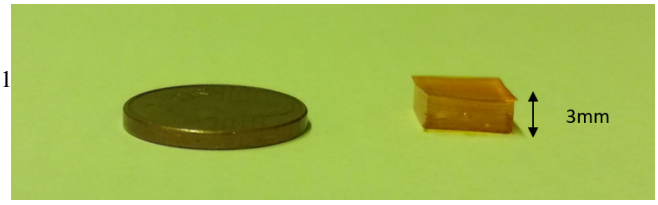

Figure 2: High-Volume 2PP-structure showing a size of 7 mm × 7 mm × 5 mm.

RESULTS AND DISCUSSION

By combining a high writing speed of 1000 mm s^{-1} with a resin based on triacrylates, it was possible to fabricate stable high-volume 2PP-structures with dimensions up to 7 mm × 7 mm × 5 mm that showed features down to 5 μm.

CONCLUSION

Material composition and the fabrication technique are crucial to increase the size of 2PP-structures while remaining the resolution of the feature size. In order to fabricate even larger up-scaled structures the materials and printing set-up need to be adapted and improved further.

REFERENCES

[1] Deubel, M.; Wegener, M.; Linden, S.; von Freymann, G.; John, S.: *"3d-2d-3d photonic crystal heterostructures fabricated by direct laser writing"*. Optics Letters, 31 (6), p. 805–807, 2006.

[2] Ovsianikov, A. et al.:*"Engineering 3D cell-culture matrices: Mul- tiphoton processing technologies for biological and tissue engineering ap- plications"*. Expert Review of Medical Devices, 9 (6), p. 613-633, 2012.

[3] Baldacchini, T. :*"Three-Dimensional Microfabrication by Two- Photon Polymerization"*. In: Generating Micro- and Nanopatterns on Polymeric Materials. WILEY-VCH, p. 6107-140, 2011.

[4] Zhou, X.; Hou, Y.; and Lin, J.:*"A review on the processing accuracy of two-photon polymerization"*. AIP ADVANCES, 5(3), 2015.

[5] Malinauskas, M.et al.:*"Two-photon polymerization for fabrication of three-dimensional micro- and nanostructures over a large area"*. Proceedings of SPIE, 7204, 2009.

[6] Kotaro, O. et al.:*"High-aspect 3D two-photon polymerization structuring with widened objective working range (WOW-2PP)"*. Light: Science and Applications, 2, 2013.

ACETAL MOIETIES AS BIODEGRADABLE FUNCTIONALITY IN PHOTOPOLYMERS FOR BONE REGENERATION

Barbara Dellago[a], Robert Liska[a,b], Stefan Baudis[a,b]

[a]E163 - Institute of Applied Synthetic Chemistry at TU Wien
[b]Austrian Cluster for Tissue Regeneration

INTRODUCTION

The most critical and costly problems in human health care is the loss or failure of an organ or tissue. Currently, the loss of an organ or tissue is treated by transplant autografts (originating from patient) or from one individual into another (allografts). This is an imperfect solution, because transplantation is limited by a critical donor shortage. Due to that the discipline of tissue engineering (TE) in life science has emerged over the last two decades. It allows to restore, maintain or improve the function of lost, damaged or diseased tissue. It is applicable for a wide range of injuries and diseases ranging from cardiovascular, skin and bone diseases. Attention lies on the biocompatibility and biodegradability of scaffolds. The scaffold completely takes over the mechanical function of the organ. In the meantime the tissue regenerates, the scaffold degrades and gives way to the new formed tissue (Figure 1). Since individual implants are necessary for each patient, the technology of additive manufacturing (AMT) was established in TE (Figure 2). This technology enables the production of complex geometries with defined porosity.[3] These properties are important for the above mentioned requirements of Tissue Engineering.

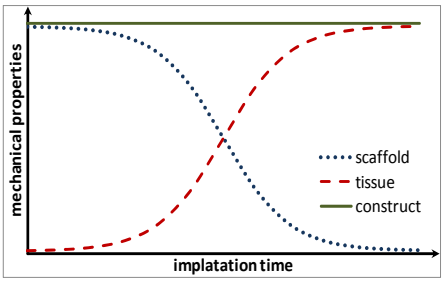

Figure 1: Ideal mechanical behaviour of the manufactured scaffold during the time of degradation and the regeneration of natural tissue.[1]

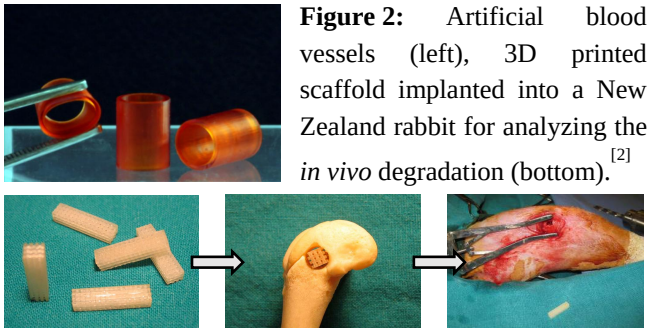

Figure 2: Artificial blood vessels (left), 3D printed scaffold implanted into a New Zealand rabbit for analyzing the *in vivo* degradation (bottom).[2]

FUNDAMENTAL OF THE PROBLEM

In this work, new bone replacement materials are developed. During bone regeneration, cells, the so called osteoclasts, degrade the bone at a pH value of about 4.5 and other cells, the osteoblasts build up new tissue.[4] The standard materials for bone replacement are polyesters, however, degrade quite slow under acidic conditions. Therefore, fast degradation should be ensured by incorporation of acetals into the polymer backbone. Acetals have the property of being stable under neutral and basic conditions but degrade fast under acidic pH value.[5]

MATERIALS AND METHODS

Acetals were synthesized by conversion of an aldehyde or ketone, e.g., terephthalaldehyde, with an alcohol, e.g., 2-hydroxyethylmethacrylate (HEMA). This way, acetal moieties were also provided with photopolymerizable groups. Methacrylates were chosen as reactive groups. Compared to acrylates, they are less toxic and have sufficient reactivity to be used in photopolymer based AMTs. The molecular structures were approved by NMR spectroscopy. In order to investigate the reactivity of the synthesized monomers, photo-DSC measurements are conducted. In addition, photorheology coupled with real-time IR measurement was chosen to determine parameters relevant for 3D printing applications. Furthermore, the degradability of photopolymerized methacrylates was tested *in vitro* at a pH typical for the osteoclasts microenvironment. Therefore, the samples were placed into an aqueous HCl (pH of 4.5) and were weighed after certain intervals.

RESULTS AND DISCUSSION

In the course of this work, monomers with acetals as cleavable moieties were be prepared in good yields with sufficient purity. These monomers were tested for their reactivity and show values expected for this class of monomers. The degradation characteristics of according polymers is promising. In Figure 3, the sample mass during degradation of the crosslinked acetal based on glycerol monomethacrylate and terephthalaldehyde (T5MA) is shown. There, a steep increase of the mass in the initial phase can be seen. It is assumed that this is the result of spontaneous swelling. The continuous mass increase in the second phase is expected to be caused by water uptake into the network owing the decreased network density as a consequence of acetal cleavage. In the third phase, elution of small molecules out of the polymer network overcompensates the mass increase by swelling and a mass decrease is finally observable.

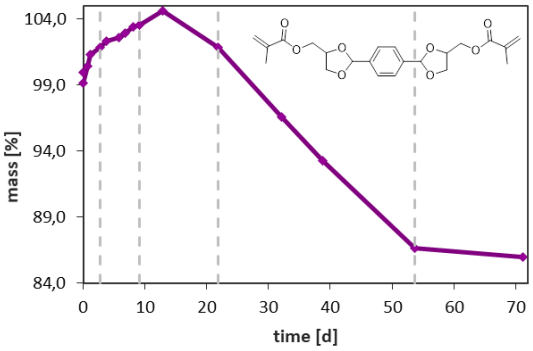

Figure 3: Degradation of T5MA under acidic pH

CONCLUSION

The synthesis of monomers with acetals as cleavable moieties was successful. Methacrylate as functional group has shown a good reactivity as investigated by Photo-DSC and real-time infrared photorheology measurements. The *in vitro* degradability tests have shown a swelling followed by a mass-erosion of photopolymerized networks. These results proof the applicability of acetals as degradability motifs in polymer networks. In addition to methacrylates as model class of photopolymerizable monomers, biocompatible vinyl esters and vinyl carbamates will be considered in future.

REFERENCES

[1] Baudis, S., Dissertation 2010, Vienna University of Technology: Vienna. p. 9.
[2] C. Heller *et al., J. Polym. Sci. A,* 2011, **49**(3) 650-661
[3] Jariwala, S. H., et al., 3D Print Addit Manuf, 2015, **2**(2): 56-64
[4] Alghazali, K. M., et al., Drug Metabolism Reviews, 2015, **47**(4): 431-454.
[5] Liu, B. and Thayumanavan, S., Journal of the American Chemical Society, 2017, **139**(6): 2306-2317.

MOLECULE-TO-BEAM HOMOGENIZATION, APPLIED TO DNA

Johannes Kalliauer[a], Gerhard Kahl[b], Stefan Scheiner[a], Christian Hellmich[a,*]

[a]E202 - Institute for Mechanics of Materials and Structures at TU Wien, Austria
[b]E136 - Institute of Theoretical Physics at TU Wien, Austria

INTRODUCTION

Mechanical properties of deoxyribonucleic acid (DNA) are of great biological interest, as duplication and expression are processes involving force-driven deformations. In traditional approaches towards understanding the mechanical behavior of DNA sequences, the latter were considered as straight and isotropic beams of cylindrical shape [1], leading, however, to unrealistic ratios between torsional and bending rigidities. In fact, DNA sequences resemble deformation characteristics (such as bending, stretching, torsion, or shearing) which are well known from a key concept of continuum mechanics, that is beam theory. On the other hand, molecular dynamics (MD)-based modeling tools, which are standardly applied nowadays to macromolecules (such as DNA), provide detailed information as to the different energy states such molecules are in under specific (thermal and mechanical) boundary conditions, but are not directly interpretable in terms of mechanical constants allowing for quantifying the aforementioned deformation modes [2]. This contribution aims at filling this gap, by providing an upscaling procedure, relating the output of MD simulations, performed on a sequence of base pairs, to beam theory-related deformation modes.

METHODS

While the subsequently described method can be applied to any kind of polymer, we here study, for the sake of demonstration, a poly(A)-poly(T)-B-DNA molecule. This molecule is reconstructed in the MD software Amber, at a length of 20 base pairs, while the molecule is clamped at both ends, see Figure 1. Then, the molecule is initially deformed to a homogeneous strain state, such as uniaxial stretch or uniaxial torsion. Eventually, the molecule relaxes, and takes up an equilibrium state.

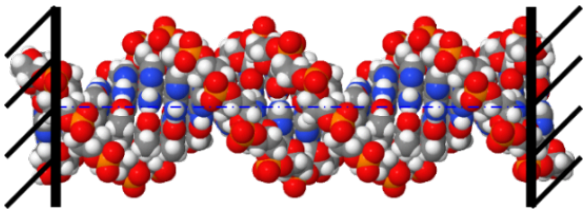

Figure 1: The DNA equilibrates, while fixing both ends at specific deformations states.

One of the key novelties of this contribution is the adaptation of the classical intersection principle ("free body diagram") to the molecular structure. In particular, the potential energies extracted from the MD simulation are translated into a corresponding system of equilibrated forces and moments [2,3], while formally representing the interaction lines between atoms as beams, see Figure 2. The forces and moments are then inserted into the principle of virtual power [4,5], which allows for "homogenizing" the molecular DNA assembly to a beam-like structural element, with corresponding bending, torsional, and axial rigidities.

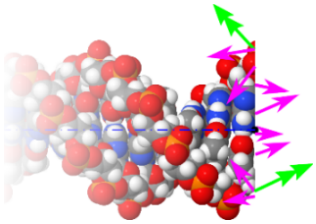

Figure 2: Potential-derived forces and moments in "beam cross sections", as input for the principle of virtual power.

RESULTS AND DISCUSSION

The molecule-to-beam homogenization method clearly evidences that the axial and torsional deformation modes of DNA are coupled; and increased stretch induced a greater rotational twist, see Figure 3. This computational result is fully consistent with experimental observations in rotor bead tracking experiments [1].

To our knowledge, the overwinding behavior of DNA, which is only known from rotor bead tracking experiments [1], could be predicted by means of computer simulations for the first time.

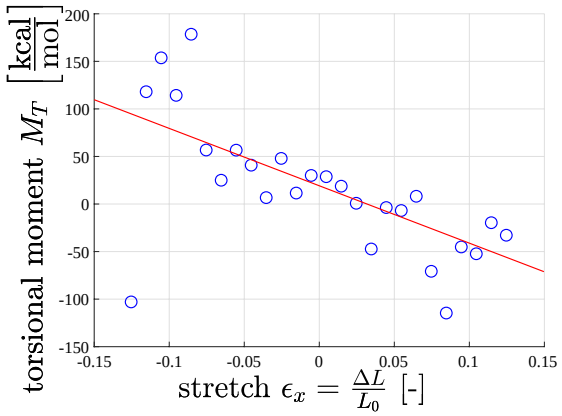

Figure 3: Overwinding behavior observed while stretching the studied DNA sequence; blue circles represent the torsional moment vs. the stretch imposed in the MD simulations, the red line represents the linear fit of the data.

CONCLUSION

This work represents an unprecedented approach a to the transition of molecular dynamics into beam theory-related mechanical properties: In the long run, the implication of this work can be potentially far-reaching. On the one hand, the replication behavior of DNA, which is believed to be influenced by its mechanical properties, potentially affects the initiations of genetic diseases such as cancer [6]. On the other hand, the proposed strategy can be straightforwardly adopted for any other chain polymer, opening a wide range of further applications.

ACKNOWLEDGMENT

The computational results presented have been achieved using the Vienna Scientific Cluster (VSC).

REFERENCES

[1] Gore, J.; Bryant, Z.; Nöllmann, M.; Le, M. U.; Cozzarelli, N. R.; Bustamante, C.: *"DNA overwinds when stretched"*. Nature, 442 (7104), p. 836-839, 2006.

[2] Boussinot, F.; Monasse, B.; Susini, J.-F.: *"Reactive programming of simulations in physics"*. International Journal of Modern Physics C, 26 (12), p. 1550132, 2015.

[3] Monasse, B.; Boussinot, F.: *"Determination of forces from a potential in molecular dynamics"*. arXiv e-prints arXiv:1401.1181, 2014. [Online]. Available: https://arxiv.org/pdf/1401.1181.pdf

[4] Germain, P.: *"The method of virtual power in continuum mechanics. part 2: Microstructure"*. SIAM Journal on Applied Mathematics, 25 (3), p. 556-575, 1973.

[5] Höller, R.; Aminbaghai, M.; Eberhardsteiner, L.; Eberhardsteiner, J.; Blab, R.; Pichler, B.; Hellmich, C.: *"Rigorous amendment of Vlasov's theory for thin elastic plates on elastic Winkler foundations, based on the principle of virtual power"*. European Journal of Mechanics - A/Solids, 73, p. 449-482, 2019.

[6] Bao, G.; Suresh, S.: *"Cell and molecular mechanics of biological materials"*. Nature Materials, 2(11), p. 715-725, 2003.

AFM-BASED MICROBEAM BENDING OF HUMAN CORTICAL BONE AT THE LAMELLAR LEVEL

Vedran Nedelkovski[a], Orestis G. Andriotis[a], Rainer Hahn[b], Paul H. Mayrhofer[b], Andreas Steiger-Thirsfeld[c], Johannes Bernardi[c], Philipp J. Thurner[a]

[a]E317 - Institute of Lightweight Design and Structural Biomechanics
[b]E308 - Institute of Materials Science and Technology
[c]E057 – University Service Center for Transmission Electron Microscopy

INTRODUCTION

Bone is a biological material with unique mechanical properties, owing to a complex hierarchical structure from the nanoscale up to the macroscale. To better understand bone mechanics, investigation of mechanical properties of structural elements on all hierarchical levels and how they interact is a promising approach. In this context, mechanical testing of individual structural elements at the microscale, such as individual lamellae, remains a challenge. Focused ion beam (FIB) milling is an attractive technique for machining microscopic bone samples. So far, animal bone microbeams[1][2][3] and micropillars[4][5][6] have been mechanically tested in bending via atomic force microscopy (AFM), or compression via conventional nanoindentation, respectively, mostly in dehydrated state except for one study. Similar experiments on human bone have, to the best of our knowledge not been reported. Here we present an AFM-based microbeam bending method applied for the micromechanical assessment of human cortical bone in both dehydrated and rehydrated state.

METHODS

Bone samples from the femoral midshaft of 4 male donors, aged 65-94y, were used and 4 microbeams per donor were produced. The FIB-machined microbeams (in cooperation with E057) were milled from a single bone lamella and were bent at multiple positions along the beam length[7] with an AFM tip furnished with a glass microsphere of 5 μm diameter for minimizing indentation effects (Fig.1A). The same microbeams were tested, first dehydrated in air, and, second rehydrated in Hank's Balanced Salt Solution (HBSS) after rehydration time of 2h. The measurement setup was previously calibrated by bending FIB-milled Si microbeams of known stiffness (in cooperation with E164) utilising an *in-situ* picoindenter situated within a scanning electron microscope (SEM). From the measured force vs. deflection curves apparent stiffness data along the microbeam length was obtained (Fig. 1B) and plotted against beam position (Fig.1C). The data was then fitted to obtain a value for the bending modulus as a fit parameter (Fig.1C). Additionally, the dissipated energy during bending of the rehydrated bone microbeams was calculated as the difference between the areas under the loading and unloading curve (Fig. 1B).

RESULTS AND DISCUSSION

Microbeams of length, width and height (25 x 4 x 1) μm^3 were made by FIB milling (Fig.1A) from a single bone lamella. Precise positioning of the microbeam within the AFM was achieved by imaging the base of the microbeam in force mapping mode (Fig. 1A). Bending modulus values obtained from bending measurements along the beam length ranged (25.1-48.7) GPa in air and (7.3-19.1) GPa in HBSS. Decrease of bending modulus up to 5 times was observed for microbeams upon rehydration. No significant change of bending modulus was observed with respect to age

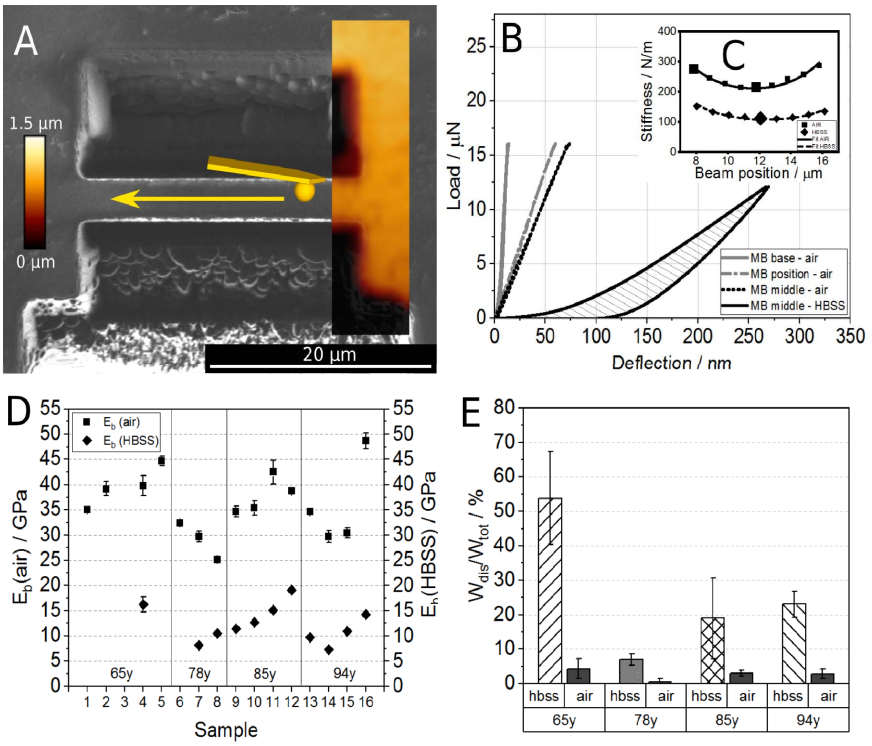

Figure 1: (A) SEM image of a bone microbeam with overlayed AFM force map (setpoint height) of the beam base. (B) Load vs. deflection bending curves at different beam positions in air (grey solid, grey dashed & black dotted) and HBSS (black solid). (C) Apparent stiffness vs. beam position from measurement (points) and fit (lines). (D) Bending moduli in air (squares) and HBSS (diamonds) of all tested microbeams from all donors. (E) Relative dissipated energy during bending vs. donor age in air and HBSS.

(Fig.1D). Moreover, bending in air exhibited linear elastic behaviour, with same apparent loading and unloading stiffness (grey solid, grey dashed and black dotted curves in Fig.1B), whereas in HBSS stiffness was higher during unloading compared to loading, and mechanical hysteresis was observed (black solid curve in Fig.1B). The dissipated energy in rehydrated samples (area between loading-unloading curves) ranged from 0.093 to 0.655 pJ (i.e. 5.8-64.5% of the total energy) and showed a trend to decrease with age (Fig.1E).

The findings show the importance of water for the micromechanical properties of bone. In air, beams appear linear elastic, whereas addition of water and salts leads to decrease of stiffness, and inelastic behaviour with significant energy dissipation. The data suggests there could be an effect of age, with possibly lower energy dissipation in bone from older donors. This in turn may play a role in decrease of fracture toughness and increased fragility of bone with age[8][9].

CONCLUSION

In conclusion, microbeam bending of single bone lamellae microbeams within an AFM was developed, both in dry and rehydrated conditions. No significant change in the elastic properties was observed with respect to age. However, our data indicates there could be a change in the viscoelastic properties and the ability to dissipate energy in bone from older donors. To further investigate these effects, the number of donors and age range should be increased and mechanical response at different loading rates should be obtained in further studies. Finally, as bone is hydrated in its physiological state and water plays a significant role in the mechanical properties of the tissue, experiments should preferentially be performed in hydrated conditions.

REFERENCES

[1] Jimenez-Palomar et al., JMBBM, 5:149-155, 2012.; [2] Jimenez-Palomar et al., JMBBM, 52:63-71, 2015.
[3] Jimenez-Palomar et al., Front. Mater., 2:1-7, 2015.; [4] Schwiedrzik et al., Nat. Mater., 13:1-8, 2014.
[5] Schwiedrzik et al., Acta Biomater., 60:302-314, 2017.; [6] Luczynski et al., JMBBM, 52:51-62, 2015.
[7] Sillero et al., J. Micromech. Microeng., 19:115016, 2009. [8] Nyman et al., Bone, 42:193-199, 2008.
[9] Manhard et al., Bone 87:1-10, 2016.

RAPID PROTOTYPING, MANUFACTURING AND APPLICATION OF ORGAN-ON-A-CHIP AND CELL BASED LAB-ON-A-CHIP SYSTEMS

Sebastian R. A. Kratz [a,b]

[a]E163 - Institute of Applied Synthetic Chemistry
[b]E164 - Institute of Chemical Technologies and Analytics

INTRODUCTION

Nowadays there are basically two pre-clinical ways to gain a better understanding how physiological parameters and drugs can influence the human organism: well-established 2D cell culturing and complex animal models. Organ-on-a-chip and lab-on-a-chip devices has been developed to create more complex 3D cell models which are exposed to dynamic ambient conditions and a proper readout of the cell behavior.

Through the last years several ways has been investigated to model a more physiological environment and to include non-invasive sensors to better predict influences on the cells in culture.

A major challenge the research of microfluidics systems are the many iteration steps which have to be taken from the first design up to the working device.

EXPERIMENTS / FUNDAMENTAL OF THE PROBLEM / EXAMINATIONS

Furthermore through the commercialization of several device the industry is seeking for suitable methods to produce cheap and robust devices with designs in the scale of micrometers. Therefore there is still a gap between the rapid manufacturing for research purpose and the industrial manufacturing for commercial devices.

To hit the challenge and overcome the gap new rapid prototyping methods has to be investigated and evaluated.

This work will investigate the applicability of new materials for the rapid prototyping and the application of those in organ-on-a-chip and lab-on-a-chip devices.

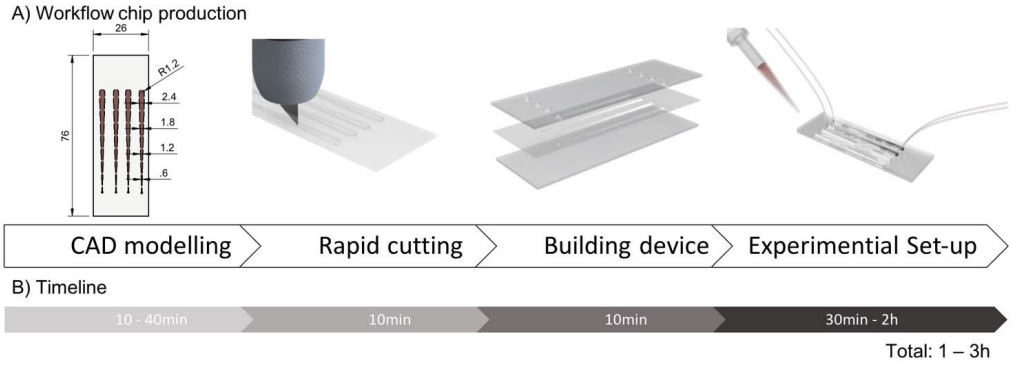

Picture 1:
A) Rapid prototyping of biocompatible pressure sensitive adhesives

B) Time line for concept-to-chip-time

One promising method is to use biocompatible pressure sensitive adhesives to establish microfluidic system for a physiological cell-like environment.

This method to assemble and built those device must be rated in regards of effort and accuracy in microfabrication as well as the bonding ability to other materials to build up multi-featured devices. Beside mechanical and chemical properties the investigation of biocompatibility is necessary to establish a proper valid cell model with in the device.

The following pressures sensitive adhesives are investigated:

Name	Total thickness	Layer thickness	Adhesives thickness	Adhesives type
ARcare 92712®	48.26 µm	12.7 µm polyester	17.78 µm	MA-93 acrylic pressure sensitive
ARcare 90445®	81.28 µm	25.4 µm polyester	27.94 µm	AS-110 acrylic medical grade
ARcare 90106®	142.24 µm	25.4 µm polyester	58.42 µm	MA-69 acrylic hybrid medical grade
ARseal 90880®	142.24 µm	50.8 µm polypropylene	45.72 µm	SR-26 silicone adhesive

Table 1 Pressure sensitive tape

RESULTS AND DISCUSSION

To analyse the cutting behaviour of pressure sensitive adhesive tapes a defined structure was cut, residual material removed and the deformation of the edges of the structure was measured.

When the digital model for the given chip design already exist, the chip structures can be cut with in minutes. By primary evaluation of the plotting resolution structures down to 100 µm are cut. The limiting factor for the machining of the pressure sensitive double-sided adhesive tapes is how easy and under which deformation the residual material of the designed structure can be peeled off. This represents the limit of the scale for cutting structures within pressure sensitive double sided adhesive tape.

The chip was built easily within 3h as described in Figure 2. The chip stayed leakage free for 7 days was perfused at the second day with 2 µl/min maintained at 37ºC. The seeded BeWo b30 cells adhered after 24h to the collagen treated membrane (see Figure 4) until day 7. Through the establishment of a monolayer of BeWo b30 cells the resistance of the cells and the membrane increases up to 0.12 kOhm and 0.17 kOhm at day 2 (see Figure 27 A). The TEER increases significantly with developing of tight junctions between the cells. This can be observed at day 2 where the slope of the TEER measurement increases and a confluent monolayer was established. Since confluence was achieved at day 2 flow was initiated to remove waste products of the cell metabolism.

CONCLUSION

The membrane- and electrode-integrated cell-based lab-on-a-chip system is established and an experiment over 7 days with BeWo b30 cells is carried out. By using pressure sensitive double-sided adhesive tapes the concept-to-chip time is under 3h. This rapid prototyping represents a very easy and fast adaption and manufacturing of the membrane- and electrode-integrated cell-based lab-on-a-chip system. There is no clean room needed and only a low investment in the manufacturing infrastructure is necessary. The adhesive tape ARcare 90445 shows suitable properties which withstand the experimental set up. ARcare 90445 was chosen to build up the membrane- and electrode-integrated cell-based lab-on-a-chip system.

The valid lab-on-a-chip system can be used to study the influence of the barrier properties through nanoparticles and drugs. Beside the TEER measurement the integrated electrodes can be used to new applications as short circuit current, action potentials of electrically active cells for electrophysiology studies, which are currently lacking in the majority of micro physiological systems.

REFERENCES

[1] Odijk, M. et al. Measuring direct current trans-epithelial electrical resistance in organ-on-a-chip microsystems. Lab Chip 15, 745–52 (2015).

SURFACE MODIFICATION OF Ti- BASED MATERIALS FOR BIOMEDICAL APPLICATION

J. Sun[a], Tz. Boiadjieva-Scherzer[a], H. Kronberger[b], K. Staats[c], J. Holinka[c], R. Windhager[c]

[a] Centre of Electrochemical Surface Technology GmbH (CEST)
[b] Technical University of Vienna, Institute of Chemical Technologies and Analytics
[c] Medical University of Vienna, Department of Orthopedics and Trauma Surgery

INTRODUCTION

Titanium metal and its alloys are the most extensively used materials for fabricating long-term implants in the biomedical sector. Despite the material choice, implants in general suffer from the drawback of susceptibility to bacteria-induced inflammation, which causes loosening of the implants and other complications [1]. Antibiotic treatment of the inflammations is increasingly becoming ineffective due to development of drug resistant bacterial strains. Currently, there are implants decorated with silver and versions dip-coated with antibiotics on the market [2], but their toxicity and effectiveness to prevent bacterial biofilm formation are questionable due to overuse.

METHODE

An alternative to antibiotics is the creation of a defined nano-topography on the surface of the implant materials, which inhibits adherence of bacterial cells to them. One of the methods used for surface nano-structuring of Ti- based materials is anodization in fluoride containing electrolytes, resulting in formation of nanotubes [3]. It has been shown that nanotubes of 100 nm diameter promote osseointegration and antibacterial efficiency even without the use of pharmaceuticals [4]. In order to enhance the antibacterial properties, the nanotubes can be loaded with antibacterial agents like Ag, Cu, Se [5] and zinc selenide [6]. Se in particular exhibits osteogenic and antimicrobial activity, while suppressing inflammations. Studies with Se nanoparticles produced from precipitation indicate decrease in the function of adhesion-mediating proteins, inducing the production of damaging reactive oxygen species and inhibition of the proliferation of macrophages [5]. Se compounds like copper selenide [7] and silver selenide are attractive for implant surface modification due to low solubility, making it suited for low long-term release of antibacterial agents.

The biocompatibility and bioactivity of the implant material can be improved by an additional coating of hydroxyapatite (HAp), which promotes bone formation and growth [8]. Crystalline HAp provides mechanical stability, but has been shown to degrade slowly in simulated body fluid leading to insufficient bone ingrowth [9]. Amorphous HAp has a slightly higher solubility, which promotes faster initial bone fixation due to resorption and bioactivity [10].

RESULTS

Surface modifications of Ti and Ti6Al4V alloys were carried out to confer antibacterial properties and improved biocompatibility to it. The materials were first subjected to anodization to nanopattern the surface. The anodization parameters (voltage and time), the electrolyte composition and acidity were varied in order to grow uniform phosphate-doped nanotube-shaped structures with a diameter of 100. Subsequently, Se and Se alloys (Ag_2Se and Cu_2Se) were uniformly incorporated into the titania nanotubes by pulse electrodeposition for enhancement of antibacterial properties. The electrochemical response of modified Ti-based substrates and the electrodeposition process of Se and Se alloys were studied by cyclic voltammetry. Se-doped hydroxyapatite top coats were then

deposited by precipitation on the nano-structured surface which acts as template and provides anchorage for HAp crystals. It was found that addition of Se to the electrolyte influences the HAp nucleation and highly facilitates its deposition and adhesion. The formation of fine globular crystal bundles on top of the HAp needles approximates a two- phase coating, expected to provide high resorption, bioactivity as well as mechanical stability. Preliminary medical in-vitro experiments show significantly better anti biofilm results for samples with Se related coatings compared to silver coated. The electrochemically and chemically treated surfaces were characterized by EDX, FE-SEM, FIB, RAMAN spectroscopy and XRD.

OUTLOOK

Current efforts focus on fabrication of nano-containers filled with potential antibacterial agents for medical testing. The fundamental theory of the nanotube formation is not yet fully understood and more insight might be obtained by planned measurements with optical waveguide spectroscopy, which will be utilized to monitor the layer formation and uniformity of nanotube loading. Medical in-vitro testing of samples for determining antibacterial properties are ongoing and future in-vivo experiments are being considered.

ACKNOWLEDGEMENTS

These investigations were performed with the support of the Austrian Science Foundation FFG under Grant 4253627.

REFERENCES

[1] Chatzopoulos, G. S.; Wolff, L. F. Implant failure and history of failed endodontic treatment: A retrospective case-control study. *Journal of Clinical and Experimental Dentistry* **2017,** *9* (11), e1322-e1328. DOI: 10.4317/jced.54277.

[2] Romanò, C. L.; Scarponi, S.; Gallazzi, E.; Romanò, D.; Drago, L. Antibacterial coating of implants in orthopaedics and trauma: a classification proposal in an evolving panorama. *Journal of Orthopaedic Surgery and Research* **2015,** *10* (1), 1-11. DOI: 10.1186/s13018-015-0294-5.

[3] Lim, Y. C.; Siti, A. S.; Amiera, P. N.; Devagi, K.; Lim, Y. P. Electrochemical deposition of copper decorated titania nanotubes and its visible light photocatalytic performance. *AIP Conference Proceedings* **2017,** *1877* (1), 070002. DOI: 10.1063/1.4999888.

[4] Su, E. P.; Justin, D. F.; Pratt, C. R.; Sarin, V. K.; Nguyen, V. S.; Oh, S.; Jin, S. Effects of titanium nanotubes on the osseointegration, cell differentiation, mineralisation and antibacterial properties of orthopaedic implant surfaces. *The Bone & Joint Journal* **2018,** *100-B* (1_Supple_A), 9-16. DOI: 10.1302/0301-620x.100b1.bjj-2017-0551.r1.

[5] Liu, W.; Golshan, N. H.; Deng, X.; Hickey, D. J.; Zeimer, K.; Li, H.; Webster, T. J. Selenium nanoparticles incorporated into titania nanotubes inhibit bacterial growth and macrophage proliferation. *Nanoscale* **2016,** *8* (34), 15783-15794. DOI: DOI: 10.1039/c6nr04461a.

[6] Mir, I. A.; Alam, H.; Priyadarshini, E.; Meena, R.; Rawat, K.; Rajamani, P.; Rizvi, M. S.; Bohidar, H. B. Antimicrobial and biocompatibility of highly fluorescent ZnSe core and ZnSe@ZnS core-shell quantum dots. *Journal of Nanoparticle Research* **2018,** *20* (7), 174. DOI: 10.1007/s11051-018-4281-8.

[7] Jagminas, A.; Kovger, J.; Selskis, A.; Rėza, A. Effect of hydrogen doping on the loading of titania nanotube films with copper selenide species via alternating current deposition. *Journal of Applied Electrochemistry* **2015,** *45* (10), 1141-1151. DOI: 10.1007/s10800-015-0883-3.

[8] Capanema, N. S. V.; Mansur, A. A. P.; Carvalho, S. M.; Silva, A. R. P.; Ciminelli, V. S.; Mansur, H. S. Niobium-Doped Hydroxyapatite Bioceramics: Synthesis, Characterization and In Vitro Cytocompatibility. *Materials* **2015,** *8* (7), 4191-4209. DOI: 10.3390/ma8074191.

[9] Bang, L. T.; Long, B. D.; Othman, R. Carbonate Hydroxyapatite and Silicon-Substituted Carbonate Hydroxyapatite: Synthesis, Mechanical Properties, and Solubility Evaluations. *The Scientific World Journal* **2014,** *2014*, 969876. DOI: 10.1155/2014/969876.

[10] Xue, W.; Liu, X.; Zheng, X.; Ding, C. Effect of hydroxyapatite coating crystallinity on dissolution and osseointegration in vivo. *Journal of Biomedical Materials Research Part A* **2005,** *74A* (4), 553–561. DOI: 10.1002/jbm.a.30323.

LITHOGRAPHY-BASED CERAMIC MANUFACTURING IN DIGITAL DENTISTRY

Malte Hartmann

E308 - Institute of Materials Science and Technology

Additive Manufacturing (AM) is a summarizing term for a quantity of technologies that enable the processing of metals, plastics or ceramics. They all have in common, that they generate physical 3-dimensional objects layer by layer. AM technologies are especially useful where small and complex parts are needed in small numbers. One of the fields that could benefit from this technological advance is the biomedical field, due to its high demand for individualization, when it comes to implants for example.

The demand for individualization is especially big in the dental industry, where aesthetic considerations like color and translucency are adding to the need for a specialized shape. To enable a successful restoration, like a crown or bridge, high precision and good surface quality are key factors.

Stereolithography is an AM method that excels in these categories and therefor is suitable for dental applications. This technology uses either LASER or Digital Light Processing (DLP) to induce finely localized photopolymerisation in a photoactive resin, as the layer generating mechanism. Fig. 1 shows a schematic setup of the DLP-based stereolithography machine used in this work. It is state of the art to use stereolithographic machines to produce models and molds from polymeric materials.

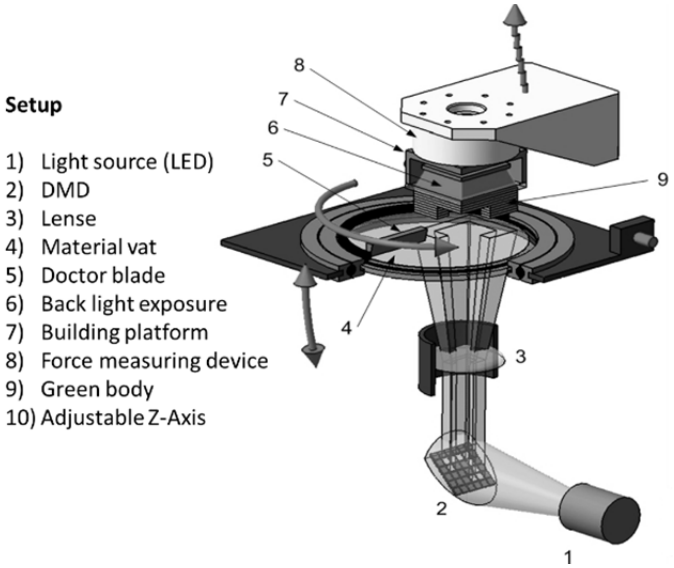

Figure 1: Schematic setup of the DLP machine at TU Wien

This work focuses on the production of full ceramic restorations by Lithography-based Ceramic Manufacturing (LCM). To achieve this, instead of a resin, a photoactive suspension is used and a thermal post-processing step (debinding and sintering) is performed after the printing process itself. Fig. 2 shows two glass-ceramic biaxial bending test plates produced by LCM. Translucency is a highly desired property in dentistry.

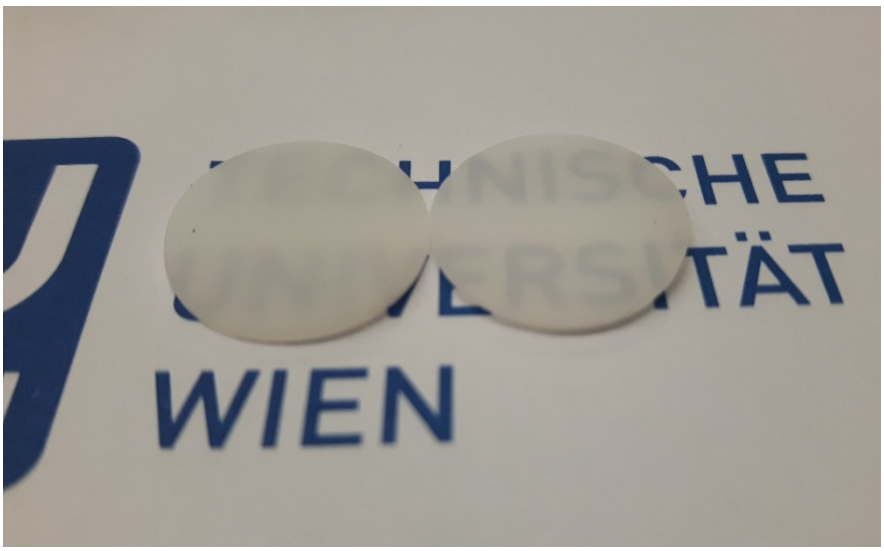

Figure 2: Translucent glass-ceramic test plates produced by LCM

The chemical and technological optimization of the LCM process is the main topic of this work. Beginning with the formulation of the suspension and its process relevant properties like rheology, to technological dependencies like construction and material choice of the coating mechanism, to post-processing issues like debinding schedules and final material properties like bending strength, all relevant steps of the process chain are discussed and analyzed. For this, a variety of analytical instruments are used, among them rheometry, thermogravimetry (TGA), thermo-mechanical analysis (TMA), scanning electron microscopy (SEM) and Weibull analysis. Fig. 3 shows an SEM image of the fracture surface of a biaxial bending test plate. No porosity is visible, which indicates densities close to the theoretical maximum.

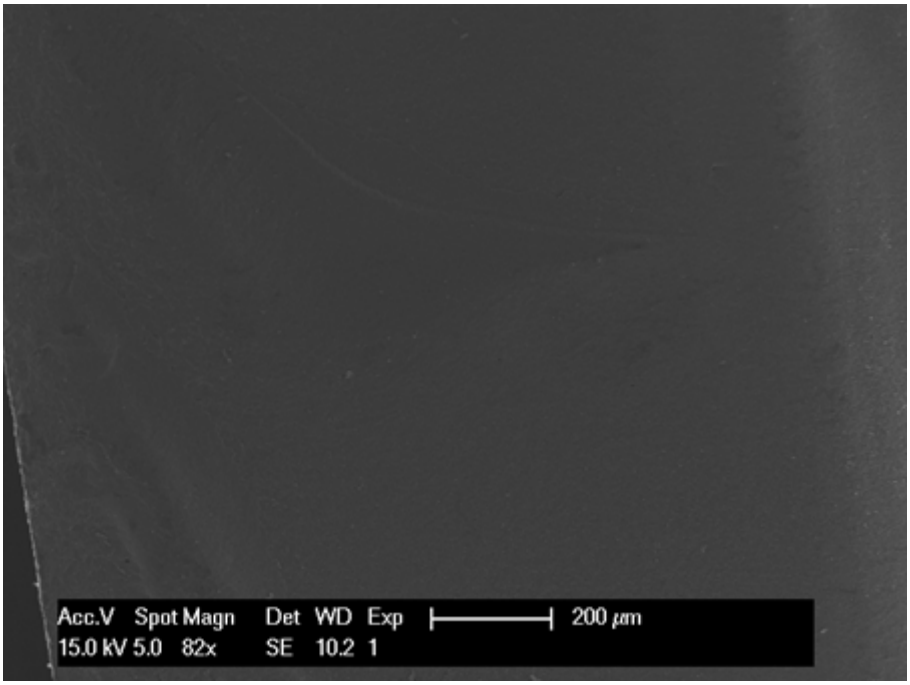

Figure 3: SEM image of the fracture surface of a glass-ceramic test plate

SIMULATION OF THE CARDIOVASCULAR AND AUTONOMIC NERVOUS SYSTEM FOR OPTIMIZATION OF AURICULAR VAGUS NERVE STIMULATION

Banbak Dabiri Razlighi, Stefan Kampusch, Eugenijus Kaniusas

Research Unit Biomedical Sensing, Institute of Electrodynamics, Microwave, and Circuit Engineering (E354), TU Wien

INTRODUCTION

Percutaneous electrical stimulation of the auricular vagus nerve (pVNS) is a promising approach in management of postoperative and chronic low back pain. pVNS has shown beneficial effects on systemic physiological parameters, such as heart rate variability. Although there are some efforts on modelling pVNS and its effects on the cardiovascular system, in order to control and optimise pVNS, the contribution of the autonomic nervous system is not modelled sufficiently yet. In this study, we model jointly the cardiovascular and autonomic nervous system, to provide a basis for the development of a feedback-based control of pVNS stimulation parameters.

METHOD

A model composed out of 3 main blocks, cardiovascular system (CVS), a chronotropic autonomic model and pVNS. CVS was optimized to keep the nominal systolic and diastolic pressure in the range of 120/80 mmHg and receives heart period as an input from baroregulation and pVNS blocks. Baroregulation system consist of carotid baroreceptors and chronotropic effect of vagal and sympathetic and total effects on heart period are summed up with pVNS effect (Fig.1).

Cardiovascular system: A minimal cardiovascular system [1] which describes the hemodynamics of heart and blood circulation was established. This model is stable in long-term and does not depend on initial values. In addition, cardiac cycles were simulated by taking into account the inertia effect on cardiac valves. Moreover, the change of thoracic pressure and its effect on cardiac output was included. Systemic resistance, which plays a major role in blood pressure, was modelled as part of the closed loop model. The model works based on pressure volume relation of every component, heart period, and systemic resistance or respiration, as changing thoracic pressure influences the heart rate variability.

Autonomic nervous system: A pulsatile heart simulation provides input for the carotid baroregulation. We used a model of carotid baroregulation [2] to simulate the baroreflex effect based on arterial pressure changes in the cardiovascular system. In this work, we focused on chronotropic effects on RR-intervals through the sympathetic and vagal efferent branches. Therefore, the vagal and sympathetic contribution will be added to the intrinsic heart period as autonomic nervous system input. Since the main contribution of pVNS on the system is not clear yet, cervical vagus nerve stimulation effects (stimulation of the cardiac vagal branch) on RR- intervals was adopted from [3], to simulate the whole structure. This can be substituted in future by pVNS.

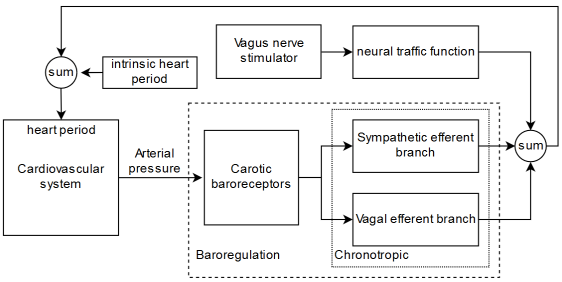

Figure 1: system block diagram.

RESULTS AND DISCUSSION

The cardiovascular system model was physiologically verified by altering the thoracic pressure, the elasticity of ventricle walls, and the systemic resistance. An increase in left ventricular stroke volume and pressure, due to doubled systemic resistance, and a decrease due to the half systemic resistance, are shown in Fig. 2. In order to investigate the respiration effect on stroke volume, the thoracic pressure was decreased from -4 mmHg to 0 mmHg. A decrease in left ventricular stroke volume and pressure was observed.

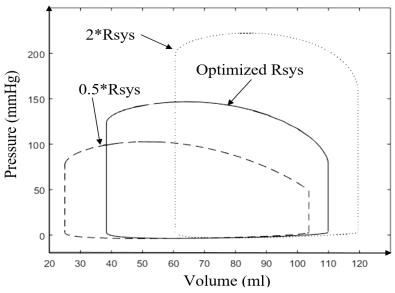

Figure 2: Systemic resistance effect.

Respiratory sinus arythmia was simulated by applying the RR- intervals from a real ECG signal to the cardiovascular system model. Fig. 3 shows aortic pressure for both conditions. A small change in the range of 5% in amplitude and different systolic and diastolic duration due to the varying RR-intervals is obvious.

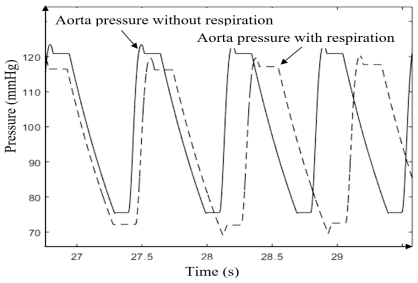

Figure 3: Respiratory effect on aortic pressure.

Autonomic nervous system simulation showed a fast response to the increase in mean aortic pressure via an increased RR-interval. A slow response was seen for a decrease in aortic pressure via a decrease in RR-intervals. Direct vagus nerve stimulation of the cardiac branch increased the RR-intervals.

CONCLUSION

In this study, we modelled a minimum dynamic cardiovascular system with autonomic nervous system and direct vagus nerve stimulation input. The model is stable and easy to solve. We verified the model by checking its response to physiologic changes. This model will allow us to optimize pVNS stimulation and build feedback based solutions. A feedback-controlled pVNS can avoid blind treatment or even help detecting non-responders by monitoring bio-signals. Simulations facilitate manipulation of physiological and stimulation parameters. In addition, simulations reduce the experimental costs and allow individualized models.

REFERENCES

[1] B. W. Smith, J. G. Chase, R. I. Nokes, G. M. Shaw, and G. Wake, "Minimal haemodynamic system model including ventricular interaction and valve dynamics," (in eng), *Med Eng Phys*, vol. 26, no. 2, pp. 131-9, Mar 2004.

[2] M. Ursino, "Interaction between carotid baroregulation and the pulsating heart: a mathematical model," (in eng), *Am J Physiol*, vol. 275, no. 5, pp. H1733-47, Nov 1998.

[3] W. Gersch and E. Dong, Jr., "A note on Warner's vagus heart rate control model," (in eng), *IEEE Trans Biomed Eng*, vol. 20, no. 2, pp. 145-8, Mar 1973.

NEURAL SIGNALLING MODELLED WITH FINITE ELEMENT METHOD

Andreas Fellner[a], Steffen Eickhoff[b], Jonathan C. Jarvis[b], Frank Rattay[a]

[a]E101 Institute of Analysis and Scientific Computing, TU Vienna, Austria
[b]Sport and Exercise Sciences, Liverpool John Moores University, United Kingdom

INTRODUCTION

Neural implants like visual prosthesis or cochlea implants are based on electrical stimulation of excitable neurons. To investigate the effects of extracellular stimulation of practical devices or to reproduce experimental results, mathematical models simulate the physiological neuronal behaviour. A common approach are Hodgkin-Huxley (HH) like cell models[1], which take the electrical properties of the cell membrane as well as ion channel kinetics in form of probability functions into account. Multi-Compartment model designs are used to implement geometric aspects of neuronal structures. However, besides the physiological cell behaviour, also the consideration of other physical effects might be crucial for a correct reproduction of cellular responses, i.e. geometric relations between neurons and electrodes, generated heat, or influences between the electrode neural tissue. These effects essentially depend on geometry of the neuron and its environment. The finite element method (FEM) provides solutions to solve complex physical interactions in space and time. Therefore, to couple cellular membrane properties with other physical phenomena, a HH cell membrane was realized in the FEM software COMSOL (www.comsol.com). This implementation is used to simulate situations where cellular responses strongly depend on the distribution of the electric field caused by stimulating electrodes, which is not only influenced by the electrodes itself but also by the neurons and their electrical activities (Figure 1).

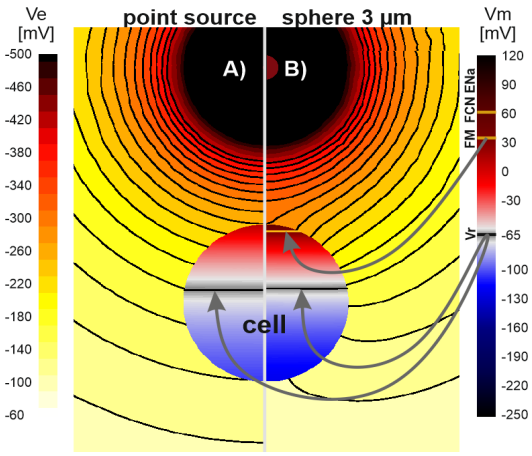

Figure 1: Difference in polarization of a spherical cell and the electrical field between idealized point source current approach (A) and FEM simulation which considers the influence of the cell itself on the electrical field (B)[2].

FUNDAMENTAL OF THE PROBLEM

Many physical phenomena addressed in neuroscience are multidimensional problems which can be described by partial differential equations (PDEs). Classical multi-compartment models are an easy and effective way to solve cellular responses of excitable cells. By utilizing symmetries in space and simplified physics for voltage distribution caused by electrodes, such models are also suitable to simulate complex extracellular stimulation situations. But, depending on the scientific question, there are electrode-neuron geometries which cannot be reproduced by multi-compartment models or assumed simplifications in physics might produce skewed results. This is in contrast to the FEM which allows to couple different physical aspects in a spatial discretized geometry which influence each other. While general electrical behaviour in and outside of a neuron is completely realized by AC/DC physics modules provided by COMSOL, the cellular kinetics were implemented as PDEs using COMSOL mathematical modules an then set as boundary conditions[3,4] at the cell membrane.

RESULTS AND DISCUSSION

Together with other necessary electrical parameters, the transmembrane current density is calculated and induced in the AC/DC physic modules of COMSOL to simulate intra- and extracellular potentials. This approach not only returns the relevant output of a nerve cell model like polarization of the surface or respective ionic currents, it also correctly reproduces the electrical effects of the electrodes and the influence of electrical neural activity on the cellular environment.

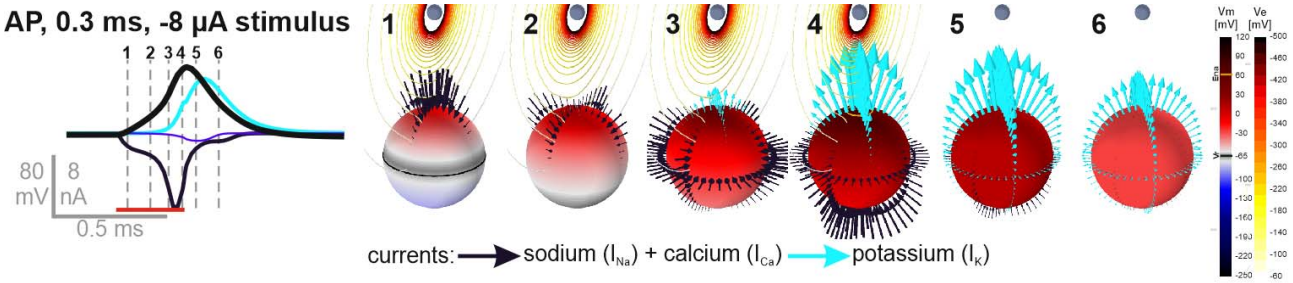

Figure 2: Polarization and ionic currents during an action potential of an extracellularly stimulated spherical cell[2]. Animated videos at: https://figshare.com/articles/Figure_9_Supplement/7624373

Among other model concepts, this method is used to investigate the upper threshold phenomenon and its causes especially for very close electrodes (Figure 2). It has been shown, that for large spherical neurons and/or a very close electrode, the influence of the neuron on the electrical field becomes a non-neglectable factor on the cell behaviour for the investigated phenomenon[2]. In an ongoing study, this model approach is being used to answer actual questions in muscle activation of in-vivo experiments done at the Liverpool John Moores University. Here, the common peroneal nerve is stimulated with two ring electrodes placed as shown in Figure 3. Due to the kind of electrode configuration and the influence of neurons on the electrical field inside the tightly packed nerve, a FEM simulation was chosen to get as meaningful results as possible.

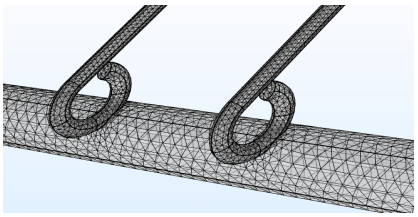

Figure 3: Example mesh of electrode configuration of a stimulated nerve.

CONCLUSION

The possibility to consider complex 3D geometries of neurons, their environment, and the actual electrode setup in combination with realistic space- and time-dependent physics, allows a precise reproduction of in-vitro or in-vivo experiments. Additional physics as provided by COMSOL are usable together with the implemented membrane kinetics. Disadvantages of this approach are the extremely high computational costs and the complexity of the models.

REFERENCES

[1] Hodgkin, A. L., & Huxley, A. F. A quantitative description of membrane current and its application to conduction and excitation in nerve. The Journal of physiology, 117(4), 500-544, 1952

[2] Fellner, A., Stiennon, I., & Rattay, F. (2019). Analysis of upper threshold mechanisms of spherical neurons during extracellular stimulation. Journal of neurophysiology.

[3] Joucla, S., Glière, A., & Yvert, B. (2014). Current approaches to model extracellular electrical neural microstimulation. Frontiers in computational neuroscience, 8, 13.

[4] Dokos, S. (2017). Modelling organs, tissues, cells and devices: using Matlab and Comsol multiphysics. Springer.

COCHLEAR IMPLANTS FOR CAT AND MAN & WHAT WE LEARN FROM A MODELING STUDY

Sogand Sajedi[a], Amirreza Heshmat[a,b], Anneliese Schrott-Fischer[b], Frank Rattay[a]

[a]E101 Institute of Analysis and Scientific Computing
[b]Inner Ear Lab, Meduni Innsbruck, Austria

INTRODUCTION

In cochlear implants, by trains of electrical pulses, neural signals are generated that should match the natural signal pattern in the auditory nerve of a normal hearing person. The auditory nerve in man consists of about 30.000 cochlear neurons connecting the sensory cells in the cochlea with the cochlear nucleus, the first auditory processing unit in the brain. Each of these neurons has a cell body (soma) and two processes (axons). Such a structure can be compared with an insulated wire, but the neuronal cable is an organic volume conductor, the insulation consists of sheets of cell membranes (myelin) and for conduction the signal (action potential) needs amplifications in active zones (non-myelinated regions, nodes of Ranvier) via a system of voltage sensitive ion channels.

Cats are experimental animals to study the relationship between stimulus currents and artificially generated signals in the auditory nerve in order to optimize stimulation parameters but this methodology caused a fundamental problem.

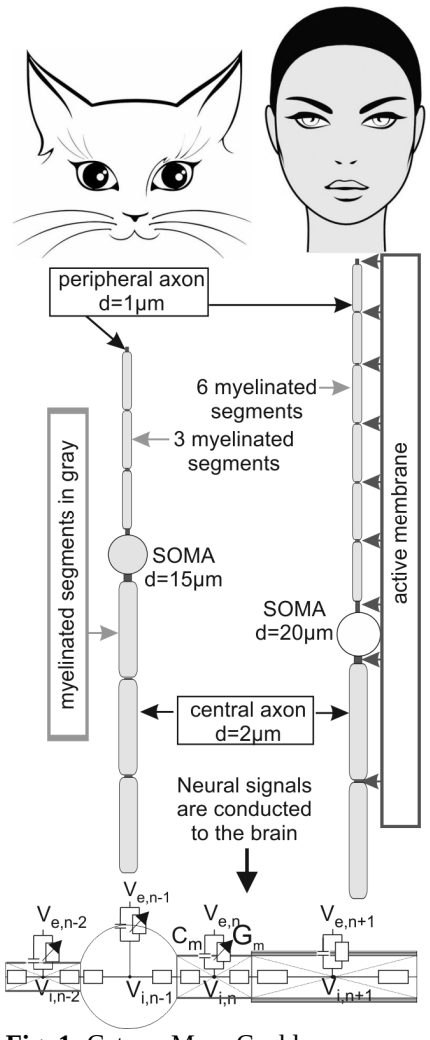

Fig. 1. Cat vs. Man: Cochlear neurons in man have longer axons, their somas are a bit larger and not myelinated [1]. Bottom: Electric circuits to simulate neural signals in a neuron.

FUNDAMENTAL OF THE PROBLEM

The main problem using experimental findings form cat data for cochlear implant stimulus parameters is the unexpected impact of the longer human peripheral axon (6 segments, Fig. 1)[1,2]. Negative stimulus pulses need essentially less intensity to generate action potentials within the peripheral axon in cat, but in man the minimum intensity is for positive pulses. As the researchers trusted on the experimental cat data this unexpected polarity effect was not considered in cochlear implants built for humans. Here, new morphometric data are used in a simplified model where the neuron's axis is a straight line to demonstrate the higher sensitivity of the human cochlear neuron to the positive stimulus polarity[1].

Voltage sensitive ion channels make the excitation of the cell membrane of a neuron possible. The excitation process of a single active part can be described by 4 non-linear differential equations[2,3]. Single active membrane segments (marked as active compartments in Fig. 1) are combined (also with passive elements) via intracellular resistances (Fig. 1, bottom). The resulting system of ordinary differential equations is stimulated either via current injection at the first compartment

(simulating natural excitation from the hair cell) or via the applied electric field that causes different extracellular potentials V_e along the neuron. For technical details see references 1, 2 and 4.

RESULTS AND DISCUSSION

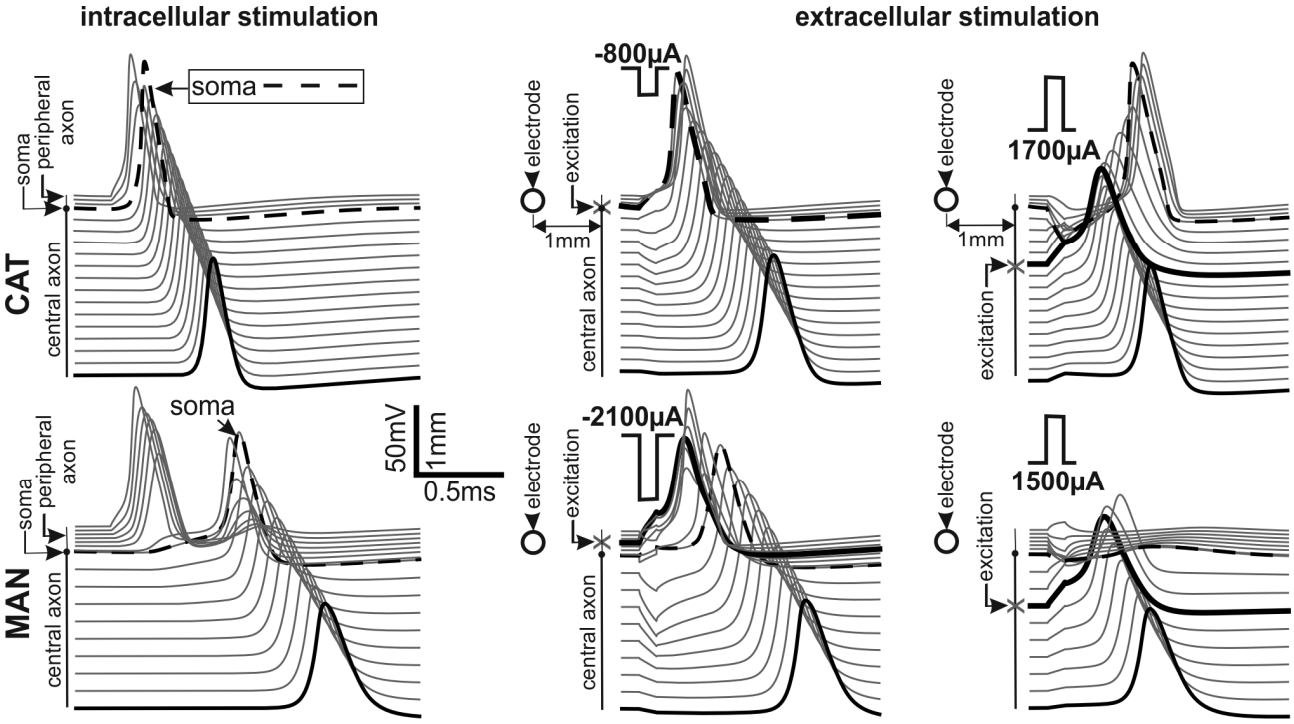

Figure 2 demonstrates two key differences between cat and man. For intracellular stimulation a 0.1ms stimulus current of 100pA is injected in the first compartment causing a propagating action potential which needs in man (because of the nonmyelinated soma[2]) about 0.68ms longer to pass the displayed 2.7mm long section on the way from the receptor cell (inner hair cell) in direction to the cochlear nucleus in the brain. Cat's signal is quicker! Most impressive is the polarity sensitivity. In cat positive pulses need about the doubled intensity to elicit an action potential, but in man it is vice versa: excitation is essentially easier with positive pulses. Note, for positive pulses excitation is generated rather far from the electrode in the central axon and that the quickest signalling with cochlear implants is expected for positive pulses – here, concerning signal speed, man is better than cat. Similar results as predicted by our simulations are seen in tests of implant users[5].

CONCLUSION

Rather small changes in geometry caused surprising results. Computer simulations reduces the importance and number of animal experiments in many cases, also in cochlear implant research.

REFERENCES

[1] Rattay, F., Potrusil, T., Wenger, C., Wise, A. K., Glueckert, R., & Schrott-Fischer, A. Impact of morphometry, myelinization and synaptic current strength on spike conduction in human and cat spiral ganglion neurons. PLoS One, 8(11), e79256, 2013

[2] Rattay, F., Lutter, P., & Felix, H. A model of the electrically excited human cochlear neuron: I. Contribution of neural substructures to the generation and propagation of spikes. Hearing research, 153(1-2), 43-63, 2001

[3] Hodgkin, A. L., & Huxley, A. F. A quantitative description of membrane current and its application to conduction and excitation in nerve. The Journal of physiology, 117(4), 500-544, 1952

[4] Rattay, F., Greenberg, R. J., & Resatz, S. Neuron modeling. In Handbook of Neuroprosthetic Methods (pp. 45-77). CRC press, 2002

[5] Spitzer, E. R., Choi, S., & Hughes, M. L. The effect of stimulus polarity on the relation between pitch ranking and ECAP spread of excitation in cochlear implant users. Journal of the Association for Research in Otolaryngology, 1-12, 2019

DNA ORIGAMI AS A NANOSCALE PLATFORM FOR T-CELL ACTIVATION

Joschka Hellmeier[a], Rene Platzer[b], Viktoria Motsch[a], Andreas Rohatschek[c], Philip Thurner[c], Johannes B. Huppa[b], Gerhard J. Schütz[a], Eva Sevcsik[a]

[a] Institute of Applied Physics, TU Wien, Wiedner Haupstr. 8-10, 1040 Vienna, Austria
[b] Center for Pathophysiology, Infectiology and Immunology,
Institute for Hygiene and Applied Immunology, Medical University of Vienna, Vienna, Austria
[c] Institute of Lightweight Design and Structural Biomechanics, TU Wien, Getreidemarkt 9,
1040 Vienna, Austria

INTRODUCTION

Every cell of our body is surrounded by a plasma membrane that separates the inside of a cell from the outside. This is not just a static barrier but the stage of an intricate interplay of invisibly small structures, proteins and even smaller lipids, that move and assemble themselves in complex ways to mediate membrane function. A special type of cells, T-cells, are major players in our immune system. One protein in their plasma membrane, the T-cell receptor (TCR), recognizes a small part of a pathogen (the antigen), which is presented by the protein mayjor histocompatibility complex (MHC) on an antigen presenting cell (APC). Upon this recognition process, the T-cell becomes activated and a series of events is initiated ultimately leading to an immune response. Deregulation of this process can lead to inadequate immune responses such as autoimmunity or immunodeficiency.

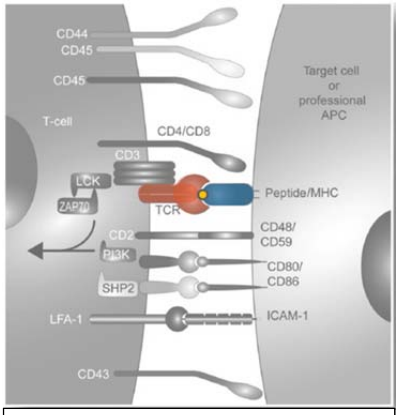

Figure 1: *Schematic overview of an immunological synapse formed by a T-cell and an APC [Huppa et al., 2004].*

T cells recognize peptide-antigens presented by MHCs (pMHCs) with remarkable specificity and sensitivity. While the molecular players in the activation cascade, as well as the sequence of events, are rather well characterized, we still do not understand how and where the decision for activation is made. It is thought that the nanoscale spatial distribution of ligand and TCR plays an essential role in the initiation of an immune response but events at this time and length scale are intrinsically hard to study in a living system.

A great asset of being part of the TU DK "Biointerface" is working with colleagues from various natural scientific fields and thus being able to combine all the expertise and benefits to view a task from every angle and perspective.

EXPERIMENTS / FUNDAMENTAL OF THE PROBLEM / EXAMINATIONS

Several studies have already tried to assess the importance of the nanoscale distribution of TCR ligands by mimicking the surface of an APC with nanostructured surfaces. So far, only static systems that do not allow for rearrangement (e.g. accumulation, segregation) of molecules within the immunological synapse during T cell activation were extensively used. Since the physiological scenario is not static at all, we were aiming for a novel nanostructured surface, which does not only allow positioning of single ligands with nanoscale precision but also permits reorganization of molecules during T-cell activation. Therefore, we use DNA origami decorated with TCR ligands anchored to a planar glass-supported lipid bilayer containing adhesion (ICAM-1) and costimulatory

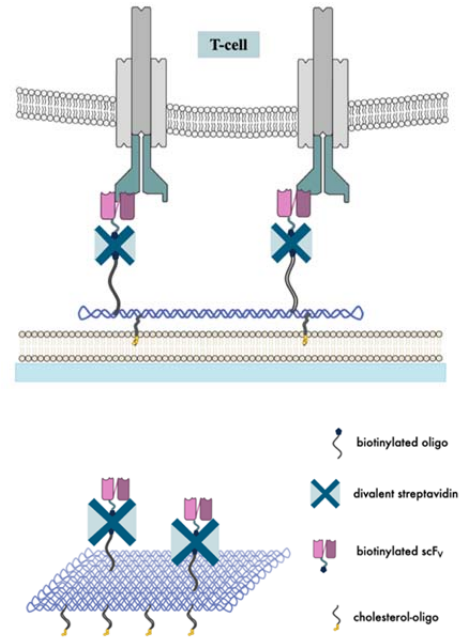

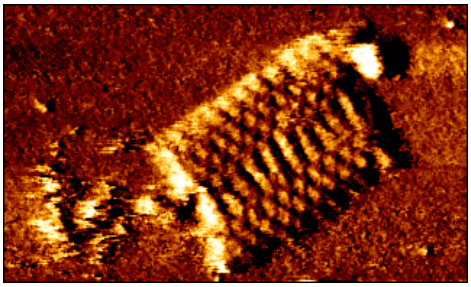

Figure 2: *Schematic overview of a T-cell interfaced with a DNA origami bilayer platform decorated with an antibody scF$_V$*

(B7-1) proteins to assess the effects of nanoscale ligand arrangement on T-cell activation. In order to achieve that, we used a sandwich structure consisting of biotinylated oligos, divalent streptavidin and biotinylated ligand labelled with a fluorophore. Intriguingly, T-cells cannot only be activated by binding to a cognate ligand (pMHC) but also by binding to antibodies. Thus, we used an antibody single chain fragment (scF$_V$) to the TCR and assessed its spatial requirements for T-cell activation. Additionally, our DNA origami platform creates an exclusion zone that prohibits the approach of ligands below a minimum distance set by the platform size. In order to observe potential differences in the T-cell response DNA origami platforms of different size and ligand occupancy were created. Actual ligand occupancies of DNA origami platforms and overall densities were determined by relating the platform brightness to the brightness of a single fluorophore.

We used intracellular calcium levels as an indicator for T cell activation. Thus, we labeled the T cells with a calcium sensitive dye to see differences in the release of calcium. Besides that, phosphorylation of the ζ-chain of the TCR, the earliest indicator of T cell activation, and subsequent recruitment of the kinase ZAP70 was determined, to be able to understand the molecular events in early t cell activation in more detail. To quantify the data, we used a positive control containing B7-1, ICAM and peptide MHC and a negative control which contained solely B7-1 and ICAM.

RESULTS AND DISCUSSION

We found a pronounced effect of ligand spacing on its potency to activate T cells. At a ligand spacing of 50nm, T cell activation was almost completely abolished. This is in line with a recent study, that varied anti-TCR antibody fragment spacings in a slightly larger size range (distances 40 – 120 nm) found an optimum spacing at 40 nm (Cai et al., 2018), albeit at much higher overall densities of immobilized Fab. In our experiments, a separation of 10 nm between ligands was 9-fold more efficient than 30 nm. Interestingly, a distance of 10nm corresponds to the spacing of two epitope-binding sites in a divalently bound antibody, a potent activator of T cell signaling... Taken together, our results suggest that single phosphorylated TCRs at distances of more than 30 nm are not signalling-competent. For efficient T cell activation, ligand and TCR need to be freely rearrangeable to from small clusters or ligand needs to be pre-arranged in dimers with a spacing of ~10 nm.

CONCLUSION

We find a pronounced influence of nanoscale ligand spacing on T cell activation. This not only sheds new light on the mechanisms of early T cell signalling but also will be important in the design of nanostructured surfaces that can be used to activate T cells in T cell immunotherapy.

DETECTOR DEVELOPMENT FOR NANOMOTION BASED MONITORING OF CELL STATES

Veronika Pfannenstill[a,b], Anne-Céline Kohler[a], Gerhard Schütz[b] and Sandor Kasas[a]

[a]Institut de Physique des Systèmes Biologiques, École Polytechnique Fédérale de Lausanne (EPFL), Lausanne, Switzerland

[b]E134 − Institute of Applied Physics − Biophysics at TU Wien

INTRODUCTION

The atomic force microscope (AFM) has provided great new insights in fields like electrochemistry, semiconductor science or molecular biology and has opened the door to a new field, we today call nanotechnology. Moreover, the development and the application of novel technologies resulted in solving important problems. In 2013, Longo *et al*. have taken advantages of the sensitivity of the cantilever to assess the viability of mammalian cells and bacteria with an unprecedented temporal resolution[1]. Further studies demonstrated the use of this technique, called nanomotion detection, to determine the effect of chemicals, such as cytochalasin D, on mammalian cells[2]. Here, we have used this technique to investigate the delivery and effect of antimitotic drugs to cancer cells and established a procedure for fast and reliable detection of the activation of Jurkat cells. The obtained results allow us to make a clear distinction between treated, untreated, activated and dead cells and pave the way towards personalized medicine.

NEW METHODOLOGY

The AFM is standardly used in a configuration that raster scans the cantilever over the “sample” probing its surface. In contrast, we mount the “sample” directly on the cantilever and use it as a sensitive probe for “sample” activity (Figure 1)[2].

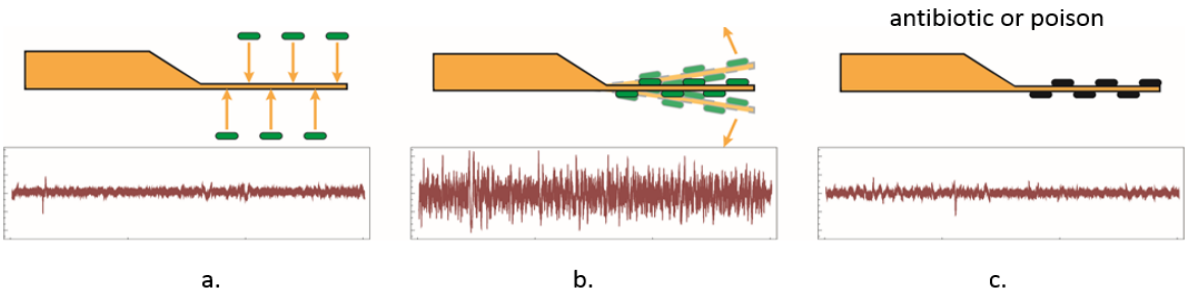

Figure 1: Schematic representation of the methodology used in this work. Upper panels show the principal experimental steps whereas the lower panels depict the cantilever movements as a function of time. a) First the specimen of interest (in green) is attached onto an AFM cantilever with molecules. b) If the specimen is alive or if it undergoes conformational changes, the cantilever oscillates. c) The presence of antibiotics or chemicals in the medium induces death or inhibition of the sample and the cantilever’s oscillations reduce or stop.

Since the movements of the tip can be accurately recorded to detect even individual atoms, it is clear that any movement of any microscopic objects, e.g. cells or bacteria, can be detected if deposited onto the cantilever. Simply, if the organism on the cantilever is alive or undergoes conformational changes it induces oscillations of the cantilever (Figure 1a,b)[1],[3]. Its extreme sensitivity allows to detect motions as small as 0.1 Å. Recently, very first experiments demonstrated that the method can be used to explore numerous types of samples, starting from single proteins to living mammalian cells[3],[4]. It has been already shown that the technique can be used for rapid, in a timeframe of minutes, detection of bacterial susceptibility to antibiotics[1]. Namely, as soon as the

sample is chemically inactivated by fixing agents, antibiotics or poisons, the oscillations of the cantilever decrease (Figure 1c). This information allows us to assess and study the sensitivity of the investigated system to the additionally injected chemical.

RESULTS AND DISCUSSION

We have applied this technique in the fields of immunology, which is, to our knowledge, the first time it has been done. The results obtained, by analysing mechanical oscillations, allow us to identify various cell states, e.g. T cell activation (Figure 2). These experiments were done by adding OKT3, an antibody that induces T cell activation, into the cell medium. Figure 2 shows a clear drop in oscillations upon addition of OKT3 which could be attributed to the spreading and reduction of motion of the cells.

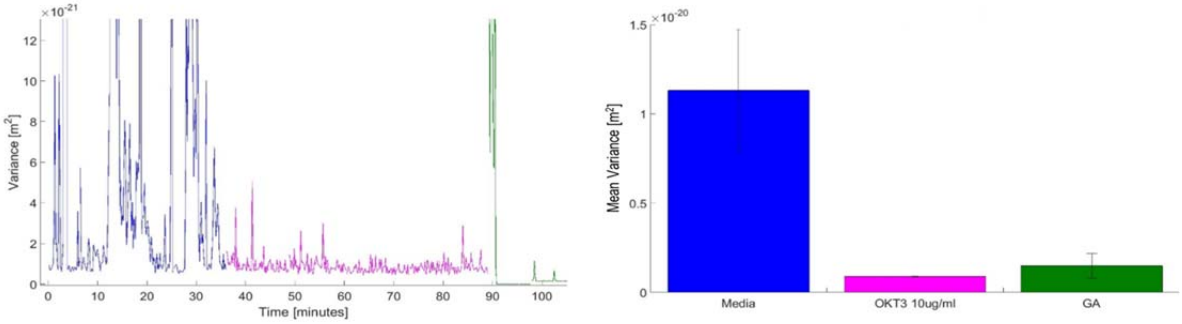

Figure 2: Nanomotion oscillation pattern of Jurkat cells exposed to OKT3 antibody that induces T cell activation. It is possible to clearly differentiate between the three states of the T cells: cells in normal media (blue), activated cells (pink) and dead cells (green).

In contrast, the control experiments with non-activating antibodies did show a constant amplitude of oscillations (data not shown). These results are of particular interest since some new cancer treatments use the patient's immune system and more specifically its T cells to kill cancer cells. A rapid test for T cell activation could therefore potentially lead to important breakthroughs and more efficient anticancer therapies in a time frame of hours/days.

CONCLUSION

It is clear that the presented AFM technique has the potential to revolutionize the fields of drug discovery, medical diagnosis and oncology as demonstrated in the presented tests (Figure 2) above. Further applications could involve sterilization assessment in hospitals and life detection in extreme environments. In addition, the technique may have the potential to serve as a biosensor and therefore change considerably the detection of toxic agents, e.g. environmental pollutants and warfare agents. The results are very encouraging and require subsequent experimental and theoretical work.

ACKNOWLEDGMENTS

This work was supported by a fellowship of the Zeno Karl Schindler Foundation (V.P.), by the Swiss-European Mobility Program (V.P.) and the FWF-Forschungsbeihilfe.

REFERENCES

[1] G. Longo *et al.*, Nat. Nanotechnol., **8** (7), pp. 522–526, 2013.

[2] S. Kasas *et al.*, Proc. Natl. Acad. Sci., **112** (2), pp. 378–381, 2015.

[3] L. Alonso-Sarduy *et al.*, PloS One, **9** (7), p. e103674, 2014.

[4] S. Kasas, P. Stupar, G. Longo, and G. Dietler, Med Sci (Paris), **31** (4), pp. 369–371, 2015.

A DYNAMIC CAUSAL SYSTEM SIMULATION APPROACH FOR ANATOMIC JOINTS

Ruth Leskovar

E101 – Institute of Analysis and Scientific Computing

MOTIVATION AND INTRODUCTION

This contribution presents a closed simulation loop for biomechanical models. This is an interdisciplinary task, since first a biomechanical model is formulated and afterwards this model is represented as dynamic system. Modelling and simulation is an important method in the field of biomechanics to analyse interactions in the human body. The knowledge of the influence of individual parts of the musculoskeletal system is necessary for treatment of diseases. Furthermore, mathematical models of parts of the human body are indispensable in the development of prostheses. Among several methods exist to model a biomechanical system, mainly two modelling approaches are used to describe these systems mathematically, partial differential equations (PDEs) and multibody models which are based on ordinary differential equations (ODEs). Both descriptions can be formulated as dynamic systems which allows to design closed simulation loops for biomechanical models. This extends possible applications and usage fields for biomechanical models as well as their influence in technology and research.

CASE STUDY – THE HUMAN KNEE JOINT

As case study, the human knee joint is a suitable starting point due to its complex structure which is a result of the interaction between rigid components as bones and soft tissues as ligaments, tendons as well as cartilage. A simplified simulation model for the flexion of the human knee joint was implemented using Simscape, the multibody library in Simulink, and COMSOL Multiphysics. The conceptual model is based on the work of Guess, Bloemker et al. [1], [2], [3].

The model contains the three main bones of the human knee, the femur, the tibia and the patella. The bones are implemented as rigid bodies and linked by two revolute joints. The patellar tendon, which attaches the patella to the femur, is implemented as linear spring-damper element. The input for the knee model is the acting force at the tibia which results in the flexion of the tibia and patella in relation to the femur. The output of the model is the angle between femur and tibia. The motion between the bodies resulting from an external force F can be described with a second order ODE [4]:

$$M\ddot{x} + J_x^T \lambda = F. \tag{1}$$

Here, M describes the mass matrix of the system, the vector x denotes the system coordinates, the matrix J_x is the Jacobian matrix of the system coordinates and λ represents the vector holding the Lagrange multipliers.

Although both simulation models are implemented using the same conceptual model, the solution is calculated in Simulink using ODE solver and in COMSOL using the finite element method. This leads to the question if both models can be described as dynamic systems. The states x in dynamic systems can be described by an ODE, dependent on time t, acting inputs u, parameters p and initial values x_0:

$$\dot{x}(t) = f(t, u(t), x(t), p), \quad x(0) = x_0. \tag{2}$$

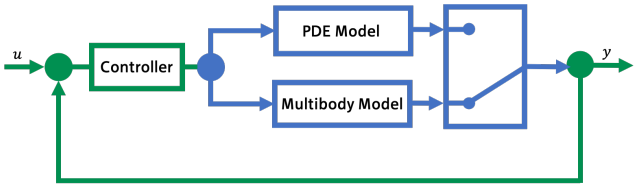

Figure 1: Design of a closed simulation loop for different biomechanical models.

The investigation of both simulation models as dynamic systems allows the design of closed simulation loops. This allows a flexible handling of the biomechanical models to different applications on the one hand and a comparison between different mathematical descriptions of biomechanical models on the other hand. As it is illustrated in Figure 1, a closed simulation loop with one degree of freedom is designed for both simulation models as plant. The simulation loop is implemented in Simulink which gives the opportunity to use its powerful control tools.

Due to the structure of the multibody model in Simscape, it is possible to define it as subsystem in Simulink and to design suitable closed loops without additional reformulations. The simulation model in COMSOL needs restrictions before it is possible to use as plant in Simulink. The dependency on time and space as well of the solution of the COMSOL simulation model requires to investigate the solution on specific points only. Ultimately, this gives various possibilities of extracting state-space representations of the COMSOL model [5].

CONCLUSION AND OUTLOOK

This work shows possibilities of representing biomechanical models as dynamic systems. This allows to use simulation models of anatomic joints as plants in closed simulation loops. Finally, it was possible to describe both models using the state space representation which allowed to use the same design of closed simulation loops. Nevertheless, disparate behaviour of the simulation models in the closed loop can be observed which is a result from their different mathematical description.

Further work will focus on the specification of the biomechanical model, e.g. ligaments will be included as non-linear spring damper elements to analyse more complex system behaviour. Moreover, the already established loop design focuses on constant reference signals. More sophisticated reference signals, the definition of a trajectory e.g., allows to simulate more realistic motion behaviour and can apply this work for gait analysis.

REFERENCES

[1] Bloemker K.H. et al.: *"Computational Knee Ligament Modeling Using Experimentally Determined Zero-Load Lengths"*. The Open Biomedical Engineering Journal 6, pp. 33–41, 2012.

[2] Guess, T.M. et al.: *"A subject specific multibody model of the knee with menisci"*. Medical Engineering and Physics 32(5), pp. 505–515, 2010.

[3] Guess, T.M. et al.: *"A multibody knee model with discrete cartilage prediction of tibio-femoral contact mechanics"*. Computer Methods in Biomechanics and Biomedical Engineering 16(3), pp. 256–270, 2013.

[4] Quental C. et al.: *"A multibody biomechanical model of the upper limp including the shoulder girdle"*. Multibody System Dynamics 28, pp. 83–108, 2012.

[5] van Schijndel, A.W.M: *"Getting state-space models from FEM simulations"*. Proceedings of European Comsol Conference, pp. 1–6, 2017.

Research Field *Fundamental Research*

Chairs and Reviewers:

Körner, Andreas
Senior Lecturer Dipl.-Ing. Dipl.-Ing. Dr.techn.

E101 - Institute of Analysis and Scientific Computing
andreas.koerner@tuwien.ac.at

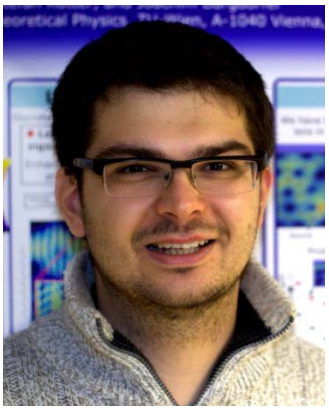

Libisch, Florian
Assistant Prof. Dipl.-Ing. Dr.techn.

E136 - Institute of Theoretical Physic
florian.libisch@tuwien.ac.at

Introduction

Modern technology has greatly affected our world - from new materials, high-speed transportation or genetically engineered plants, to powerful computers. All these applications are firmly based on fundamental research in the basic sciences, which revealed the underlying chemical, mathematical or physical principles governing our world. For example, the revolutionary impact of the internet on culture, commerce, and technology, including the rise of near-instant communication, is based on algorithms and basic protocols that seemed of little practical use at their time.

The same is true today: many active current developments in fundamental research will form the scaffold for new technologies in the coming decades. We will need these technologies to meet the rising global challenges in sociology, environmental research, and renewable energies.

There is a plethora of examples for fundamental research and its envisioned applications in different fields: An entire class of novel low-dimensional materials, spearheaded by the discovery of graphene a few years ago, promises new approaches for battery design, spray- on solar cells or flexible nanoelectronics. Conceptual characterizations based on first principles and behavioural modelling of complex systems are found in applications from smart cities and modelling of electrical grids to telecommunication and information science. New approaches in designing hybrid materials and biomaterials promise highly efficient catalysis, artificial noses or renewable biofuels. Methods from the field of dynamic systems and partial differential equations enable the characterisation, simulation and analysis of technical and socioeconomic systems.

This symposium covers all fundamental research performed at TU Wien. Beyond the natural sciences its scope also extends to application of mathematical, physical and chemical methods in electrical, mechanical or civil engineering as well as in architecture and spatial planning. Its highly interdisciplinary nature implies a crossover of all focal areas: Computational Science, Quantum Technologies, Materials and Matter, Information and Communication Technologies, as well as Energy and Environment. As such, we welcome and invite contributions from diverse research fields and all Faculties at TU Wien involved in fundamental research.

MULTIPHOTON DOUBLE IONIZATION OF HELIUM

Manuel Ederer, Stefan Donsa, Fabian Lackner, Iva Březinová, Joachim Burgdörfer

E136 Institute of Theoretical Physics

INTRODUCTION

Double ionization of helium by bright, ultra-short laser pulses is a prototypical test case to study strong electron correlations. Since both electrons leave the nucleus within a fraction of a femtosecond (10^{-15} s) they can share the energy of the absorbed photons via Coulomb interaction. We study the imprint of this interaction for different photon energies on the fully differential two-electron wave function.

THEORETICAL BACKGROUND

The dynamics of the helium atom in a laser field is governed by the time-dependent Schrödinger equation

$$i\partial_t \Psi(\mathbf{r}_1,\mathbf{r}_2,t) = \left[\frac{\mathbf{p}_1^2}{2} + \frac{\mathbf{p}_2^2}{2} - \frac{2}{r_1} - \frac{2}{r_2} + \frac{1}{|\mathbf{r}_1-\mathbf{r}_2|} + (\mathbf{r}_1+\mathbf{r}_2)E(t)\right]\Psi(\mathbf{r}_1,\mathbf{r}_2,t), \tag{1}$$

where $E(t)$ is the electric field and $\mathbf{r}_i$ and $\mathbf{p}_i$ are the relative coordinates and momenta of the electrons. We solve Eq. 1 employing the time-dependent close coupling method [1]. After the conclusion of the laser pulse we project the final wave function $\Psi(\mathbf{r}_1,\mathbf{r}_2,t_f)$ onto the symmetrized product of Coulomb waves to obtain the fully differential double ionization probability $P^{DI}(\mathbf{k}_1,\mathbf{k}_2)$ which is experimentally accessible [2].

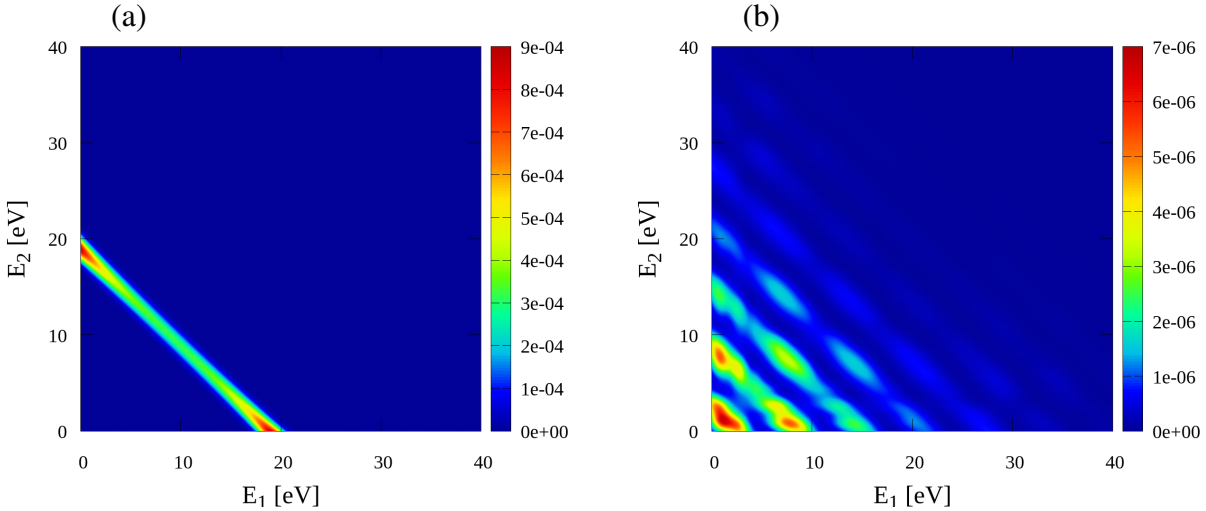

Figure 1: Double-ionization spectra $P(E_1,E_2)$ as a function of the electron energies E_1 and E_2 for a laser pulse with (a) wavelength $\lambda = 25.1$ nm ($\cong 49.4$ eV), intensity of $I = 10^{14}$ W/cm^2 and total duration of 4 fs and a pulse with (b) $\lambda = 197$ nm ($\cong 6.3$ eV), $I = 10^{15}$ W/cm^2 and total duration of 8 fs.

RESULTS AND DISCUSSION

The angle integrated doubly-differential double ionization spectrum depends strongly on the energy of the absorbed photons. For an energy of 49.4 eV double ionization can only occur if two photons are absorbed and the electrons share the energy because the energy of one photon is smaller than the second ionization potential of helium. This is referred to as two-photon non-sequential double ionization, see [3]. The resulting energy distribution shows a characteristic band along the total energy $E_1 + E_2 = 2\omega$ with maxima where one of the electrons ends up with close to the total energy, see Fig. 1(a). For photon energy of 6.3 eV where at least 13 photons have to be absorbed to overcome the double ionization potential of ~ 79 eV the energy distribution shows considerable differences compared to the two-photon case. We observe multiple bands where each band along constant total energy corresponds to absorption of an additional photon. Angular resolved quantities like the joint-angular distribution $P(\theta_1 = \phi_1 = \phi_2 = 0°, \theta_2)$ at equal energy sharing ($E_1 = E_2$) provide even more insight, see Fig. 2. For photon energies of 49 eV the joint-angular distribution shows a pronounced minimum for emission of both electrons into the same direction independent for both two or three photon absorptions, due to the electron-electron repulsion. However, for two-photon absorption we observe a distinct maximum for back-to-back emission ($\theta_2 = 180°$) while three photon absorption shows a node at $\theta_2 = 180°$ as this process would violate parity conservation.

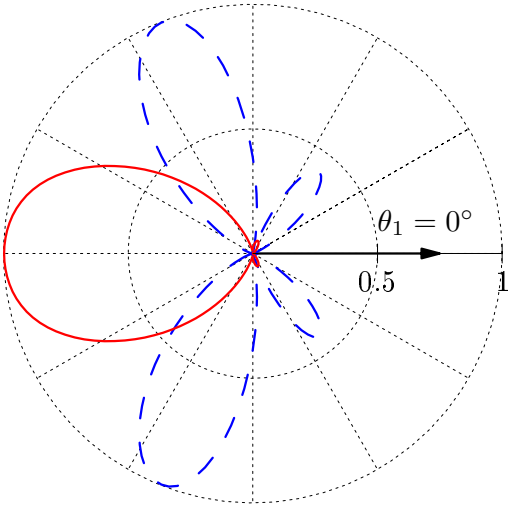

Figure 2: Joint angular distribution $P(\theta_1 = \phi_i = 0°, \theta_2)$ with equal energy sharing ($E_1 = E_2$). Solid line: absorption of two photons with photon energy $\omega = 49$ eV. Dashed line: absorption of three photons with photon energy $\omega = 29$ eV. The direction of the first electron is indicated by the arrow.

CONCLUSION

We investigate double ionization of atomic helium by short, intensive laser pulses with photon energies from 100 eV down to a few eV. The fully-differential energy spectra allow insights into the properties of electronic correlations. In the future we will use fields approaching the infra-red limit (800 nm) and explore the influence of elliptical polarization on multi-photon double ionization.

REFERENCES

[1] M. S. Pindzola and F. Robicheaux. *Time-dependent close-coupling calculations of correlated photoionization processes in helium*. Phys. Rev. A **57**, 318 (1998).

[2] R. Dörner, V. Mergel, O. Jagutzki, L. Spielberger, J. Ullrich, R. Moshammer, and H. Schmidt-Böcking. *Cold Target Recoil Ion Momentum Spectroscopy: a 'momentum microscope' to view atomic collision dynamics*. Physics Reports **330**, 95 (2000).

[3] J. Feist, S. Nagele, R. Pazourek, E. Persson, B. Schneider, L. A. Collins, and J. Burgdörfer. *Nonsequential two-photon double ionization of helium*. Physical Review A **77** (2008).

BUCKLING OF A CLAMPED-CLAMPED BEAM DUE TO INITIAL CURVATURE

Christian Schmidrathner, Yury Vetyukov

E325 - Institute of Mechanics and Mechatronics at TU Wien

INTRODUCTION

Modern beam theory has a broad range of potential applications. Buckling of beams due to a compressive force is commonly known since Euler. Nowadays, lots of articles are published, where this kind of stability loss is addressed including functionally graded materials and shear effects, often paired with various temperature distributions across the beams cross section [1]. These temperature distributions have similar effect as eigen stresses, which is our chosen approach. Usually, these observation are made in a two-dimensional analysis. As a result to this restriction, these structures become instable only if the resulting normal force is a compressive one.

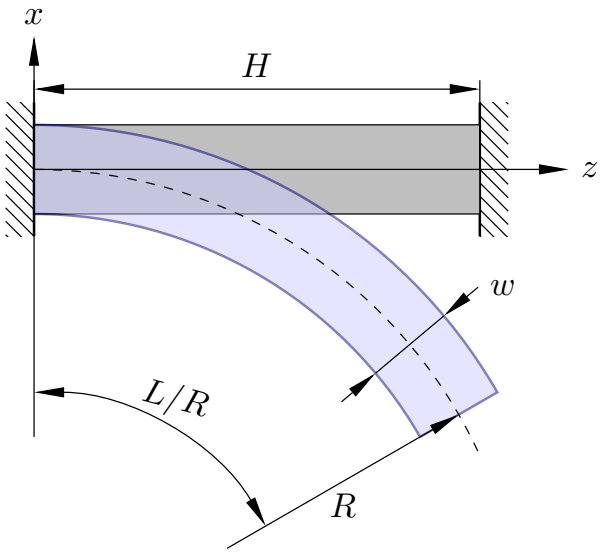

Figure 1: Clamped and free curved beam

During the validation of finite element schemes for belt drives including natural curvature as imperfections, which are currently developed in our research group, we observed some buckling phenomena even with beams under tension, which we want to study in this work. Hence, in contrast to above, we consider the three-dimensional deformation of the beam, which allows for an additional displacement component as well as torsion. Another interesting and similar problem is the buckling of a flat ring due to initial curvature [2].

PROBLEM STATEMENT AND SOLUTION

We consider a beam with rectangular cross section, which is clamped at both ends. The unclamped beam is curved and its length is unequal to the distance of the clamping conditions, see Fig.1. Due to these initial curvature $\Omega^0 = 1/R$ and pretension ε^0, the straight configuration of the clamped beam is loaded by a normal force as well as a moment. Solving the equations of equilibrium,

$$\mathbf{M}' + \mathbf{r}' \times \mathbf{Q} = 0, \quad \mathbf{Q}' = 0 \qquad (1)$$

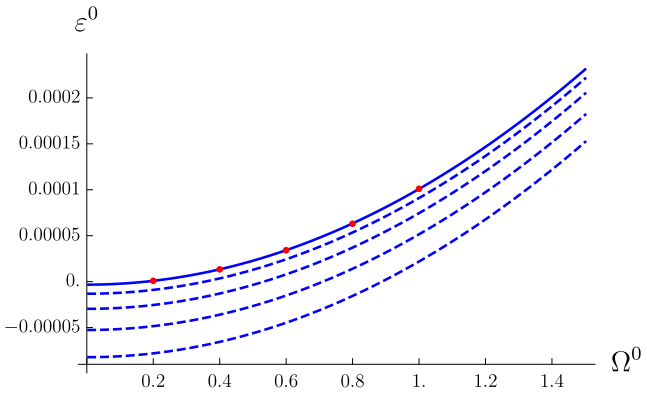

Figure 2: Critical parameters of the clamped beam for $H = 2$, $w = 0.01$ and thickness $h = 0.002$

with moment $\mathbf{M}$, force $\mathbf{Q}$ and position vector $\mathbf{r}$, and their derivatives $()'$ with respect to the material length. We find that the straight configuration is one possible solution. Next, we disturb this equilibrium state and solve the incremental form of the equilibrium equations. An equilibrium solution

for a beam without natural curvature but with gravity forces was found and then disturbed by a small initial curvature Ω^0 in the previous study [3]. In contrast to that article, here we obtain a system of homogeneous differential equations for three small rotations, describing the buckling modes of the system. Searching for non-trivial solutions, we find critical combinations of Ω^0 and ε^0. Whereas for vanishing initial curvature we reproduce the Eulerian buckling load, it is also possible to find buckling modes mainly determined by the pre-curvature Ω^0. Further insight will give Ritz-approximations of the corresponding shell problem.

Comparison with finite element solutions of both, beam and shell models show excellent agreement of the critical values of pretension and curvature, see Fig.2. The blue lines are the stability curves for different buckling modes, where the solid line is the critical one. The red dots show points where the stiffness matrix of finite element solutions become singular. It has been observed, that if the beam becomes strip-like, a nonlinear coupling between torsion and tension, altering the torsional rigidity, becomes crucial, which again is in good agreement with shell solutions. The first mode of stability loss of the shell model is presented in Fig.3.

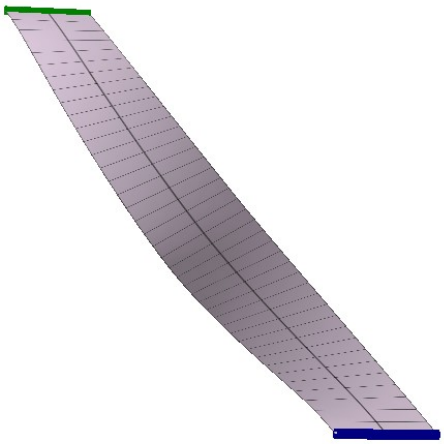

Figure 3: Deformed shell with clamped ends

CONCLUSION

We have seen, that a natural curvature, which is inherent in practical applications like belt drives, may cause interesting buckling phenomena. Although it is interesting from the academical point of view, this study also provided us with a novel benchmark test for the mentioned finite element code.

ACKNOWLEDGEMENTS

The authors thank for the support of the Austrian Research Promotion Agency (FFG), project number 861493.

REFERENCES

[1] Kiani Y., Eslami M.R., *Thermal buckling analysis of functionally graded material beams*, Int J Mech Mater Des, 2010.

[2] Vetyukov Y., *Stability and Supercritical Deformation of a Circular Ring with Intrinsic Curvature*, in Irschik H., Belyaev A., Krommer M, *Dynamics and Control of Advanced Structures and Machines*, p.23-32, Springer (2017)

[3] Vetyukov Y., Schmidrathner C., *A rod model for large bending and torsion of an elastic strip with a geometrical imperfection*, Acta Mech (Accepted).

EDGE FREE GRAPHENE NANOSYSTEMS

Thomas Fabian, Florian Libisch

E136 - Institute of Theoretical Physics at TU Wien

INTRODUCTION

We simulate electronic transport through nanostructures in the ballistic regime. This means that we use quantum mechanics – especially the Schrödinger equation – to investigate the properties of novel materials.

Only few problems in quantum mechanics can be solved by hand, with pen and paper. But the equations can easily be discretized and turned into matrix equations, which can then be solved numerically. In practice this requires reasonable approximations of the Schrödinger equation – approximative enough that the problem at hand can be solved by a (super)computer, yet accurate enough that it captures all the essential features.

Since the first experimental realization of graphene – a one-atom thin sheet of carbon atoms – lots of effort has been undertaken to study this and similar materials. One is eager to find and understand mechanisms that make a material ideal for a special application. As an example, one might want to have materials which can efficiently convert light to electricity – as is done in photovoltaic cells. One might try to conduct electricity without resistance – as we find in a superconductor. We can also think of controlling individual quantum states to eventually obtain a quantum computer.

Our group contributes to the world-wide effort to better understand such nanostructures by close collaboration with experimentalists and by accurate modeling of their current work. Good models improve the understanding of the underlying mechanisms and can further be used to make predictions and suggestions for future lines of research.

SIZE QUANTIZATION IN GRAPHENE AND BILAYER GRAPHENE NANORIBBONS

Quantum mechanics predicts that in a ribbon of a certain width W, the current propagates in so-called modes. These modes resemble the oscillations in a vibrating string. By increasing the vibrational energy, the string (and the quantum mode) at some point obtains enough energy to form an additional node (a node is a point with constant vanishing amplitude). In a quantum transport measurement this sudden increase in the allowed number of modes leads to a sudden, step-like increase in the current we can send through the system.

Unfortunately in all graphene nanoribbons the edge – which means adsorbates, defects, roughness – washes out these clean conductance steps. The group of Christoph Stampfer at the RWTH Aachen recently undertook the effort [4] to improve the resolution of individual quantum states by additionally tuning the edge away with an electric potential. In this setting we investigated the evolution of quantum states in a magnetic field B, see 1.

Researchers at the ETH Zürich and the Karlsruhe Institute of Technology ([1, 3]) were able to electrostatically define a channel in a bilayer graphene ribbon. Bilayer graphene consists – as the name suggests – of two layers of graphene stacked on top of each other. In this system a spatially varying electric potential landscape leads to different potential on the two graphene layers, which can be used

to define a channel without the usual rough edges for the current measurement. In this system it is possible to measure the quantum mechanical modes with unprecedented accuracy.

We come back to monolayer graphene where it is under certain circumstances (a high magnetic field, which quantum mechanically confines electrons to fixed energies) also possible to define an edge free "quantum dot". This is for example done in the group of Markus Morgenstern in Aachen where a scanning tunneling microscope creates a potential well in the graphene sample. After we have collaboratively studied the effects of a substrate [2] our group is currently investigating the influence of lattice defects on individual energy levels.

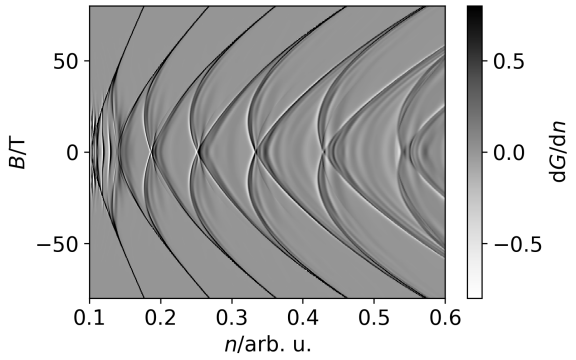

Figure 1: Crossover to Landau quantization in a graphene nanoribbon

CONCLUSION AND OUTLOOK

We have studied several ways to cleanly (edge-free) confine electrons in graphene nanostructures. We have shown that we experimentally and theoretically understand and are able to control individual quantum levels in these systems.

Future lines of research will be the investigation of electrostatically confined quantum dots in bilayer graphene, as well as the investigation of mechanisms which can control an additional defining property of states in graphene called "valley"

REFERENCES

[1] R. Kraft, I. V. Krainov, V. Gall, A. P. Dmitriev, R. Krupke, I. V. Gornyi, and R. Danneau. Valley subband splitting in bilayer graphene quantum point contacts. *Phys. Rev. Lett.*, 121:257703, Dec 2018.

[2] Nils M. Freitag, Tobias Reisch, Larisa Chizhova, Péter Nemes Incze, Christian Holl, Colin R. Woods, Roman Gorbachev, Yang Cao, Andre K. Geim, Kostya S. Novoselov, Joachim Burgdörfer, Florian Libisch, and M Morgenstern. Large tunable valley splitting in edge-free graphene quantum dots on boron nitride. *Nature Nanotechnology*, 13, 08 2018.

[3] Hiske Overweg, Angelika Knothe, Thomas Fabian, Lukas Linhart, Peter Rickhaus, Lucien Wernli, Kenji Watanabe, Takashi Taniguchi, David Sánchez, Joachim Burgdörfer, Florian Libisch, Vladimir I. Fal'ko, Klaus Ensslin, and Thomas Ihn. Topologically nontrivial valley states in bilayer graphene quantum point contacts. *Phys. Rev. Lett.*, 121:257702, Dec 2018.

[4] Sowmya Somanchi, Thomas Fabian, Florian Libisch, Kenji Watanabe, Takashi Taniguchi, Bernd Beschoten, and Christoph Stampfer. Crossover from size quantization to landau quantization in graphene quantum point contacts.

MONITORING OF ALPINE SNOW CONDITIONS USING C-BAND SAR

Claudio Navacchi, Bernhard Bauer-Marschallinger, Wolfgang Wagner

E120 - Department of Geodesy and Geoinformation

INTRODUCTION

Aperture synthesis in radar imaging has allowed the acquisition of high-resolution earth observation data. This data is commonly referred to as synthetic aperture radar (SAR) imagery [1]. Many SAR systems operate in the C-band to take advantage of its significant sensitivity to one of the most abundant molecules on Earth: water. It has proven to be an indispensable way of monitoring processes taking place within the cryosphere, e.g. iceberg monitoring, wet snow extent or snow property mapping.

Recent radar satellite missions as well as in-situ snow profile measurements offer a valuable basis for investigating the relationship of both high-resolution SAR backscatter and snow parameter data. Profound relations shall be determined by correlating snow parameters such as snow height, grain size and snow wetness with backscatter. This backscatter can be transformed to different representations, where the most suitable ones need to be identified to finally be able to derive maps indicating snow conditions.

INTERACTIONS OF MICROWAVES WITH MULTI-LAYERED SNOW PACKS

The fundamental background of all models describing the interaction of electromagnetic (EM) waves with media is based on the radiative transfer theory, which is very complex in the presence of a dense medium as it is the case for an aged snow pack (cf. Fig. 1).

Yet, assumptions in terms of the composition of the snow pack or the propagation characteristics of the radiation allow to derive certain snow parameters. This has been shown in past studies, e.g. an estimation of grain size, snow density and snow depth using the polarimetric properties of SIR-C's X/C-band sensor [2] or mapping extents of a wet snow pack with the aid of change detection [3].

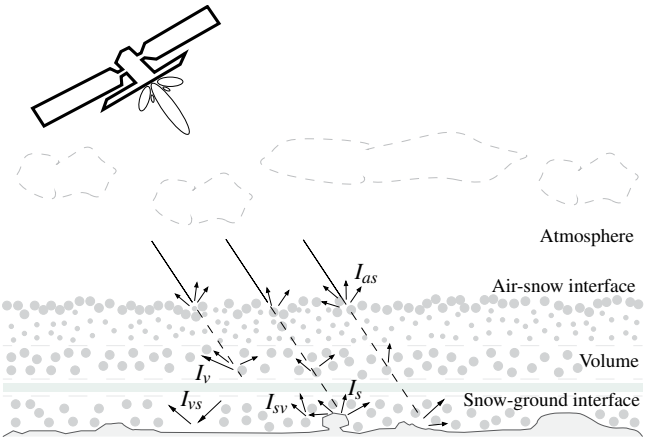

Figure 1: Interaction of radiation with a multi-layered snow pack.

EXPERIMENTS

A comparison of C-band SAR backscatter data from ESA's Sentinel-1 satellites with snow profile measurements offered by the *Lawinenwarndienst Tirol* was proceeded for the timespan summer 2015 to autumn 2017. The geographical scope was limited to an alpine area being 100 $\times$ 100 km wide and covering the North and South Tyrolean alps.

A plausible correlation of the data sets mentioned above demands to adjust the backscatter data, which is strongly influenced by the observation geometry in steep terrain or, in other words, the variability of the incidence angle. Since a snow profile measurement was rarely performed at the same location, the dependency of backscatter on incidence angles has to be eliminated. To do so, various methods, both model based and data-driven, have been presented.

One method belonging to the former category is radiometric terrain flattening, which simulates the local illuminated area based on a Digital Elevation Model (DEM) and utilises it during radiometric normalisation. If many observations at different incidence angles are available, linear regression can be used to normalise backscatter to a certain reference incidence angle. In addition, a novel data-driven normalisation technique relying on the percentiles derived for each orbit was introduced in this study. Well-known quantities such as backscattering differences originating from change detection or polarisation ratios were also created to support an extensive comparison with snow data.

RESULTS AND DISCUSSION

As a measure of predictability, the Pearson correlation coefficient was chosen to compare a subset of snow parameters with the aforementioned backscatter representations. Normalised backscatter by means of linear regression and VH polarisation appeared as the best setup. Results were enhanced by spatio-temporal filtering of backscatter data leading to a partial increase in correlation by nearly 0.2. The most meaningful, consistent correlation of -0.64 was found with respect to maximum snow wetness when doing change detection, which approves presented methodologies to map wet snow [3]. When computing such differences, normalised and not-normalised backscatter perform equally well, since steady effects like the dependency on incidence angles cancel out. Snow height was characterised by the highest positive correlation (0.67), but its significance is questionable, because dry snow is likely a transparent medium for C-band radiation. On the other hand, an aged snow pack containing larger grains can alter the radiation and its state of polarisation to a larger extent being visible in cross-polarisation ratios at the end of the snow melt season.

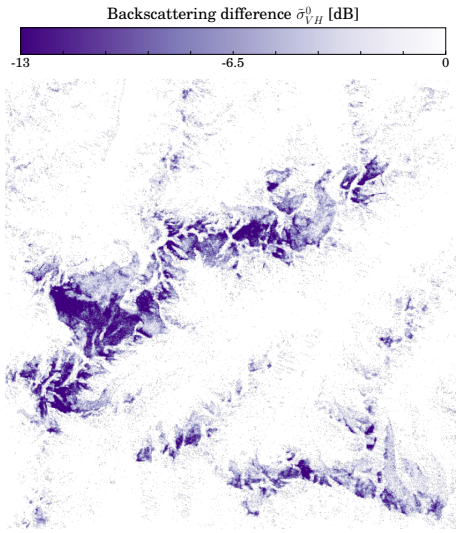

Figure 2: Backscattering differences indicating wet snow (Equi7 grid system).

CONCLUSION

This study has shown, that snow wetness is indeed the most promising quantity to be derived from single-frequency, cross-polarised C-band SAR backscatter data. Fortunately it is not necessary to put effort in normalisation, since the difference formation eliminates terrain effects. Filtering both data sets by time (e.g., separating winter from snow melt season) could be interesting for further research, but more data would be needed to preserve significance. Useful information for run-off models and for determining fragile snow packs is offered by the herein presented wet and dry snow maps aiding in the prediction of avalanche risk assessment.

REFERENCES

[1] Moreira, Alberto et al.:*"A tutorial on synthetic aperture radar"*. IEEE Geoscience and remote sensing magazine 1.1, p. 6-43, 2013

[2] Shi, J.; Dozier J.: *"Estimation of snow water equivalence using SIR-C/X-SAR. II. Inferring snow depth and particle size"*. IEEE Transactions on Geoscience and Remote Sensing 38.6, p. 2475-2488., 2000

[3] Nagler, T.; Rott H.: *"Retrieval of wet snow by means of multitemporal SAR data"*. IEEE Transactions on Geoscience and Remote Sensing 38.2, p. 754-765, 2000

DEVELOPING A NEW SUBSTITUTE FOR IVORY USING LITHOGRAPHY BASED ADDITIVE MANUFACTURING

Thaddäa Rath[a], Bernhard Steyrer[b], Richard Addison[c], Elena Holzhausen[d], Jürgen Stampfl[a]

[a] E308 - Institue of Materials Science and Technology
[b] Cubicure GmbH, Vienna, Austria
[c] Addison KG, Vienna, Austria
[d] Erzdiözese Wien, Vienna, Austria

INTRODUCTION

Due to its convenient mechanic workability and general popularity, ivory was used for art, religious and everyday objects for hundreds of years. Nowadays the resources are limited due to the ivory trading ban, which was set in place for ethical reasons. The price of legally available ivory from remaining stocks is, therefore, very high. The wish to restore sometimes very fragile and delicate cultural artefacts, thus, requires the development of a high-quality substitute material. Most of all, it is necessary to replicate the aesthetic characteristics of ivory by means of the color, translucency and haptic. This also includes the recreation of in ivory specific pattern, which is especially visible at the cross-section of an elephant tusk, as shown in Figure 1. This pattern is also called Schreger lines.

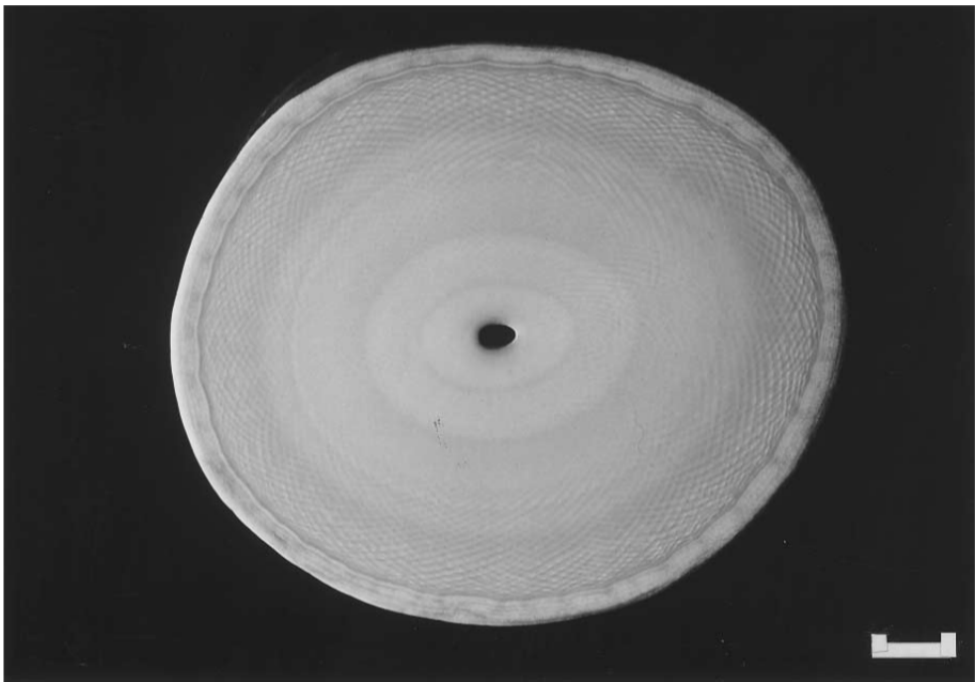

Figure 1:Crosssection of an elephant tusk with Schreger lines visible. The scaling bar equals 4 cm[1].

METHODS

Ivory consists of an organic matrix with embedded calcium phosphate and carbonate. To imitate the morphology a composite was formed, consisting of a photopolymer filled with calcium phosphate particles. In addition, color pigments were mixed into the compound to adjust the base color. In order to remodel the column capital of the cabinet of king Friederick the Fair, micro computed tomography was utilized. A computer-aided design program was used to apply a surface texture that imitates the appearance of the Schreger lines. The model was then sliced into 0.5 µm thick layers. The composite was solidified using lithography based additive manufacturing and, subsequently, the surface was dyed and polished.

RESULTS

Choosing a degree of filling of 55 wt-% calcium phosphate, the Young's modulus, the density and the translucency of the material are comparable to natural ivory. The generation of the surface texture is a simple way to mimic the Schreger lines. However, further post processing of the surface is necessary for an optical imitation of ivory. Figure 2 shows the column capital of the cabinet of king Friederick the Fair, recreated by additive manufacturing compared to the original artefact.

Figure 2: Comparison of the manufactured (left) and the original (right) column capital of the cabinet of king Friederick the Fair.

CONCLUSIONS

Considering the cost, time and ethical aspects it is reasonable to use a substitute material for restoring ivory artefacts. Since the building technology is additive manufacturing, also individual and detailed geometries are possible. This new solution for substituting ivory shows promising results and advantages over existing substitute materials.

REFERENCES

[1] Raubenheimer EJ, Bosman MC, Vorster R, Noffke CE, Histogenesis of the chequered pattern of ivory of African elephant (Loxodonta Afircana), Archives of Oral Biology, 43:6, 969-977, 1998

ELECTRONIC TRANSPORT MEASUREMENTS UNDER UNIAXIAL PRESSURE IN CUPRATE SUPERCONDUCTORS

Benjamin Klebel, Wojciech Tabis, Neven Barišić

E138 - Institute of Solid State Physics

INTRODUCTION

Despite the cuprates (copper-oxide superconductors) being under close scrutiny by the scientific community since their discovery thirty years ago, the phenomenon of high-transition-temperature (high-T_c) superconductivity arising in this class of materials remains unresolved. [1] The richness of the phase diagram originates from strong electron correlation effects, and an intrinsic complexity of these materials. Several coexisting (in some cases competing) phases, and differences in the crystal structures between individual compounds, make it difficult to ascertain the intrinsic and universal properties of the cuprates. One important problem to resolve is the nature of the pseudogap (PG), a regime at moderately low doping, where partial gaps open at the Fermi level, transforming a large hole-like Fermi Surface (FS) into disconnected Fermi arcs.

PHASE DIAGRAM OF THE CUPRATES – REVISITED

The cuprates are a group of compounds in which the common building block, the CuO_2 layers, are separated by material specific charge reservoir layers. The parent compounds are charge-transfer insulators, while various phases and regimes emerge upon doping, in particular superconductivity (Fig.1). In the hole-doped cuprates, superconductivity exists in a doping range between $p_{\min} \approx 0.05$ and $p_{max} \approx 0.3$. In the heavily overdoped regime, above $p_{\max}$, the cuprates exhibit characteristics of a conventional Fermi liquid (FL). For example, the electrical resistivity follows a quadratic temperature dependence, and a large, hole-like Fermi surface is experimentally well documented [2,3] and consistent with band structure calculations. [4] Upon decreasing the doping (below $p_{\max}$), T_c first increases to its highest value at optimal doping ($p_{opt} \approx 0.18$) and then decreases on the underdoped side of the phase diagram, to vanish below p_{min}. [1] In recent work, the electronic scattering rate $1/\tau$ was demonstrated to be quadratic in temperature, and universal (compound and doping independent). [5–7] This result implies that the PG emerges as an effect of a gradual localization of one carrier per unit cell, upon decreasing the doping and/or temperature, marked by T^{**} in Fig. 1. [8–10] This allows for a simple description of the evolution of the carrier density from $n = 1 + p$ at the overdoped side, to $n = p$ on the underdoped side. [3,11] The strange-metal (SM) regime, where the resistivity exhibits a linear temperature dependence, can be explained by evoking thermally excited charge carriers contributing to the electronic transport, effectively masking the underlying Fermi-liquid scattering rate.

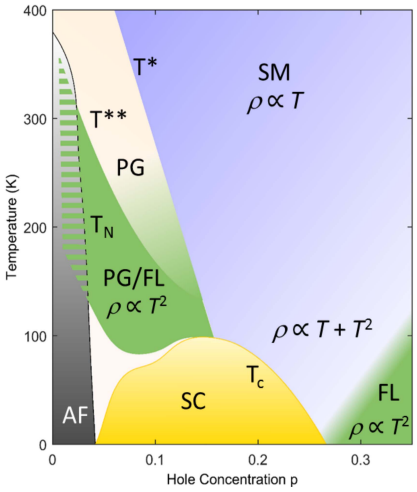

Figure 1: Generic resistivity phase diagram of the cuprates. [5]

SPATIALLY INHOMOGENEOUS LOCALISATION OF ONE CARRIER

The proposed phenomenological model is in its essence percolative, with small patches of the material becoming superconducting a few Kelvin above the actual T_c. Superconductivity results

from a coexistence of two electronic subsystems – itinerant holes and holes which are localised (in the PG regime one carrier per unit cell). [10] The latter subsystem is separated from the Fermi level by an energy gap which is inhomogeneous, both in real and momentum space. As the charge becomes localised (when traversing the phase diagram from high to low temperature/doping), the corresponding states at the Fermi level are being supressed, giving rise to the transformation of the large hole-like FS into Fermi arcs. Moreover, the localized carrier serves as the superconducting pairing "glue" for the itinerant electrons. However, the details of the microscopic mechanism responsible for the pairing/localization, where presumably the intrinsic structural inhomogeneity of the cuprates plays an important role, are still under investigation [12]. Therefore, our goal is to establish the relation between T_c and the details of the crystal lattice and its symmetry. To control these parameters, we developed a novel uniaxial pressure setup, which permits performing various measurements on a single sample while modifying its lattice symmetry. Results obtained from these measurements will be compared with the results from various compounds exhibiting distinct structures and distinct T_c's.

RESISTIVITY UNDER UNIAXIAL PRESSURE

I will present preliminary results of electronic transport measurements performed under uniaxial pressure in single crystals of $Nd_{2-x}Ce_xCuO_4$. This material has a tetragonal crystal structure, which we distort by applying uniaxial pressure within the *ab*-plane. According to the discussed phenomenological model, we expect this distortion to lower the T_c, as the tetragonal symmetry is lost. At room temperature, the *c*-axis resistivity decreases linearly with pressure, reverting to its original value upon releasing pressure. The superconducting transition shifts towards lower temperatures, in contrast to a general increase of T_c under isotropic pressure (Fig. 2). Thus, it is successfully demonstrated that superconductivity is affected by the structural changes of the lattice symmetry.

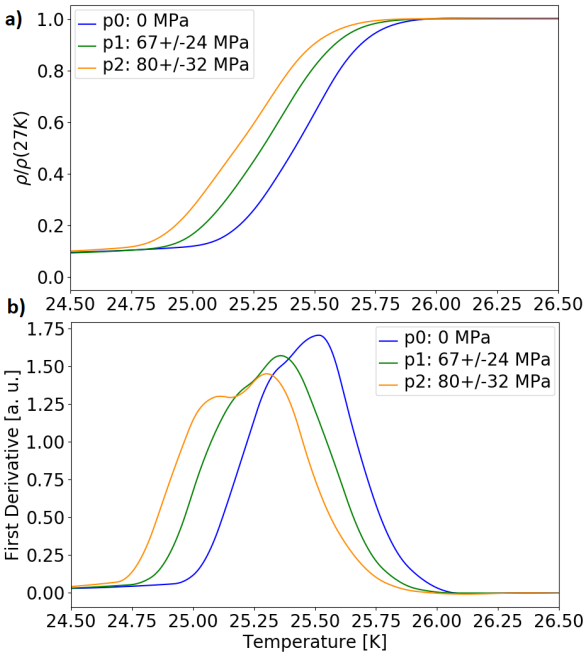

Figure 2: Variation of Tc with uniaxial pressure applied along the [100] crystallographic direction. (a) In-plane resistivity and (b) first derivative.

REFERENCES

[1] B. Keimer, Nature **518**, 179 (2015).
[2] S. Nakamae, Phys. Rev. B **68**, R100502 (2003).
[3] B. Vignolle, Nature **455**, 952 (2008).
[4] C. O. Rodriguez, Phys. Rev. B **49**, 1200 (1994).
[5] N. Barisic, Proc. Natl. Acad. Sci. U. S. Am. PNAS **110**, 12235 (2013).
[6] M. K. Chan, Phys. Rev. Lett. **113**, 7005 (2014).
[7] N. Barišić, ArXiv E-Prints **1507**, arXiv:1507.07885 (2015).
[8] D. Pelc, Nat. Commun. **9**, 4327 (2018).
[9] P. Popčević, Npj Quantum Mater. **3**, 42 (2018).
[10] D. Pelc, Sci. Adv. **5**, eaau4538 (2019).
[11] A. P. Mackenzie, Phys. Rev. B **53**, 5848 (1996).
[12] D. Pelc, ArXiv E-Prints **1902** arXiv:1902.00529 (2019).

BACKGROUND SIMULATION STUDIES FOR THE CRESST AND COSINUS DIRECT DETECTION DARK MATTER EXPERIMENTS

Alexander Fuss

E141-03 - Institute of Atomic and Subatomic Physics, Research Unit of Nuclear and Particle Physics
HEPHY - Institute of High Energy Physics of the Austrian Academy of Sciences

INTRODUCTION: DARK MATTER SEARCH WITH SCINTILLATING CALORIMETERS

Dark matter (DM) is one of the big mysteries still persistent in the physical picture of our universe. According to the standard cosmological model, visible matter contributes less than 20% to the total existing matter content. Among the experiments searching for DM via direct detection are CRESST (Cryogenic Rare Event Search with Superconducting Thermometers), a long-standing pioneer in the direct search for very low-mass DM particles, and COSINUS (Cryogenic Observatory for SIgnatures seen in Next-generation Underground Searches), a more recently initiated project which is only starting to build up the experiment this year. As the interaction between DM and standard model particles is presumably very weak, a crucial task for both experiments is background minimization and optimal understanding of residual background signals.
CRESST and COSINUS are searching for signatures of DM particles scattering elastically off nuclei in their detectors. Both experiments operate their scintillating target crystals ($CaWO_4$ in CRESST, NaI in COSINUS) at mK-temperatures and employ a two-channel readout – using transition edge sensors (TESs) developed in CRESST – allowing to simultaneously measure the phonon (heat) and the scintillation light signal. This feature provides the possibility to distinguish β/γ-backgrounds from the expected nuclear recoils. However, neutrons entering the detectors can easily mimic signals of the sought-after DM particles, which is why we consider them as the most dangerous background. We distinguish radiogenic neutrons, originating from spontaneous fission and (α,n) reactions due to environmental radioactivity and radioactive contaminations inside materials surrounding the detectors, and cosmogenic neutrons produced in interactions of cosmic muons.

BACKGROUND MODELING FOR CRESST

Searching for the very rare DM-nucleus scattering processes is like looking for a needle in a haystack, if the detectors are not shielded optimally against any kind of background in the signal region. For this reason, the CRESST experiment is located undergound at the Laboratori Nazionali del Gran Sasso (LNGS), where a rock overburden of 3600 meter water equivalent reduces the cosmic muon flux by a factor of 10^6 with respect to the surface. Furthermore, the detectors have to be surrounded by a dedicated shielding setup. A classical approach uses a sequence of an outer shield made of a low-Z material to moderate ambient neutrons, a high-Z shield mitigating the ambient gamma flux and an inner (thin) low-Z layer shielding against neutrons produced in the high-Z materials. Additionally, plastic scintillator panels are used as an active muon veto. The respective shielding structure of CRESST is shown in Fig. 1. For developing a neutron background model, we use the Monte Carlo toolkit Geant4 [1], in which a detailed geometry of the experimental setup has been implemented.

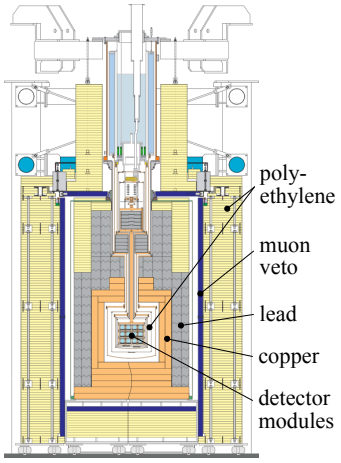

Figure 1: The shielding setup of CRESST.

Currently, we are studying radiogenic backgrounds, for which we feed energy spectra and fluxes of neutrons obtained with the SOURCES4C [2] code to the Geant4 simulations, where we have developed a dedicated primary particle generator, which allows us to efficiently simulate radioactive contaminations. As an example, Fig. 2 shows the detector carousel and a homogeneous radioactive contamination in all its Cu parts. Additionally, an enhanced detector response model is under development, which will allow us to include the energy resolution of our multiple detectors and to directly compare simulated to real data.

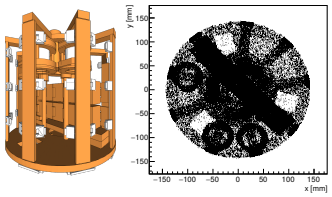

Figure 2: left: CRESST detector carousel visualized in Geant4. right: radioactive contamination in its Cu parts

DEVELOPING A SHIELDING CONCEPT FOR COSINUS

In COSINUS, our current simulation task focuses on evaluating an optimal shielding structure for the eventual buildup of the experiment. The idea is to use an approach, in which the outer low-Z shield consists of a big steel tank filled with ultra-pure water, as schematically depicted in Fig. 3. An advantage of this structure is, that the water tank can serve two tasks simultaneously. First, it acts as a passive shield against ambient radioactive decay particles and second, it can be instrumented with photomultiplier tubes to function as an active Cerenkov muon veto. Results of our simulation studies let us conclude that inner layers made of polyethylene and lead (see Fig. 3) should likely be omitted, due to higher radiogenic and cosmogenic neutron yields, respectively. We find that 3 m of water together with an inner layer of 8 cm copper would be sufficient in reducing ambient particle fluxes, while at the same time minimizing the expected background. In addition, a dedicated optical simulation of the Cerenkov light produced in the water tank is employed to estimate the efficiency of the muon veto system. All results of these simulations contribute to the conceptual design report of COSINUS, which is currently being written up.

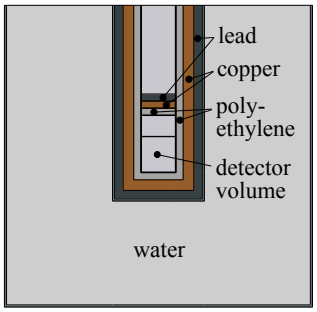

Figure 3: Schematic design of the COSINUS shielding.

CONCLUSION

A main task in rare event search experiments is optimal background mitigation and modeling of residual backgrounds. For CRESST, developments both in enhancing the simulation code and improving the post-processing of simulated data are thus ongoing. Eventually, all radiogenic and cosmogenic background contributions shall be analyzed, leading up to a background model for the experiment. For COSINUS, current simulations are laying ground for the shielding concept of the experiment and help estimating the efficiency of the muon veto, resulting in important contributions to the conceptual design report.

ACKNOWLEDGEMENTS

This work would not be possible without the collaborative efforts within CRESST and COSINUS and the support of my work by the Austrian Science Fund FWF, Doctoral program No. W1252-N27.

REFERENCES

[1] S. Agostinelli et al. *"Geant4–a simulation toolkit"*. NIMA 506.3 (2003), pp. 250-302.

[2] W. B. Wilson et al. *"SOURCES 4A: A Code for Calculating (α,n), Spontaneous Fission, and Delayed Neutron Sources and Spectra"*. LA-13639-MS (1999).

INVERSE MAGNETISATION PROBLEM FOR THE ANCIENT ROCKS: A FRUITFUL ENCOUNTER OF HARMONIC ANALYSIS AND PALEOMAGNETISM

Dmitry Ponomarev[a], Laurent Baratchart[b], Juliette Leblond[b], Eduardo Andrade Lima[c]

[a]E101 - Institute of Analysis and Scientific Computing, TU Wien
[b]FACTAS/APICS team, INRIA, Sophia Antipolis, France
[c]Department of Earth, Atmospheric and Planetary Sciences, MIT, Cambridge, USA

INTRODUCTION / PHYSICAL MOTIVATION

Earth rocks and meteorites may preserve invaluable records of ancient planetary and solar nebula magnetic fields in the form of remanent magnetization. Recent advances in magnetometry have made it possible to measure magnetic fields of very low intensity generated by some rocks, and extraction of this relict magnetic information has become reality in cases that were previously inaccessible using standard rock magnetometers. An endeavor to develop a robust and efficient method for processing these data leads to a number of challenging problems such as effective extension of the restricted measurement data and extraction of certain features of the magnetization (typically, its mean value) that may still allow for retrieving those primordial records without having to solve the entire inverse problem for the underlying spatial distribution of magnetic sources.

In particular, we are concerned with the setup corresponding to a SQUID scanning microscope which operates in a horizontal plane above the sample and measures the vertical component of the magnetic field produced by the sample (a slice of the magnetized rock).

We employ two different solution techniques based on asymptotic analysis and original data continuation approach (involving the use of a priori unknown quantities) which lead to explicit analytical formulas for the magnetic moments in terms of measurement data (see formulas (1)-(2)). One of these techniques is Kelvin transformation followed by asymptotic spherical harmonics projections whereas the second is asymptotic analysis of Fourier integrals in vicinity of the origin. Both methods are novel and lead to essentially identical results which prompts one to explore a deeper connection between elementary ”discrete” and ”continuous” harmonic analysis tools.

MATHEMATICAL FORMULATION

The following setting is a three-dimensional version of what has been previously discussed (see the references in [2]). As follows from Maxwell equation for the stationary field, scalar potential Φ of the magnetic field produced by magnetization $\vec{M}$ (a compactly supported distribution whose support Q is known and corresponds to the area occupied by the magnetic sample) satisfies Poisson equation: $\Delta\Phi = \nabla\cdot\vec{M}$. This establishes a link (in the form of three-dimensional convolution integral) between the unknown magnetization M and the measured quantity $B_3 = -\mu_0\frac{\partial\Phi}{\partial x_3}$ available on a bounded subset (which we take to be a disk of area A) of a horizontal plane at some height above the sample, μ_0 is a physical constant (magnetic permeability of vacuum). Severe ill-posedness of the reconstruction problem for the whole magnetization distribution and physical interest in overall strength and direction magnetization of a sample lead us to a hope for recovery of the net magnetization vector (essentially, an average magnetization of the sample) $\vec{m} := \iiint_Q \vec{M}(t_1,t_2,t_3)\,d^3t$ which is called magnetic moment.

RESULTS AND DISCUSSION

By using specially developed "discrete" and "continuous" harmonic analysis tools mentioned in Introduction and detailed in [1,2], we conclude that the suitable integrals of the measured data provide good approximation to magnetic moment components with the accuracy growing with the size of the measurement area A:

$$m_j = \frac{2}{\mu_0} \iint_{D_A} \left(1 + \frac{4x_j^2}{3A^2}\right) x_j B_3(x_1, x_2)\, dx_1 dx_2 + \mathcal{O}\left(\frac{1}{A^2}\right), \quad j = 1,2, \tag{1}$$

$$m_3 = \frac{2}{\mu_0 A} \iint_{D_A} B_3(x_1, x_2)\, dx_1 dx_2 + \mathcal{O}\left(\frac{1}{A^2}\right). \tag{2}$$

As shown on Figure 1 obtained for a synthetic example, the method is robust with respect to the 10-percent (i.e. SNR=20 dB) Gaussian white noise once a simple data preprocessing is done. The latter concerns only one component of the magnetization moment whose recovery relies on a necessity dictated by physics implying the vanishing of the total integral of B_3 over the horizontal plane above the sample.

CONCLUSION AND OUTLOOK

We have developed data continuation/analysis techniques which prove to be efficient in a particular inverse magnetization problem (the source enters the governing PDE in the divergence form and the available data is one component of the gradient of the potential field). This naturally raises a question to define a scope of other source-characterization problems (i.e. the triples of source, data and source-related object of interest) where the general philosophy of "recursive" data continuation and asymptotic harmonic analysis can be used with the same success and at the same time being physically interesting.

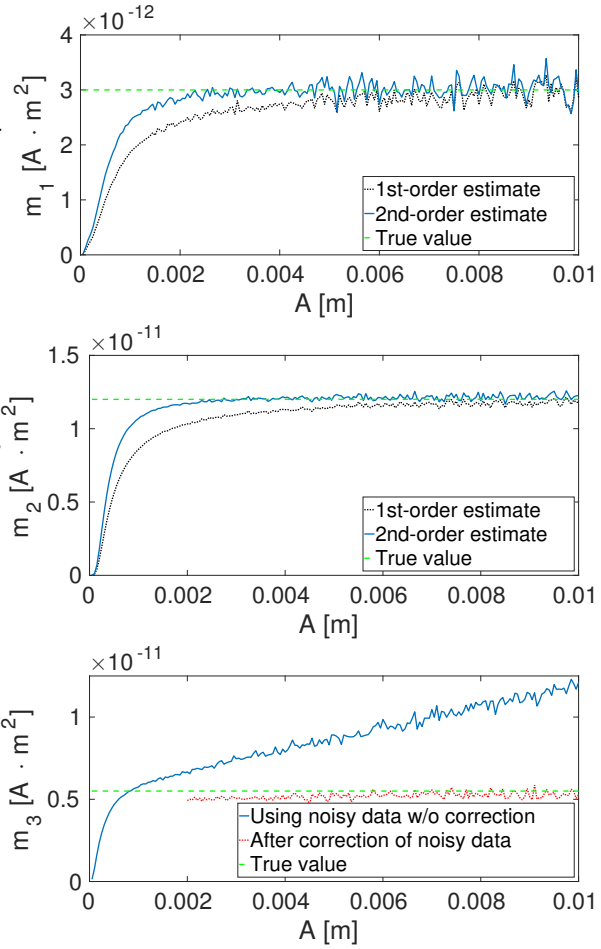

Figure 1: Estimates for components of magnetization moment versus radius A of measurement area

ACKNOWLEDGEMENT

The authors acknowledge the support of MIT-France seed funding grant (IMPINGE project) under which present results were obtained. D. Ponomarev is currently supported by Austrian Science Fund (FWF project I3538-N32).

REFERENCES

[1] Ponomarev D 2016, *Some inverse problems with partial data*, PhD thesis (University of Nice)

[2] Baratchart L, Leblond J, Lima E, Ponomarev D, 2017 Magnetization moment recovery using Kelvin transformation and Fourier analysis, *J. Phys.: Conf. Ser.* **904**

REPROCESSING OF HIGH DENSITY POLYETHYLENE

Hoai Maria Nguyen Thu, Michael Preschl, Thomas Koch, Vasiliki-Maria Archodoulaki

E308-02-1- Institute of Material Science and Technology- Research Group Structural Polymers
TU Wien

INTRODUCTION

Plastics have made modern life possible and have become an integral part of our everyday life. In 2017 the worldwide plastic manufacturing reached about 350 million tonnes[1]. Plastic disposal has become a global problem since plastic scraps are released into the environment during its production and as waste after usage. Mechanical recycling is a common way to re-process waste materials. However, the mechanical properties of the material are maybe affected, which can lead to a reduction of the quality of the manufacture. 92% of the worldwide plastic production is allocated among 7 different types of plastic. With 36% polyethylene leads the world market [2].

This work deals with the simulation of mechanical recycling of high density polyethylene (PE-HD). In literature the data are incomplete concerning an industrial upscaling, since the processing temperatures used in research are too low[3] which comes along with a low extruder throughput and therefore low profit. Besides, little attention was payed which catalyst system was used to produce PE-HD[3],[4]. Ziegler Natta leads to chain scission and further degradation. Whereas Phillips can cause crosslinking, and the thermoplastic becomes a thermoset, which excludes the re-processing through film blowing[5]. The influence of the pre-treatment method (pelletising or grinding) is also a point of interest, since additional mechanical degradation can occur.

EXPERIMENTS / FUNDAMENTAL OF THE PROBLEM / EXAMINATIONS

To simulate mechanical recycling 10 extrusion cycles were done on the single screw extruder Ex-18-26 with a screw rotating speed of 75 rpm and two different processing temperature sets from the first zone to the third zone were applied. The first one with 130°C-180°C-200°C follows the approach in literature and the second one with 130°C-240°C-240°C represents processing temperatures from industry. Two PE-HD types were investigated. One made through a Ziegler Natta catalyst named Hostalen GF 4750 purchased from LyondellBasell and the Phillips type Marlex 5502BN provided by Chevron Phillips Chemical. Moreover, the manufacturing processes of pelletizing and grinding were simulated. Pelletizing was conducted through cutting and grinding was done with the universal cutting mill Pulverisette 19 (Fritsch). After 1 and 10 extrusion cycles tensile tests (Zwick 050) according to DIN ISO 527-2 and tensile impact strength tests (Instron Ceast 9050) according to DIN ISO 8256 were done. The influence of the processing of the specimens (injection moulded and compression moulded) is also investigated. To determine the crosslinking content, the samples were heated at 140°C for 24h in xylene according to ASTM D2765-01.

RESULTS AND DISCUSSION

At 180°C and by pre-treating the material via cutting, in comparison to the first cycle extruded samples, the 10 times extruded PE-HD had higher impact tensile strength. This was found for both catalyst systems (Figure 1). No changes in strain at break were observed

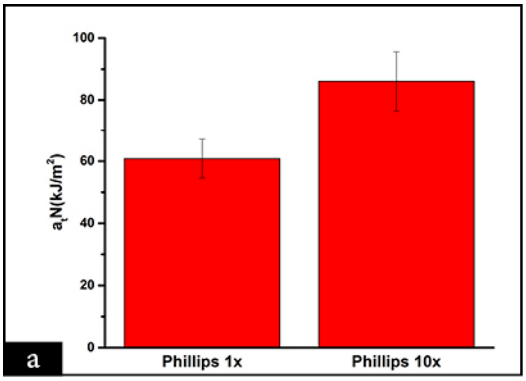

between the single extruded samples and the 10 times extruded Phillips PE-HD. For the 10 times extruded injection moulded Ziegler Natta PE-HD samples the strain at break doubled (Figure 2b). Due to chain scission of the longest chains, the new medium sized chains have a higher mobility, which causes a weakening of the polymer network. Therefore, the rigidity decreases and the elasticity rises[6].

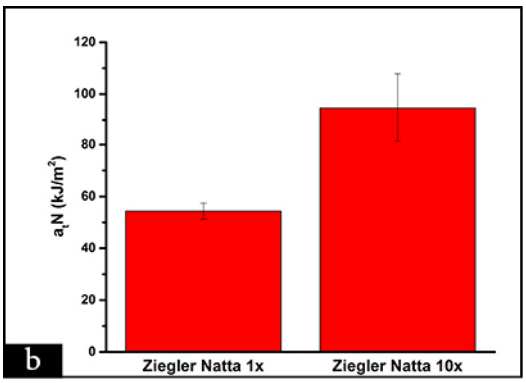

Figure 1: a) tensile-impact strength for Phillips PE-HD, b) tensile-impact strength for Ziegler Natta PE-HD

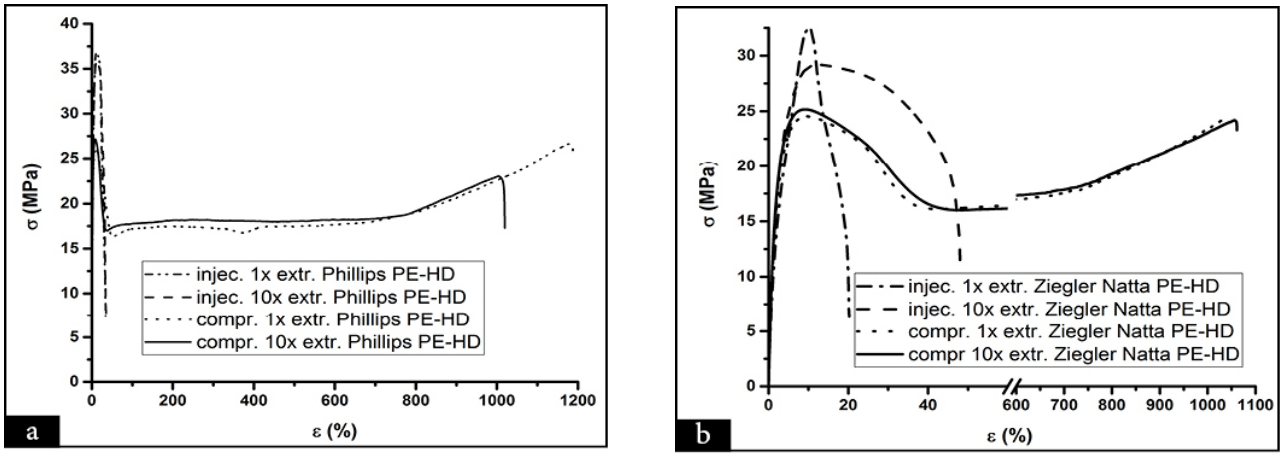

Figure 2: a) stress- strain diagram for Phillips PE-HD, b) stress- strain diagram for Ziegler Natta PE-HD

CONCLUSION

The obtained results show a strong dependence on the processing parameters and the used PE-HD type. The gentlest re-treatment process for each polymer must be identified. Further PE-HD types with other melt flow index values and PE-HD from post-consumer waste must be investigated, in order to ensure a proper recycling method.

REFERENCES

[1] https://www.plasticseurope.org/en/resources/market-data

[2] Geyer, Roland et al. “Production, use, and fate of all plastics ever made” *Science advances* vol. 3,7 e1700782. 19 Jul. 2017

[3] Mylläri, V. et al. “Detergent impurity effect on recycled PE-HD: Properties after repetitive processing” J. Appl. Polym. Sci., vol. 133, issue 31, 43776, 2016

[4] Oblak, Pavel et al. “Processability and mechanical properties of extensively recycled high density polyethylene” Polymer Degredation and Stability, vol. 114, 133-145, 2015

[5] Moss, Serge et al. “Degradation and stabilization of high density polyethylene during multiple extrusions” Polymer Degredation and Stability, vol. 25, issues 2-4, 1989

[6] Benoit, N., González-Núñez, R., & Rodrigue, D. “High Density Polyethylene Degradation Followed by Closed-loop Recycling” Progress in Rubber, Plastics and Recycling Technology, 33(1), 17-38, 2017

FILLING OF SINGLE-WALLED CARBON NANOTUBES WITH LEAD HALOGENIDES

Marianna V. Kharlamova, Dominik Eder

E165 - Institute of Materials Chemistry, TU Wien

INTRODUCTION

Single-walled carbon nanotubes (SWCNTs) attract ever increasing attention of researchers in fundamental science. They possess extraordinary physical and chemical properties and unique one-dimensional structure[1]. As-synthesized nanotube samples represent mixtures of nanotubes with different atomic structures and electronic properties[2]. However, fundamental research requires the SWCNTs with homogeneous properties.

To controllably modify the electronic properties of SWCNTs, several methods were established. They include the covalent and noncovalent modification of the outer surface of SWCNTs, substitution of atoms in the SWCNT walls by other atoms, intercalation of bundles of SWCNTs and filling of internal channels of SWCNTs[3]. Among these methods, the filling of SWCNTs is a promising approach of tailoring the electronic properties of SWCNTs, because the channels of nanotubes can be filled with different substances[4]. The SWCNTs were filled with metals and non-metals, inorganic compounds (metal halogenides, metal chalcogenides, metal oxides), molecules (fullerenes and their derivatives, metallocenes, metal acetylacetonates).

Here, we perform the filling of SWCNTs with lead halogenides ($PbCl_2$, $PbBr_2$ and PbI_2). We investigate the filling ratio of SWCNTs by high-resolution scanning transmission electron microscopy (HR STEM) and the modified electronic properties of SWCNTs by spectroscopic techniques (Raman spectroscopy and X-ray photoelectron spectroscopy (XPS)).

EXPERIMENTAL

The SWCNTs synthesized by the arc-discharge method (1.4 nm ArcSO type, Meijo-Nanocarbon Co.) were used as starting material. The SWCNT ends were opened by annealing in air at 500°C for 30 min. After that the SWCNTs and powders of lead halogenides were put into a quartz ampoule, evacuated (10^{-6} mbar) and sealed. The ampoule was heated in a tube furnace until a temperature 100°C above the melting point of each lead halogenide: 601°C for $PbCl_2$, 471°C for $PbBr_2$ and 502°C for PbI_2, kept at this temperature for 6 hours and cooled at rates of 0.05-1.5°C/min to obtain one-dimensional crystals of the salts.

The HR STEM imaging was conducted using a Nion UltraSTEM 100 microscope operated at an accelerating voltage of 60 kV. Samples were prepared by drop casting dispersions of filled SWCNTs in isopropanol onto carbon-coated gold grids. Raman spectroscopy measurements were performed using Horiba Jobin Yvon LabRAM HR800 spectrometer equipped with a tuneable ArKr laser (Coherent Innova 70c) (458, 488, 514, 531, 568 and 647 nm) and a HeNe laser (633 nm). The measurements were performed directly on the buckypapers. The experimental accuracy is 2 cm^{-1}. The Raman spectra were fitted to Voigtian and Fano peaks and the area intensities were calculated with PeakFit v4.12. XPS spectra were measured with a SPECS spectrometer equipped with a monochromatized AlK_α (1486.6 eV) X-ray gun (μFocus 350 μm) and a hemispherical Phoibos 150 WAL analyzer. Buckypapers (5 mm × 5 mm) were mounted on a sample holder using double-sided carbon tape. The pass energies for detailed and survey XPS scans were 30 and 100 eV, respectively.

RESULTS AND DISCUSSION

The HR STEM data proves the filling of SWCNTs with lead halogenides. Figure 1 presents an example of image of bundles of SWCNTs filled with lead iodide. The filling ratio differs for different lead halogenides. According to the XPS data, the filling ratio is maximal in the case of PbI_2 and minimal in the case of $PbBr_2$.

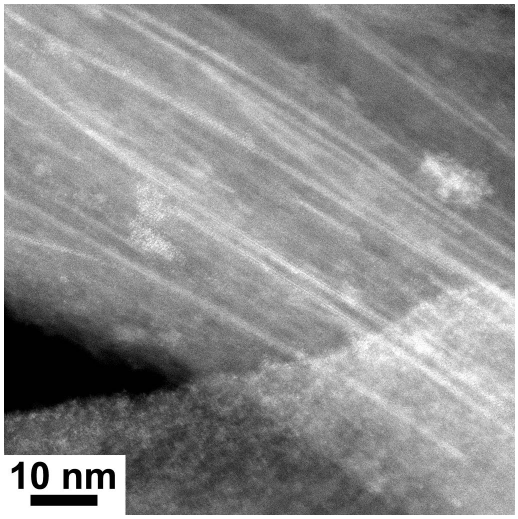

Figure 1: The HR STEM image of lead iodide-filled SWCNTs.

Raman spectroscopy and XPS testify to p-doping of SWCNTs by the encapsulated compounds. The strong modifications of radial breathing mode and G-bands of Raman spectra are observed. They include shifts of the peaks and changes in their relative intensities. The C 1s XPS spectra demonstrate shift of the peak towards lower binding energies, which is caused by increasing the work function of SWCNTs as a result of a downshift of the Fermi level of SWCNTs due to the charge transfer from the nanotubes to the encapsulated salts. Both Raman spectroscopy and XPS data prove that the doping efficiency differs for different lead halogenides. The effect is strongest for PbI_2, followed by $PbCl_2$ and $PbBr_2$.

There are several factors that influence the doping level of filled SWCNTs. Firstly, the doping level depends on the chemical and physical properties of the encapsulated compounds. There is a gradual change in the properties of lead halogenides, such as anion radius and electron affinity of halogen, in the line $PbCl_2$ - $PbBr_2$ - PbI_2. However, this does not explain the observed variation of the doping level of SWCNTs. Secondly, the doping level depends on the filling ratio of SWCNTs. The XPS investigations showed that the nanotubes have different filling ratios with different lead halogenides. This is in line with the observed differences in the doping efficiency of SWCNTs.

CONCLUSION

To summarize, the SWCNTs were filled with one-dimensional nanocrystals of $PbCl_2$, $PbBr_2$ and PbI_2. The filling of SWCNTs was confirmed by HR STEM. Raman spectroscopy and XPS proved that lead halogenide nanocrystals result in p-doping of the nanotubes accompanied by a downshift of the Fermi level of SWCNTs. The doping level varies for different lead halogenides: the doping effect is the largest for PbI_2 and the smallest for $PbBr_2$.

REFERENCES

[1] Saito R, Dresselhaus G, Dresselhaus MS (1998) Physical properties of carbon nanotubes. Imperial College Press, London

[2] Joselevich E, Dai HJ, Liu J, Hata K, Windle AH (2008) Carbon nanotube synthesis and organization. In: Jorio A, Dresselhaus G, Dresselhaus MS (eds) Carbon nanotubes: topics in applied physics, vol 111. Springer, Berlin, pp 101–164

[3] Kharlamova MV (2013) Electronic properties of pristine and modified single-walled carbon nanotubes. Phys Usp 56:1047–1073

[4] Kharlamova MV (2016) Advances in tailoring the electronic properties of single-walled carbon nanotubes. Prog Mater Sci 77:125–211

STUDY OF INTERACTIONS OF CHEMIRESISTORS ARRAYS TOWARDS VOCs

Katarina Kumpf[a], Filippo Fedi[b], Johannes Bintinger[b],
Wolfgang Knoll[b], Bernhard Lutzer[a] and Philipp Fruhmann[a]

[a]Center for Electrochemical Surface Technology, Konrad-Lorenz-Straße 24, 3430 Tulln/Donau
[b]Austrian Institute of Technology GmbH, Konrad-Lorenz-Straße 24, 3430 Tulln/Donau

Gas sensors are key elements in many aspects that affect the quality of our life as well as the efficiency of industrial production[1]. Within different classes of gas sensors, resistive gas sensors are found to be one of the most investigated type of electrochemical gas sensors. They gained much attention based on their possibility to be employed under atmospheric conditions, cost efficiency and flexibility in production. Their working principle is based on the change of the resistance that the gas-sensing material experiences once it is exposed to the target analytes. Due to their simplicity and tuneability, many different gases are detectable by this principle. In this work we study and compare the interaction between volatile organic compounds (VOCs) with two different sensor arrays. The first array were made out of four commercial metal oxides (MOx) chemiresistors (Figure 1 a,b,c), while the second one were based on chemiresistors with four tailored organic semiconductors (OSs) (Figure 1,d) as sensitive layer.

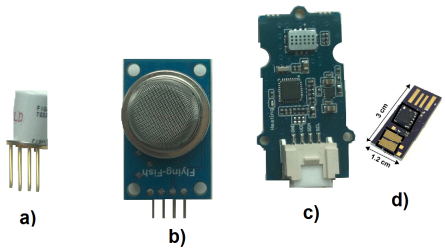

Figure 1: In figure are shown the commercial MOx sensor (a,b,c) and the OS sensor (d).

MATERIALS AND METHODS

The core part of the monitoring system is based on an Arduino UNO microcontroller and connected with four sensors as well as with a temperature and humidity sensor (Figure 2). Arduino is an open-source electronics platform based on easy-to-use hardware and software[2]. The Arduino UNO board is based on the ATmega328 - 8- bit microchip, which has 14 digital input/output pins and 6 analog inputs, which allow the connection of up to 6 different sensors. The open-source Arduino Software (IDE) is a cross-platform Software, whose environment is written in Java and based on an open-source software[2]. Also, Arduino Software contains several libraries that are easily accessible and free, allowing easy programming. During the measurements, which gives the opportunity to plot the signal in real time based on the serial communication. Within the experiments several different OSs were used and the sensors were prepared by casting some microliters of a OSs solution in chloroform on each electrode arrays [3]. Based on the different nature of the different OSs, different responses for our target analytes were finally achieved.

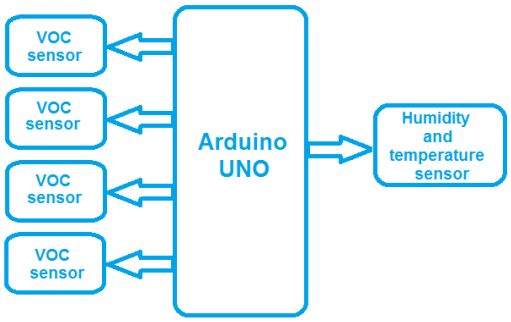

Figure 2: Hardware module of the systems

RESULTS AND DISCUSSION

Commercial MOx sensors usually have a wide detection range between 1 ppm (parts per million) and 1000 ppm. The sensing element is in most cases based on SnO_2. MOx sensors are easily accessible on the market, prices are affordable and according to the datasheets, they own a long stability in time.

In contrast to them, the use of OSs are a promising and already used technology in organic electronic devices. This is mainly based on their intrinsic affinity towards reducing and oxidizing analytes.

In our experiments, we are employed two types of resistive gas sensors: commercial ones based on MOx[3] and some tailor-made sensors on OSs[4]. In both cases, the materials undergo changes in the electrical resistance when interacting with gases and vapors. In order to optimize the sensing responses, we examined the sensing performance under same conditions measuring simultaneously. We employed an array of four commercial MOx sensors and array four OSs sensors. In addition, we monitored the humidity and the temperature in our experiments in order to achieve reproducible results. The arrays behave different due to the diverse characteristic of the sensing materials. The MOx based sensors showed slow operation time due the required pre-heating step, since their operating temperature is in the range of 300 - 450 °C. Once the analyte is removed, this high temperature allows to achieve a full recovery of the signal. The platform made with OSs are faster and more reactive, but in some cases, they have slower and inefficient recovery. For both materials there are still controversial opinions about the charge transfers mechanisms and the resulting sensor signal. With this work we were therefore aimed to establish a simple sensor platform which could be utilized with different sensor types in order to create tailor-made sensor arrays within scientific and industrial applications.

CONCLUSION

In our work we compared the behaviours of two different arrays of chemiresistors towards VOCs. Advantages and disadvantages between sensors based on MOx and OSs will be shown. Further experiments will be performed using other toxic gases like CO, NH_3, NO_2 and the influence of humidity and temperature will be studied.

REFERENCES

[1] Erfan, M. et al. (2016) "On-Chip Micro–Electro–Mechanical System Fourier Transform Infrared (MEMS FT-IR) Spectrometer-Based Gas Sensing." Applied Spectroscopy (2016): 70(5), pp. 897–904.

[2] https://www.arduino.cc/

[3] Wang, Yin, et al. "Metal oxide gas sensors: sensitivity and influencing factors."Sensors (2010): 10(3), 2088-106.

[4] Yang, Shyuan, et al. "Inexpensive, Versatile, and Robust USB-Driven Sensor Platform." IEEE sensors letters 1.6 (2017): 1-4.

CONTROLLING THE ELASTICITY OF CALCITE SUSPENSIONS WITH SIMPLE IONS

Teresa Liberto[a,b], Catherine Barentin[b], Jean Colombani[b], Marie Le Merrer[b]

[a]E207 - Faculty of Civil Engineering, Center for Building Materials and Materials Technology, Adolf Blamauergasse 1-3 A-1030 Vienna, Austria

[b]Université de Lyon, Université Claude Bernard Lyon 1, CNRS, Institut Lumière Matière, F-69622, Villeurbanne, France

INTRODUCTION

Calcite is an ubiquitous mineral employed in many industrial fields such as paper filling, pharmaceutical, art or construction. In particular the suspension of its particles is used to mimic early stage cementitious materials. In order to control the mechanical properties of calcite paste it is necessary to understand the role of the interaction forces between its particles. In this regard, this study show how a macroscopic quantity of the calcite suspensions, namely the elasticity, measured by rheological measurements can be linked to microscopic interactions, via DLVO analysis. Our calcite pastes are weakly attractive systems, showing a typical colloidal gel behavior, and characterized by an elastic shear modulus and a critical strain. We have tuned the interaction forces between particles by addition of simple ionic species (Ca^{2+} and OH^{-}). Rheological measurements are compared to DLVO calculations, obtained by chemical speciations and ζ potential measurements on dense suspensions.

MATERIALS AND METHODS

Socal 31 calcite powder (Imerys) with an average particle diameter of 70 nm is dispersed in various solutions to obtain several calcite suspensions [1,2]. The initial calcite volume concentration is fixed to $\phi = 10\,\%$. To investigate the effects of simple ionic additives, we disperse calcium hydroxide $Ca(OH)_2$ (concentrations c ranging from 3 to 50 mM) or sodium hydroxide NaOH (concentration 100 mM) in deionized water.

Rheological measurements are made with a plate-plate geometry (gap width 1 mm) [1,2]. The measurements consist in a pre-shear step with 1 minute imposed shear rate of $\dot{\gamma} = 10\ s^{-1}$ and then a constant deformation of $\gamma = 0.01\,\%$ at frequency $f = 1$ Hz during 10h. In particular, the imposed deformation is small enough to remain in the linear regime [1] and allows to measure the temporal evolution of the storage modulus $G'(t)$ of the samples. **DLVO calculation** (Derjaguin-Landau-Verwey-Overbeek) between parallel planes [2] is used to characterize the strength of particle interaction [3]. **Zeta potential measurements** are carried out directly on the concentrated calcite suspensions with an electroacoustic technique (ZetaProbe) [2,4]. The suspension **chemical speciations** (i.e. full ionic compositions) are obtained with the freeware Visual MINTEQ [2,5]. For all the samples, pH measurements are made directly on the fresh suspensions.

RESULTS AND DISCUSSION

As shown in Figure 1, addition of calcium hydroxide improves the initial workability of the paste by lowering the elastic modulus of the paste (G'), which is further recovered upon carbonation (in time) in contact with atmospheric carbon dioxide. To estimate the change of interaction nature with the calcium hydroxide concentration, we have computed the value of the DLVO potential and its

maximum energy barrier W_{max} against pH, as shown in Figure 2(b). Its evolution is strongly non linear, with a sharp maximum at pH $\simeq$ 12. The initial elastic modulus of the paste in the same pH range is presented in Figure 2(a). The evolution of interaction potential and mechanical property are strongly correlate. The weaker the attraction, the softer the gel. The $G'(0)$ minimum and W_{max} maximum match perfectly at pH $\approx$ 12. Below this pH, the main effect is a change in surface potential with calcium concentrations, while at high pH, modifications of the ionic strength and Debye lengths are dominant. We also demonstrate that the addition of NaOH completely screens the charges and leads to a strongly interacting and rigid paste [2].

CONCLUSION

We have shown in this study how simple ions modifies significantly the mechanical behavior of a calcite paste. We found a direct correlation between the elastic modulus of colloidal calcite paste and the energy barrier calculated using the classical DLVO potential. A practical consequence of our findings is that calcium hydroxide could be used as an admixture to get more workable calcium carbonate pastes, considering that the induced extra-fluidity spontaneously disappears, by simple contact with air, to give good final mechanical properties. The perspective of this work is to applied an analogous procedure to cementitious material in order to connect the macroscopic behavior of the paste with the microscopical interaction.

REFERENCES

[1] T. Liberto et al., Soft Matter, 2017,13, 2014-2023

[2] T. Liberto et al., *in preparation*, 2019

[3] J. Israelachvili, Academic Press, London, 1992.

[4] A. Dukhin et al., Langmuir, 1999,15, 6692-6706

[5] Visual MINTEQ version 3.1, https://vminteq.lwr.kth.se

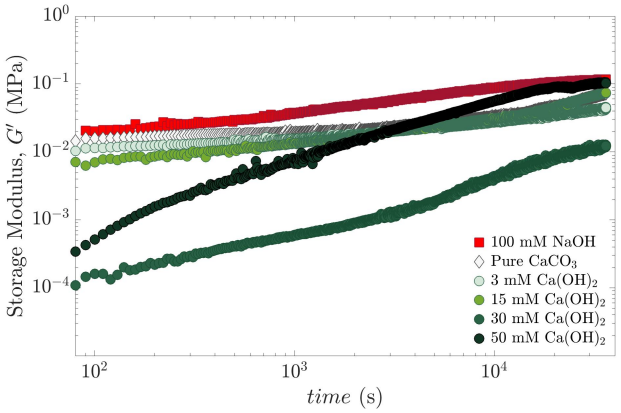

Figure 1: Time evolution of the storage modulus G' of calcite suspensions of concentration $\phi = 10\,\%$, for increasing c and a sample containing NaOH.

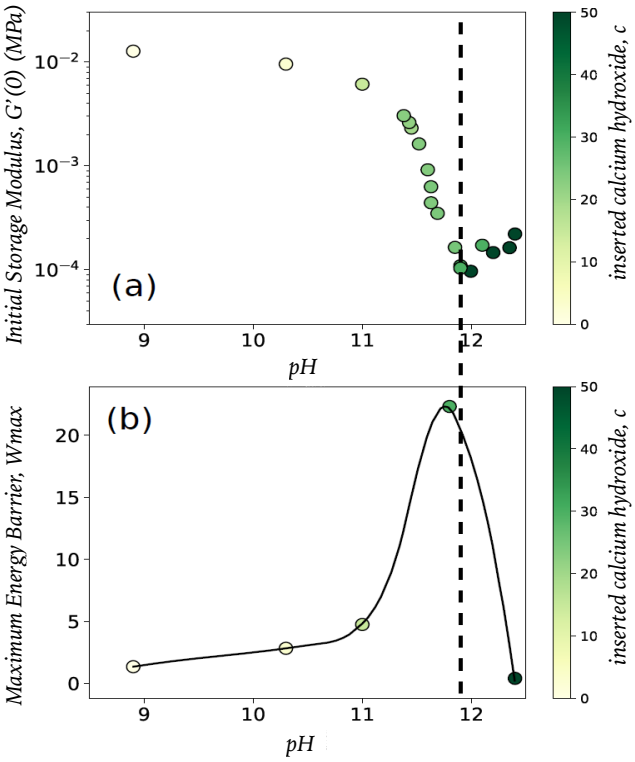

Figure 2: (a) Initial storage modulus $G'(0)$ as a function of pH. (b) Maximum energy barrier, W_{max} as a function of pH. The different data points correspond to various $Ca(OH)_2$ oncentrations (c).

SEMI-VOLATILE ORGANIC TRACE QUANTIFICATION OF EMISSION SAMPLES WITH PTR-TOF-MS

Bernadette Kirchsteiger [a], Dusan Materic [b], Rupert Holzinger [b], Franziska Klauser [c], Harald Stressler [c], Rita Sturmlechner [c] and Anne Kasper- Giebl [a]

[a] E164- Institute of Chemical Technologies and Analytics
[b] Utrecht University, 5386 Utrecht, Netherlands
[c] BIOENERGY 2020+ GmbH, 8010 Graz, Austria

INTRODUCTION

Carbonaceous compounds represent a major fraction of atmospheric aerosols. This holds true for ambient particulate matter, but is even more obvious when emission samples from residential wood combustion are evaluated. Moreover, biomass combustion is also a source for volatile organic compounds (VOCs) which may interact with carbonaceous compounds in particulate matter. Routinely carbonaceous compounds are quantified with a thermal-optical method, differentiating between organic and elemental carbon. In this study, we will investigate the impact of semi-volatile organics on the evolution of elemental carbon with this method.

STUDY DESIGN

This study focusses on the amount of semi-volatile organic trace compounds in emission samples from different firewood combustion devices. Sampling differentiated between hot and cooled total suspended particle (TSP) samples, “cooled-phase samples” were diluted with compressed air. A comprehensive chemical characterization of both sample fractions was carried out. The analysis of organic carbon (OC) and elemental carbon (EC) was performed in duplicates by an OCEC analyzer (Sunset Laboratory Inc.), applying the EUSAAR_2 protocol in the transmission mode[1]. Different contributions of the carbonaceous aerosol fractions could be observed in both sample fractions. Hot-phase samples consist primarily of EC while OC concentrations dominate cooled-phase samples. For hot-phase samples the filter transmittance signal was very low caused by the relative high filter loadings, which made OC charring difficult to detect. Based on a first evaluation, hot-phase samples were divided into samples showing “early burning EC” (EB-EC) and “late burning EC” (LB-EC). EB-EC samples showed a rapid evolution of EC during the first temperature step and right after switching to the oxidative phase. While LB-EC samples showed the opposite effect, where the evolution of EC took place during the last and highest temperature step within the oxidative phase.

Liu et al. reported that the presence of oxygenated species in particulate matter samples may be associated with premature EC evolution [2]. To investigate this effect for emission samples under evaluation, semi-volatile trace quantification of both sample fractions will be carried out using a Proton Transfer Reaction “Time-of-Flight” Mass Spectrometer (PTR-TOF-MS). This method couples high sensitivity with high mass resolution for multiple semi-volatile organics emitted from biomass burning.

PRELIMINARY RESULTS

This study evaluates the separation between the carbonaceous fraction EC and OC and its dependence on other constituents of particulate matter formed during biomass combustion of different residential firewood devices. Special focus will be put on semi-volatile organics. PTR-TOF-MS enables a real-time detection of semi-volatile organics during the different temperature steps which were used for OC and EC quantification. Results will be compared with data from the thermal-optical method. Statistical analysis will be performed with mentioned data and will give insights in the impact of semi-volatile organics on the premature evolution of EC. Detailed interaction of VOCs and carbonaceous fraction emitted from residential firewood combustion devices will be presented at the symposium.

CONCLUSIONS AND OUTLOOK

Here we will present the comprehensive characterisation of emission samples, which serves as a basis for the calculation of up to date emission factors. The obtained results will give insights in the interaction of semi-volatile organics and elemental carbon.

Furthermore, this work aims to establish awareness on the advantages and limitations of the quantification of OC and EC with a thermal-optical method.

REFERENCES

[1] Cavalli et al., Toward a standardized thermal-optical protocol for measuring atmospheric organic and elemental carbon: the EUSAAR protocol, Atmos. Meas. Techn.3, p. 79-89, 2010

[2] Liu et al., Uncertainties in thermal-optical measurements of black carbon: Insights from source and ambient samples, Science of the Total Environment, p. 239-249, 2019

THERMAL AND FRICTIONAL AGING IN TRIBOLOGY - STATUS ANALYSIS OF ENGINEERING AND HIGH-PERFORMANCE THERMOPLASTICS

Latifeh Nasseri, Haris Kovacevic, Bernadette Duscher, Thomas Koch, Vasiliki-Maria Archodoulaki

E308-02-1- Research Group for Structural Polymers at TU Wien

INTRODUCTION

Tribology as a relevant knowledge for many fields of engineering consists in optimization of mechanical properties by reducing friction and wear related energy and material losses. Hence, study the influence of important parameters such as contact temperature, environmental temperature, sliding velocity and load on the wear and friction coefficient is very important. Thermoplastics are especially found in applications of non-conformal tribological contacts such as gears or bearings. Between most frequently used engineering thermoplastics, aliphatic polyketone (APK), polybutylenterephthalat (PBT) and polyoxymethylene (POM) are widely used for tribological applications due to their high abrasion and heat resistance. For comparison reasons, the tribological tests are also performed for polyether ether ketone (PEEK) and polysulfone (PSU).

Numerous studies show that abrasive wear processes in polymers are complex and hardly to generalize. Unal et al. [1, 2] investigated the impact of sliding speed and applied normal pressure on the tribological performance of different polymers including POM and APK at room temperature. They concluded that with increasing the pressure the coefficient of friction decreases linearly, whereas wear rate showed less sensitivity to the applied pressures and sliding speed. Unal et al. [3] has also shown that the wear rate of POM and APK decreases with the increase in sliding distance. However, the influence of the environmental temperature on the tribological performance of these materials is not found in the literature.

The aim of this study is a fundamental and systematic approach of the interaction between microstructure, mechanical, and tribological properties. Studies have shown that polymer wear undergoes two main mechanisms, deformation wear and interfacial wear [4]. Deformation wear involves abrasive and fatigue wear while the interfacial wear involves adhesive or transfer wear. Wear of polymers is influenced by sliding contact conditions, the bulk mechanical properties of the polymer and properties of a third body, which generally appears as transfer film or loose degraded polymer particles [5]. The performance of a tribological system is governed by the interplay of these three groups which is in focus of this study.

EXPERIMENTS / FUNDAMENTAL OF THE PROBLEM / EXAMINATIONS

In this study, the wear deformations on the polymer surface are investigated when a steel ball is loaded against a polymer specimen (ball-and-plate test), a polymer pin is loaded against a steel disk (pin-on-disc test) and when the aforementioned tests are performed at temperatures below and above the glass transition temperature of the polymers. Hence, to determine the wear behavior in a dry sliding environment, tribological tests are performed for two sliding speeds 0.075 m/s and 0.15 m/s, and for two normally applied loads 30 N and 60 N, under two different measurement temperatures 23°C and 80°C. Since the surface roughness has impact on wear rate and friction coefficient [6], the surface roughness is modified to reach a high and a low roughness value.

RESULTS AND DISCUSSION

Figure 1 represents the variation of friction force with time for POM and PEEK, performed on a pin-on-disc apparatus for 6 hours under 0.075 m/s sliding speed and normal load value of 30 N at room temperature. The coefficient of friction can be calculated by dividing the friction force by the normal force. It is evident from this picture that the friction force increases rapidly at the early stages due to the formation of ridges on the surface, and reaches a stable plateau as the test progresses and a layer of wear debris is built on the surface. Besides, based on the measured weight loss of pins after each measurement it is clear that the weight loss of PEEK is about 5 times higher than POM.

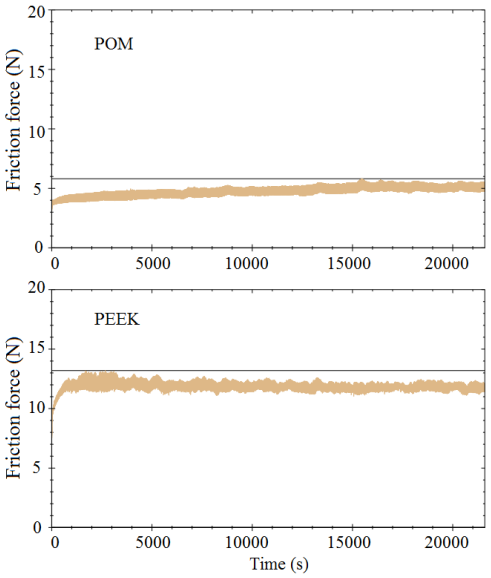

Figure 1: Friction force as function of time resulted from the pin-on-disc test

Figure 2 represents the variation of friction force with time for POM and PEEK performed on a ball-and-plate apparatus for 6 hours under 0.075 m/s sliding speed and normal load value of 30 N at room temperature. Both surfaces were prepared with a defined low roughness value. As it can be seen, the friction force of PEEK is almost two times higher than of POM and increases constantly during the testing time up to a maximal value of about 12 N or a coefficient of friction of 0.4.

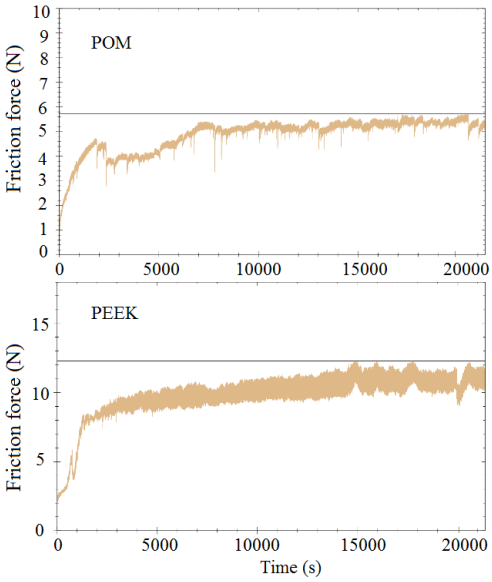

Figure 2: Friction force as function of time resulted from the ball-and-plate test

CONCLUSION

The wear rate and frictional behavior are significantly influenced by the surface roughness and sliding distance. Future experiments will include performance of the tribological measurements at temperatures above the glass transition temperature. Furthermore, measurements with different load conditions will be also carried out.

REFERENCES

[1] H. Unal, U. Sen, A. Mimaroglu, Dry sliding wear characteristics of some industrial polymers against steel counterface, Tribology International, Volume 37, Issue 9, 2004.

[2] H. Unal, A. Mimaroglu, T. Arda, Friction and wear performance of some thermoplastic polymers and polymer composites against unsaturated polyester, Applied Surface Science, Volume 252, Issue 23, 2006.

[3] H. Unal, A. Mimaroglu, V. Serdar, Dry sliding performance of thermoplastics against reinforced unsaturated polyester (BMC): In use in electrical contact breakers components. Wear. 261, 2006.

[4] B. Briscoe, Tribol Int14, 231, 1981.

[5] B. J. Briscoe and S. K. Sinha, Proc. Inst. Mech. Eng. Part J J. Eng. Tribol.216, 401, 2002.

[6] Ovaert, T.C. and Cheng, H.S.,Counterface topographical effects on the wear of polyetheretherketone and polyetheretherketone-carbon fiber composite, Wear, Vol. 150, 1991.

BITUMEN AGEING AND ITS EFFECT ON THE SURFACE MICROSTRUCTURES

Ayse Nur Koyun, Hinrich Grothe

E165 - Institute of Materials Chemistry at TU Wien

INTRODUCTION

Ageing of roadwork materials causes microstructural changes of the asphalt binder. Therefore, fast ageing simulations of roadwork materials, such as Viennese Ageing Procedure (VAPro) or Pressure Ageing Vessel (PAV)[1], can be conducted in laboratory to determine the asphalt long-time performance on the streets in a quick process. Topological deformations caused by ageing can be detected with cryo-ESEM and Atomic Force Microscopy (AFM). Fluorescence Spectroscopy is used to track the ageing state of the asphalt binder.

EXPERIMENTS / FUNDAMENTAL OF THE PROBLEM / EXAMINATIONS

Sunlight (photo-oxidation), atmosphere (reactions of bitumen with reactive oxygen species (ROS)), rain water (dissolving acids and oxygen containing species) and thermal oxidation (during treatment process in refinery, during transportation from refinery to pavement area and the embedding process itself) are the main factors for the change over its lifetime. The main bitumen components are Asphaltenes, Saturates, Aromatics and Resins. Negative electrospray ionization Fourier transform ion cyclotron resonance mass spectrometry [ESI(-)] FT-ICR-MS experiments show that ageing reduces condensed aromatic compounds to alicyclics and open chain aliphatics [2]. The overall fluorescence intensity decreases with oxidation state (see figure 1) and structural changes can be observed on the surface of the roadwork material with cryo-ESEM.

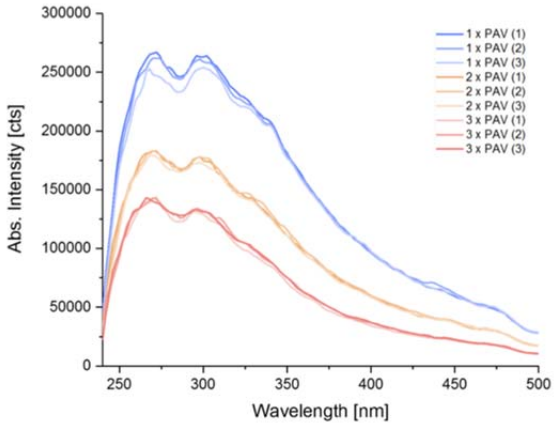

Figure 1: Fluorescence spectra of PAV aged samples. Decrease in overall absolute Intensity.

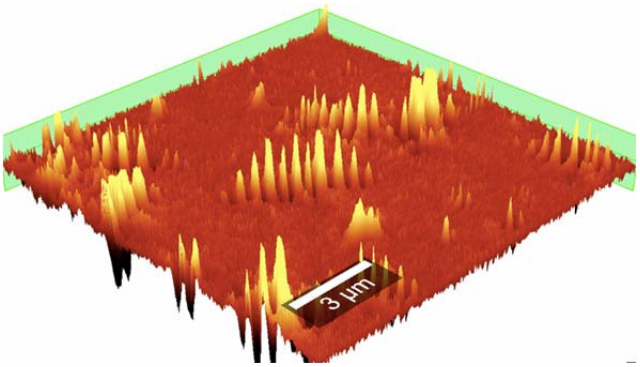

Figure 2: Non - aged AFM of bitumen after 24 h relaxation time.

Cryo-ESEM shows an increase of the surface microstructures with increasing the oxidation state with PAV. A change in the size distribution is observed, where the size of the surface structures alters from 2 – 10 µm in length and up to 1 µm in width.

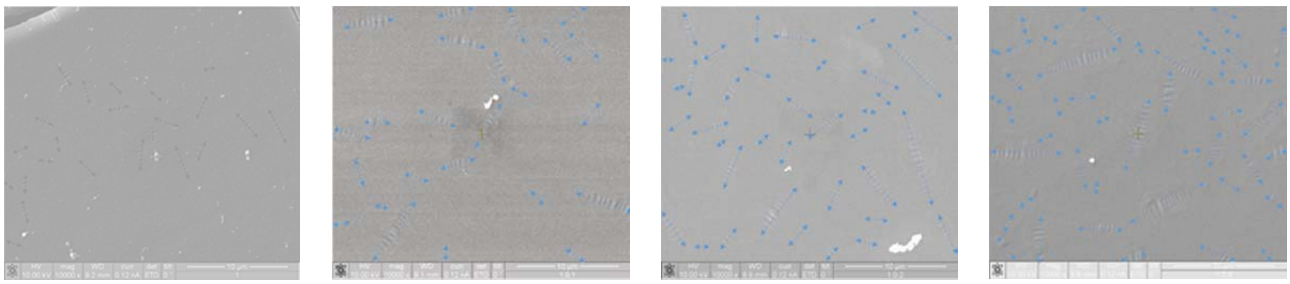

Figure 3a - d: cryo – ESEM of (a) non - aged, (b) 1 x PAV (c) 2 x PAV (d) 3 x PAV aged bitumen samples

A higher resolution of the surface microstructures can be achieved with AFM. A dependence of the ageing state with the surface morphology can be seen during the microstructure formation process. The surface roughness increases with the ageing state (see figures 4a -c).

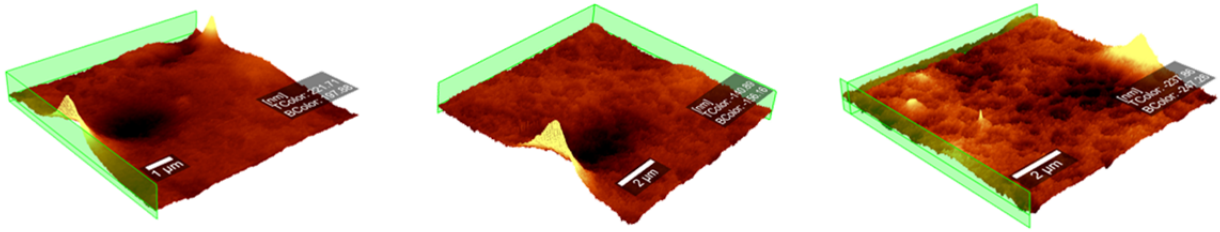

Figure 4a - c: AFM of (a) 1 x PAV rms = 22,41 nm (b) 2 x PAV rms = 34,05 (c) 3 x PAV rms = 46,64 nm aged bitumen samples.

CONCLUSION

A strong correlation between the PAV ageing state and surface properties could be observed. Since microchanges can pave the way to macrochanges (embrittlement and cracks visible to the eye), it is worth to look at the correlations and to elucidate methods that can predict a materials performance to save resources and energy.

ACKNOWLEDGEMENT

The authors would like to thank the analytical instrumentation center for the AFM facilities. FEG-SEM measurements were carried out using facilities at the University Service Centre for Transmission Electron Microscopy, TU Wien. We also would like to thank the FFG for the financial support.

REFERENCES

[1] Daniel Steiner, Bernhard Hofko, Markus Hospodka, Florian Handle, Hinrich Grothe, Josef Füssl, Lukas Eberhardsteiner & Ronald Blab (2016) Towards an optimised lab procedure for long-term oxidative ageing of asphalt mix specimen, International Journal of Pavement Engineering, 17:6, 471-477. DOI: 10.1080/10298436.2014.993204

[2] Florian Handle, Mourad Harir, Josef Füssl, Ayşe N. Koyun, Daniel Grossegger, Norbert Hertkorn, Lukas Eberhardsteiner, Bernhard Hofko, Markus Hospodka, Ronald Blab, Philippe Schmitt-Kopplin, and Hinrich Grothe (2015)Tracking Aging of Bitumen and Its Saturate, Aromatic, Resin, and Asphaltene Fractions Using High-Field Fourier Transform Ion Cyclotron Resonance Mass Spectrometry. Energy & Fuels 2017 31 (5), 4771-4779. DOI: 10.1021/acs.energyfuels.6b03396

LASER-ASSISTED SYNTHESIS OF GRAPHITE ENCAPSULATED ALLOY NANOPARTICLES FOR ENERGY CONVERSION APPLICATIONS

Niusha Lasemi[a*], Christian Rentenberger[b], Robert Pospichal[c], Alexey S. Cherevan[a], Dominik Eder[a], Gerhard Liedl[c], Martin Pfaffeneder-Kmen[d]

[a] E165 - Institute of Materials Chemistry, TU Wien
[b] Institute of Physics of Nanostructured Materials, University of Vienna
[c] E311 - Institute of Production Engineering and Photonic Technologies, TU Wien
[d] Institute of Physical Chemistry, University of Vienna

INTRODUCTION

Pulsed laser ablation in liquids (PLAL) is a novel technique to produce nanomaterials with higher purity for various applications such as biomedicine [1], energy conversion and catalysis. Ultrashort laser pulses are practically important as the physicochemical processes occur in timescales comparable to the natural atomic and molecular oscillation time from femtosecond (10^{-15} s) up to picosecond regime (10^{-12} s) [2]. Moreover due to the thermal non-equilibrium situation of electrons and lattice, the precise and localized material processing with less energy loss can be expected [3]. Graphite shell nanomaterials due to their outstanding optical, mechanical, thermal, electrical properties and high surface area attract more attention in energy conversion applications. They showed a promising potential in transistor, battery, supercapacitor and biosensor. As the efficient heat transfer in electronic packages is of importance, the thermal interface materials (TIMs) were mainly introduced in high-density electronics. Commercial TIMs are generally composed of highly conductive particles such as graphite particles and a matrix for an efficient heat transfer. In the presented work, Ni/Au bimetallic oxide nanoparticles (BONs) with a few nanometer graphitic shell and median size of 10nm were generated by femtosecond laser pyrolysis of butanol solvent on Ni/Au target.

EXPERIMENTAL

The Ni/Au platelets were positioned in a glass cell (height of 15mm) with an optical window allowing the horizontal access of the laser beam (Picture 1). The nanoparticle production was carried out using a commercial femtosecond titanium-sapphire laser (SPECTRA-PHYSICS®, ≤400mW, 800nm, 10 fs, 75 MHz and beam diameter ca. 6 mm). The chirped pulse amplification (CPA) were applied before transferring the seed laser pulse to the Pockels cell [4]. The powermeter (OPHIR Photonics) was placed after diaphragm A3. The maximum output power for the system is ≤1 W. The focus position at various liquid media were experimentally evaluated by measuring the ablation area on a silicon target (ImageJ software) as a function of the distance of the focusing parabolic mirror (focal length 101.16 mm). The Gaussian beam radius of 87 micron was calculated. The size distribution study and electron diffraction patterns of laser-synthesized nanoparticles were studied by transmission electron microscope; Philips CM200 TEM (LaB6 cathode, acceleration

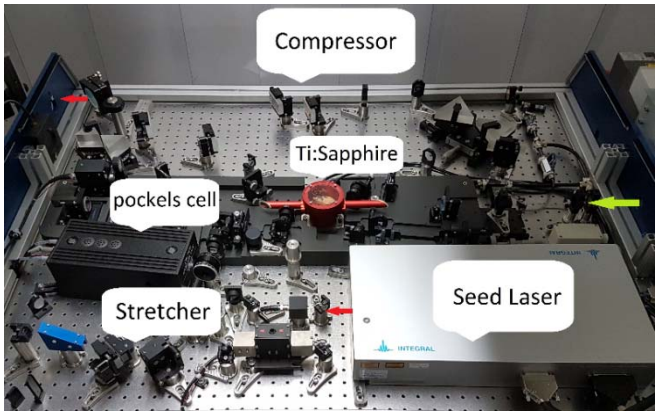

Picture 1: The schematic of femtosecond laser set up. The system connected to the motorized XYZ-scanning stage controlled by CNC computer program.

voltage of 200kV, Gatan Orius CCD camera). Energy-dispersive X-ray spectroscopy (EDX) in connection with TEM served for chemical composition studies. High resolution transmission microscopy (HRTEM) was performed by FEI Titan 80-300 equipped with an imaging Cs corrector. The squared diameter of the ablated area (D^2) which is evaluated by optical microscopy is correlated to the Gaussian beam radius (w_0), the pulse energy (E) and the threshold pulse energy (E_{th}) with the assumption of a Gaussian beam profile;

$$D^2 = 2w_0^2 ln\left(\frac{E}{E_{th}}\right)$$

The laser energy was chosen around 250 μJ to decrease the energy losses during the synthesis. The solvent evaporation by laser cause scattering and shielding of the laser energy and consequently lower productivity. Moreover, the filamentation of ultrashort laser beam in fluid at higher fluences can contribute to energy losses [5].

RESULTS AND DISCUSSION

The femtosecond laser ablation of Ni/Au target in butanol at fluence (F) about 1 J.cm^{-2} and number of pulses (N) of 1000 led to crystalline Ni/Au BONs with median size of 10 nm. BF-TEM is shown various forms of crystallographic systems and defects (Picture 2). The HRTEM of Ni/Au BONs presented a few atomic layers of graphite shell. The lower polydispersity and median size are observed similar to isopropanol solvent and in comparison to ethanol. In fact, solvents with higher carbon chain length led to the formation of carbonaceous shells, e.g. graphite due to pyrolysis of solvents on hot metallic surface [6-7]. The sublimation, evaporation and disintegration of the solid material occur due to the interaction of the high intensity laser pulse with the surface of the material. Moreover, due to the heat transfer from the molten metal layer and plasma plume to the solvent at the liquid-metal interface, the supercritical liquid can be formed [8]. This can contribute to solvent decomposition and generation of carbonaceous species inside the colloidal solutions.

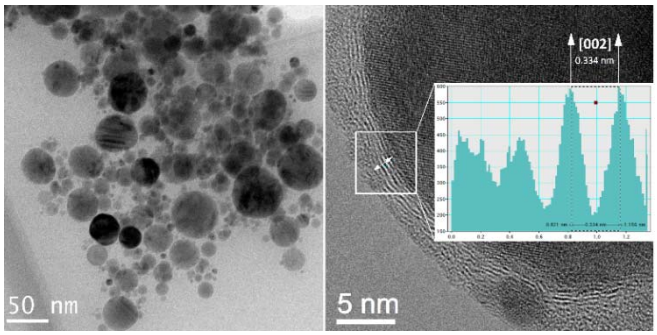

Picture 2: BF-TEM, HRTEM and intensity profile of femtosecond laser-synthesized Ni-Au BONs in butanol. (N = 1000, F = 1 Jcm^{-2}).

CONCLUSION

Graphite encapsulated Ni/Au BONs with a thin graphitic shell of a few atomic layers and median size of 10nm were synthesized by femtosecond laser-induced disintegration of butanol solvent. One can assume that the nature of the solvent may play a role in the final chemical composition of nanomaterials. The graphitization of Ni/Au BONs in butanol triggered more colloidal stability due to less agglomeration and particle diffusion.

REFERENCES

1. N. Lasemi, O. Bomatí, R. Lahoz, V.V. Lennikov, U. Pacher, C. Rentenberger, W. Kautek, 19, 1414-1419 (2018).
2. S.K. Sundaram, E. Mazur, Nature Materials, 1, 217 (2002).
3. S.P. Murzin, G. Liedl, R. Pospichal, A.A. Melnikov, Journal of Physics: Conference Series, 1096, 012138 (2018).
4. A. Fernandez, T. Fuji, A. Poppe, A. Fürbach, F. Krausz, A. Apolonski, Optics Letters, 29, 1366-1368 (2004).
5. A. Hahn, S. Barcikowski, B.N. Chichkov, Journal of Laser Micro/Nanoengineering, 73-77 (2008).
6. V. Amendola, G.A. Rizzi, S. Polizzi, M. Meneghetti, Journal of Physical Chemistry B, 23125-23128 (2005).
7. N. Lasemi, U. Pacher, C. Rentenberger, O. Bomatí-Miguel, W. Kautek, ChemPhysChem,18, 1118-1124 (2017).
8. C.-Y. Shih, C. Wu, M.V. Shugaev, L.V. Zhigilei, Journal of Colloid and Interface Science, 489, 3-17 (2017).

PERFORMANCE CHARACTERIZATION OF A TECHNOLOGY FOR THERMAL ENERGY STORAGES

Stefan Krimmel[a,b], Romeo Ralon[a], Anastasia Stamatiou[b], Jörg Worlitschek[b], Heimo Walter[a]

[a]E302 - Institute for Energy Systems and Thermodynamic
[b]University of Applied Sciences Lucerne - T&A, CC TES, Switzerland

INTRODUCTION

In the case of latent thermal storage units with indirect heat transfer technologies, the output is still sufficient for the design process even with a high degree of solidification. Due to an insulating layer of solidified storage material, a liquid-solid phase change material (PCM), the efficiency decreases over the time drastically. To reduce this effect, the surface of the heat exchanger is enlarged by finned tubes or by tube bundles. The fins and the high number of tubes will increase the costs and reduce the specific power and capacity of the storage.

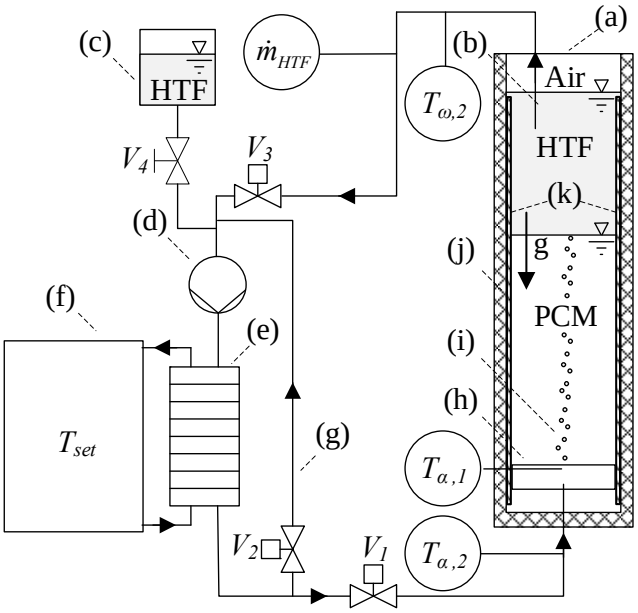

Figure 1: Flow chart of experimental set-up.

(a) Storage tank; (b) outlet extraction; (c) expansion tank; (d) pump; (e) plate heat exchanger;(f) thermostat unit; (g) by-pass; (h) nozzle plate; (i) droplet flow, ascending against the gravity; (j) insolation; (k) plate LED strips.

The heat transfer concept of direct contact in theory promises to reach high specific power and capacity without the named disadvantages. By this technology, a heat transfer fluid (HTF) that is not soluble with the PCM flows directly through the liquid PCM as a swarm of droplets, see Figure **1** (i). Even the complete PCM is solidified a flow of the HTF is due to channels in the solidified matrix still possible.

The presented research work investigates the dominant heat transport mechanisms in a latent direct contact storage. The aim of this research is the mathematical description of the thermal performance curve via the degree of solidification as well as the identification of design guidelines in order to adapt the performance curve to the process requirements during design. Experimental investigations are carried out on a 12 l storage tank in the laboratory and numerical investigations in 2- and 3-dimensional space.

The results of a series of preliminary tests with one nozzle and the material combination H2O - thermal oil are presented. The performance curves during solidifying and melting are discussed on the basis of dimensionless key figures and image recordings of phase change process with regard to the identification of the dominant heat transport process. In the field of numerical investigations, the models and initial results of a sensitivity analysis are presented and discussed.

EXPERIMENT

The test rig shown in Figure 1 is used for the experimental investigation. The storage tank is optically accessible through an insulating glass pane. This enables the solidification and melting processes to be observed. From the observations, explanatory approaches for the course of heat transfer performance can be derived.

Seven preliminary tests will be carried out, whereby the nozzle Reynolds number ranges from 600 to 6000 and the thermal power from 250 to 2500 W. Orifices with a diameter of 2 and 5 mm are used as nozzle.

EXPERIMENTAL RESULTS

The courses of the measured temperatures and calculated powers are evaluated dimensionless. The evaluation shows that there is obviously a critical charge level of the storage as a function of the nozzle Reynolds number. Up to this critical charge level, the power decreases linearly. From the critical charge level onwards, the transmitted power decreases drastically. The optical documentation allows to identify the critical charge state as the state in which the dominant heat transfer mechanism changes from liquid-liquid to liquid-solid. This information is important for the definition of the suitability for further nozzle arrangements.

NUMERICAL MODEL

The numerical investigations are performed in ANSYS Fluent. The Volume of Fluid approach is chosen for the illustration of the multiphase flow. The aim of the simulation on one hand is to be able to map the influences of fluidic installations and on the other hand to map parameters of the material pairings on the system behaviour. In 2-dimensional space, the influences of internals on the multiphase flow are investigated. In 3-dimensional space, the influence of the material pairing and the temperature stroke on the solidification and melting process is mapped.

NUMERICAL RESULTS

The simulations of multi-phase flows require very fine network resolutions and short time steps, as a result of which high computing power is required. Even if the calculations are carried out on the Vienna Scientific Cluster (VSC-3), the dimensions of the laboratory storage device are too large as a reference for the simulation. The results of the solidification of a single droplet are shown and the sensitivity to network resolution and time step is discussed.

CONCLUSION

The evaluation methodology was confirmed as suitable in the preliminary test series. To optimize the documentation, an optically fully accessible and higher storage device is built. The influence of the number of nozzles and the fluid-dynamic cross-sectional load on the position of the critical charge level is to be determined at this accumulator.

The modelling for the simulations has been completed and the first parameter studies can be carried out. These can only be evaluated qualitatively and not quantitatively until the results have been validated. For validation, a suitable compromise between the size of the domain and that of the storage tank must be found.

THE USE OF FLY ASH FOR THE SYNTHESIS OF INSULATING MATERIALS

Elżbieta Jószczuk, Piotr Zabierowski, Paweł Baran, Katarzyna Zarębska

AGH University of Science and Technology, Cracow, Poland
zarebska@agh.edu.pl

INTRODUCTION

Power generation in Poland is mainly based on coal and lignite as fuels. Consequently the power generation sector has become a major source of waste production. Extensive efforts are made to reuse fly ash as much as possible. The research is a new proposal for waste management of fly ash from the energetical sector in Poland. The main target in this study was to obtain insulating material based on fly ash with a perlite addition. The refractory of the obtained material and its thermal conduction coefficient were examined.

EXPERIMENTS / FUNDAMENTAL OF THE PROBLEM / EXAMINATIONS

The main target of this research was to obtain a material with good thermal insulation properties. As regards to the research part, certain amounts of fly ash, perlite, sodium water glass and NaOH were used to synthesis the material. All the ingredients were mixed into a smooth, homogeneous mass using a magnetic stirrer. The obtained mixture was transferred to a form, which was made in accordance with PN-EN 196-1 (Picture 1) and heated for 24 hours at 60°C. Then the sample was seasoned for 60 days. After this time, the insulating and refractory properties of the obtained material were examined. The study included examining its thermal conduction coefficient and refractory.

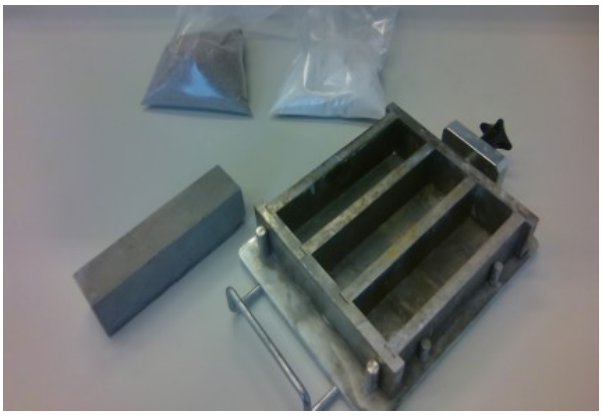

Picture 1: Form for synthesis

RESULTS AND DISCUSSION

The insulation and refractory properties of the obtained material were tested. The synthesized material is characterized by thermal conduction coefficient of 0,107 W/(m·K), which is a good result compared to commercially used materials. The examination of refractory, which is 115 sP means that the material is fireproof up to 1150°C. Analysing literature, materials are classified as fireproof if they do not deform up to 1580°C [2].

Picture 2: Obtained material

Thermal conduction coefficient	Refractory
0,107 W/(m·K)	115 sP

Table 1: Results of the study: value of thermal conduction coefficient and refractory

CONCLUSION

The research has shown that the obtained material is characterized by good thermal insulation properties and slightly worse refractory properties. In the future compressive strength examination should be carried out. However literature reports that geopolymers synthesized from fly ash have a high compressive strength value [1]. With such a low thermal conduction coefficient and probable high compressive strength, the obtained material may be an alternative insulation and construction material for commonly used products.

REFERENCES

[1] Baran P., Zarębska K., Kanciruk A., Nazarko M., Obal M., Effect of synthesis parameters on the compressive strength of geopolymers obtained from fly ashes. Przemysł Chemiczny, nr 96, 2017, 19–23

[2] Szczerba J., Klasyfikacja materiałów ogniotrwałych według zunifikowanych norm europejskich. Materiały ceramiczne, nr 1, 6–16, 2006

THE USE OF THE HYDROTHERMAL METHOD FOR SORBENTS SYNTHESIS

Agata Popiela, Natalia Czuma*, Paweł Baran, Katarzyna Zarębska

AGH University of Science and Technology, Cracow, Poland
*nczuma@agh.edu.pl

INTRODUCTION

The energy industry in the world is still mainly based on fossil fuels. Due to the growing awareness of society and the interest in environmental protection, it is gradually moving away from it and new waste recycling methods are being sought. The source of waste is, among others, combustion by-products generated during the operation of power facilities that burn a variety of solid fuels. The global production of fly ash exceeds 500 million ton/year. However, only 15% are reused. Thanks to the in-depth knowledge of the physicochemical properties of fly ashes and the ability to use their specific features, their use has increased. New products began to be developed, in which fly ash is the main ingredient. The fly ash in its structure has a significant content of silicon and aluminum, thanks to which it is a good substrate for the synthesis of zeolites. Due to its huge diversity, there is no universal method of converting them into zeolitic material[1,2]. The aim of the thesis was to select the optimal parameters in the hydrothermal method of zeolite synthesis, in order to obtain the zeolite material with the highest possible efficiency.

EXPERIMENTS

The hydrothermal method is one of the best known methods of zeolite synthesis. It is a complex physicochemical process, taking place in the liquid phase, in an alkaline environment. The process involves solid substances (amorphous and crystalline). The temperature range in which the synthesis is carried out is 80-200 °C. Application of too high temperatures can lead to damage to zeolite structures. The most important parameters for the synthesis of zeolites are: temperature, time and pressure. The process can take place in two variants: under increased pressure in the autoclave and under atmospheric pressure. Both stages differ only in the value of the pressure over the reacting slurry. It is usually one-step process **(Picture 1)**[1].

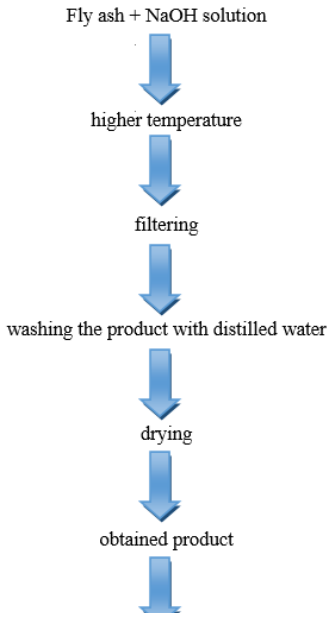

Picture 1: Scheme of hydrothermal synthesis of zeolites from fly ash [1]

RESULTS AND DISCUSSION

After the test, the obtained sample was analyzed by X-ray diffraction at room temperature. Based on the obtained spectra, it was possible to identify the resulting zeolite form.

The XRD diffraction pattern before synthesis (**Chart 1**) , shows the presence of basic constituents in the studied fly ash.. They are: quartz, mullite and calcium carbonate.

On the diffractogram of fly ash after synthesis (**Chart 2**), characteristic reflections for sodalite can be observed. It means that the proposed method of conducting the synthesis process was correct. No other zeolite forms were found in the tested material. Characteristic reflections from quartz and mullite are still present. The intensity of reflections from quartz decreased. No reflections from calcium carbonate were observed.

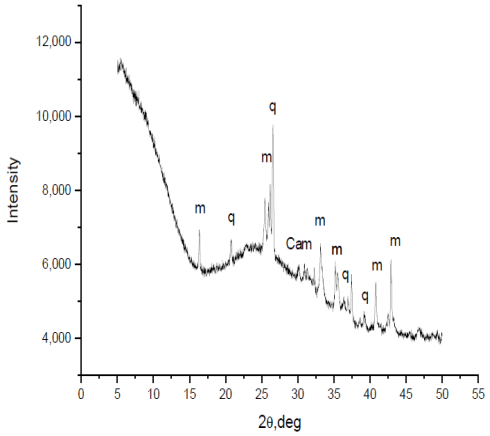

Chart 1: XRD diffractogram of fly ash from coal combustion in EDF power plant before the synthesis, where: m-mullite, q-quartz, Ca-calcium carbonate

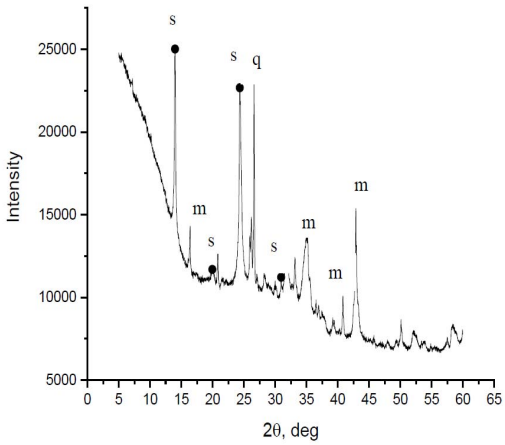

Chart 2: The fly ash diffractogram after hydrothermal synthesis, where: s-sodalite, m-mullit, q-quartz

CONCLUSION

After the hydrothermal synthesis, the product was identified by X-ray diffraction (XRD). This made it possible to confirm the presence of zeolite with a crystalline structure. The obtained zeolite is sodalite. It is built of cuboctahedrons, connected with each other by square walls. There are 24 silicon or aluminum ions in each of the cuboctahedron that combine with the oxygen anions at the endings. Its structure includes 8 hexagonal and 6 square front faces[3].

Its chemical formula is: $Na_8[Cl_2(AlSiO_4)_6]$[4]

The hydrothermal method is the most common method of fly ash zeolite synthesis. The process takes place in a liquid environment, thanks to which synthesis is easy to perform. It is less energy-intensive compared to other methods. Also from an economic point of view, this method is relatively low cost. For this reason, it is possible to obtain zeolites on an industrial scale. The disadvantage of the hydrothermal method is the formation of highly alkaline wastewater, which must be disposed of later. It also occurs with lower efficiency compared to, for example, the fusion method.

REFERENCES

[1] Czuma N., Baran P., Franus W., Zabierowski P., Zarębska K.., Synthesis of zeolites from fly ash with the use of modified two-step hydrothermal method and preliminary SO_2 sorption tests, Adsorption Science & Technology, 37, 1–2, 61-76 (2019)
[2] Czuma N., Zarębska K., Baran P., Additives for the hydrothermal fly ash zeolites synthesis, SGEM 2016, Vienna, Austria, (2016)
[3] http://www.zeo4.info/zeolity-budowa-podzial-i-charakterystyka/
[4] http://www.webmineral.com/data/Sodalite.shtml#.XIQEcihKhPY

SYNTHESIS OF NOVEL ALLOY CLUSTERS USING LIGAND EXCHANGE REACTION

Ibuki Kobayashi,[a] Sayaka Hashimoto,[b] Sakiat Hossain,[a] Yuchi Negishi,[a,b]

[a] Graduate School of Science, Tokyo University of Science, Tokyo, Japan
[b] Tokyo University of Science, Tokyo, Japan

INTRODUCTION

Thiolate protected gold clusters ($Au_n(SR)_m$) exhibit high stability against degradation and show various size-specific function unlike bulk gold. In these gold clusters, gold 25-atom clusters research has been most-actively conducted (Figure 1). Other group reported that when gold 25 clusters ($Au_{25}(SC_2H_4Ph)_{18}$) and *tert*-butylbenzenthiol ($HSPh^tBu$) are reacted, the different core size cluster (gold 28 clusters) could be synthesized.[1] These gold 28 clusters are known that it's formed by the fusion of icosahedron cores which gold 25 clusters have (Figure 2). Also, research in alloy clusters has recently become hot topic. Alloy clusters ($Au_{24}M(SR)_{18}$) exhibit functionalities unlike those of single metal clusters (Figure 3). In this research, we applied this reaction to alloy clusters which exhibit functionalities unlike those of single metal clusters.[2] We used Pd doped alloy cluster to synthesis new alloy clusters.

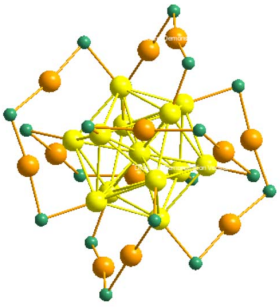

Figure 1. $Au_{25}(SR)_{18}$

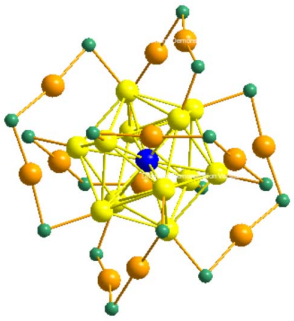

Figure 3. $Au_{24}M(SR)_{18}$

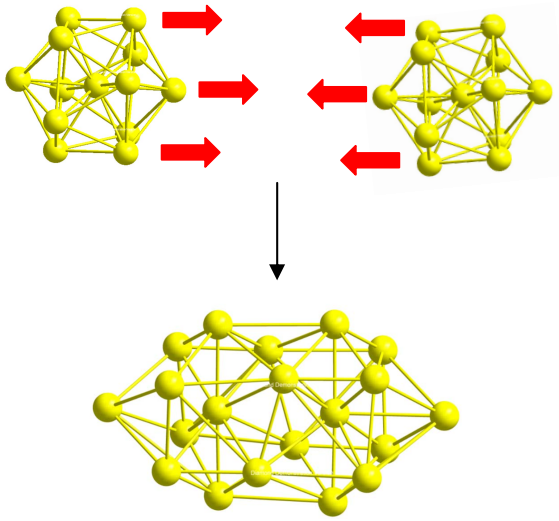

Figure 2. Fusion of icosahedron cores

EXPERIMENTS

The precursor cluster $Au_{24}Pd(SC_2H_4Ph)_{18}$ was synthesized by the method we reported in the past.[3] The $Au_{24}Pd(SC_2H_4Ph)_{18}$ was mixed with $HSPh^tBu$ in toluene at room temperature. Reaction solutions of 0 h, 2 h, 4 h, 6 h, 8 h, and 16 h were collected and the product was evaluated using reverse phase high performance liquid chromatography (RP-HPLC).[4] In addition, reaction products at each time were evaluated by ultraviolet-visible absorption spectroscopy and electrospray ionization mass spectrometry (ESI-MS).

RESULTS AND DISCUSSION

Figure 4 shows the UV chromatogram of the product at each reaction time. Multiple peaks appear in each UV chromatogram. As time passes, the retention times are getting longer than those of $Au_{24}(SC_2H_4Ph)_{18}$ which is a precursor cluster. Since SPh^tBu is less polar than SC_2H_4, it is interpreted that such a peak shift occurred with ligand exchange. Figure 5(a) and 5(b) show ultraviolet-visible absorption spectra of clusters before reaction (0 h) and after 16 h reaction, respectively. The absorption spectrum of the cluster after 16 h reaction is largely different from that

before the reaction. These results strongly suggest that a new metal cluster was formed by the ligand exchange reaction. Indeed, several peaks attributed to clusters of chemical composition which are not reported in the past ware observed in the ESI mass spectrum of the cluster after 16 h reaction. (Figure 6)

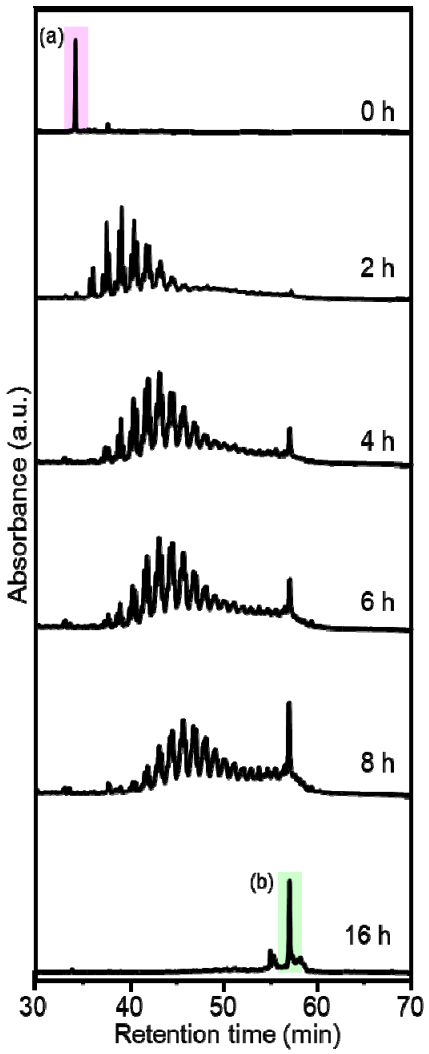

Figure 4. The UV chromatogram of the cluster of each reaction time

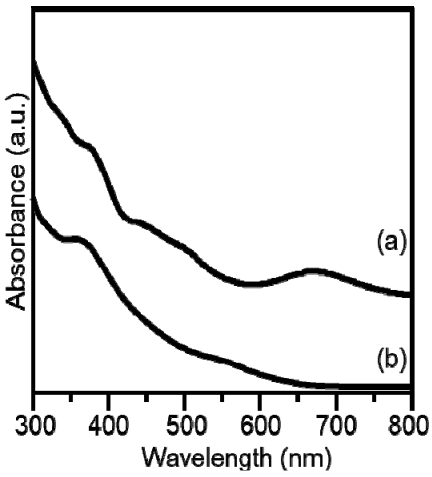

Figure 5. Ultraviolet-visible absorption spectrum of cluster (a) before reaction (0 h) (b) after 16 h reaction

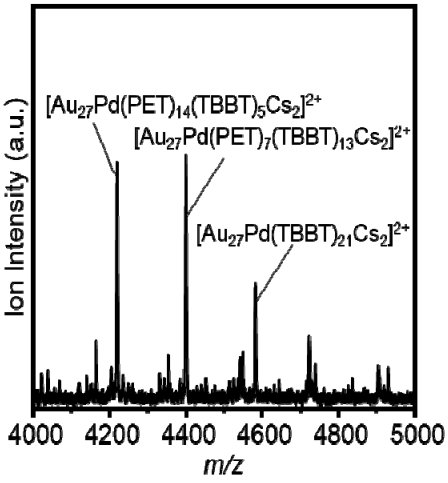

Figure 6. ESI mass spectra of clusters after 16 h reaction

CONCLUSION

This work implied that we succeeded in synthesizing a new alloy cluster. In future, we will work on isolation and single crystal X-ray structural analysis in order to determine the geometry of new alloy clusters.

REFERENCES

[1] R. Jin *et al.*, *J. Am. Chem. Soc.*, 135, 10011−10013 , 2013.

[2] Y. Negishi *et al., Phys. Chem. Chem. Phys.*,12, 6219−6225, 2010

[3] Y. Negishi *et al., Nanoscale,* 6, 7889−7896, 2014,

[4] Y. Negishi, *et al.*, *J. Phys. Chem. C*, 120, 25861−25869, 2016,

INFLUENCE OF TANTALUM ON THE PHASE STABILITY AND MECHANICAL PROPERTIES OF WB_2 THIN FILMS

C. Fuger[a], V. Moraes[a,b], R. Hahn[a], M. Arndt[c], H. Bolvardi[c], P. Polcik[d], P.H. Mayrhofer[a,b], and H. Riedl[a,b]

[a] CDL-AOS at the Institute of Materials Science and Technology, TU Wien, Austria

[b] Institute of Materials Science and Technology, TU Wien, Austria

[c] Oerlikon Balzers, Oerlikon Surface Solutions AG, Liechtenstein

[d] Plansee Composite Materials GmbH, Germany

Future tasks in many different fields of academia and industry are directed towards environmental sustainability, asking also for new advance in the field of protective coatings. Especially, transition metal diboride based films exhibit a great potential to be applied in various applications because of their excellent thermal and chemical stability, high hardness as well as electrical conductivity. Latest studies on diborides showed that this material class prefers to crystallize in two related hexagonal crystal structures: α-AlB2 or ω-W2B5-x prototype, respectively. In a previous ab initio study, we proposed single phased α-W1-xTaxB2 as a material system where the addition of Ta promises to only slightly decrease the excellent mechanical properties (e.g. ductile behavior of α-WB_2) by simultaneously increasing its phase stability.

For an experimental validation of these predictions, we deposited the full compositional range of $W_{1-x}Ta_xB_2$ thin films using magnetron sputtering. On behalf of structural investigations, we could confirm that single phased structured α-$W_{1-x}Ta_xB_2$ thin films are formed up to Ta contents of 26 at.%. These films were investigated by nanoindentation and in-situ micromechanical bending tests to evaluate the mechanical properties. As depicted in Figure 1 $W_{1-x}Ta_xB_2$ thin films outperform well-known systems in terms of fracture tolerance [1].

Based on our results, we can conclude that the experimental investigations are in excellent agreement to the theoretical predictions and the fracture toughness decreases with increasing Ta content only from 3.7 to 3.0 MPa√m.

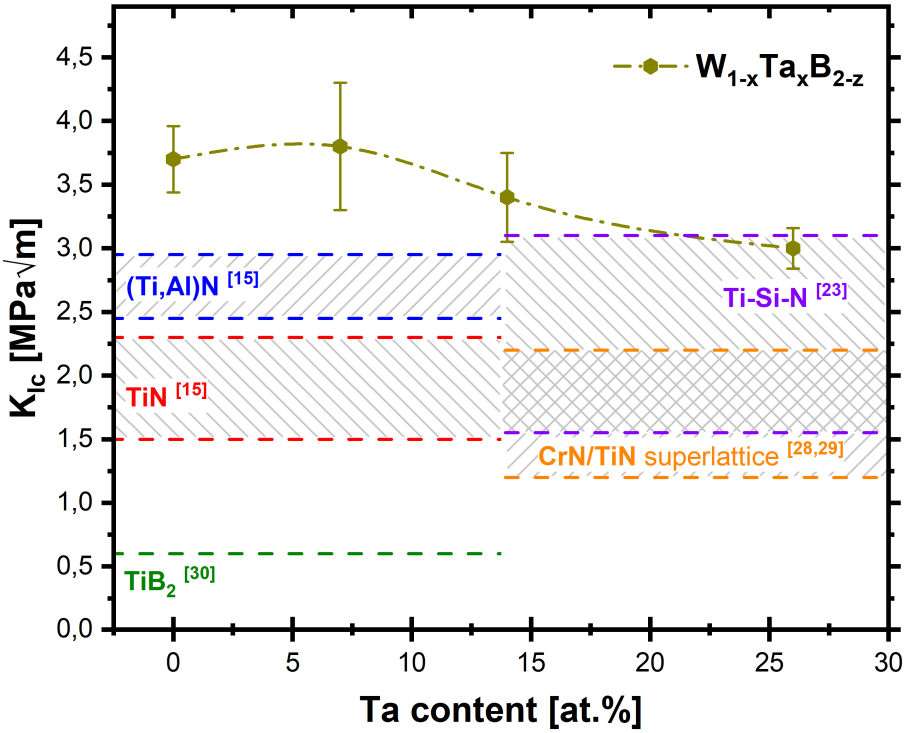

Figure 1: Critical stress intensity factor (K_{IC}) values determined by micromechanical bending tests of microscopic cantilevers, produced from the coatings. The tests were carried out with the following samples: $WB_{1.78}$, $W_{0.93}Ta_{0.07}B_{1.76}$, $W_{0.86}Ta_{0.14}B_{1.83}$ and $W_{0.74}Ta_{0.26}B_{1.87}$. Literature values of (Ti,Al)N, CrN/TiN, Ti-Si-N, TiN and TiB_2 are indicated by the blue, orange, purple, red and green areas and lines, respectively.

REFERENCES

[1] Fuger, Christoph, Vincent Moraes, Rainer Hahn, Hamid Bolvardi, Peter Polcik, Helmut Riedl, and Paul Heinz Mayrhofer. n.d. “Influence of Tantalum on Phase Stability and Mechanical Properties of WB2.” MRS Communications, 1–6. Accessed March 15, 2019.

FRACTURE PARAMETERS OF ALKALI-ACTIVATED MATRIX BASED COMPOSITES

Hana Šimonová[a, b], Bojan Poletanović[a], Ildikó Merta[a]

[a]E207-01 − Institute of Material Technology, Building Physics and Building Ecology, Research Unit Building Materials and Technology
[b]Brno University of Technology, Faculty of Civil Engineering, Institute of Structural Mechanics, Brno, Czech Republic

INTRODUCTION

Although cement based composites are the most commonly used quasi-brittle structural materials in the building industry in the world, the environmental aspects related with their production and using of cement are increasingly being discussed. Their manufacturing process significantly contributes to the global emissions of CO_2[1]. Therefore, there has been an increasing effort to develop and use some alternative binders instead of ordinary Portland cement (OPC) during the recent decades. The alkali-activated aluminosilicate materials (AAMs) are one representatives of such type of binders. These binders are created through mixing of some non- or poorly-crystalline aluminosilicate based materials, such as blast furnace slag or fly ash, with an alkaline activator (hydroxides, carbonates or the most preferably silicates) and water [2, 3].

Like OPC based composites, AAMs also belong to quasi-brittle materials with a low energy absorption capacity under tensile load. Different types of steel or synthetic fibres can be used to overcome this problem. However, the environmentally guided requirements force to use sustainable alternatives to steel and synthetic fibres. Natural plant fibres (e.g. hemp, flax) which grown locally ensure a renewable, and relatively cheap alternatives [4].

Knowledge of mechanical fracture parameters of composites based on brittle matrixes is essential for both the quantification of their resistance against crack initiation and propagation as well as for the definition of material models used to simulate the quasi-brittle behaviour of the structures or their components made from this type of composite materials.

EXPERIMENTS / METHODS

An extensive research work aimed to investigate the effect of different fly ash and slag types, their dosage and the dosage of hemp fibres within the matrix on the durability, mechanical and fracture parameters of alkali-activated mortars was performed. In this contribution, the fracture parameters of one selected alkali-activated fly ash mortar (AAFAM) with 1 vol% of hemp fibres are presented and compared with reference AAFAM without fibres. The locally available fly ash from power plant in Serbia was used to produce AAFAM specimens. Sodium silicate solution (Na_2SiO_3) with a modulus of n = 1.91 was chosen as an alkali activator (AA). The AA solution concentration was 10% of Na_2O in respect to the dry fly ash weight. Mortar specimens were prepared using river sand with maximum grain size of 8 mm. The hemp fibres (Cannabis Sativa L) cultivated and processed in Hungary were used, the fibres length was approximately 10 mm.

The standard prismatic mortar specimens with nominal dimensions 40 × 40 × 160 mm were produced and provided with an initial central edge notch before testing and subsequently subjected to the fracture tests in the three-point bending configuration. The nominal depth of notch was about 1/3 of the specimen height and span length was set to 120 mm. The test procedure requires a constant increment of displacement which was set to 0.02 mm/min during the loading test.

The displacement was continuously recorded using the inductive sensor connected to the data logger during the loading test. In this way, the diagram of loading force F in relation to the displacement d (deflection in the middle of the span length) during the fracture test was recorded.

After the appropriate processing of measured diagrams, at first the initial parts of F–d diagrams were used to estimate the modulus of elasticity E values. Afterwards, the effective crack elongation and effective fracture toughness K_{Ice} values were determined using the Effective Crack Model[5]. The work of fracture and the consequent specific fracture energy G_F values were obtained from the whole F–d diagrams according to the RILEM method[6].

RESULTS / CONCLUSIONS

Results in the form of arithmetic mean (coefficient of variations) from three independent measurements of the specimens measured bulk density ρ, compressive strength f_c, flexural strength f_f, and mechanical fracture parameters obtained from recorded F–d diagrams are shown in Table 1.

Table 1 Selected mechanical fracture parameters of AAFAM specimens

Parameter / Mixture	ρ (kg/m^3)	f_c (MPa)	f_f (MPa)	E (GPa)	K_{Ice} (MPa·m$^{1/2}$)	G_F (J/m^2)
AAFAM_REF	1850 (3.6)	30.7 (5.9)	4.3 (7.4)	16.0 (4.9)	0.554 (6.3)	43.5 (22.9)
AAFAM_1.0	1860 (2.0)	27.6 (5.1)	4.0 (8.5)	11.9 (7.8)	0.616 (7.7)	158.5 (8.2)

From the presented experimental research results the following conclusions can be drawn:

- The compressive and flexural strength of AAFAM decreased up to 10 % with the addition of hemp fibres;
- The modulus of elasticity decreased about 25% with the addition of hemp fibres;
- On the contrary, the fracture parameters increased up to 10% with addition of hemp fibres in the case of effective fracture toughness and about 265% in the case of specific fracture energy.

The addition of fibres into alkali-activated matrix should lead to reduced cracking tendency and improved tensile properties of these materials. It seems that the obtained results comply with these assumptions − fracture parameter values increased with the addition of hemp fibres. On the other hand, it is necessary to perform more tests or determine other parameters to affirm these results. One of the issue is also the degradation of natural fibres in alkaline environment, therefore it is important to monitored fracture behaviour during the materials ageing.

ACKNOWLEDGEMENT

This outcome has been achieved under the research mobility at TU Wien within the project CZ.02.2.69/0.0/0.0/16_027/0008371. The support of project No. 8J18AT009 and project No. 18-12289Y is gratefully acknowledged.

REFERENCES

[1] Aïtcin P C, Mindess S 2011 Sustainability of concrete (New York: Spon Press)

[2] Provis J L and van Deventer J S (eds) 2014 Alkali activated materials: state-of-the-art report, RILEM TC 224-AAM (Dordrecht: Springer)

[3] Shi C, Krivenko P V, Roy D 2006 Alkali-activated cements and concretes (London: Taylor & Francis)

[4] Zhou X, Kastiukas G 2017 Frontiers in Building Environment **3** pp 1–9

[5] Karihaloo B L 1995 Fracture Mechanics and Structural Concrete (New York: Longman Scientific & Technical)

[6] RILEM TC-50 FMC Recommendation 1985 Materials & Structures **18** pp 285–290

MODIFICATION OF THE LABORATORY EQUIPMENT USED TO ASSESS THE SPONTANEOUS COMBUSTION SUSCEPTIBILITY OF COAL

Agnieszka Kuźmik, Katarzyna Czerw*, Katarzyna Zarębska, Paweł Baran

AGH University of Science and Technology, Faculty of Energy and Fuels, Aleja Mickiewicza 30, 30-059 Krakow, Poland
* kczerw@agh.edu.pl

INTRODUCTION

The self-heating process and, as a consequence, the spontaneous combustion of coal is associated with the sorption of oxygen on the surface of grains, in the porous structure of the carbonaceous matter. If the heat generated during the process is not sufficiently discharged outwards, ignition occurs. Endogenous fires in the coal mines, caused by this phenomenon, have a negative impact on the natural environment, as well as on the mining industry, raising the cost of fire prevention and coal extraction. Nowadays, in order to assess the spontaneous combustion susceptibility of coal, fully automated methods and instrumental techniques are used. First of all they allow to determine the self-heating rate, the amount of heat generated, and to estimate the concentration and composition of gases emitted during the oxidation. The presented research focuses on Örsat gas analyzer (Fig.1.) which was patented in 19th century but still is considered a reliable measurement method non inferior to modern techniques. The analyzer is based on the selective absorption of individual gas component especially CO_2, O_2 and CO in the adsorption pipettes containing appropriate solutions[1]. Coal samples from Sobieski, Brzeszcze and Pniowek coal mines with the grain size 0.1-0.7 mm were used in the analysis. In order to obtain post-reaction gases, the coal samples were submitted to low-temperature oxidation with a hydrogen peroxide solution, as in reported method [2].

EXPERIMENTS

The difference between the most commonly used Örsat gas analyzer and the apparatus described in this research was the method of sample delivery. Thus, in order to test the reaction gasses obtained after the oxidation of coal, a reactor in form of a beaker with rubber cork was added to apparatus and then attached to the burette. 3 grams of coal was placed in beaker, next the 1 cm^3 of distilled water and 9 cm^3 of 20% hydrogen peroxide solution was added. A thermometer was placed in the reactor via a fitted slot and the burette was filled to approximately 100 cm^3 with saturated NaCl solution. During the reaction, the temperature on the thermometer was read every five minutes, and the evolution time of post-reaction gases was also noted. When the reaction was over, the sample of gas was pushed to the first absorption bulb filled with potassium hydroxide solution to absorb CO_2. The bottle filled with NaCl solution was brought down so that the

Figure 1: Örsat gas analyzer used during the research

gas was rushed to the burette and the volume increase of liquid in burette was measured.

RESULTS AND DISSCUSION

Coal sample	Content of element C [%]	Moisture content [%]	Volume of post-reaction gas [cm^3]	Concentration of CO_2 in gas [%]
Sobieski	66.85	6.13	11	1.76
Brzeszcze	77.53	2.3	0	0
Pniowek	81.17	0.68	0	0

Table 1. Basic specification of coal samples and the results obtained after using Örsat analyzer

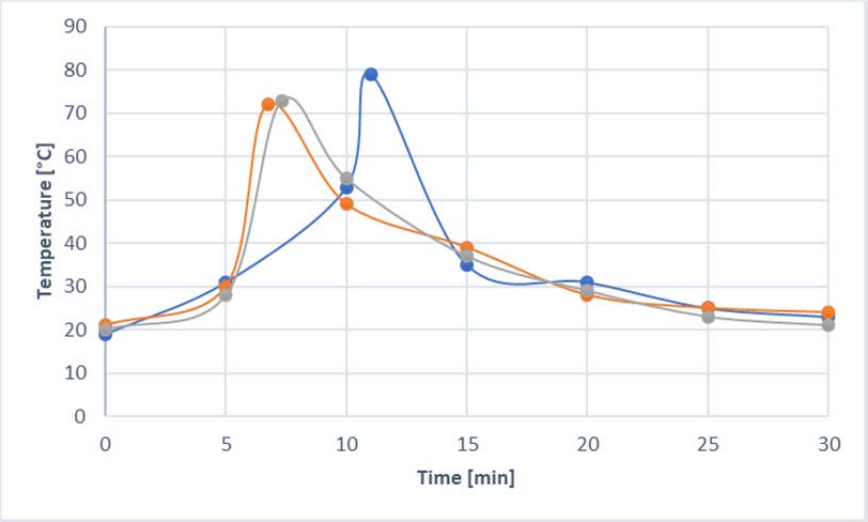

Figure 2: The rate of temperature change for samples from the Sobieski coal mine

Due to the use of the Lasoń method, the tendency of the coals to spontaneous combustion was determined[2]. Figure 2 shows a rapid increase in temperature in the Sobieski coal and perhydroxic acid system (reaching almost 80°C). Also in the case of coal from the Sobieski mine, the gas bubbles evolved in the beaker from the very first moment of measurement. However, the collection of reaction gases to the burette was observed for a very short time, which was related to the rapid decomposition of hydrogen peroxide. The concentration of carbon dioxide in the gas was significant. Neither for coal from the Brzeszcze mine nor for the coal from the Pniowek mine, no signs of the reaction of carbon with hydrogen peroxide were observed, including a lack of the emergence of post-reaction gases (Table 1.) and constant temperature in the rector.

CONCLUSIONS

The results obtained suggest that coal from the Sobieski mine shows a significant tendency to self-ignition. However, the Brzeszcze and Pniowek coals did not show a similar susceptibility as a temperature during the measurement remained constant and no gas was emitted. The Örsat analyzer presented in the research is relatively easy to use and can be successfully used as a replacement for automatic apparatus.

REFERENCES

[1] Cygankiewicz J., *Prognozowanie procesu samozapalania węgla w podziemiach kopalń,* Główny Instytut Górnictwa, Katowice (2018)

[2] Brzóska K., Ceglarska-Stefańska G., Małysa E., Marecka A., Orzechowska-Zięba A., *Wybrane zagadnienia z fizykochemii węgla kamiennego,* Wydawnictwo AGH, Kraków (2003)

COMPARISON OF DATA MODELLING POSSIBILITIES IN HYBRID MODELS

Stefanie Winkler

E101 - Institute of Analysis and Scientific Computing

MOTIVATION AND INTRODUCTION

The accumulation of data in various applications, platforms and software enforces researchers to look for powerful methods to process big data structures which makes data modelling one of the leading research areas. Despite this trend there are several research fields where system behaviour is still described using physical laws and mathematical formulations. Psichogios and Ungar [1] give an example of a possible combination of both approaches. Complex structures often require different methods and models, e.g. a mixture of discrete and continuous descriptions called hybrid models. Considering a model containing discrete and continuous processes where a neuronal network is used to determine these parameters. For example in automotive industry this combination was implemented to optimize a combination of different LTI systems, see Lu et al. [2]. In the following we will present the basic structure of hybrid models and neural networks and the possibilities to combine these approaches implementing a basic example.

MODELLING APPROACH

Hybrid Modelling. In modelling and simulation the term hybrid describes a certain collection of modelling approaches to describe the system behaviour. A hybrid automaton is a possible illustration of such complex behaviours consisting of different nodes symbolising various states of the system. Speaking of a hybrid dynamical system the nodes characterise the discrete or continuous system behaviour in form of ODEs, DAEs, DEVS or similar. The lines connecting these nodes define the conditions to enable transitions from one node to the other.

Neural Networks. In general neural networks are based on the biological nerve structure of human brains. The basic structure consists of three components: the input, the hidden and the output layers. The most interesting one is the hidden layer which contains a specific activation function to process the incoming signal. The weights of the edges can only be specified using training data consisting of input and corresponding output data as references.

RESULTS AND DISCUSSION

In the following the bouncing ball, an academic example of hybrid systems, is discussed. Regarding the bouncing ball the bounce itself represents the discrete part of the model and only occurs for a single point in time where the ball changes its direction and decreases its total velocity. This behaviour can be described with physical basics defining the corresponding ODE system and the state space description, respectively. The hybrid model description then consists of the state space description, the jump and the jump condition. Due to the fact that there exists an analytical solution to this problem training data for the neural network can be generated.

In the current setting the results of the neural network can be used to predict the next event of the hybrid system. Additionally the peak of the current bounce is calculated. Compared to the numerical simulation in MATLAB, where the behaviour of the system is given for every point in time, the

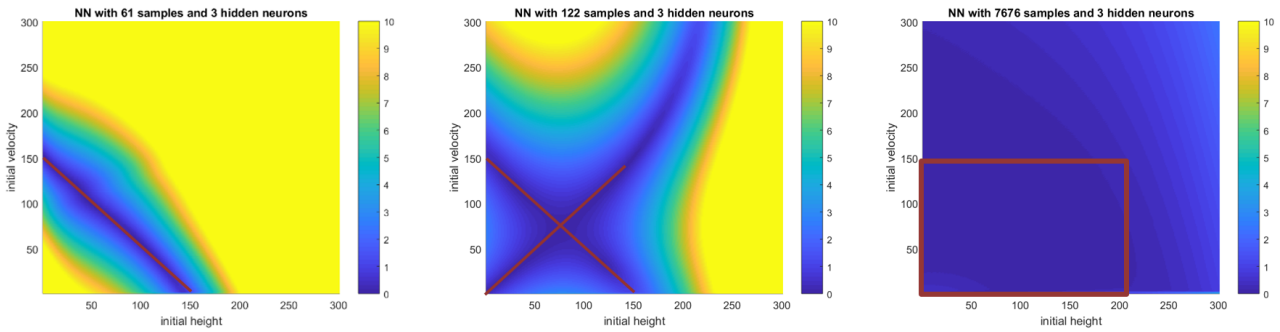

Figure 1: Depending on the number of data points in the training set the accuracy of the neural network is shown.

enabled analysis for the neural network is limited. Another possible implementation could predict only the height of the ball for the next time steps. This might be useful if such neural network would be embedded in a bigger real time system to calculate approximations to determine e.g. machine settings.

K. Hornik [3] claims that feed-forward networks are capable of arbitrarily accurate approximation to any real-valued continuous function over a compact set. Therefore it is not surprising that the accuracy of the neural network compared to the analytical solution is acceptable, as shown in Figure 1. The influence of the network structure and training set to the performance is here depicted. The results encourage the usage of neural networks for hybrid models.

OUTLOOK

This work was just a first step in answering the question if neural networks and hybrid modelling can be combined or even be used as replacement. The approach of Martinus and Lambert [4] could be useful to cope the challenging zeno effect typical for hybrid models. In order to explore the possibility to predict system behaviour, the training data has to be defined differently. Following this, the gathered knowledge will be applied to a more sophisticated example to analyse the system behaviour and provide possible answers to some of the following questions: What model structures can be replaced by neural networks? Which type of hybrid models benefit from embedded neural networks? What are the limits of this approach in hybrid modelling? The last question can never be fully answered but it is important to look for new enhancements and combinations of existing model approaches to keep pace with development and technology.

REFERENCES

[1] D. C. Psichogios and L. H. Ungar. *A Hybrid Neural Network-First Principles Approach to Process Modeling* AIChE Journal vol. 38, No. 10, pages 1499-1511, 1992.

[2] W. Lu, P. Zhu und S. Ferrari. *A Hybrid-Adaptive Dynamic Programming Approach for the Model-Free Control of Nonlinear Switched Systems.* IEEE Transactions on Automatic Control vol. 61, No. 10, pages 3203-3208, 2016.

[3] Hornik K., *Multilayer Feedforward Networks are Universal Approximators.* In: Neural Networks, vol 2, pp.359-366. 1989.

[4] Martinus G., Lampert C.H., *Extrapolation and learning equations.* 2016. arXiv preprint https://arxiv.org/abs/1610.02995.

TUNING STRUCTURE AND MECHANICAL PROPERTIES OF Ta-C COATINGS BY N-ALLOYING AND VACANCY POPULATION

T. Glechner[a,b], P.H. Mayrhofer[a], R. Hahn[a], T. Wojcik[a], D. Holec[c], S. Fritze[d], D. Primetzhofer[e], H. Bolvardi[f], S. Kolozsvári[g], H. Zaid[h], S. Kodambaka[h], and H. Riedl[a,b]

[a] Institute of Materials Science and Technology, TU Wien, Austria
[b] CDL-SEC at the Institute of Materials Science and Technology, TU Wien, Austria
[c] Department of Materials Science, Montanuniversität Leoben, Austria
[d] Department of Chemistry - Ångström Laboratory, Uppsala University, Sweden
[e] Department of Physics and Astronomy, Uppsala University, Sweden
[f] Oerlikon Balzers, Oerlikon Surface Solutions AG, Liechtenstein
[g] Plansee Composite Materials GmbH, Germany
[h] Department of Materials Science and Engineering, University of California Los Angeles, USA

Transition metal carbides and nitrides are well established in various thin film applications due to their outstanding properties including extreme hardness, chemical inertness and highest melting temperatures. They exhibit a mixture of strong ionic, covalent, and metallic bonds but their application as structural components as well as thin films is limited by their poor fracture tolerance. Therefore, enhancing their fracture toughness, while retaining other thermo-mechanical properties is desirable for increasing the use of transition metal carbides in any application.

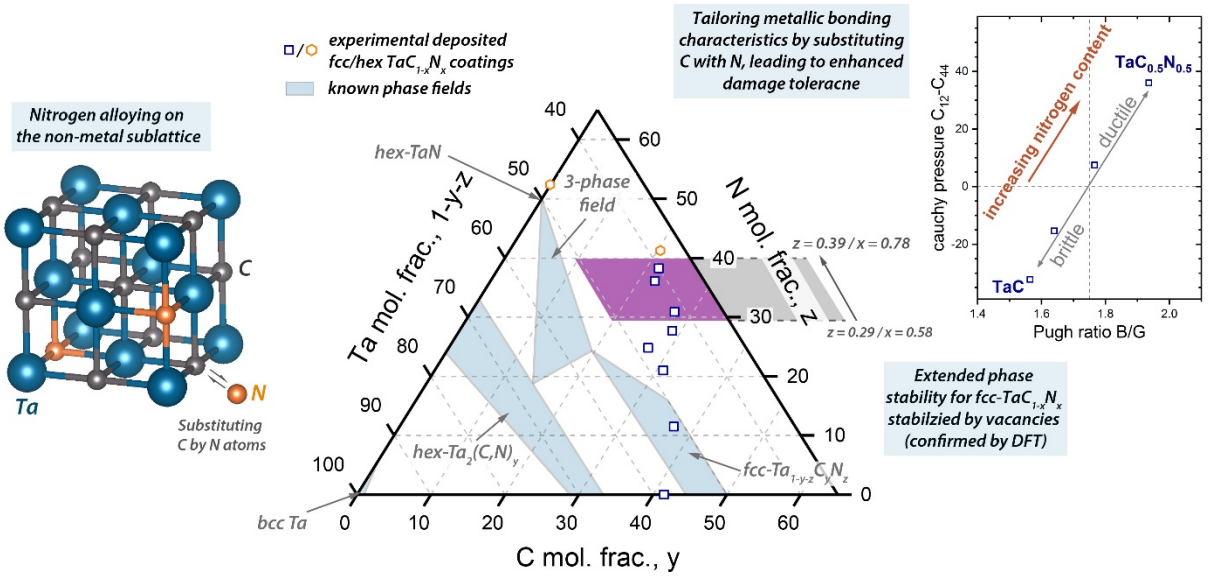

One conceptional approach is non-metal alloying, involving the exchange of C by N or vacancies on the non-metallic sublattice. Based on its high thermal stability as well as hardness Ta-C is used as a base system. Ta-C thin films were synthesized via non-reactive sputtering, while ternary Ta-C-N coatings have been deposited in N_2/Ar gas mixtures. Based on ab initio calculations, we could experimentally verify that structural defects, especially Ta vacancies, stabilize the preferred cubic structure for high N contents. We found single phase cubic structure up to a nitrogen content of about 68 % on the non-metallic sublattice. Furthermore, our DFT results predicted a softening of the films (confirmed by nanoindentation) and an increase of ductility—according to the Pugh's and Pettifor's criterion—with increasing N content. During uniaxial compression of superhard (43.3 GPa) 110-oriented $Ta_{0.47}C_{0.34}N_{0.19}$ pillars, we observed yielding at 16.9 GPa followed by plastic deformation where we identified {111} <01$\bar{1}$> as the most active slip system. From micro-

cantilever tests, we determined K_{IC} values of 2.9 compared to 1.8 MPa$\sqrt{m}$ for $Ta_{0.47}C_{0.34}N_{0.19}$ and $Ta_{0.55}C_{0.45}$ respectively, indicating that Ta-C-N exhibits indeed superior fracture tolerance compared to Ta-C.

This study gives a promising outlook on how mechanical properties can be tuned through alloying on the non-metal sublattice in transition metal carbides and nitrides based compounds.

NEW TOOLS FOR THE ON-SITE DETECTION OF WATER POLLUTANTS: ION-SELECTIVE ELECTRODES AND LATERAL FLOW DEVICES

Lisa Mayerhuber[a], Kathrin Lauter[b], Gabriele Weigelhofer[c], Sabine Baumgartner[b], Philipp Fruhmann[a]

[a]Competence Center for Electrochemical Surface Technologies (CEST), Wr. Neustadt, Austria
[b]University of Natural Resources and Life Sciences Vienna (BOKU), Center for Analytical Chemistry, Tulln, Austria
[c]University of Natural Resources and Life Sciences Vienna (BOKU), Institute of Hydrobiology and Aquatic Ecosystem Management, Vienna, Austria

INTRODUCTION

The occurrence and fate of pharmaceutical contaminants in water is a complex and important topic which is directly related to the environment and human health. A wide range of different pharmaceuticals are released in the environment, either direct or indirect. The most common way of these substances in the environment is via excretion or disposal (Fig.1). Depending on their structure and reactivity they are only slowly transformed or can even remain unchanged due to their persistence. The most common way for the quantification of different contaminants are chromatographic based methods such as GCMS and LCMS. The aim of this work was the development of ion-selective electrodes and lateral flow devices (LFDs), as economic and fast tools for the on-site determination of different pharmaceutical residues.

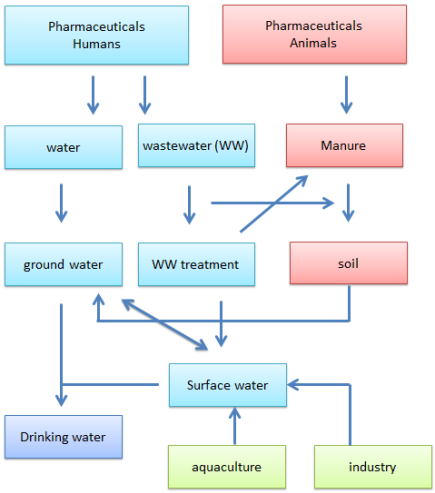

Figure 1. Distribution of pharmaceutical active compounds in water

Antipyrine and metamizole (Fig.2) were chosen as target analytes since both molecules are nitrogen containing pollutants, which makes their detection via metallacarborane complexes possible. Metamizole is an analgesic and antipyretic drug and has anti-inflammatory effects. It is a pro-drug which breaks down after oral administration to structurally related compounds like Antipyrine.

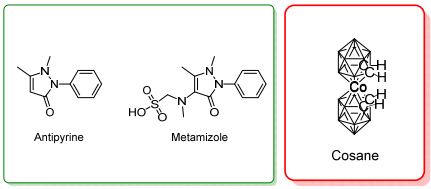

Figure 2. Target molecules (left) and cosane, which was used for the complex synthesis

BACKGROUND

The most important part of an ion selective electrode is the membrane, which is responsible for its sensitivity and selectivity. The developed and optimized membrane consists of three core parts, which are: polymer matrix, plasticizer and ionophore. The ionophore is an ion pair complex formed between analyte and carborane (Fig.2). The characterization of the electrodes was done in a classical two electrode setup using a reference electrode and the prepared working electrode (Fig.3). The performance of the ISEs were characterized by their detection limit and slope of the calibration curve.

Lateral flow devices (LFDs) are commonly used for testing concentrations of different drugs, biomarkers or other target molecules in different media and are a valuable alternative approach for

the detection of pollutants in low concentrations. The most prominent example of this technique is the standard pregnancy test, which indicates pregnancy by showing two purple lines. The huge advance of LFDs is their portability and easiness.

RESULTS AND DISCUSSION

Based on recent results in comparable experiments [1,2] a similar membrane composition was used and optimized in order to achieve a good selectivity and long-term stability. The best results were achieved with a membrane composition of 4.0 wt% ion-pair complex, 33 wt% PVC and 63 wt% plasticizer. A serial dilution of each analyte was measured, three times with each electrode, from lower to higher concentrations and the obtained values were plotted against the signal. Based on the obtained data it was possible to evaluate the limit of detection (LoD), linearity/working range, slope, stability and the reproducibility (Fig.3).

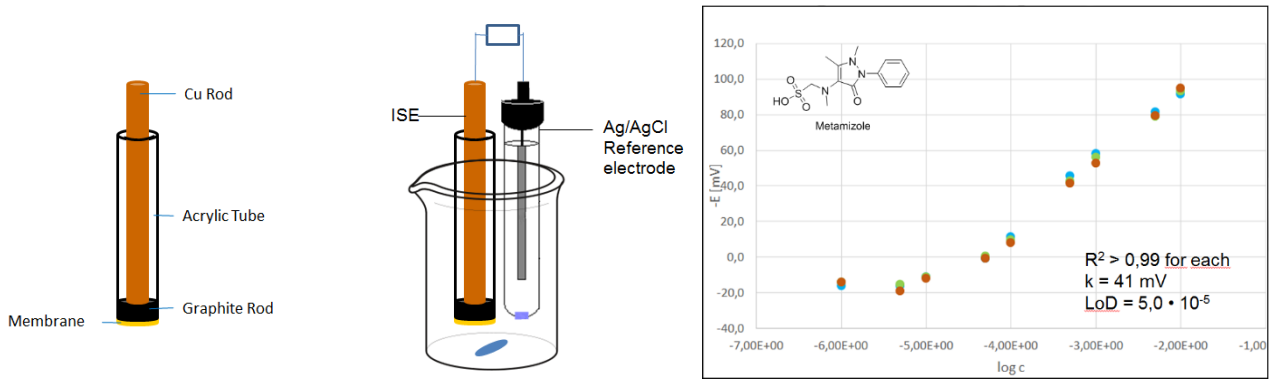

Figure 3. Experimental two electrode setup (left) and the obtained results for metamizole.

Beside the analytical parameters, the developed electrodes are robust and can be stored and re-used during a period of months. This demonstrates the capability of the developed electrodes to be used under harsh on-site conditions. Although there is still room for improvement regarding the slope, composition and linear range, it was demonstrated that it is possible to sense the target analytes with cosane based ion-pair complexes. The results further demonstrate the usability of the developed simple and cost-effective electrodes which provide a rapid response and shows a good reproducibility.

Beside the ion-selective approach, an additional focus was the development of a lateral flow device for metamizole, in order to provide a complementary system for the detection of the proposed target analytes. First results are really promising and will be presented in detail during the symposium.

OUTLOOK

Within the future, the detection limit of the electrodes should be improved in order to reach a limit of detection below 10^{-6} mol/L. Beside this, a lateral flow device with an even higher sensitivity as an alternative quantification method will be developed.

ACKNOWLEDGEMENT

The authors would like to thank the NÖ Forschungs- und Bildungsges.m.b.H. (NFB), grant agreement No. SC15-004 for funding.

REFERENCES

[1] Stoica A.-I., Vinas, C., Teixidor, F., Cobaltabisdicarbollide anion receptor for enantiomer-selective membrane electrodes, ChemComm, **2009**, 0, 4988-4990

[2] Bliem, C., Fruhmann, P., Stoica, A.-I., Kleber, C., Development and Optimization of an Ion-selective Electrode for Serotonin Detection, Electroanalysis, **2017**, 29, 1635-1642

DEVELOPMENT OF A NOVEL OPTOELECTRONIC SENSOR PLATFORM

Richard Mócsa[a], Ulrich Ramach[a], Patrik Aspermair[a,b], Anil Bozdogan[a], Philipp Fruhmann[a], Johannes Bintinger[c], Wolfgang Knoll[a,c]

[a]Competence Center of Electrochemical Surface Technologies (CEST), Wr. Neustadt, Austria
[b]Université de Lille, Lille, France
[c]Austrian Institute of Technology, Vienna, Austria (AIT)

INTRODUCTION

As of now, countless sensors have been created with various applications within the health industry, to monitor the well-being of a person and to screen for diseases. However, most of these sensors have inherent limitations such as size, cost, relatively high limits of detection and they do not provide real-time- and point-of-care measurements. An ideal biosensor would be of compact and portable design and would perform non-invasive (from saliva, urine, etc.), real-time-measurements of the biomarkers of interest in a reliable and fast manner. The following concept is one attempt, to conquer this huge challenge. In this approach, two sensor techniques (SPR and FET – optical and electronic) are combined, to complement each other.

BACKGROUND

Since its introduction in the 1990s, Surface Plasmon Resonance (SPR) has proven to be among the best technologies to investigate the specificity, affinity and binding/dissociation kinetics of macromolecules. SPR has also been commercialized and used for routine analysis in laboratories all over the world (e.g. Biacore, GE Healthcare). For detecting interactions with the SPR, no labels are required, which bypasses such problems, as steric hindrances or structural changes due to labeling.(*2*) The sensing principle is based on surface plasmons which are created on a flat metal-dielectric interface (in SPR sensors, usually gold is used as metal) upon radiation with a laser. In the Kretschmann geometry (Fig 1.), polychromatic light travels through a high refractive index prism at a specific angle, exciting plasmons on the surface of the metal, which drops the intensity of the light entering the detector. This angle is called a resonance angle. Upon a binding event on the surface the refractive index of the metal surface changes and thus also the resonance angle is modified.(*3*) Despite the many advantages of this method, SPR devices are usually very big benchtop systems, expensive (>10k €) and have an intrinsic size limitation of the analyte (> 3 kDa).

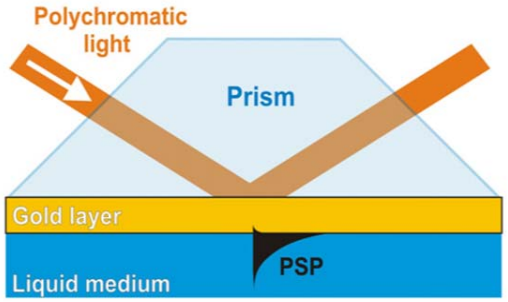

Figure 1. The excitations of PSP's in the Kretschmann geometry of an ATR method by a polychromatic light (3)

In search of solving some of the above-mentioned problems, the concept of a field-effect transistor (FET)-based biosensor has attracted a lot of attention over the last decade. A FET consists of an insulator, a semiconductor and three electrodes. The *source* and the *drain* electrodes are in direct contact with the semiconductor, while the third, the *gate*, is isolated from the semiconductor by the *insulator*. (Fig 2.) By applying a voltage between the *gate* and the *source/drain*

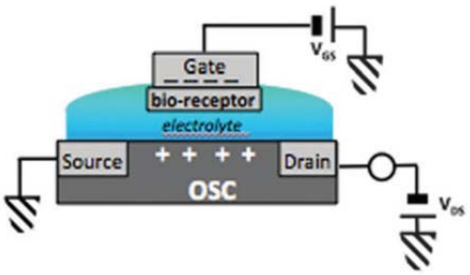

Figure 2. Schematics of an OFET. OSC designates organic semi-conductor (1)

electrodes, charges of opposite sign are induced at the semiconductor-dielectric interface. Because the charges in the semiconductor are mobile, current will flow in the channel when an additional voltage is applied between *source* and *drain*. If a biorecognition event is taking place on either the *gate* or semiconducting interface, the change in capacitance will modulate the overall source-drain current (Equation 1).(*4*) Hence, even small molecules (<200 Da) can introduce signal changes and allow for ultra-low detection. However, one of the main challenges of electronic biosensing are reproducibility and the prevention of unspecific binding events.

$$I_{DS}^{sat} = \frac{W}{2L} C_i \mu (V_{GS} - V_T)^2$$

Equation 1. The relationship between voltage and current within a FET

RESULTS AND DISCUSSION

Considering the weaknesses of both systems, the idea arose to combine optical- (SPR) and electronic (FET) sensors, to develop a novel optoelectronic biosensing platform, where both techniques could be implemented at the same time, complementing each other and negating the drawbacks of the individual approaches. We benchmark the experimental FET sensors with more established SPR tools in order to test for the scope and limitations of the new system. In our prototype a flow cell design is used, containing a gold surface which simultaneously acts as the *gate* of a FET and source of surface plasmons. In between, an electrolyte containing the analyte is used as a dielectric material, enabling ultra-low voltage operations. (Fig. 3)

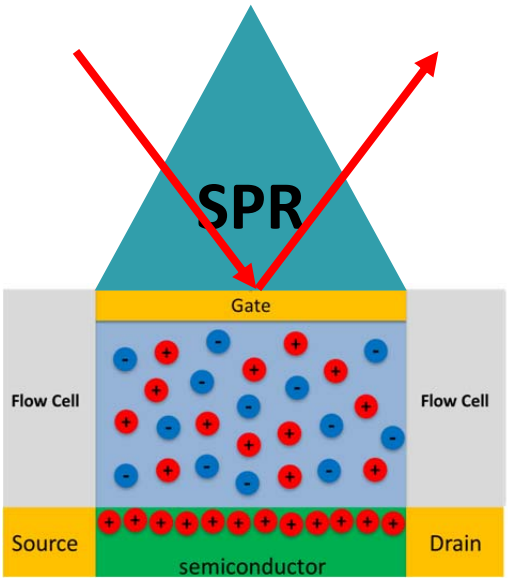

Figure 3. The scheme of the prototype set-up

In preliminary results we demonstrate the capability of the system for biotin-neutravidin as well as PNA-DNA and layer-by-layer (LBL) sensing. With our new platform we can simultaneously investigate a biosensing event from an optical and electronic point of view. One advantage of this system is the possibility to separate mass from charge, with the SPR measuring the mass of the bound analyte and with the FET measuring its charge. Currently we also use this tool for smell sensing applications. For this, odorant binding proteins (OBPs) are used as biorecognition elements for odor molecules (<200 Da).

OUTLOOK

One could also use this system e.g. for blood analysis and obtain not only the information about the quantity and quality of selected biomarkers, but also obtain information about their biological state (isoelectronic point) and pH of the solution at the same time.

REFERENCES

1. L. Torsi, M. Magliulo, K. Manoli, G. Palazzo, Organic field-effect transistor sensors: a tutorial review. *Chem Soc Rev* **42**, 8612-8628 (2013).
2. H. H. Nguyen, J. Park, S. Kang, M. Kim, Surface plasmon resonance: a versatile technique for biosensor applications. *Sensors (Basel)* **15**, 10481-10510 (2015).
3. H. Sipova, J. Homola, Surface plasmon resonance sensing of nucleic acids: a review. *Anal Chim Acta* **773**, 9-23 (2013).
4. M. Y. Mulla *et al.*, Capacitance-modulated transistor detects odorant binding protein chiral interactions. *Nat Commun* **6**, 6010 (2015).

PRODUCTION OF VERY FINE GRAINED TUNGSTEN CARBIDE POWDERS BY THE $WO_2(OH)_2$ TRANSPORT REACTION

Markus Ostermann, Roland Haubner

E164 - Institute of Chemical Technologies and Analytics, TU Wien

INTRODUCTION

The production of very fine grained WC powders is interesting for high performance hardmetal applications because of the positive effects of smaller grain sizes on properties like the hardness of hardmetals [1]. However, it is difficult to achieve nanometer grain sizes with traditional processes, which makes it interesting to develop alternatives for the production of these WC powders [2-3].

In this study, the chemical vapour transportation (CVT) reaction of WO_3 with H_2O is used to generate gaseous $WO_2(OH)_2$ [4], which directly reacts with a H_2/CH_4-gas mixture to WC. Due to the reactions in the gas phase, nano-sized WC powder can be obtained. Additionally, it would be a one-step process from WO_3 to WC in contrast to established processes. With the variation of process parameters such as furnace temperature, humidity and gas flows, their effect on the product was investigated and the process further improved.

EXPERIMENTAL

The equipment consisted of two concentric, externally heated quartz tubes. In the smaller tube WO_3-powder was placed in a quartz boat to generate $WO_2(OH)_2$ by passing humid argon. This $WO_2(OH)_2$ flowed into the big quartz tube through a small hole located at the end of the small tube. A mixture of H_2 and CH_4 was lead in the big quartz tube to directly transform the $WO_2(OH)_2$ into WC. The obtained powders were collected in the colder parts of the outer quartz tube. The products were characterized by X-ray diffraction (XRD) and transmission electron microscopy (TEM).

RESULTS AND DISCUSSION

In the SEM micrograph (Figure 1), merely agglomerates are visible due to the small crystallite sizes. To specify the crystallite sizes and microstructures TEM investigations were necessary. The grain sizes of the WC powders are in the single-digit nanometer range (about 3-7 nm) (Figure 1). Additionally thin amorphous layers are observed on the particle surfaces, which could be free carbon resulting from the methane decomposition. The electron diffraction pattern (Figure 1) corresponds to the calculated pattern of a NaCl-type (cubic) WC_{1-x} with a lattice parameter of a = 4,239 Å [3]. Weaker reflexes indicate small amounts of hexagonal WC. WC_{1-x} is considered as a metastable high temperature modification of WC, which can be stabilized at low grain sizes [3, 5].

The X-ray diffraction patterns (Figure 1) of the samples show that beside the hexagonal-WC other phases such as WC_{1-x}, W_2C and W are present. These are formed most likely due to an incomplete carburization reaction. The rare occurrence of oxidic tungsten species in the product indicates that the reduction process is faster than the carburization process.

Additionally, the influences of different process parameters on the product were investigated. Higher Ar-flowrates, higher water concentrations and higher temperatures enhance the transport of $WO_2(OH)_2$. This increases the yield of powder on one hand, while on the other hand it can result in oxidic tungsten species in the product. The situation is similar with a strong increase of the CH_4-flow, which results in free carbon in the product. Therefore, it is important to balance the process

parameters, which enhance the transport reaction, with the reducing and carburating agents H_2 and CH_4.

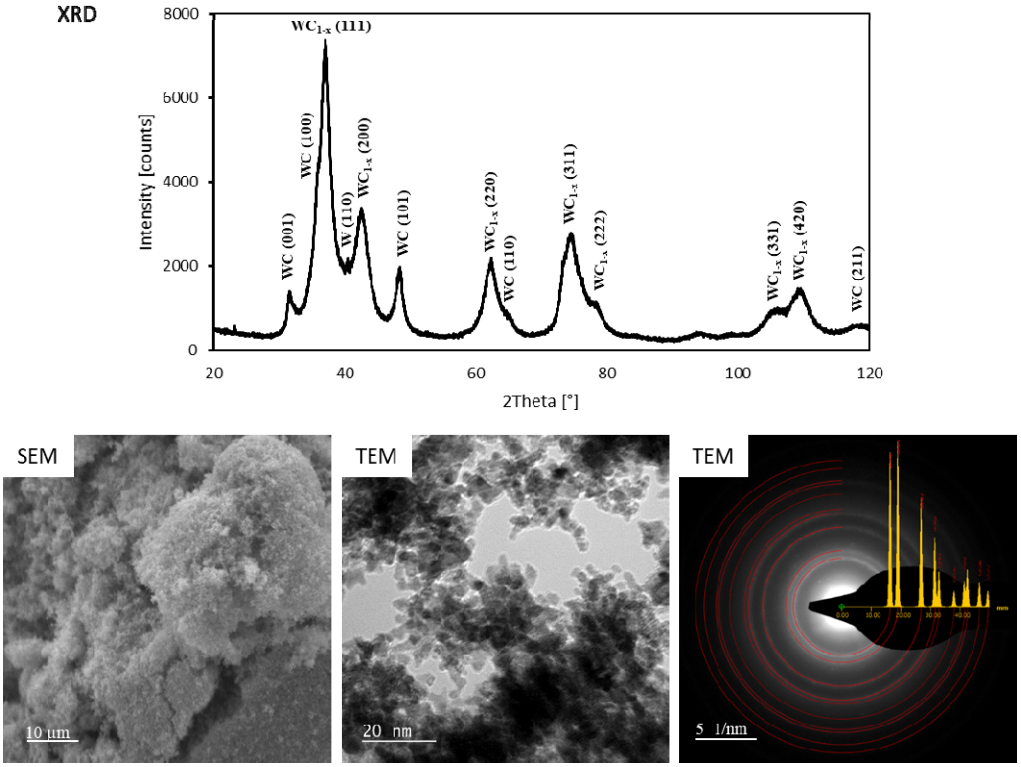

Figure 1: X-Ray diffraction pattern, SEM and TEM micrograph of a produced tungsten carbide powder, measured electron diffraction pattern of the sample with the calculated pattern of WC_{1-x}

CONCLUSION

Using this CVT-based process, the production of tungsten carbide powders with grain sizes in the single-digit nanometer range in a one-step process was achieved. As a result of the small grain sizes a high amount of cubic WC_{1-x} instead of the hexagonal WC is formed. Further characterization will be executed by Raman spectroscopy to investigate the presence of amorphous carbon. The powders could be applicated in the hardmetal section and in catalysis as an alternative to noble metal catalysts for example for the conversion of methane to synthesis gas [6].

ACKNOLEDGEMENTS

The TEM measurements were carried out using facilities at the University Service Centre for Transmission Electron Microscopy, Technische Universität Wien, Austria.

REFERENCES

[1] Schubert W.D., *Feinst- und Ultrafeinkornhartmetalle – vom Pulver zum Werkzeug*, Keramische Zeitschrift 67, 365-376, 07/2015

[2] Kim J.C. et al., *Synthesis of nanosized tungsten carbide powder by the chemical vapor condensation process*, Scripta Materialia 50, 969-972, 2004

[3] Abdullaeva Z. et al., *High temperature stable WC_{1-x}@C and TiC@C core-shell nanoparticles by pulsed plasma in liquid*, RSC Advances 3, 513-519, 2013

[4] Glemser O. et al., *Gasförmige Hydroxide IV. Über gasförmige Hydroxide des Molybdäns und Wolframs*, Z. Anorg. Allg. Chem. 316, 168-181, 1962

[5] Zavodinsky V.G., *Small tungsten carbide nanoparticles: Simulation of structure, energetics, and tensile strength*, International Journal of Refractory Metals and Hard Materials 28, 446-450, 2010

[6] Claridge J.B. et al., *New Catalysts for the Conversion of Methane to Synthesis Gas: Molybdenum and Tungsten Carbide*, Journal of Catalysis 180, 85-100, 1998

RADICAL INDUCED CATIONIC FRONTAL POLYMERIZATION OF EPOXY SYSTEM

Anh Dung Tran, Patrick Knaack, Nicolas Klikovits, Robert Liska

E163 - Institute of Applied Synthetic Chemistry-Polymer Chemistry and Technology at TU Wien

INTRODUCTION

Radical induced cationic frontal polymerization (RICFP) is an elegant technique to cure epoxy resin. Combining advantages of thermal curing (bulk curing) and photopolymerization (fast curing, low energy consumption, and long pot-life) make the RICFP beneficial in industrial applications.[1] A formulation for RICFP consists of an epoxy monomer, e.g. bisphenol-A-diglycidylether (BADGE), tetraphenyl-1,2-ethanediol (TPED) as a radical thermal initiator, and an antimonite (I-Sb) or aluminate (I-Al) based diaryl iodonium salts as a photoacid generator. The presence of the two initiators allows the RICFP to be initiated by UV light or a thermal stimulus. The so liberated acid initiates a cationic ring opening polymerization of the epoxy rings of the resin. This exothermic reaction generates the heat necessary to cleave the radical thermal initiator, which provides radicals that can undergo a redox reaction with the photoacid generator causing again acid liberation (Figure 1).[2,3]

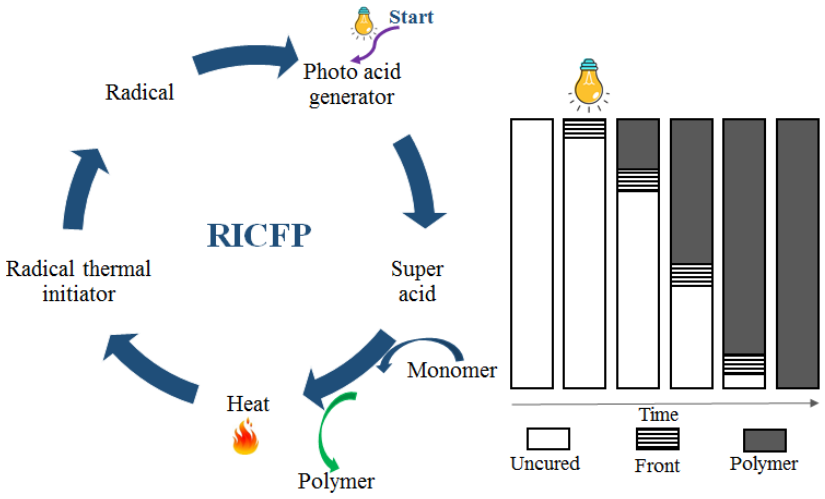

Figure 1: Mechanism and scheme of RICFP

With these advantages, the RICFP deserves to be deeply investigated for composite manufacturing which is commonly performed at elevated temperature, for many hours. Furthermore, the RICFP is a promising technique for applications like chemical anchor bolts (Figure 2) and under water curing which were difficult to carry out with conventional techniques until now.

EXPERIMENTS

The RICFP was conducted in a PTFE mold. An UV/Vis-light of 320 to 500 nm and a light intensity of 3 W/cm^2 at tip of a light guide were used to initiate the frontal polymerization. After initiation, the reaction will propagate without further irradiation being necessary.

RICFP under water: the standard formulation for RICFP contains BADGE, TPED as the thermal radical initiator, and I-Al as the photoacid generator. To test the possibility to conduct the RICFP under water, process of filling the mold with the formulation and irradiation step were done underwater.

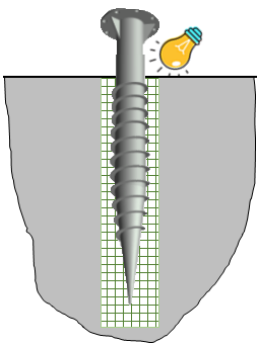

Figure 2: Chemical anchor bolts RICFP experiment

Chemical anchor bolt: this is a way to fix screws or bolts in walls without the need of common anchor bolts. In a common brick, holes of 5 mm diameter and 30 mm depth were drilled. Then, the prepared solution was filled in the drilling holes and a screw with 3 mm diameter was positioned in the center of the hole. Excessive formulation was removed before the initiation of the RICFP (Figure 2).

RICFP for epoxy composites: various fillers and fibers were used. Due to high viscosity and low reactivity of the BADGE, some reactive diluents were tested. The filler and fiber were used from low to high content to investigate the RICFP.

RESULTS AND DISCUSSION

RICFP underwater: the experiment indicated that the RICFP was successfully conducted under water (Figure 3). This result can be used for applications that had been very difficult to carry out until now, such as filling underwater cracks in bridge pillars or dams, or repairing pipes during ongoing operation.[4]

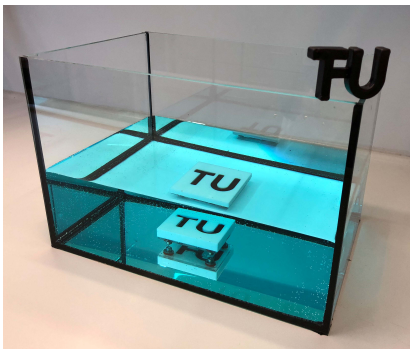

Figure 3: RICFP under water experiment

Chemical anchor bolts: the whole polymerization of the anchor bolt was done in a very short period of time by the RICFP. The stability of the specimen were tested by pull-out resistance. The result illustrated that the anchor bolt can resist the pull-out force up to 1000 N.

The RICFP for composite was successfully conducted with various fillers, for instance aluminum, milled carbon fiber, glass microspheres, aluminum nitride, silicon carbide, copper, graphite, mica, and carbon nano tubes (Figure 4). Furthermore, formulation containing reactive diluent can be used to produce composites with high filler content up to 75 vol% glass microspheres, 40 vol% milled carbon fiber, and 30 vol% aluminum nitride. The RICFP for fiber reinforced epoxy composite was investigated with carbon fiber and glass fiber.[4] 35 vol% of each fiber can be added in the specimen. Tensile testing revealed that the tensile strength, Young's modulus, and elongation at break of the composite prepared by RICFP were held at the same level of those value of the specimen cured by the conventional technique.

Figure 4: Composite specimens

CONCLUSION

The RICFP can be conducted under water. The mechanically stable anchor bolt were successfully prepared by RICFP. The RICFP for composite was not only successfully conducted with variety of fillers and fibers, but also very high filler content.

REFERENCES

[1] Pham, H.Q., Marks, M. J., Epoxy Resins, in Encyclopedia of Polymer Science and Technology. **2004**.

[2] Bomze, D., Knaack, P., Liska, R., Polymer Chemistry, 6 (47), pp. 8161-8167, **2015**

[3] Bomze, D., Knaack, P., Koch, T., Jin, H. F., Liska, R., Journal of Polymer Science Part A: Polymer Chemistry, 54 (23), pp. 3751-3759, **2016**.

[4] https://www.tuwien.ac.at/en/news/news_detail/article/125878/

CHARACTERISATION OF NANOSTRUCTURED HARD COATINGS PRODUCED BY CHEMICAL VAPOUR DEPOSITION

Elisabeth Rauchenwald[a], Mario Lessiak[b], Ronald Weissenbacher[b], Roland Haubner[a]

[a]E164 - Institute of Chemical Technologies and Analytics
[b]Boehlerit GmbH & Co. KG, Kapfenberg, Austria

INTRODUCTION

The use of nanostructured materials as wear resistant coatings on cutting tools has emerged, due to their superior physical properties. Novel analytical techniques allow the study of nanostructures and therefore their modification by parameter changes during the production process. Especially nanoscale multilayers show improved hardness and toughness, owing to the hindering of dislocation motion [1, 2]. The recent development of nanostructured AlTiN by spontaneous self-organisation, using chemical vapour deposition (CVD) suggests, that this technique can be extended to other metal nitride combinations [3]. AlZrN presents itself as a promising candidate for coating applications, as ZrN has similar properties to TiN, with advantages in drilling tests and a lower friction coefficient [4, 5]. HfN on the other hand shows good chemical inertness as well as thermal stability and when combined with aluminium nitrides in a mixed layer, wear resistance properties comparable with those of CrAlN [6]. However, knowledge about AlZrN and AlHfN coatings deposited by CVD is scarce.

The objective of this work is the production and investigation of chemical vapour deposited AlZrN and AlHfN coatings. The main focus is set on analysing the microstructure, crystal structure and elemental composition of the coatings, as well as optimising the deposition processes.

EXPERIMENTAL PROCEDURE

AlZrN and AlHfN coatings were produced using CVD based on previous work [7]. By overflowing metallic Zr/Hf and Al pellets at elevated temperature with HCl gas in two separate reactors, gaseous metal chlorides were produced in situ. Using H_2 as the carrier gas, the $AlCl_3$ and $ZrCl_4$ respectively $HfCl_4$ gases were then mixed and subsequently transported to the deposition reactor. Due to temperatures above 900 °C and the separately introduced mixture of NH_3 and N_2, the coatings were deposited on hardmetal inserts, which were coated with a TiN intermediate layer beforehand. All experiments were conducted at a deposition time of 25 min.

RESULTS AND DISCUSSION

AlZrN and AlHfN coatings with layer thicknesses up to 30 µm were generated, which indicates a high reactivity of the reaction gases. The SEM images of both coatings showed homogeneous surface structures with small cracks, which most likely occur due to differences in the thermal expansion coefficient, leading to residual stresses in the coatings.

Throughout the cross section of the AlZrN coatings, a gradient of the elemental composition was observed. Zooming in, a porous, nano-crystalline ZrN layer on the TiN could be detected, which then transforms into a dense pillar structure, as soon as Al is built into the coating (Fig. 1). This suggests either the preferred nucleation of ZrN on the TiN surface or a faster reaction of $ZrCl_4$ with NH_3 and N_2 compared to $AlCl_3$. Further investigations of the pillar structure led to the observation of slightly higher amounts of Zr in correlation with crystalline phases in the columns, surrounded by

more amorphous Al rich phases. This indicates the influence of the crystallinity by the amount of Al and Zr in the coating.

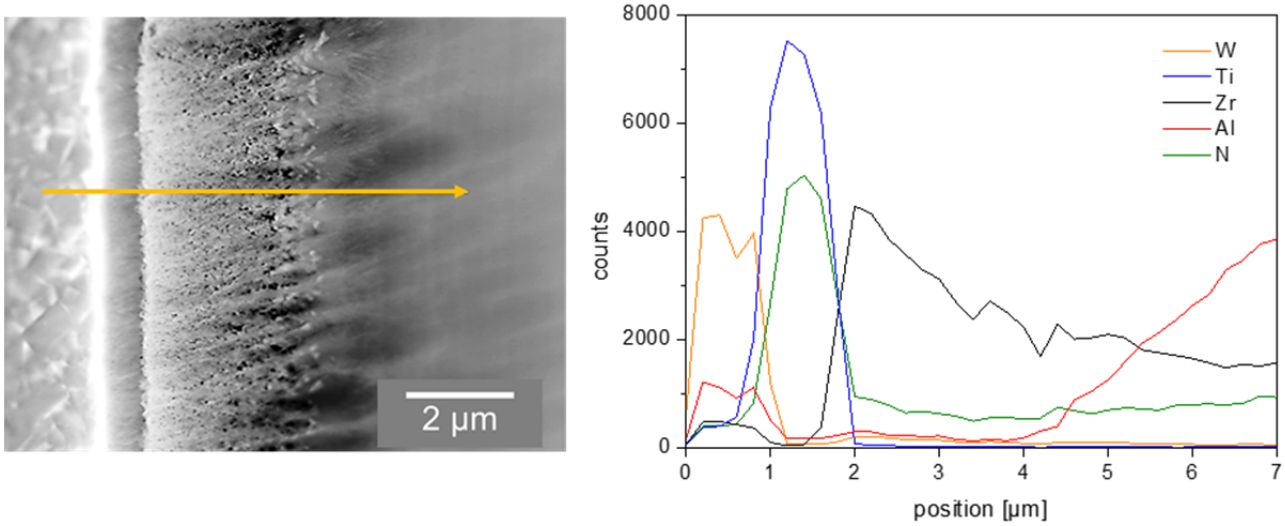

Fig. 1: EDX line scans, using TEM, examining the cross-section of the AlZrN coating.

The results of AlHfN revealed the formation of dense coatings with columnar microstructures, which occur due to changes of the phase composition. Additionally an amorphous HfN intermediate layer in the range of 2 nm between TiN and AlHfN was found.

CONCLUSION

Nanostructured AlZrN and AlHfN coatings were generated by CVD. The high reactivity of the reaction gases led to high deposition rates, which influenced the structure and elemental composition of the coatings. Additionally, a correlation between the Al/Zr or Al/Hf ratio in the coatings and the crystallinity of the structures was observed. We suspect, that by lowering the deposition rates more uniform structures and homogeneous elemental compositions throughout the coatings are achievable. The obtained results give new information on structures of AlZrN and AlHfN coatings, which will further help to optimise CVD processes.

ACKNOLEDGEMENTS

Financial support was provided by the Austrian research funding association (FFG) (grant ID 858484). The TEM measurements were carried out using facilities at the University Service Centre for Transmission Electron Microscopy, Technische Universität Wien, Austria.

REFERENCES

[1] L. Rogström et al., „Phase transformations in nanocomposite ZrAlN thin films during annealing,“ *Journal of Materials Research*, Bd. 27, pp. 1716-1724, 2012.

[2] J. Keckes et al., „Self-organized periodic soft-hard nanolamellae in polycrystalline TiAlN thin films,“ *Thin solid films*, Bd. 545, pp. 29-32, 2013.

[3] A. Köpf et al., „Nanostructured coatings for tooling applications,“ *International Journal of Refractory Metals and Hard Materials*, Bd. 62, pp. 219-224, 2017.

[4] J. J. Araiza et al., „Influence of aluminium incorporation on the structure of ZrN films deposited at low temperatures,“ *Journal of Physics D: Applied Physics*, Bd. 42, p. 115422, 2009.

[5] D. Holec et al., „Phase stability and alloy-related trends in Ti-Al-N, Zr-Al-N and Hf-Al-N systems from first principles,“ *Surface and Coatings Technology*, Bd. 206, pp. 1698-1704, 2011.

[6] R. Franz et al., „Investigation on structure and properties of arc-evapourated HfAlN hard coatings,“ *Journal of Vacuum Science \& Technology A: Vacuum, Surfaces, and Films*, Bd. 28, pp. 528-535, 2010.

[7] E. Rauchenwald et al., „Chemical vapour deposition of ZrN using in situ produced ZrCl4 as a precursor,“ *Ceramics International*, 2018.

Experimental Studies of Measurement Uncertainty Relations studied in Neutron Optics

Stephan Sponar

Atominstitut - TU Wien, Stadionallee 2, 1020 Vienna, Austria

Neutron interferometry [1], where an interference effect of matter-waves passing through a perfect silicon-crystal interferometer is observed, and neutron polarimetry (also referred to as spin-interferometry) have established as a powerful tool for investigation of fundamental quantum mechanical concepts using massive particles. The former technique enabled several textbook experiments, such as demonstrations of 4π spinor symmetry of spin - $1/2$ particles, spin superposition, gravitationally induced phase and topological phase effect, as well as studies of characteristics of intra-partite entanglement, i.e., entanglements between different degrees of freedom. The latter was utilized for demonstration of anti-commuting properties of Pauli spin matrices, topological phase measurements, and tests of alternative theories of quantum mechanics [2].

Heisenberg's uncertainty principle [3] is without any doubt one of the corner stones of modern quantum physics and not only known by scientists but also to the layman. However, the present perception of quantum mechanics has deviated from Heisenberg's empiristic assumptions, reflected in his famous gamma-ray microscope where a measurement process is the source of uncertainty, resulting in a version of the uncertainty relation expressed as a product of widths of probability distributions, i.e., standard deviations (independent of any measurement). These types of uncertainty relations set limits on how sharp the values of two observables can be determined if measured separately, but provide no information of the error when measuring one observable and the thereby induced disturbance on another subsequently (or simultaneously) measured observable. However, a naive product-type error-disturbance uncertainty relation (EDUR) is not valid in general.

Recently, Heisenberg's error-disturbance uncertainty relation has been studied in neutronic and also photonic quantum systems. In 2003, Ozawa thus proposed an improved EDUR, based on rigorous and general theoretical treatments of quantum measurements which is usually refereed to as an *operator-based* approach [4]. In my talk, I am going to give an overview of our neutron optical approaches for investigation of error-disturbance uncertainty relation via a successive measurement of incompatible neutron spin observables (e.g. $\hat{A} = \hat{\sigma}_x$ and $\hat{B} = \hat{\sigma}_y$) [5, 6, 7]. The disturbance $\eta(\hat{B})$ on the observable $\hat{B}$ is induced by the measurement of the observable $\hat{A}$ with error $\varepsilon(\hat{A})$. Though universally valid Ozawa's relations is not optimal. Recently, Branciard [8] has derived a tight EDR, describing the optimal trade-off relation between error $\varepsilon(\hat{A})$ and disturbance $\eta(\hat{B})$. Our experimental results clearly demonstrate the validity of Ozawa's and Branciard's EDRs and that the original Heisenberg EDR is violated throughout a wide range of experimental parameters.

Another more recent experiment tests so called *operational* definitions of error and disturbance developed by Busch and his co-workers. In this theoretical framework error and disturbance are evaluated from the difference between output probability distributions of the successive measurement and reference (ideal) measurements. Despite the ongoing controversy of the two competing approaches, in the case of projectively measured qubit observables, such as non-commuting neutron spin components,

both approaches lead to the *same* outcomes [9].

In our recent experiments information-theoretic, or entropic, definitions of error (in this theoretical framework referred to as *noise*) and disturbance are studied. Here, noise and disturbance are defined via correlations between the input states and measurement outcomes. We successfully carried out an experimental test of a newly derived, *tight* noise-disturbance uncertainty relation for general qubit measurements. The noise associated to the measurement of an observable is defined via conditional Shannon entropies and a tradeoff relation between the noises for two arbitrary spin observables is demonstrated [10]. The optimal bound of this tradeoff is experimentally obtained for various non-commuting spin observables. For some of these observables this lower bound can be reached with projective measurements, but we observe that, in other cases, the tradeoff is only saturated by general quantum measurements (i.e. positive-operator valued measures POVMs) as predicted theoretically. These results showcase experimentally the advantage obtainable by general quantum measurements over projective measurements when probing certain uncertainty relations.

References

[1] H. Rauch and S. A. Werner, *Neutron Interferometry* (Clarendon, Oxford, 2000).

[2] J. Klepp, S. Sponar, and Y. Hasegawa, Prog. Theor. Exp. Phys., **2014**, 082A01.

[3] W. Heisenberg. *Über den anschaulichen Inhalt der quantentheoretischen Kinematik und Mechanik. Z. Phys.*, 43:172–198, 1927.

[4] M. Ozawa. *Universally valid reformulation of the Heisenberg uncertainty principle on noise and disturbance in measurement. Phys. Rev. A*, 67:042105, 2003.

[5] J. Erhart, S. Sponar, G. Sulyok, G. Badurek, M. Ozawa, and Y. Hasegawa. *Experimental demonstration of a universally valid error-disturbance uncertainty relation in spin-measurements. Nature Physics*, 8:185–189, 2012.

[6] G. Sulyok, S. Sponar, J. Erhart, G. Badurek, M. Ozawa, and Y. Hasegawa. *Violation of Heisenberg's error-disturbance uncertainty relation in neutron-spin measurements. Phys. Rev. A*, 88:022110, 2013.

[7] S. Sponar, G. Sulyok, J. Erhart, and Y. Hasegawa. *Error-disturbance uncertainty relations in neutron-spin measurements. Adv. High Energy Phys.*, 44:36–44, 2015.

[8] C. Branciard, Proc. Natl. Acad. Sci. USA **110**, 6742 (2013).

[9] G. Sulyok and S. Sponar. *Heisenberg's error-disturbance uncertainty relation: Experimental study of competing approaches. Phys. Rev. A*, 96:022137, 2017.

[10] B. Demirel, S. Sponar, A. A. Abbott, C. Branciard and Yuji Hasegawa *Experimental test of an entropic measurement uncertainty relation for arbitrary qubit observables. New J. Phys*, 21:013038, 2019.

RESPONSIBLE TOURISM TO CLIMATE CHANGE: A SYSTEM APPROACH FOR ALTERNATIVE SUSTAINABLE TRANSPORT

Amphai Wejwithan[a], Hermann Knoflacher[a], Helga Kromp-Kolb[b] ,Tanawan Sintunawa[c]

[a] E230-01 - Research Centre of Transport Planning and Traffic Engineering, Institute of Transportation, Vienna University of Technology
[b] Centre for Global Change and Sustainability, Institute of Meteorology BOKU University, Austria
[c] Faculty of Natural Resource Studies, Mahidol University ,Green Leaf Foundations, Thailand

INTRODUCTION

This main idea is a showcase in urban tourism by promoting responsible mobility in a new emerging tourism destination in Thailand namely Koh Pha-ngan (Pha-ngan island). Koh Pha-Ngan is located in the southern part of the Gulf of Thailand, in Suratthani province. As like other tourism destinations in Thailand, motorized oriented mode of transport has dominated tourism mobility to respond to mass tourism growth. Pha-ngan island's topography is very supportive of climate friendly and environmentally friendly transport modes for both daily use and tourism activities. System thinking and system dynamics will be used to asses possible policy options for climate friendly tourism in the destination.

FUNDAMENTAL OF THE PROBLEM

System Dynamics Approach is applied for behaviour overtime analyses and modelling. The identification of needed data and information collections, primarily survey and reviews of literatures are conducted. Comparison of system behaviours and reference modes for an understanding of what influence system behaviours through behavioural analysis of modelling processes are using for the system approach and modelling. Transforming data from clausal loop diagram (CLD) and collecting data into a simulation model has done by simulation and modelling steps. The Final step is policy alternatives recommended as the results of system modelling.

The study is focusing on how the cause and effect of tourism to the environment and climate change. Transportation causes around 75% of the CO_2 emissions generated by tourism, with aviation representing the bulk part of it (40%). Although tourism transport has a relatively small share in current global emissions, there is a need to develop effective mitigation measures, considering its projected dynamic growth. In the mitigation efforts technological development is still a key tool, but it is unable to solve the problem of climate change on its own. Therefore, for effective mitigation in the transport sector there is a need to implement a mix of measures, including technological improvements, regulatory and market based measures, as well as behaviour changes. In any market-based measures the position of developing countries should be considered carefully to ensure that poverty reduction objectives are not jeopardized which might imply increasing flights to deliver tourism exports.[5] Since transportation is the main part that contributes CO_2 in the tourism business and it is the most complicated part in this sector, and its impact are vastly. Transport modes in the destination are used as a key indicator for a modal shift for the sustainable mobility

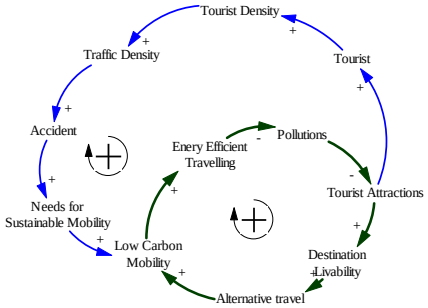

Figure 1 causal loop diagram about the sustainability tourist destination Source: Author, 2019

in tourism destinations.

Figure 1 is a causal loop diagram that represents the number of tourists cause more accidents and consume more energy consumption. These are the reasons that can cause air pollution and leads to a decline in tourist attractions. The increasing number of tourists makes traffic high density, especially in the group of tourists traveling by car and motorcycle users in areas. Low carbon travel is one way to make tourist attractions can be attractive.

RESULTS AND DISCUSSION

The survey result in Figure 2 shows that motorcycle is the highest mode of transport which used for commuting in Pha-Ngan. Walking and cycling are more popular modes for tourists while they were staying on this island, higher than travelled by cars. Modal splits are key points which influence tourist's decision for choosing their travel. Total of trips done by using low carbon modal splits from walking, cycling and public services which are local buses, tuk- tuk is 49 %.

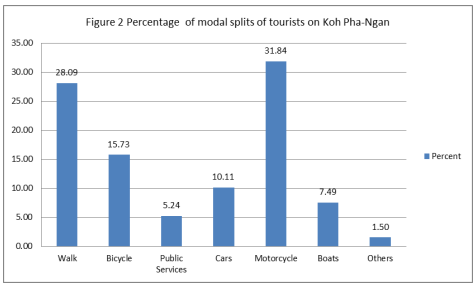

Source: Project survey complied by Author, 2018-2019

Transforming CLD to System Dynamics Model stimulates assumption behaviour of the system. In the stimulated year, 2018-2019 will be the turning point of the tourism industry in this business as usual behaviour. Sustainable travel is decided to be an alternative option copes with energy efficiency and pollutions. Boosting a better environmentally friendly tourist destination needs to improve transportation systems in the area.

CONCLUSION

Car and motorcycle users change their mobility behaviour to low carbon styles by walking and using bicycles that will reduce the CO_2 emission from transport. The systems thinking will show how changing behaviour can impact on the effects of climate change can be achieved by promoting non-motorized mode. For example, encouraging more walking and cycling in tourist destinations, the number of car users or the people who use motorise mode will decrease. Energy consumption will be reduced accordingly. Tourism policy- making for the whole country can be applied by using results from this study.

ACKNOWLEDMENT

This study has a grant from Balaton Group as Donella Meadows Fellowship project in 2017-2018 and funding from Health Promotion and Climate Friendly Bicycles in tourism attractions project under the Green Leaf Foundation and Thai Health Foundation.

REFERENCES

[1] Hall CM, Scott D and Gössling S.. The Primacy of Climate Change for Sustainable International Tourism. Sustainable Development 21, 112–121 Published online in Wiley Online Library (wileyonlinelibrary.com) DOI: 10.1002/sd.1562. 2013.
[2] Ian Jenkins Sustainability and Climate Change; Sustainability in Tourism.Springer Fachmedien Wiesbaden. 2013.
[3] Meadows, D. H. Thinking in systems: A primer, chelsea green publishing. 2008.
[4] Knoflacher, H., & Ocalir-Akunal, E. V. (Eds.). Engineering Tools and Solutions for Sustainable Transportation Planning. IGI Global. 2017.
[5] World Tourism Organization and United Nations Environment Programme Climate Change and Tourism – Responding to Global Challenges. World Tourism Organization, Madrid, Spain 2008. p.9

FIXED-PARAMETER TRACTABLE FRAGMENTS OF CONJUNCTIVE QUERIES AND CONSTRAINT SATISFACTION PROBLEMS

Georg Gottlob[a,b], Matthias Lanzinger[a], Reinhard Pichler[a]

[a]E192 - Institute of Logic and Computation

[b]University of Oxford, United Kingdom

INTRODUCTION

Conjunctive query (CQ) answering is one of the most fundamental problems in computer science. On the theoretical side, CQs are equivalent to constraint satisfaction problems (CSPs) and the homomorphism problem; the central problem of model theory. On the practical side, CQs are the foundation of modern database systems [1] and are widely used – often in the form of CSPs – to implement state of the art scheduling and planning solutions in industry applications.

It is therefore unfortunate that answering CQs belongs to the class of NP-complete problems; which means that all known methods of solving CQs and CSPs require computational effort – and therefore, time – that grows exponentially in the size of the problem, e.g., the database. Considering the scope of modern databases — which frequently exceeds multiple terabytes — it is of great importance for practical applications to study the theory of what precisely makes the problem hard and how to identify and evaluate easy cases. Identifying fragments of the problem, i.e., classes of conjunctive queries that exhibit some specific property, for which evaluation requires subexponential time is one of the main themes in this line of research in general and the presented work in particular.

FUNDAMENTALS OF THE PROBLEM

The problem has been heavily studied in the literature, starting with the well known treewidth which has found wide adoption throughout theoretical computer science as well as real-world applications [2]. Treewidth has some significant shortcomings in the context of CQs and more general methods, based around the idea of structurally decomposing the query, have subsequently been developed to address these shortcomings [3]. In particular, the study of (generalized) hypertree width and its fractional generalization has led to important results, identifying large fragments for which the CQ problem is indeed *tractable*, i.e., solvable in polynomial time.

Recent results have identified even more general fragments — identified by their *submodular width* [4] — for which *fixed-parameter tractable* (fpt) evaluation is possible. In fpt algorithms, the execution time may depend superpolynomially only on *part of the problem* (the namesake fixed parameter). In the context of database queries fixed-parameter tractability becomes very attractive in practice as the query itself is usually vanishingly small in comparison to the size of the database.

RESULTS AND DISCUSSION

In our ongoing research we bring together the principles of structural decomposition that have already been proven successful in this context with another classical theme of CQ research; query minimization and semantic equivalence of queries [5]. We call two queries *semantically equivalent* if they always return the same results over any database. The idea is then to compute the answer to a query by instead computing the answer of an equivalent query with the simplest structure. The main prob-

lem then is that there exist infinitely many equivalent queries, making it very difficult to find the best one. We formalize this plan by introducing the notions of *semantic fractional hypertree width* and *semantic submodular width* as the minimal respective widths over all equivalent queries. In our main result we are able to precisely identify those structures for which these widths are minimal and show that both properties identify significant and new fpt fragments of CQs. Semantic submodular width in particular is shown to induce the most general known fpt fragment, subsuming all other fragments identified in the literature.

CONCLUSION

Figure 1 illustrates our contributions in the context of other important properties from the literature that identify (fixed-parameter) tractable fragments of CQs. These new classes represent a significant advancement over previous results and are a significant step towards the ultimate goal — for theory and applications — of fully characterizing all fixed-parameter tractable conjunctive queries. Furthermore, our approach is the first to combine all the main threads of CQ research, providing a first holistic view of the problem and thereby laying the foundation for new fields of research.

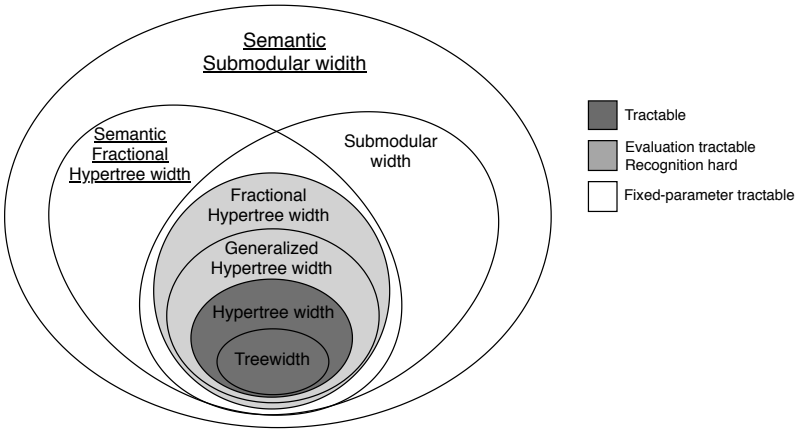

Figure 1: Properties used to identify (fixed-parameter) tractable fragments of CQs. New classes introduced in the presented work are underlined.

This work was supported by the Austrian Science Fund (FWF):P30930-N35.

REFERENCES

[1] S. Abiteboul, R. Hull, and V. Vianu, *Foundations of databases: the logical level*. Addison-Wesley Longman Publishing Co., Inc., 1995.

[2] T. Kloks, *Treewidth: computations and approximations*. Springer Science & Business Media, 1994, vol. 842.

[3] G. Gottlob, G. Greco, N. Leone, and F. Scarcello, "Hypertree decompositions: Questions and answers," in *Proceedings of the 35th ACM SIGMOD-SIGACT-SIGAI Symposium on Principles of Database Systems*. ACM, 2016, pp. 57–74.

[4] D. Marx, "Tractable hypergraph properties for constraint satisfaction and conjunctive queries," *Journal of the ACM*, vol. 60, no. 6, p. 42, 2013.

[5] A. K. Chandra and P. M. Merlin, "Optimal implementation of conjunctive queries in relational data bases," in *Proceedings of the ninth annual ACM symposium on Theory of computing*. ACM, 1977, pp. 77–90.

POINT DEFECT PHONON SCATTERING: FUNDAMENTALS AND IMPORTANCE

Bonny Dongre[a], Ankita Katre[b], Jesús Carrete[a], Natalio Mingo[c], and Georg K H Madsen [a,*]

[a] E165 Institute of Materials Chemistry
[b]Savitribai Phule Pune University, Pune, India
[c]CEA-Grenoble, Grenoble Cedex, France

INTRODUCTION

The present work deals with understanding the effect of point-defect phonon scattering on the thermal transport properties of semiconductors. Phonons are the main heat carriers in semiconductors and insulators [1]. Various point defects like vacancies, interstitials, and impurities are inherently present in such materials. These defects introduce mass and interatomic force constant (IFC) perturbations that cause a hindrance to the flow of phonons and determine the phonon scattering characteristics of a particular point defect. The higher the scattering caused by a point defect, the larger the induced reduction in the lattice thermal conductivity (κ_ℓ). Experimentally, it is challenging to retrieve the phonon scattering rates of individual defects. However, recent advances on the theoretical and computational fronts have facilitated understanding and dealing with such a problem. In this regard, the T-matrix atomistic Green's functions (AGF) approach combined with inputs from density functional theory (DFT) facilitates the treatment of the perturbation to all orders and parameter-free calculation of scattering rates [2].

AGF have been successfully applied for studying defects like vacancies, extrinsic dopants, nanoparticles, and dislocations [3]. Here we explain the drastic reduction in κ_ℓ of cubic SiC (3C-SiC) in the case of boron doping based on the enhanced phonon scattering it causes [4]. The underlying factors in the AGF that result in such enhanced scattering are studied in detail. It is established that the smaller the asymmetry in the atomic relaxation around the defect, the higher the IFC perturbation, and the higher the phonon scattering [5].

THEORETICAL FOUNDATION

The scattering rate due to point-defect phonon interactions can be calculated as:

$$\frac{1}{\tau_{i\mathbf{q}}} = \pi n_{\text{def}} V_{\text{uc}} \frac{1}{\omega_{i\mathbf{q}}} \sum_{i'\mathbf{q}'} \left| \left\langle i'\mathbf{q}' \left| \mathbf{T} \right| i\mathbf{q} \right\rangle \right|^2 \delta\left(\omega^2_{i'\mathbf{q}'} - \omega^2_{i\mathbf{q}} \right), \tag{1}$$

where where n_{def} is the volumetric concentration of the point defects, V_{uc} the volume of the unit cell, and ω the angular frequency of phonons. The sum is taken over all the possible outgoing phonons of wave vector $\mathbf{q}'$ and branch index i' for an incoming phonon $i\mathbf{q}$ scattered from a point defect. The $\mathbf{T}$ matrix is defined as, $\mathbf{T} = (\mathbf{I} - \mathbf{V}\mathbf{g}^+)^{-1}\mathbf{V}$, where $\mathbf{g}^+$ is the retarded phonon Green's function of the unperturbed host lattice. $\mathbf{V}$ is the total perturbation matrix calculated as, $\mathbf{V} = \mathbf{V}_M + \mathbf{V}_K$. Here, $\mathbf{V}_M$ and $\mathbf{V}_K$ are the mass and IFC perturbation matrices, respectively.

RESULTS AND DISCUSSION

In 3C-SiC, we observed that nitrogen doping in polycrystalline samples reduces κ_ℓ only slightly as compared to the undoped ones, in excellent agreement with experiments [4]. However, addition

of boron to the system in amounts much smaller than nitrogen leads to a huge reduction in κ_ℓ. This reduction is caused by the enhanced scattering rates of the neutral B defect as compared to N, see Fig. 1, which shows the scattering rates of B- and N-doped 3C-SiC and diamond in different charge states. Boron shows resonant phonon scattering at ≈ 33 rad/ps and the scattering rates are two orders of magnitude larger than the N ones. This was found to be directly related to the fact that the B atom relaxes slightly asymmetrically, away from one of the Si atoms in the nearest neighbor Si atom tetrahedron around it, as shown in Fig. 2. This resulted in a large IFC perturbation which is essential for enhanced scattering. However, for B- and N-doping in diamond, it is observed that the N atom relaxes highly asymmetrically and causes an IFC perturbation smaller than B which relaxes slightly asymmetrically. Despite producing equally large IFC perturbations no enhanced scattering is observed in diamond because of its low phonon density of states.

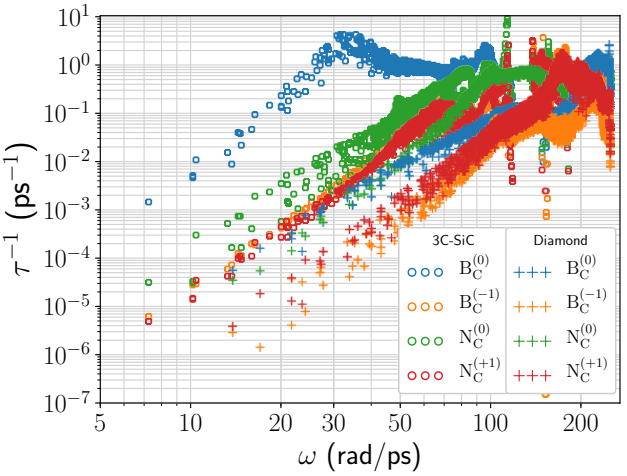

Figure 1: Scattering rates of different dopants in 3C-SiC and diamond [4]-Reproduced by permission of The Royal Society of Chemistry.

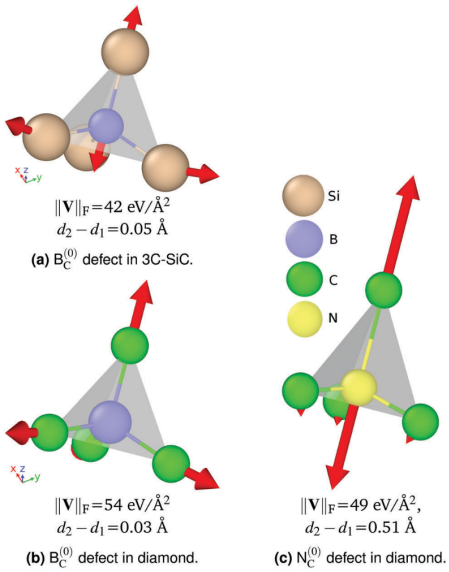

Figure 2: Asymmetrical relaxation of different defects in 3C-SiC and diamond [5]-Reproduced by permission of The Royal Society of Chemistry.

CONCLUSION

We have shown how certain point defects scatter phonons more strongly than others and can greatly reduce κ_ℓ. Asymmetrical relaxation of the defect in the system is an important ingredient to resonant scattering. In future, we plan to perform a high-throughput study of all the possible points defects in many different semiconductor materials with an aim of identifying other such super-scatterers.

REFERENCES

[1] Ziman, John M. *"Electrons and phonons: the theory of transport phenomena in solids"*. Oxford university press, 2001.

[2] Mingo, Natalio, et al. *"Cluster scattering effects on phonon conduction in graphene"*. Physical Review B, 81 (4), p. 045408, 2010.

[3] http://katalog.ub.tuwien.ac.at/AC15312589

[4] Katre, Ankita, et al. *"Exceptionally strong phonon scattering by B substitution in cubic SiC"*. Physical review letters, 119 (7), 075902, 2017.

[5] Dongre, Bonny, et al. *"Resonant phonon scattering in semiconductors"*. Journal of Materials Chemistry C, 6(17), 4691-4697, 2018.

ORGANIC HIGH-PERFORMANCE MATERIALS VIA HYDROTHERMAL SYNTHESIS

M. Josef Taublaender[a,b], Miriam M. Unterlass[a,b,c,*]

[a]E163 - Institute of Applied Synthetic Chemistry
[b]E165 - Institute of Materials Chemistry
[c]CeMM - Research Center for Molecular Medicine of the Austrian Academy of Sciences, Vienna, Austria

INTRODUCTION

We recently established a novel synthetic preparation method for various organic high-performance materials which solely employs water under high-temperature and high-pressure conditions as reaction medium. While classical protocols for generating the substances we are interested in require toxic solvents and often yield harmful reaction byproducts, our strategy does not pose any risk for environment and health. In fact, our technique can be considered as inherently "green", since water is the only solvent used as well as the only reaction byproduct formed. Hence, handling and disposal of harmful substances can be completely avoided just by replacing the usual synthetic methods by ours based on high-temperature water.

THEORETICAL BACKGROUND

These so-called hydrothermal (HT) preparation techniques are inspired by natural mineral formation processes taking place in the earth's crust. There, it can occur that subterranean, entrapped water in close proximity to magma chambers is heated to elevated temperatures (T > 100 °C). Due to the constraint space, the resulting hot steam cannot evaporate and consequently autogenous pressure (p > 1 bar) arises – similar to what happens in an ordinary pressure cooker some of us frequently use for cooking. Under HT conditions certain physico-chemical properties of water change, allowing for dissolution of a plethora of compounds that are virtually insoluble in water at ambient conditions. In addition to that, HT water can also facilitate certain types of chemical reactions – among others condensations. In nature, this enables the formation of various highly crystalline minerals. By using autoclaves, which are basically high-end pressure cookers, we can mimic such HT systems in our laboratory and take advantage of the altered properties of water in order to prepare advanced organic high-performance materials.

RESULTS AND DISCUSSION

We have already successfully demonstrated that HT conditions are perfectly suitable for not only synthesizing, but also crystallizing highly aromatic, low-molecular weight compounds.[1] Interestingly, HT conditions are also nicely suitable for generating polymers, *i.e.* high-molecular weight compounds. If our synthetic approach is applied to synthesize polymers, it is generally termed hydrothermal polymerization (HTP). Besides other types of polymers, HTP is especially well-known for generating various polyimides. By carefully choosing monomers as well as optimizing reaction conditions, it has been shown that even highly crystalline polyimide microparticles can be synthesized in solely HT water (see Figure 1).[2,3]

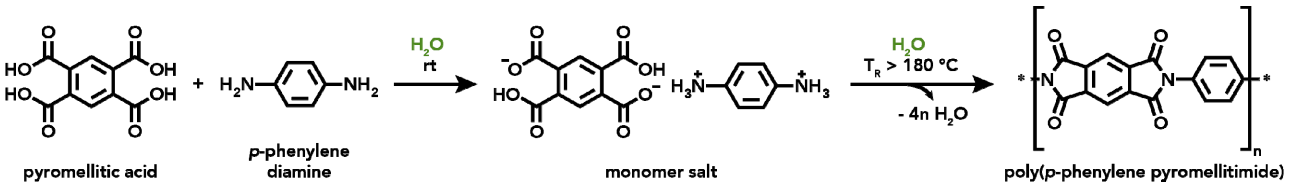

Figure 1: HTP of the polyimide poly(*p*-phenylene pyromellitimide) from its monomers *via* a monomer salt intermediate. Both reaction steps are carried out in solely H_2O.

This is a truly startling finding considering the polymeric nature of these material. The obtained high crystallinities are a significant advantage compared to classical polyimides prepared in toxic, harmful solvents which only show low degrees of crystallinity. It is a well-known fact that with increasing crystallinity several materials properties such as mechanical, chemical and thermal stability improve.

Furthermore, it has also been shown that by applying environmentally benign additives and co-solvents during HTP polyimide microparticles of different morphologies can be obtained while maintaining the highly promising feature of extraordinarily high crystallinity. The morphological possibilities include microsheets, various types of magnificent flower-like structures as well as nano-structured microparticles (see Figure 2).[4,5] Such particles of different size, shape and morphology have different surface areas and show different degrees of anisotropy regarding various physical properties such as thermal conductivity and mechanical strength. By using such microparticles as light-weight organic fillers for high performance matrices, composite materials with various properties can be obtained.

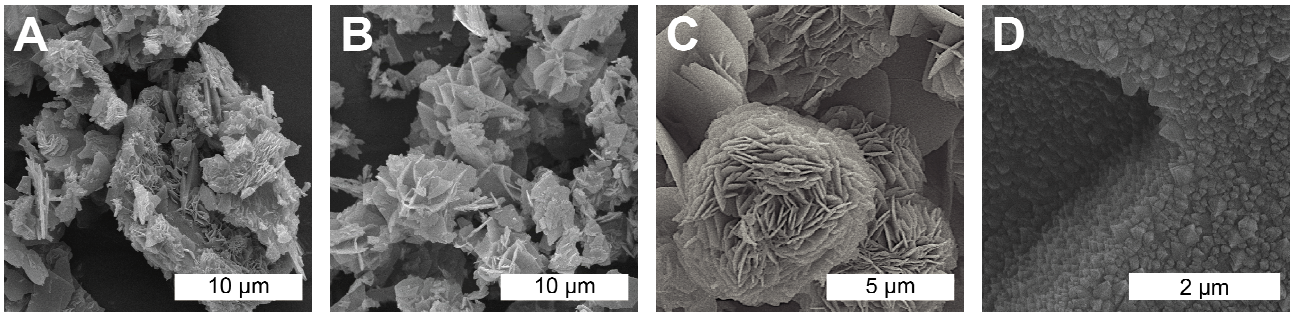

Figure 2: SEM micrographs of hydrothermally synthesized polyimides: A, B – intergrown and decorated polyimide microsheets as well as flower-like structures obtained using solely H_2O; C – densely packed polyimide microflower generated in the presence of an additive; D – nanostructured PI microparticle synthesized by applying a co-solvent.

CONCLUSION

Together with their environmentally benign origin the enhanced properties as well as the simplicity of morphological tuning are most important for the future perspective of HTP as synthetic approach since only such novel and green processes have realistic chances to replace existing methods if they yield products of at least equal or even improved quality.

REFERENCES

[1] M. J. Taublaender, F. Glöcklhofer, M. Marchetti-Deschmann, M. M. Unterlass, *Angew. Chem. Int. Ed.* **2018**, *57(38)*, 12270.

[2] B. Baumgartner, M. J. Bojdys, M. M. Unterlass, *Polym. Chem.* **2014**, *5*, 3771.

[3] Baumgartner, M. J. Bojdys, P. Skrinjar, M. M. Unterlass, *Macromol. Chem. Phys.* **2016**, *217*, 485.

[4] M. J. Taublaender, M. Reiter, M. M. Unterlass, *Macromol. Chem. Phys.* **2017**, *219(3)*, 1700397.

[5] M. J. Taublaender, M. Reiter, M. M. Unterlass, *submitted*, **2019**.

LADEINFRASTRUKTUR FÜR ELEKTROFAHRZEUGE: BEDARF, KOSTEN UND AUSWIRKUNGEN AUF DIE ENERGIEVERSORGUNG IN ÖSTERREICH BIS 2030

Thomas Bruckmüller

E315 - Institut für Fahrzeugantriebe und Automobiltechnik

EINLEITUNG

Die derzeit noch niedrigen BEV-Bestände beim PKW und leichten Nutzfahrzeug (LNF) unterliegen aufgrund der stark zunehmenden Neuzulassungen einem beachtlichen Wachstum. Daraus ergeben sich zahlreiche Fragen in Hinblick auf die erforderliche Ladeinfrastruktur, welche in dieser Arbeit bis 2030 untersucht werden. Zusätzlich werden die Auswirkungen höherer BEV-Bestände bis hin zu 100 % untersucht.

METHODISCHER ANSATZ UND NEUE ASPEKTE

Der wesentliche neue methodische Beitrag besteht in der Berechnung des Ladeinfrastrukturbedarfs ausgehend vom Mobilitätsverhalten österreichischer Fahrzeug- nutzer. Dabei werden ausgehend von der Bestandsentwicklung und einer detaillierten Mobilitätsdatenerhebung der österreichischen PKW-Nutzer, der Leistungsgang (Leistungsverlauf) sowie die gleichzeitig benutzten Ladestellen (Gleichzeitigkeit) berechnet. Es werden zusätzlich der BEV-Verbrauch und die Umgebungstemperatur berücksichtigt. Des Weiteren wird nach Ort (Bundesland bzw. Stadt), Jahreszeit, Wochentag, Erwerbsstatus des Fahrers, Zweck der Fahrt sowie Fahrtziel differenziert. Der daraus resultierende Leistungsgang und die Gleichzeitigkeit liefern die benötigte Leistung, Energie und Anzahl der Ladestellen. Diese Parameter sind insbesondere für Energieversorger, Netz- und Ladestellenbetreiber von größter Bedeutung. Es werden die Auswirkungen auf das lokale Verteilernetz in verschiedenen Modellen (ländlich, klein- und großstädtisch) untersucht. Anschließend werden die Kosten für die Errichtung der Ladestellen abgeschätzt. Eine Untersuchung der Ladeinfrastruktur für E-Fahrzeuge mit einem derartigen methodischen Ansatz, in diesem Detailierungsgrad und unter Vereinigung der Fahrzeug- und Netzseite, ist bisher nicht verfügbar.

ERSTE ERGEBNISSE

Bis 2030 wird ein BEV-Bestand von 11 % beim PKW bzw. 6,5 % beim LNF (leichtes Nutzfahrzeug) erwartet. Deren Ladevorgänge erzeugen eine Spitzenlast von 1,1 GW. Das entspricht ca. 11 % der derzeitigen Spitzenlast. Bei 100 % BEV-Bestand (PKW & LNF) ergibt sich durch die Ladung eine Spitzenleistung von 9,4 GW bzw. 93 % der derzeitigen Spitzenlast. Der zusätzliche Energiebedarf im Jahr 2030 beträgt 2,2 TWh bzw. 3,2 % des derzeitigen Bedarfs. Bei 100 % BEV-Bestand ergibt sich ein Mehrbedarf von 28 % bzw. 19,8 TWh.

Die benötigte Anzahl an Ladestationen ist nach Ort und Ladeleistung unterschiedlich. Im Jahr 2030 werden insgesamt für ganz Österreich 857.000 Ladestellen benötigt, davon 154.000 in Wien. 29 % der Ladestellen in Österreich werden am Straßenrand (Parkstreifen) benötigt. In Wien sind 67 % der benötigten Ladestellen am Straßenrand, was auf die geringe Anzahl an Personen mit eigenen Stellplätzen zurückzuführen ist. Mit 73 % wird die Mehrheit der Ladestellen in Österreich mit 11 bzw. 22 kW erwartet. Bei 100 % BEV-Bestand werden 7,2 Mio. Ladestellen in Österreich benötigt, davon 1,2 Mio. in Wien.

Die Untersuchung typischer lokaler Verteilernetzmodelle (ländlich, klein- und großstädtisch) zeigt, dass bis 2030 keine unzulässigen Überschreitungen in einem typischen Netz erwartet werden. Es sind daher bis 2030 keine Netzerweiterungs- maßnahmen zu erwarten. In Einzelfällen, in denen bereits jetzt eine hohe Netzauslastung vorliegt, können Netzerweiterungsmaßnahmen nicht ausgeschlossen werden. Die jeweiligen Grenzen der betrachteten Verteilernetze werden bei BEV-Beständen PKW & LNF von 30 % & 18 % (ländlich), 56 % & 33 % (kleinstädtisch) bzw. 48 % & 28 % (großstädtisch) erwartet.

Die Errichtungskosten für die benötigten Ladestellen bis 2030 werden mit 6,1 Mrd. € in Österreich, davon 2,1 Mrd. € in Wien, erwartet. Das entspricht 9.800 €/Fahrzeug, was bei 0,2 €/kWh Stromkosten und 25 kWh/100km Verbrauch den Energiekosten für 196.000 km pro Fahrzeug entspricht. 62 % der Kosten in Österreich entfallen auf

Ladestellen am Straßenrand. Aufgrund der geringen Anzahl an eigenen Stellplätzen, werden in Wien 81 % der Kosten für Ladestellen am Straßenrand erwartet. Da Ladestellen am Straßenrand in der Regel nicht durch den Fahrzeugnutzer selbst errichtet werden können, lässt sich daraus schließen, dass die Mehrheit der Kosten für den Ausbau der Ladeinfrastruktur durch öffentliche Stellen oder Ladestellenbetreiber getragen werden müssen. Bei 100 % BEV-Bestand ergeben sich Kosten in der Höhe von 51 Mrd. € (exkl. Netzerweiterungen) in Österreich, davon 17 Mrd. € in Wien.

Zusammenfassend lässt sich feststellen, dass für den Ladeinfrastrukturbedarf durch die zunehmende Anzahl an E-Fahrzeugen in den nächsten Jahren ein starker Anstieg erwartet wird. Im Vergleich zum Gesamtbedarf an elektrischer Energie ergibt sich bis 2030 nur eine geringe Zunahme der benötigten Energie und Leistung durch E- Mobilität. Für typische lokale Verteilernetze sind bis 2030 keine Probleme durch das Laden batterieelektrischer Fahrzeuge zu erwarten. Für die Errichtung der benötigten Ladestellen werden aufgrund der hohen Anzahl und der hohen Einzelkosten für Ladestationen im öffentlichen Bereich, hohe Gesamtkosten erwartet.

Author Index

Presenting authors in bold letters

A

Addison, R. FUR.5
Amorrortu, O. CAT.24
Andriotis, O.G. ENM.4
Archodoulaki, V.-M. FUR.9, FUR.14
Arndt, M. FUR.21
Aspalter, A. CAT.7
Aspermair, P. FUR.27

B

Bao, X. CAT.23
Baran, CAT.11, CAT.12
Baran, P. CAT.10, CAT.13 FUR.18, FUR.19, FUR.23
Baratchart, L. FUR.8
Barentin, C. FUR.12
Barišić, N. FUR.6
Barrabés, N. CAT.3 **CAT.9**, CAT.24, CAT.26
Baudis, S. ENM.2
Bauer-Marschallinger, B. FUR.4
Baumgartner, S. FUR.26
Bernardi, J. ENM.4
Bintinger, J. FUR.27, FUR.11
Boiadjieva-Scherzer, T. ENM.6
Bolvardi, H. FUR.21, FUR.25
Bommarius, A.S. CAT.1
Bozdogan, A. FUR.27
Brezinova, I. FUR.1
Bruckmüller, Th. **LION.2**
Burgdörfer, J. FUR.1

C

Čalkovský, M. CAT.2
Carrete, J. FUR.34
Casanova, I. CAT.20
Chen, H. **CAT.23**
Cherevan, A. CAT.8
Colombani, J. FUR.12
Ćwik, A. CAT.20
Czerw, K. CAT.10, FUR.23
Czuma, N. CAT.11, CAT.12 CAT.13, FUR.19, CAT.20

D

Dabiri Razlighi, B. **ENM.8**
De Vrieze, J.E. CAT.22
Dellago, B. **ENM.2**
Diebold, U. CAT.2, CAT.23
Dobrezberger, K. **CAT.7**
Dong, S. **AUP.19**
Dongre, B. **FUR.34**
Donsa, S. FUR.1
Duscher, B. FUR.14

E

Eder, D. FUR.10, CAT.8, FUR.16
Ederer, M. **FUR.1**
Eickhoff, S. ENM.9
Enzlberger, L. CAT.25

F

Fabian, Th. **FUR.3**
Fadai, A. AUP.10
Fedi, F. FUR.11
Fellner, A. **ENM.9**
Feroz, S. CAT.1
Fleck, K. CAT.15
Flegar, M. **AUP.5**
Föttinger, K. CAT.7, CAT.22, CAT.25
Franchini, C. CAT.2
Fried, R. **CAT.15**
Fritze, S. FUR.25
Fruhmann, P. FUR.27, FUR.11, FUR.26
Fuger, Ch. **FUR.21**
Fuss, A. **FUR.7**

G

Gantner, F. **ENM.1**
Garcia, C. **CAT.26**, CAT.9
Giannopoulos, I. AUP.4
Glechner, Th. **FUR.25**
Gottlob, G. FUR.33
Griessler, T. CAT.15
Grothe, H. FUR.15
Gruber, P. ENM.1

H

Hahn, R. ENM.4, FUR.21, FUR.25
Haroshka, D. **AUP.11**
Hartmann, M. **ENM.7**
Hashimoto, S. FUR.20
Haubner, R. FUR.28, FUR.30
Haunold, Th. **CAT.5**
Hellmeier, J. **ENM.11**
Hellmich, Ch. ENM.3
Herwig, Ch. CAT.21
Heshmat, A. ENM.10
Holec, D. FUR.25
Holinka, J. ENM.6
Holzhausen, E. FUR.5
Holzinger, R. FUR.13
Hossain, S. FUR.20
Huber, M. CAT.7
Huber, T. CAT.17
Huppa, J.B. ENM.11

I

Idiskut, H. **AUP.14**

J

Jarvis, J.C. ENM.9
Jenewein, M. **AUP.18**
Jonas, A. AUP.13
Jószczuk, E. **FUR.18**

K

Kahl, G. ENM.3
Kalliauer, J. **ENM.3**
Kampusch, S. ENM.8
Kaniusas, E. ENM.8
Kasas, S. ENM.12
Kasper-Giebl, A. FUR.13
Katre, A. FUR.34
Kharlamova, M. **FUR.10**
Kirchsteiger, B. **FUR.13**
Klauser, F. FUR.13
Klebel, B. **FUR.6**
Klikovits, N. FUR.29
Knaack, P. FUR.29
Knoflacher, H. FUR.32
Knoll, W. FUR.27, FUR.11
Kobayashi, I. **FUR.20**
Koch, Th. FUR.9, FUR.14
Kodambaka, S. FUR.25
Kohler, A.-C. ENM.12
Kolozsvári, S. FUR.25
Kovacevic, H. FUR.14
Koyun, A.N. **FUR.15**
Kratz, S. **ENM.5**
Krimmel, S. **FUR.17**
Kromp-Kolb, H. FUR.32
Kronberger, H. ENM.6
Kühner, L. CAT.15
Kumpf, K. **FUR.11**
Kuźmik, A. **FUR.23**

L

Lackner, F. FUR.1
Lanzinger, M. **FUR.33**
Lasemi, N. **FUR.16**
Latschka, M. **CAT.22**
Lauter, K. FUR.26
Le Merrer, M. FUR.12
Leblond, J. FUR.8
Lelek, V.E. **AUP.9**
Leskovar, R. **ENM.13**
Lessiak, M. FUR.30
Li, X. **CAT.6**
Liberto, T. **FUR.12**
Libisch, F. FUR.3
Liedl, G. FUR.16
Ligęza, O. **CAT.11**
Lim, Ch. **CAT.14**
Lima, E. FUR.8
Lindenthal, L. **CAT.4**, CAT.18
Liska, R. ENM.2, FUR.29
Liu, Y. CAT.23
Lizarazu, J. **CAT.24**

Lunzer, M. ENM.1
Lutzer, B. FUR.11

M

Madsen, G.K.H. FUR.34
Magierło, M. **CAT.10**
Mahdavi, A. AUP.3, AUP.5, AUP.7 AUP.12, AUP.13, AUP.15
Mansouri , H.R. **CAT.1**
Materic, D. FUR.13
Mayerhuber, L. **FUR.26**
Mayr, J. **AUP.6**
Mayrhofer, P.H. ENM.4, FUR.21, FUR.25
Mc Cutchan, M. **AUP.4**
Merta, I. FUR.22
Mihovilovic, M. CAT.1, CAT.15
Mingo, N. FUR.34
Mócsa, R. **FUR.27**
Montes, M. CAT.24
Moraes, V. FUR.21
Mostrou-Moser, S. CAT.22
Motak, M. CAT.12, CAT.16, CAT.19
Motsch, V. ENM.11

N

Nagl, A. CAT.22
Nandan, S.P. **CAT.8**
Nasseri, L. **FUR.14**
Navacchi, C. **FUR.4**
Nedelkovski, V. **ENM.4**
Negishi, Y. FUR.20
Nenning, A. CAT.4, CAT.18
Neuhauser, J. CAT.7
Nguyen Thu, H.M. **FUR.9**
Novak, K. **CAT.21**
Nowak, W. CAT.11
Nowotarski, M. **CAT.13**

O

Opitz, A.K. CAT.4, CAT.18
Oprea, I. CAT.15
Ostermann, M. **FUR.28**
Ovsianikov, A. ENM.1
Öztal Oktay, S. AUP.4

P

P. Goncalves , L.Ch. CAT.1
Pacholik, G. **CAT.25**
Pfaffeneder-Kmen, M. FUR.16
Pfannenstill, V. **ENM.12**
Pflügl, S. CAT.21
Pichler, R. FUR.33
Pillwein, S. **AUP.8**
Platzer, R. ENM.11
Polcik, P. FUR.21
Poletanović, B. FUR.22
Pollice, R. CAT.14
Pollitt, S. CAT.9
Ponomarev, D. **FUR.8**
Pont, U. AUP.3, AUP.5, AUP.7 AUP.12, **AUP.13**, AUP.15
Popiela, A. **FUR.19**
Popovic, J. CAT.4, CAT.17, CAT.18
Pospichal, R. FUR.16
Pramhaas, V. CAT.6
Preschl, M. FUR.9
Priebernig, H. AUP.13
Primetzhofer, D. FUR.25

R

Radwańska, G. **CAT.12**
Rajagopal, A. CAT.8
Ralon, R. FUR.17
Ramach, U. FUR.27
Rameshan, Ch. CAT.4, CAT.5 CAT.6, CAT.17, **CAT.18**
Rameshan, R. CAT.4, **CAT.17**, CAT.18
Raschhofer, J. CAT.4, CAT.17, CAT.18
Rath, T. **FUR.5**
Rattay, F. ENM.9, ENM.10
Rauchenwald, E. **FUR.30**
Reimer, F. **AUP.2**
Reisinger, J. **AUP.16**
Rentenberger , Ch. FUR.16
Reticcioli, M. CAT.2
Riedl, H. FUR.21, FUR.25
Rohatschek, A. ENM.11
Roiaz, M. CAT.6
Rudroff, F. CAT.1, CAT.15
Ruh, Th. CAT.18

Rühe, E. CAT.15
Rupprechter, G. CAT.3
CAT.5, CAT.6, CAT.7
CAT.24, CAT.26, CAT.9

S

S. Cherevan, A. FUR.16
Saeys, M. CAT.22
Sajedi, S. **ENM.10**
Samojeden, B.
CAT.13, CAT.16, CAT.19
Santana Sosa, A. **AUP.17**
Sanz, O. CAT.24
Sarikaya, C. **AUP.12**
Scheiner, S. ENM.3
Schmid, M. CAT.2
Schmidrathner, Ch. **FUR.2**
Schnürch, M. CAT.14
Schober, P. AUP.7, AUP.13
Schrott-Fischer, A. ENM.10
Schuss, M. AUP.7
Schütz, G. ENM.11, ENM.12
Setvin, M. CAT.2
Sevcsik, E. ENM.11
Shahabian, A. **AUP.10**
Šimonová, H. **FUR.22**
Sintunawa, T. FUR.32
Sobala, J. **CAT.20**
Sokolović, I. **CAT.2**
Sperka, K. **AUP.3**
Spettel, M. CAT.14
Spiegel, F. CAT.15
Sponar, S. **FUR.31**
Staats, K. ENM.6
Stamatiou, A. FUR.17
Stampfl, J. FUR.5
Steiger, W. ENM.1
Steiger-Thirsfeld, A. ENM.4
Steyrer, B. FUR.5
Streb, C. CAT.8
Stressler, H. FUR.13
Stropp, J. CAT.7
Sturmlechner, R. FUR.13
Summa, P. **CAT.16**, CAT.19
Sun, J. **ENM.6**
Swoboda, S. AUP.13
Szczurowski, J. CAT.10
Szymaszek, A. CAT.16, **CAT.19**

T

Tabis, W. FUR.6
Taublaender, M.J. **LION.1**
Thurner, P. ENM.4, ENM.11
Tran, A.D. **FUR.29**
Truttmann, V. **CAT.3**, CAT.9
Tsigkanos, C. **AUP.1**

U

Unterlass, M.M. LION.1

V

van Bokhoven, J.A. CAT.22
Vetyukov, Y. FUR.2

W

Wagner, W. FUR.4
Walal, K. **AUP.15**
Waldmayer, F. AUP.13
Walter, H. FUR.17
Weigelhofer, G. FUR.26
Weissenbacher, R. FUR.30
Wejwithan, A. **FUR.32**
Windhager, R. ENM.6
Winkler, S. **FUR.24**
Wojcik, T. FUR.25
Wölzl, M. **AUP.7**
Worlitschek, J. FUR.17

Y

Yang, F. CAT.23

Z

Zabierowski, P. FUR.18, CAT.20
Zaid, H. FUR.25
Zarębska, K. CAT.10, CAT.11
CAT.12, CAT.13, FUR.18
FUR.19, CAT.20, FUR.23